

Regulation of septin filament formation and cholesterol production by DHCR7

Dissertation zur Erlangung des akademischen Grades

Doktor der Naturwissenschaften (Dr. rer. Nat.)

Des Fachbereichs Chemie der Technischen Universität Dortmund

Angefertigt am

Max-Planck-Institut für Molekulare Physiologie

Vorgelegt von

Yashar Sadian

Geboren am 30.05.1983, Teheran, Iran

Dortmund, Dezember 2012

Die vorliegende Arbeit wurde in der Zeit von Januar 2009 bis Dezember 2012 am Max-Planck-Institut für Molekulare Physiologie in Dortmund unter der Anleitung von Dr. Stefan Raunser durchgeführt.

1. Gutachter: Prof. Dr. Roger S. Goody

2. Gutachter: Prof. Dr. Roland Winter

Hiermit versichere ich an Eides statt, dass ich die vorliegende Arbeit selbständig und nur mit den angegebenen Hilfsmitteln angefertigt habe.

Yashar Sadian

Dortmund

We have not the reverent feeling for the rainbow that a savage has,
because we know how it is made. We have lost as much as we
gained by prying into that matter.

Mark Twain

TABLE OF CONTENTS

ABBREVIATIONS	4
ABSTRACT	6
1) INTRODUCTION.....	9
1.1) INTRODUCTION INTO SEPTIN	9
1.1.1) BUDDING YEAST AS A MODEL TO STUDY CELL DIVISION	9
1.1.2) GENETICS OF CELL DIVISION IN BUDDING YEAST	10
1.1.3) SEPTINS	13
1.1.3.1) GENETICS OF SEPTINS	14
1.1.3.2) STRUCTURE OF SEPTIN.....	16
1.1.3.3) BIOCHEMISTRY OF SEPTIN AS A GTPASE	23
1.1.3.4) FUNCTIONS OF SEPTIN	25
1.1.3.5) ESTABLISHMENT OF POLARITY, COOPERATION BETWEEN SEPTIN AND CDC42P	30
1.2) INTRODUCTION INTO DHCR7.....	36
1.2.1) CHOLESTEROL	36
1.2.2) CHOLESTEROL BIOSYNTHESIS.....	37
1.2.3) REGULATION OF CHOLESTEROL BIOSYNTHESIS	38
1.2.4) 7-DEHYDROCHOLESTEROL REDUCTASE (DHCR7).....	39
1.2.4.1) GENETICS OF DHCR7	40
1.2.4.2) PROTEIN STRUCTURE OF DHCR7	40
1.2.4.3) ENZYMATIC ACTIVITY OF DHCR7	42
1.2.4.4) DISEASE	43
1.3) METHODOLOGY.....	44
1.3.1) MEMBRANE PROTEIN EXPRESSION AND PURIFICATION	44
1.3.2) ELECTRON MICROSCOPY (EM)	45
1.3.2.1) SINGLE PARTICLE ANALYSIS	46
1.3.2.2) CRYO-ELECTRON TOMOGRAPHY (CRYO-ET)	47
1.3.2.3) ELECTRON CRYSTALLOGRAPHY	48
2) MATERIALS AND METHODS	51
2.1) MATERIALS	51
2.1.1) CHEMICALS	51
2.1.2) BUFFERS AND SOLUTIONS.....	53
2.1.3) MEDIA	59
2.1.4) BACTERIAL STRAINS, YEAST, INSECT AND MAMMALIAN CELLS	60
2.1.5) OLIGONUCLEOTIDE VECTORS	60
2.1.6) ANTIBODIES	61
2.1.7) CONSUMABLES.....	62
2.1.8) INSTRUMENTS	62
2.1.9) SOFTWARE	64
2.2) METHODS	64
2.2.1) EXPRESSION SCREENING.....	64

2.2.1.1) EXPRESSION SCREENING IN <i>E. COLI</i>	64
2.2.1.2) EXPRESSION IN INSECT CELLS	65
2.2.2) PROTEIN PURIFICATION	65
2.2.2.1) PURIFICATION OF YEAST SEPTIN COMPLEX (YSC)	65
2.2.2.2) PURIFICATION OF GIC1	66
2.2.2.3) PURIFICATION OF CDC42P	67
2.2.2.4) PURIFICATION OF HSSD	67
2.2.2.5) PURIFICATION OF CDHCR7.....	68
2.2.2.6) PURIFICATION OF HDHCR7-EGFP	68
2.2.3) CELL LYSIS AND MEMBRANE STRIPPING	69
2.2.4) SOLUBILIZATION SCREENING.....	69
2.2.5) DETERGENT EXCHANGE.....	70
2.2.5.1) ON-COLUMN EXCHANGE	70
2.2.5.2) DURING GEL FILTRATION.....	70
2.2.6) PROTEIN CONCENTRATION ESTIMATION	71
2.2.6.1) BRADFORD ASSAY	71
2.2.6.2) BCA.....	71
2.2.7) SEMIDENATURING SDS POLYACRYLAMIDE GEL ELECTROPHORESIS (SDS-PAGE)	71
2.2.8) WESTERN BLOTTING.....	71
2.2.9) PREPARATION OF SEPTIN FILAMENTS.....	72
2.2.10) ADSORPTION TO LIPID MONOLAYER	73
2.2.11) ELECTRON MICROSCOPY	73
2.2.12) CRYO ELECTRON TOMOGRAPHY (CRYO-ET).....	73
2.2.13) IMAGE PROCESSING OF NEGATIVELY STAINED SAMPLES	74
2.2.14) PLASMID CONSTRUCTION FOR YEAST TWO-HYBRID ASSAY	75
2.2.15) YEAST TWO-HYBRID ASSAY	75
2.2.16) NUCLEOTIDE EXCHANGE OF CDC42P.....	75
2.2.17) HIGH PRESSURE LIQUID CHROMATOGRAPHY (HPLC)	76
2.2.18) ANALYTICAL GEL FILTRATION ANALYSIS	76
2.2.19) CELL CULTURE	76
2.2.20) FLUORESCENCE IMAGING	77
2.2.20.1) PREPARATION OF HEK CELLS	77
2.2.20.2) MICROSCOPY.....	78
2.2.20.3) IMAGE PROCESSING	78
2.2.21) MEASUREMENT OF CHOLESTEROL	78
2.2.21.1) KIT TO QUANTIFY TOTAL CHOLESTEROL (AXIOM DIAGNOSTICS)	78
2.2.21.2) GAS CHROMATOGRAPHY	78
2.2.22) 2D CRYSTALLOGRAPHY	79
2.2.23) 3D CRYSTALLOGRAPHY	80
2.2.24) NBD-7DHC BINDING ASSAY	80
3) RESULTS	81
3.1) RESULTS AND DISCUSSION OF SEPTIN, GIC1 AND CDC42P	81
3.1.1) FILAMENT FORMATION AND BUNDLING BY GIC1	81
3.1.1.1) YEAST SEPTIN COMPLEX (YSC) STRUCTURAL ORGANIZATION	81
3.1.1.2) FILAMENT FORMATION AND ENHANCEMENT OF BUNDLING BY GIC1	83
3.1.1.3) TIME-DEPENDENT BINDING OF GIC1 TO SEPTIN FILAMENTS.....	86

3.1.1.4) ANALYSIS OF BINDING SITE OF Gic1 USING AN α -Cdc11 ANTIBODY	87
3.1.1.5) ANALYSIS OF SEPTIN-EGFP FILAMENTS	88
3.1.1.6) ANALYSIS OF Cdc10 Δ AND Cdc11 Δ FILAMENTS	89
3.1.1.7) YEAST-TWO HYBRID ASSAY CONFIRMS <i>IN VITRO</i> DATA	90
3.1.1.8) C-TERMINUS OF GIC1 IS THE SEPTIN-BINDING DOMAIN	91
3.1.1.9) BINDING OF GIC1 TO FILAMENTS VS. OCTAMERS	92
3.1.1.10) GIC1 CONFERS RESISTANCE TO SEPTIN FILAMENTS AGAINST HIGH SALT	94
3.1.2) CDC42P REGULATES ASSEMBLY OF SEPTIN FILAMENTS	95
3.1.2.1) CDC42P(GDP) ENHANCES DISASSEMBLY OF THE FILAMENTS	95
3.1.2.2) ADDITION OF GIC1 TO BROKEN SEPTIN FILAMENTS RESTORES THE RAILWAY STRUCTURE	99
3.1.2.3) MECHANISM OF DISASSEMBLY	100
3.1.3) CDC42P(GppNHP) MECHANISTICALLY REGULATES THE SEPTIN-Gic1 COMPLEX	104
3.1.3.1) CDC42P(GppNHP) BUT CDC42P(GDP) BINDS TO GIC1	104
3.1.3.2) THE SEPTIN-GIC1 COMPLEX DISASSEMBLES AT HIGH CONCENTRATION OF CDC42P(GppNHP).....	105
3.1.3.3) SIMULTANEOUS ADDITION OF Gic1 AND CDC42P TO FILAMENTS.....	108
3.1.4) EFFECT OF NUCLEOTIDES ON SEPTIN FILAMENTS	109
3.1.4.1) GTP DESTABILIZES THE FILAMENTS BUT NOT THE SEPTIN-Gic1 COMPLEX	109
3.1.4.2) GDP AND GMP HAVE NO EFFECTS ON FILAMENTS OR SEPTIN-Gic1 COMPLEX	112
3.1.4.3) CDC42P(GDP) AND GTP GENERATE TETRAMERS TOGETHER.....	112
3.1.5) CRYO-ELECTRON TOMOGRAPHY (CET) OF SEPTIN FILAMENTS	113
3.2) RESULTS OF DHCR7	121
3.2.1) EXPRESSION AND PURIFICATION OF DHCR7	121
3.2.1.1) PURIFICATION OF HSSD	121
3.2.1.2) PURIFICATION OF CDHCR7.....	124
3.2.1.3) PURIFICATION OF HDHCR7	128
3.2.2) BINDING OF NBD-7DHC TO CDHCR7	130
3.2.3) <i>IN VIVO</i> REDUCTASE ASSAY	132
3.2.4) 2D CRYSTALLOGRAPHY OF CDHCR7	134
3.2.5) LOCALIZATION OF HDHCR7-EGFP IN HEK-293 CELL	135
3.2.5.1) CO-LOCALIZATION OF DHCR7 WITH GOLGI MARKER.....	136
3.2.5.2) CO-LOCALIZATION OF DHCR7 WITH PEROXISOME MARKER.....	139
4) REFERENCES.....	143
5) SUPPLEMENTARY INFORMATION.....	163
5.1) PROTEIN SEQUENCE OF SEPTIN SUBUNITS	163
5.2) ALIGNMENT OF Cdc3, Cdc10, Cdc11 AND Cdc12	164
5.3) PHYLOGENY TREE OF Cdc3, Cdc10, Cdc11 AND Cdc12	165
5.4) SEQUENCE OF DHCR7	165
5.5) ALIGNMENT OF DHCR7.....	166
5.6) PHYLOGENY TREE OF DHCR7.....	167
5.7) GC-MS MEASUREMENT OF CHOLESTEROL	167
6) GLOSSARY.....	168
7) INDEX.....	172

Abbreviations

7-DHC	7-dehydrocholesterol
AU	Absorbance Units
CCD	Charge coupled device
Cdc	Cell division control
Cdk	Cyclin dependent kinase responsible for phosphorylation during mitosis
CET	Cryo-electron tomography
CHAPS	3-[(3-Cholamidopropyl)dimethylammonio]-1-propanesulfonate
CLSM	Confocal laser scanning microscopy
CRIB	Cdc42/Rac-interactive binding
CYP51A	Lanosterol 14-alpha-demethylase
DDM	Lauryl- β -D -maltoside
DHCR7	7-Dehydrocholesterol reductase
cDHCR7	DHCR7 of <i>Coxiella burnetii</i>
hDHCR7	DHCR7 of <i>Homo sapiens</i>
IDHCR7	DHCR7 of <i>Legionella longbeachae</i>
pDHCR7	DHCR7 of <i>Plesiocystis pacifica</i>
DHCR24	24-Dehydrocholesterol reductase
DM	n-Dodecyl β -D-maltoside
DMPC	1,2-Dimyristoyl- <i>sn</i> -Glycero-3-Phosphocholine
DOPC	1,2-dioleoyl- <i>sn</i> -glycero-3-phosphocholine
EGFP	Enhanced green fluorescent protein
EM	Electron microscopy
ER	Endoplasmic reticulum
Fos-choline-12	n-Dodecylphosphocholine
Fos-choline-13	n-Tridecylphosphocholine
GalT	Galactose-1-phosphate uridylyltransferase
GAP	GTPase activating protein
GC-MS	Gas chromatography-mass spectrometry
GDP	Guanosine diphosphate
GEF	GTPase exchange factor
Gic	GTPase interacting component
GMP	Guanosine diphosphate
GppNHp	5'-Guanylyl imidodiphosphate
GTP	Guanosine triphosphate
HMGCS1, HMGCS2	Hydroxymethylglutaryl-CoA-synthase 1/2
HPLC	High pressure liquid chromatography
IPTG	Isopropyl β -D-1-thiogalactopyranoside
MEN	Mitosis exit network
MNG-3	Maltose neopentyl glycol
NADPH+H ⁺	Nicotinamide adenine dinucleotide phosphate (reduced form)

NMR	Nuclear magnetic resonance
NSDHL	NADPH steroid dehydrogenase-like
OG	<i>n</i> -octyl- β -D-glucoside
PAGE	Polyacrylamide gel electrophoresis
PIP2	phosphatidylinositol-4,5-bisphosphate
RFP	Red fluorescent protein
SC5D	Sterol C5 desaturase
SDS	sodium dodecyl sulfate
Shh	Sonic hedgehog
SLOS	Smith Lemli Opitz syndrome
TEV	Tobacco Etch Virus
Y2H	Yeast two-hybrid assay
YSC	Yeast septin complex

Abstract

In English:

Electron microscope (EM) is a strong tool to study the structure of molecules. It can be used to investigate the structure of macromolecules such as filaments or protein complexes in the native environment. Electron microscope can also be used to study the structure of membrane proteins in a lipid bilayer, which resist crystallization. In this work, we used EM to study the structure of septin filaments and the structure of DHCR7, the final enzyme in the cholesterol biosynthesis pathway.

Septins are a family of GTPases that polymerize to form non-polar multimers as the basic unit. These basic units polymerize end-to-end to form filaments, which are present in the budding neck of the budding yeast. Recruitment of septins to the budding neck depends on the initial signal of Cdc42p and two of its effectors namely, Gic1 and 2. Upon bud formation, septins form filamentous arrays that run along the membrane to serve a scaffold for other proteins and also a diffusion barrier. It was previously shown that Gic proteins interact directly with septin. However, the structural features and significance of this interaction is unknown. We used negative staining and cryo-electron tomography to study the septin-Gic1 complex. We showed that Gic1 binds to Cdc10-Cdc10 interface and connects up to six septin filaments to form a very flexible complex. Furthermore, Cdc42p(GDP) disassembled the septin filaments at the Cdc10-Cdc10 interface by binding to the first 29 amino acids of Cdc10. Notwithstanding, Gic1 competes with Cdc42p to bind to Cdc10 but it still binds to Cdc10(30-322). We showed that Cdc42p(GppNHp) bound to Gic1 and at a high concentration, it disassembled the septin-Gic1 complex into short but yet filamentous structures. Furthermore, we studied the effect of GTP on the filaments. GTP replaced the GDP in Cdc11 and caused conformational changes in the NC-interface of Cdc11-Cdc11 to disassemble the septin filaments. Our studies provided a model of how Cdc42p, GTP and Gic1 regulate filament assembly and disassembly *in vitro*.

DHCR7 is the ultimate enzyme in the cholesterol biosynthesis pathway. It reduces C7-8 double bond of 7-dehydrocholesterol by using NADPH to produce cholesterol. The absence of its activity leads to an autosomal syndrome known as Smith-Lemli-Opitz syndrome (SLOS) in human. We purified the DHCR7 from human, *Coxiella burnettii* and *Plesiocystis pacifica* to investigate the structure of function of this enzyme. In this regard, we reconstituted the DHCR7 from *Coxiella burnettii* into a lipid bilayer and obtained a 2D crystal, which we studied using an electron microscope. The obtained crystal was too small to be tilted for data acquisition and requires improvement in future experiments. Furthermore, the function of DHCR7 was studied *in vivo* using ergosterol as a substrate and measured its conversion to brassicasterol using gas chromatography-Mass spectrometry (GC-MS). Our results provided an assay, which can be used to test the functionality of different DHCR7 mutants in primary *dhcr7^{-/-}* cell lines. Besides, localization of DHCR7 was studied in HEK-293 cells and we showed that DHCR7 localized to the Golgi apparatus and not only to the ER.

In German:

Elektronenmikroskopie (EM) ist eine hervorragende Methode um die Struktur von Proteinkomplexen in ihrer nativen Umgebung zu studieren. In dieser Arbeit verwendeten wir zum einen Einzelpartikelelektronenmikroskopie und Elektronentomographie um die Struktur von Septinfilamenten und deren Interaktion mit anderen Proteinen zu untersuchen. Zum anderen züchteten wir zweidimensionale Kristalle der Dehydrocholesterinreduktase DHCR7, um in Zukunft deren Struktur elektronenkristallographisch bestimmen zu können.

Septine gehören zur Familie der GTPasen und bilden große Polymere, deren Untereinheiten aus nicht-polaren Multimeren bestehen. Die Polymere wiederum bilden Filamente, die im Knospungshals von sprossenden Hefen zu finden sind. Die Rekrutierung der Septine zum Knospungshals ist abhängig von dem Signalprotein Cdc42p und zwei seiner Effektoren, Gic1 und Gic2. Die Septinfilamente lagern sich auf der Oberfläche von Membranen an und bilden dadurch zum einen ein Gerüst und zum anderen eine Diffusionsbarriere für Proteine. Obwohl man weiß, dass Gic-Proteine direkt mit Septinen interagieren, sind die strukturellen Gegebenheiten und die Signifikanz dieser Bindung bislang unbekannt.

In dieser Arbeit konnten wir zeigen, dass Gic1 an der Bindungsfläche zwischen den Septinen Cdc10-Cdc10 bindet und dabei bis zu sechs Septin-Filamente zu einem flexiblen Septin-Gic-Komplex verbindet. Die Bindung von Cdc42p(GDP) an die ersten 29 Aminosäuren von Cdc10 induziert die Dissoziation der Septinfilamente. Cdc42p(GppNHp) hingegen interagiert nicht mit Septinen, sondern bindet direkt an Gic1. Interessanterweise führen hohe Konzentrationen von Cdc42p(GppNHp) dabei zu einer Dissoziation des Septin-Gic-Komplexes. Ebenso haben wir den Effekt von GTP auf die Filamente selbst untersucht. GTP ersetzt GDP in Cdc11 und verursacht eine Konformationsänderung an der Bindungsfläche von Cdc11-Cdc11 was zu einer Dissoziation der Septinfilamente führt. Die vorliegende Studie liefert ein Modell für den durch Cdc42p, GTP und Gic1 gesteuerte Auf- und Abbaus von Septinringen während des Zellzyklus.

Die Dehydrocholesterinreduktase DHCR7 reduziert im letzten Schritt der Cholesterin-Biosynthese die C7-C8-Doppelbindung von 7-Dehydrocholesterin unter Verbrauch von NADPH. Eine Fehlfunktion der DHCR7 führt beim Menschen zu dem Smith-Lemli-Opitz Syndrom (SLOS). Eine atomare Struktur der DHCR7, die es bislang nicht gibt, würde die mechanistischen Grundlagen der enzymatischen Funktion des Proteins erklären und Aufschlüsse über dessen Fehlsteuerung im Krankheitsfall geben.

Die vorliegende Arbeit beschäftigte sich deshalb mit der Isolierung, Aufreinigung und zweidimensionalen Kristallisation der menschlichen Dehydrochlosterinreduktase-7 und deren bakteriellen Homologe aus *Coxiella burnettii* und *Plesiocystis pacifica*.

Für DHCR-7 aus *Coxiella burnettii* konnten kleine zweidimensionale gezüchtet werden, die allerdings in Zukunft verbessert werden müssen, um sie elektronenkristallographisch zu analysieren. Um die Funktion der Reduktase *in vivo* zu studieren, wurde die DHCR-7-katalysierte Umwandlung von Ergosterol zu Brassicasterol mit Hilfe von Gaschromatographie gekoppelt mit Massenspektrometrie (GC-MS) quantifiziert. Des Weiteren zeigte eine Lokalisationsstudie in HEK293-Zellen, dass DHCR7 neben dem ER auch im Golgi-Apparat lokalisiert ist.

1) Introduction

1.1) Introduction into septin

1.1.1) Budding yeast as a model to study cell division

Use of a model organism has been a common practice in classical and modern cell biology. Biological models are nonhuman organisms used to study certain aspects of biochemical and cellular pathways from which conclusions can be drawn as how the related pathways function in human cells. Specific model organisms are usually chosen when performing an experiment on humans is either technically unfeasible or unethical. Conservation of the majority of metabolic and signaling pathways through evolution, availability of genomic data and sophisticated experimental tools have made it possible to discover the homologues of many human proteins. Choice of the model depends on the particular biological theme to be studied, ease of maintenance, availability of genomic and proteomic data and also the span of the cell cycle. Usually, *E. coli* is used as a model to study prokaryotic cells while there are a number of different models for eukaryotic cells. *C. elegans*, *Danio rerio* (zebrafish), *Drosophila melanogaster* (fruit fly), *S. pombe* (fission yeast) and *S. cerevisiae* (budding yeast) are the common eukaryotic models, which have provided an invaluable tool to unravel the details of cell division and development (Field and Johnson, 2005).

Saccharomyces cerevisiae originally used in winemaking, bakery and brewery has served as the main model to study eukaryotic cell division. *S. cerevisiae* is a small 5-10 μm long ovoid cell, with a doubling time of 1-2 hours. It has two distinct life cycles in which it exists either as a haploid (vegetative) or a diploid (sporulative) form. In the vegetative cycle, haploid cells divide mitotically through an asymmetric division known as budding, hence also known as budding yeast. Budding usually commences early in the cell cycle and culminates with mitosis when the daughter cell has the same size as the mother cell. Upon mating of two haploid cells, a diploid cell forms, which also divides mitotically. But under stressful conditions, cells enter a sporulative cycle in which they divide meiotically to form four haploid cells that grow again when normal conditions are restored (Herskowitz et al., 1988). The haploid genome of *S. cerevisiae* facilitates functional characterization of genes by taking advantage of modern molecular biology techniques such as gene knockout, recombination and mutational analyses. Moreover, the genome of budding yeast is devoid of extensive non-coding DNA. The simple genomic features and relatively fast doubling time have made budding yeast a suitable organism to study the cell cycle (Botstein et al., 1997).

1.1.2) Genetics of cell division in budding yeast

Cells in order to propagate run a set of coordinated events that ultimately lead to separation of two cells. Upon receiving an external signal, cells become committed to pursue multiple steps up to the final point of cell division. First, cells make sure that they have access to enough external resources to produce materials required for each step of the cell cycle. The first stage of the cell cycle is called G1. In the G1 phase, cells become committed to cell division and pass an irreversible decision called *start point* in lower eukaryotes and *restriction point* in mammals (Csikász-Nagy et al., 2011). During this point, cells monitor the availability of growth hormones and external nutritious materials utilized for internal synthesis of molecules. In the second phase of the cell cycle known as S phase, the genetic content of the cell is duplicated. This phase is probably the most scrutinized step to ensure that DNA has been flawlessly synthesized. In the third phase known as G2, cells undergo multiple checkpoints to monitor if there was an error in DNA duplication. If an error exists, the cycle is halted until errors are corrected (Csikász-Nagy et al., 2011). In the last step, cells disjoin physically and each cell inherits equal genomic and proteomic materials except in cells that undergo asymmetric division such as budding yeast or stem cells where one cell inherits less of the cytoplasm and its contents leading to emergence of two types cells.

Each step of the cell cycle is under tight scrutiny to guard the integrity of genetic material. Proteins responsible to regulate the entry or passage through each step are cyclins and their corresponding cyclin-dependent kinases (Cdk). Budding yeast owns nine cyclins (Cln1, 2 and 3 and Clb1, 2, 3, 4, 5 and 6) and a single Cdk (Cdc28) (Cross et al., 2011). Combination of Cdc28/Cln1, 2 and 3 are involved in passage through the *start point*. Cdc28/Clb5 and 6 control the initiation of DNA replication by phosphorylating proteins that sit on the origin of replication. Cdc28/Clb3 and 4 are active during early mitosis and finally Cdc28/Clb1 and 2 are active at different stages of mitosis. Ultimately, cyclins are destructed and their level drops in the cell, which leads to chromosome separation and passage through the *finish point* (Csikász-Nagy et al., 2011) (Fig. 1.1).

There are two separate regulatory machineries active during two distinct phases of the cell cycle. The first one is a complex of Cdc28/Clb2 and the second is Cdh1/APC with the earlier being active during S-G2-M phases and the later during G1 phase (Cross et al., 2011; Csikász-Nagy et al., 2011). Cdc28/Clb1 and 2 reach the peak of their activity in the late mitosis and can be regulated in different ways. First, the anaphase-promoting complex (APC) with the help of Cdc20 phosphorylates and sets Cdc28/Clb2 for destruction at the end of mitosis and early G1 leading to mitotic exit and commencement of a new cycle. On the other hand, APC together with Cdh1 have an inhibitory relation to Cdc28/Clb2 (Csikász-Nagy et al., 2011). Interestingly, Cdh1 is also phosphorylated and inhibited by Cdc28/Clb2 creating a negative feedback loop between Cdc28/Clb2 and Cdh1. At the beginning of the cycle when the level of APC is low, Clb2 accumulates and phosphorylates Cdh1 (Cross et al., 2011; Csikász-Nagy et al., 2011). But at the end of the mitosis when APC activity is stark, Cdh1 becomes activated and they together inhibit Clb2 and target it for destruction. At the beginning of the cell cycle when the level of Clb2 is low Cln1, 2 and 3

start to accumulate as they are not substrates for APC (Zacharia et al., 1999). Cdc28 together with Cln1, 2 and 3 promote the cell to pass the *start* point by activating transcription factors of Clb molecules. Simultaneously, they phosphorylate and inactivate Cdh1 to allow accumulation of Clb molecules for the next phases. Therefore, cells pass to the S-G2-M phase with high levels of Clb and low levels of Cln cyclins. At the end of the cell cycle, Cdc20/APC degrade the Clb molecules and together with Cdc28/Clb2 activate Cdc14 phosphatase, which reverts the Cdc28/Clb mediated phosphorylation events and thereby reactivates Cdh1 to further inhibit Clb cyclins (Novak et al., 2007; Chen et al., 2004; Zacharia et al., 1999; Csikász-Nagy et al., 2011).

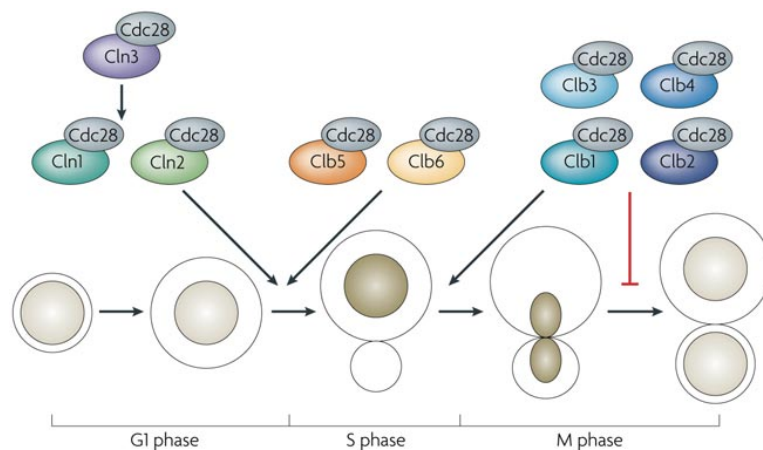


Fig. 1.1. Cyclins and cyclin-dependent kinases in different stages of the cell cycle. Concerted production and targeted degradation of cyclins lead to furtherance of mitosis in budding yeast (taken from Bloom and Cross, 2007). A single Cdk (Cdc28p) is in complex with Cln1, 2 and 3 in G1 but at late G1 and early S phase, Clb5 and 6 replace Cln cyclins. During mitosis, Clb1, 2, 3 and 4 constitute the main body of cyclins in the cell. For details refer to the text.

Another interesting feature of cell division in *S. cerevisiae* is an emergence of a bud as the cell proceeds through the stages of the cell cycle. Late in G1, bud emerges usually next to the bud scar (a landmark left after the previous budding) when cells make the decision to enter the cell cycle. Now, cells require multiple checkpoints to ensure that duplicated chromosomes pass to the daughter cell. The first checkpoint is called morphogenesis checkpoint during which, cells make sure that the bud has successfully formed. At this stage, actins become polarized and form filaments that point towards the bud (Cid et al., 2002). Septins also become localized to the bud neck and form arrays of parallel filaments, which act as a scaffold for assembly of other molecules. Proteins such as Hsl1, Hsl17 and Swe1 localize to the bud side of the septin ring and Hsl1 recruits other proteins to the budding neck to guarantee the

degradation of Swe1 to allow further activation of mitotic kinases. By means of this mechanism, cells ascertain that the bud formation has been successfully achieved (Cid et al., 2002).

The second checkpoint entails monitoring of spindle orientation before cells can proceed to the next stage. Cells have to make sure that both the bud and mother cells receive equal amount of genetic material. Therefore, the spindle pole bodies (SPB) and cytoplasmic microtubules (cMT), which emanate from the SPB, are under continual scrutiny by redundant pathways (Merlini and Piatti, 2011). One pathway, which utilizes Kar9, captures cMTs on the bud cortex. Kar9 is localized to the old SPB and associates with the plus-end microtubule protein Kip2 and orientates the spindle. The second pathway uses dynein to move cMTs along the bud axis. Asymmetric localization of dynein to the bud-side SPB is also vital for cell viability and is achieved by Clb1, 2, Elm1, Gin4 and Hsl1 whose asymmetric localization is guarded by septin (Merlini and Piatti, 2011) (Fig. 1.2).

At this stage, Bub2 interacts with Bfa1 and this binary complex binds to Cdc3 subunit of septin to localize at the bud site of the septin (Kirshnan et al., 2000). These proteins act as a GTPase activating protein (GAP) for Tem1, which is part of the mitotic exit network (MEN) crucial for mitotic exit. Additionally, a protein kinase called Kin4 phosphorylates Bfa1 and keeps it active. Elm1 is a kinase that phosphorylates Kin4 directly and PP2A^{ts1} is a phosphatase that ensures restriction of Kin4 activity in the mother cell (Siller and Dou, 2009). Furthermore, Lte1 a GTPase exchange factor (GEF) of Tem1 is also constrained in the bud cell most likely via the diffusion barrier function of septin to guarantee constant and localized activity of Bub2/Bfa1 on the spindle pole body pulled to the bud cell. Hence, Bub2 and other proteins make sure that the spindle has positioned properly and passed through the bud, which makes a cell committed for advancement to cytokinesis (Adams et al., 2001; Lee et al., 2001; Krishnan et al., 2000). Ultimately, MEN is activated by its major player Cdc5, a polo kinase, which interacts with septin and acts in activating other component of the MEN (Stegmeier et al., 2002; Song et al., 2000). MEN components are not only responsible to initiate the signaling cascade that leads to exit from the cell cycle but also, they are active much earlier during metaphase and directly activate Kar9 (Hotz et al., 2012a and 2012b). By means of concerted action of Lte1 as an activator in the bud cell, Kin4 as an inhibitor in the mother cell and numerous other kinases and phosphatases, cells guarantee the fidelity of cell division.

As mentioned above, septin is one of the many molecules that play a crucial role in establishment of polarity during cell division. Septin localizes to the budding neck by attaching to the underlying membrane to prevent the diffusion of molecules, thereby constricting them to certain compartments. It also serves as a scaffold for other proteins to place them in the proper location in the cell to execute their function. The precise and detailed function of septins is discussed in the following sections.

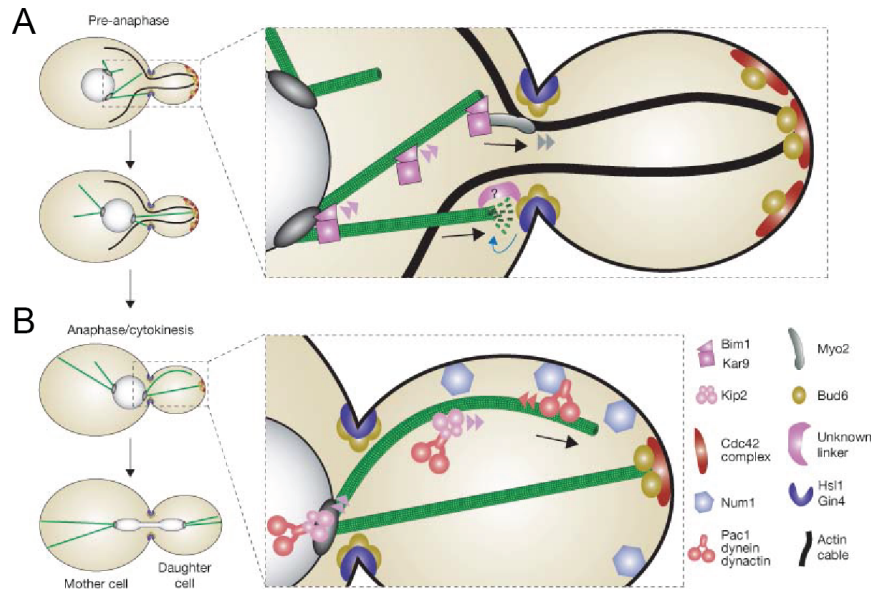


Fig. 1.2. Polarization in budding yeast. (A) Early pathway in which Kar9 interacts with Myo2 and pulls the spindle into the daughter cell. (B) Late pathway in which dynein is transported to the bud cell in a Kip2-dependent pathway. There it is activated and the dynein-dynactin-Num1 complex pulls the spindle into the bud cell (taken from Siller and Dou, 2009).

1.1.3) Septins

Septins were discovered in budding yeast as temperature-sensitive mutations in four genes (*cdc3*, *cdc10*, *cdc11* and *cdc12*). The mutants were defective in fulfillment of cytokinesis that resulted in formation of elongated multinucleated cells, which failed to separate from the mother cells. The execution point of each of these genes were determined to be approximately 0.08 fraction of the cell cycle for *cdc11*, which is in early G1, 0.27 for *cdc3* that occurs during S phase and finally 0.58 for *cdc10* that is concomitant with G2. It was concluded that these genes and therefore bud emergence is not a prerequisite for completion of DNA synthesis and nuclear division but rather they are needed for cell abscission (Hartwell, 1971). The name ‘Septin’ was coined in the laboratory of John Pringle in 1980’s, which reflects their role in septation between mother and daughter cell (Hall and Russell, 2012).

Since their discovery, septins have been extensively studied in yeast and mammalian cells. Septins play various roles in cell division (Kinoshita et al., 2006), actin organization (Kinoshita et al., 2002), microtubule organization (Silverman-Gavrila et al., 2008), cancer (Hall et al., 2012), spermeiogenesis (Tourte et al., 2011), exocytosis (Younghoon et al., 2010) and neuronal spine development (Xie et al., 2007). The detailed biochemistry and function of septins is discussed in the following sections.

1.1.3.1) Genetics of septins

Mining of the available genomic data has broadened the overall knowledge about the genomic organization of septins in different organism. By careful analysis of genomes of various organisms using bioinformatics tools, it was shown that septins exist in all eukaryotes except in plants. However, different organisms have accommodated diversity by means of gene duplication to create numeracy in gene number and structure. *Chlamydomonas* has only one septin gene while *Caenorhabditis elegans* has two (*unc-59* and *unc-61*). The yeast genome encodes seven genes, four of which are expressed continually during its lifespan (*cdc12*, *cdc11*, *cdc10* and *cdc3*) but two are only expressed during sporulation (*Spr3* and *Spr28*) and one during germination (*Shs1*). The *Drosophila* genome encodes five genes (*Sep1*, *Sep2*, *Sep4*, *Sep5* and *Pnut*) and the human genome expresses thirteen different genes and at least 11 pseudogenes. Notwithstanding the observed diversity, all septin genes share certain features. Septins contain a conserved G-domain, which binds to either GTP or GDP. Another conserved feature of all septins is the presence of the N- and C-termini (also known as C-terminal extension) with varying length that provides the basis for classification of septins in different groups (Hall and Russell, 2012; Barral and Kinoshita, 2008).

The C-terminal extension of septins is the most variable domain from which classification of septins stems. There are four general groups of human septins with parallel homologues in yeast. The SEPT2 group is comprised of SEPT1, 2, 4 and 5 all of which have two coiled coil domains in their C-termini. The SEPT6 group members have only one coiled coil and include SEPT6, 8, 10, 11 and 14. SEPT3, 9 and 12 have no coiled coil domains, which are categorized as SEPT3 group. Finally SEPT7 is a single-member group. Some phylogenetic studies classify SEPT13 together with SEPT7 whereas others consider SEPT13 as a pseudogene of SEPT7 (Hall and Russell, 2012). A notable point in septin genomics is the presence of multiple pseudogenes, which have arisen as a result of gene duplication. Moreover some septins have many transcripts and isoforms, which originate from extensive splicing of each transcript. In spite of studies that targeted some isoforms (e.g. *SEPT9_v4*), the majority of isoforms are yet poorly characterized (Hall and Russell, 2012). A detailed profile of septin genes and pseudogenes are listed in table 1.1.

Name	Location	Septin class	Locus type	Known transcripts	Known isoforms
SEPT3	22q13.2	I	Protein coding	6	4
SEPT9	17q25	I	Protein coding	11	5
SEPT12	16p13.3	I	Protein coding	1	1
SEPT6	Xq24	II	Protein coding	8	5
SEPT8	5q31	II	Protein coding	14	10
SEPT10	2q13	II	Protein coding	14	10

SEPT11	4q21	II	Protein coding	16	9
SEPT14	7p11.2	II	Protein coding	2	1
SEPT1	16p11.1	III	Protein coding	1	1
SEPT2	2q37.3	III	Protein coding	48	22
SEPT4	17q23	III	Protein coding	15	7
SEPT5	22q11.2	III	Protein coding	15	8
SEPT7	7p14.2	IV	Protein coding	7	1
SEPT2P1	1p21.1	-	Processed pseudogene	1	0
SEPT7L	10p11.21	-	Duplicated pseudogene	9	1?
SEPT7P1	14q13.2	-	Processed pseudogene	1	0
SEPT7P2 (SEPT13)	7p12.3	-	Duplicated pseudogene	9	0
SEPT7P3	7p14.2	-	Duplicated pseudogene	1	0
SEPT7P4	7q11.21	-	Duplicated pseudogene	1	0
SEPT7P5	7q11.21	-	Duplicated pseudogene	1	0
SEPT7P6	7q36.1	-	Processed pseudogene	1	0
SEPT7P7	9q22.33	-	Processed pseudogene	1	0
SEPT7P8	19q13.42	-	Processed pseudogene	1	0
SEPT10P1	8q12.1	-	Processed pseudogene	1	0

Table 1.1: Current knowledge about septin genomics (taken from Hall and Russell, 2012).

Alternative splicing is a molecular way to create diversity. In this way, many transcripts of any given gene can be made, which have specific characteristics. Some transcripts can differ in their untranslated regions playing a regulatory function and some can produce different proteins. One of the best-characterized septin splice variants is *SEPT9_v4*. This gene has two distinct transcripts, namely *SEPT9_v4* and *SEPT9_v4**, which differ in the 5' UTR and the first exon. *SEPT9_v4* is widely expressed in all tissues of an adult under normal conditions while in hypoxia, cap-dependent translation is halted and thus *SEPT9_v4** is translated (Kostic and Shaw, 2000). One of the main genes, which are activated as a result of hypoxia and response to DNA damage, is p53. The p53-binding sites have been identified upstream of the first exon of *SEPT9_v4** while these sites are infrequent in other isoforms of SEPT9. In this manner, the cell guarantees the expression of SEPT9 under normal and stress conditions by creating different splice variants (Hall and Russell, 2012).

Complete knowledge of septin transcriptomics necessitates comprehensive studies to investigate the expression and localization of each septin transcript and isoform in different tissues in health and disease. A few studies targeted the expression pattern of a certain septin gene using a low-resolution microarray technique (Yagi et al., 1998, Zieger et al., 2000 and Bartsch et al., 2010). However, lack of suitable probes directed against septin genes and their transcripts, complexity of septin expression pattern in health and disease states and ultimately poor understanding of septin function have limited uncovering all the expressed transcripts (Hall and Russell, 2012).

Complexity of septins is not only restricted at the genomics level. Septins can adopt different localization and function. In budding yeast, septins are associated with actin filaments and act as a diffusion barrier (Barral and Kinoshita, 2008 and Hu et al., 2010). They are present in cellular projections such as primary cilium (Tada et al., 2007), in neuronal spikes to assist in dendrite formation (Xie et al., 2007 and Cho et al., 2011) and they are also involved in spermatogenesis (Ihara et al., 2005). It is noteworthy that not all septin isoforms form filaments. *SEPT9_i1* has a nuclear localization signal that enters the nucleus to modulate the HIF1a-mediated gene expression (Amir et al., 2006). Therefore, the complexity and numeracy of transcripts compels detailed functional studies to unravel roles of different septin genes in miscellaneous cellular mechanisms. The catalogue of septin genomics and transcriptomics remains still sketchy and hinges on insightful characterization of septins in different tissues.

1.1.3.2) Structure of septin

Septins belong to a superfamily of P-loop GTPases characterized by the Ras superfamily, OBG/HflX superfamily and translocation factors. These proteins are recognized by an α - β - α core structure and a nucleotide binding domain. Sequence alignment shows that septins have a high degree of homology to Ras proteins and share the same structural features (Leipe et al., 2002). In the classification, paraseptins, which exist in bacteria and include Toc34, are the closest proteins to septins in the phylogenetic tree (Fig. 1.3). This suggests a lateral transfer of genes from bacterial ancestors to eukaryotes during the course of evolution (Barral and Mansuy, 2007 and Weirich et al., 2008).

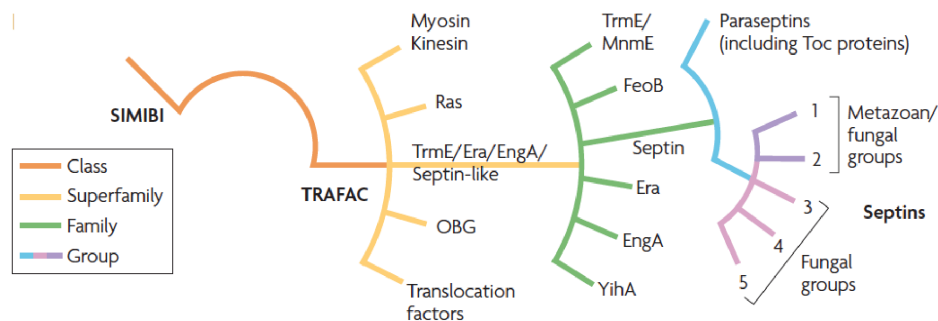


Fig. 1.3. Phylogenetic study of septins. A schematic representation of the phylogenetic tree of P-loop NTPases (taken from Weirich et al., 2008).

Septins are organized in five discrete domains: a variable N-terminus, which can have different lengths, a polybasic region, which is responsible for binding to membrane, a septin-specific sequence in the N-terminus, a G domain that binds to nucleotides and a coiled coil at the C-terminus, which can have variable lengths or even be non-existent (Weirich et al., 2008).

The crystal structure of the human septin revealed many structural details and their organization into polymers (Sirajuddin et al., 2007 and Sirajuddin et al., 2009). The human SEPT2 was crystallized in its GDP and GppNHP bound states alone and also with SEPT6 and SEPT7. The SEPT2 eluted as a monomer and a dimer during gel filtration analysis but crystallized in its dimeric form (Sirajuddin et al., 2007). The structure of SEPT2 resembled the canonical G domain exemplified by the Ras protein. The Ras proteins have six β -strands and five α -helices but SEPT2 has additional features including an α -helix at the N-terminus, named α_0 (to maintain the G domain nomenclature), α_5 between α_4 and β_6 , two additional anti-parallel β -strands named β_7 and β_8 , and another α helix at the C-terminus called α_6 tilted by 90° from the G domain (Sirajuddin et al., 2007) (Fig. 1.4). The SEPT2 in the dimeric structure face each other on their nucleotide binding pockets making an interface called the G-interface. However, dimers in the crystal associated with each other via the N- and C-termini of the proteins to give rise to another interface called the NC-interface (Sirajuddin et al., 2007).

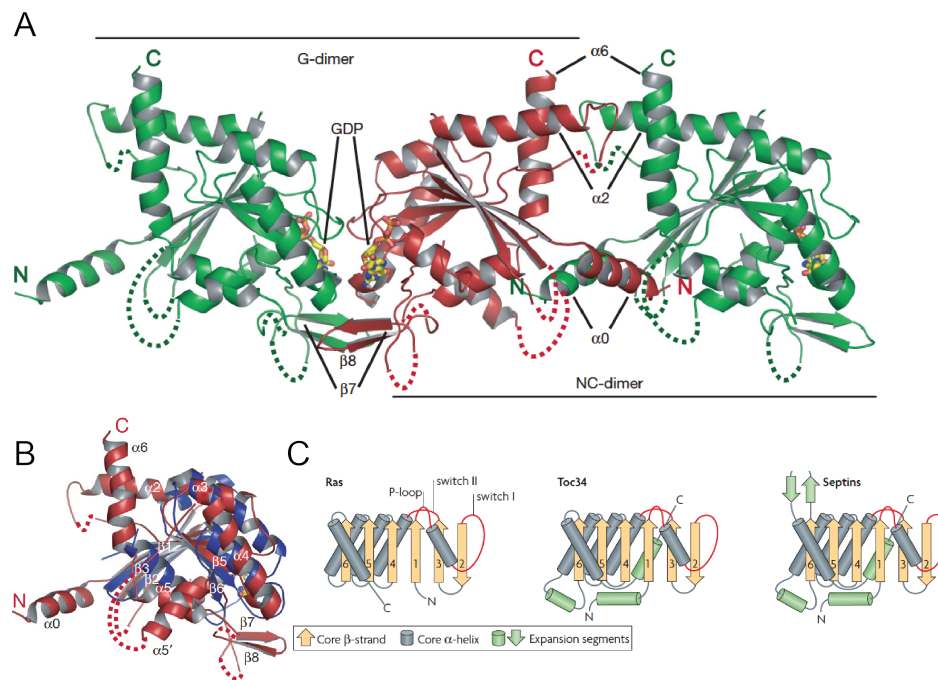


Fig. 1.4. Crystal structure of the human SEPT2 in the GDP bound state. (A) Protein eluted as a dimer during gel filtration and existed as a filament in the crystal structure, which gave rise to two different interfaces namely, G- and NC-interface. **(B)** Superimposition of

SEPT2(GDP) and Ras(GppNHP) (taken from Sirajuddin et al., 2007). **(C)** Comparison of the structures of Ras, septin and Toc34 (taken from Weirich et al., 2008).

The structure shown above (Fig. 1.4) corresponds to septin in its GDP bound state. The crystal structure of the SEPT2 in its GppNHP bound state manifested the conformational changes conferred to the protein upon binding to a tri-phosphate guanosine nucleotide (Sirajuddin et al., 2009). Likewise the previous structure, SEPT2(GppNHP) dimerized via its G-interface but existed as a dimer in the crystal. However, the GppNHP-interface had a much larger buried surface than the GDP-interface implying tighter packing

upon binding to GppNHp. In contrast to the previous structure, an extra $\beta 9$ is observed between $\beta 7$, $\beta 8$ and $\alpha 5$ that is due to the higher resolution of the crystal structure (2.9 Å versus 3.4 Å) (Sirajuddin et al., 2009). Superimposition of the two structures showed dramatic movements of β -strands while α -strands remained unchanged. The beta strands $\beta 2$ and $\beta 3$ were tilted roughly 20° compared to the GDP-bound structure (Sirajuddin et al., 2009). These two strands are in the vicinity of switch regions and $\beta 2$ should remain hydrogen-bonded to $\beta 3$. Therefore upon binding to GppNHp, the N-terminal part of the $\beta 2$ -strand moves and clashes with $\alpha 0$, which leads to conformational changes on the N-terminus of the protein (Fig. 1.5). The GppNHp bound SEPT2 remained as dimer in the crystal while the GDP bound state polymerized to form filaments in the crystal. This observation hints on a possibly significant and unknown function of the nucleotides in septin polymerization (Sirajuddin et al., 2009).

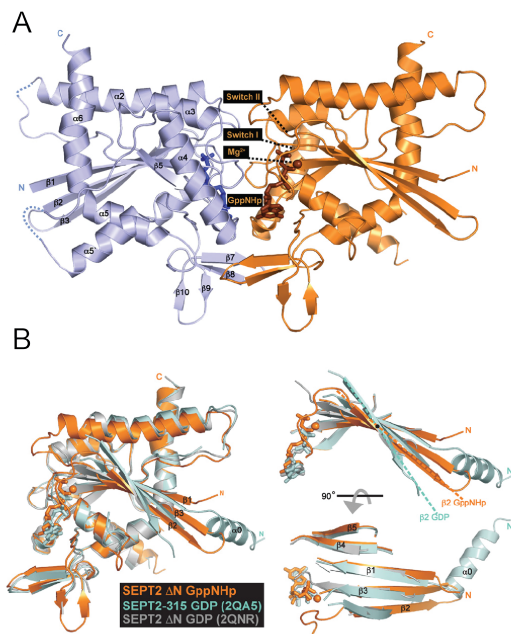


Fig. 1.5. Crystal structure of SEPT2 bound to GppNHp . (A) Crystal structure of dimeric SEPT2 with GppNHp. (B) Superimposition of the GDP and GppNHp-bound SEPT2 structures. SEPT2 Δ N (GppNHp) (33-306) (PDB ID 3FTQ), SEPT2-315 (GDP) (PDB ID 2QA5) and SEPT2 Δ N (GDP) (PDB ID 2QNR), are shown in gold, cyan and grey respectively. Upon binding to GppNHp, the N-terminus of the protein is tilted which alters the NC-interface (taken from Sirajuddin et al., 2009).

The binding of a pair of SEPT2(GDP) is mediated via interaction of Phe 156 in both subunits of the dimer and also interaction of His 270 with Trp 260. Whereas, in the GppNHp bound structure, Asp 107 of the switch II region interacts with His 158 of the other subunit, which is in turn stabilized by Glu 202 (Sirajuddin et al., 2009). The Yeast Septin Complex (YSC) has a high homology with the human septin. His 158 is present in Cdc12, Cdc11 and Cdc3 but absent in Cdc10 and its mutation causes temperature-sensitivity only in Cdc3 (Sirajuddin et al., 2009). Moreover, in the crystal structure of the SEPT7(GDP), residues other than those involved in SEPT2-SEPT2 interaction were also noticed (Zent et al., 2011).

The hexameric human septin complex consisting of SEPT2, SEPT6 and SEPT7 was also crystallized at 4 Å resolution (Sirajuddin et al., 2007) (Fig. 1.6A). The structure depicted a two-fold rotational symmetry that formed a nonpolar hexamer. A dimer of SEPT2 occupied the central position but unlike the crystal structure of the SEPT2 dimer, they bound via their NC-interface. A pair of SEPT6 interacted with SEPT2

on both sides via the G-interface and SEPT7 occupied the terminal position. The filament formation in the SEPT2-6-7 complex is mediated via the G-interface of SEPT7, which leads to formation of circular filaments and bundles (Fig. 1.6B) (Sirajuddin et al., 2007; Kinoshita et al., 2002). However, it was also shown that another septin subunit, SEPT9 could bind to SEPT7 to serve as the terminal subunits. Different isoforms of SEPT9 with specific structural characteristics could modulate the size of the disk-shaped filaments *in vivo* suggesting a possible role for SEPT9 to control and alter filament properties (Kim et al., 2011; Sellin et al., 2012). Of significance, only the larger isoform of SEPT9 (*SEPT9_i1-3*) incorporates into larger assemblies and the truncated isoform (*SEPT9_i4*) can displace the larger SEPT9 from the filaments (Sellin et al., 2011; Chacko et al., 2005).

SEPT7 can form a complex with SEPT2 and SEPT6 in fibroblast (Joberty et al., 2001) or alternatively with SEPT5 and SEPT11, SEPT9b and SEPT11 or SEPT5 and SEPT3 in neurons (Xie et al., 2007; Nagata et al., 2004; Fujishima et al., 2007). Yeast two-hybrid and three-hybrid assays have strengthened the previously believed opinion that members of the SEPT6 can bridge between members of the SEPT2 and SEPT7. Besides, members of the SEPT3 were shown to form a complex with SEPT6 and SEPT7 group members. However, no interactions of SEPT9 with SEPT2 could be detected due to the drawback of the three-hybrid system that can detect only a limited number of possible interactions (Sandrock et al., 2011).

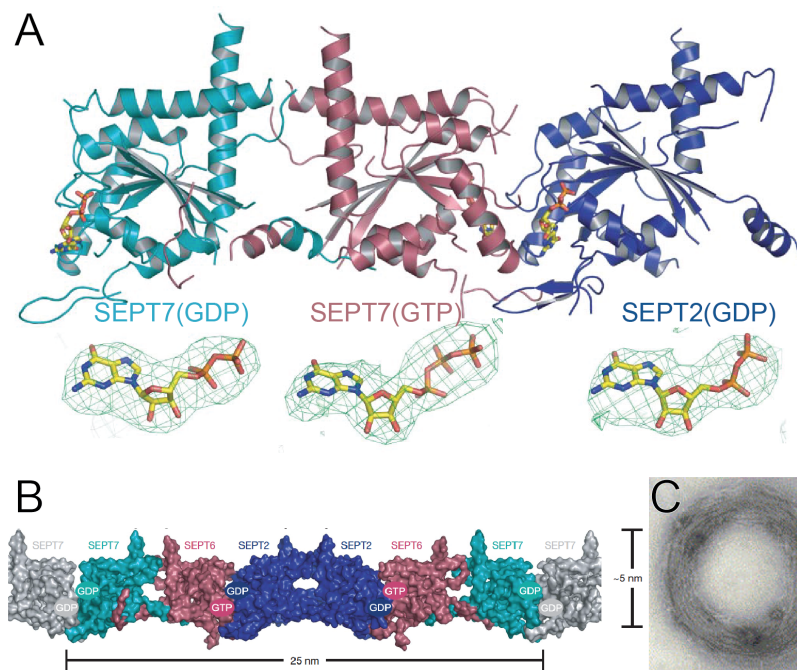


Fig. 1.6. The crystal structure of SEPT2-6-7 complex and their corresponding filamentous structure. (A) Ribbon model of the crystal structure of SEPT2-6-7 and $F_o - F_c$ electron density map around their nucleotide binding pockets. **(B)** Surface representation of the human septin complex of SEPT2-6-7 crystal structure at 4Å (taken from Sirajuddin et al., 2007). **(C)** An electron microscope (EM) image of septin filaments

composed of SEPT2-6-7 that form circular bundles (taken from Kinoshita et al., 2002).

Surprisingly, the C-termini of septin subunits in the crystal structure had no electron density although there was enough space between pairs of filaments. Single particle analysis was also performed on a negatively stained sample of the hexameric human septin sample (Sirajuddin et al., 2007). The class averages also showed no clear density corresponding to the C-terminal extensions of the subunits. In another study, the native septin complex was purified from the rat brain, which consisted of SEPT3, SEPT5 and SEPT7. The structure of the hexameric complex was reconstructed from cryo-EM images at a final resolution of 27 Å (Lukoyanova et al., 2008). It revealed a hexameric 27-nm long asymmetrical filament. Both in the class averages and in the final 3D reconstruction, no obvious electron density was observed for the C-termini of septin subunits. The most reasonable explanation could be that the coiled coil regions at the C-termini of subunits are highly flexible and thus they are lost during averaging. However, it was shown that the C-terminal extensions play a vital role in stability and interaction of septin subunits (De Almeida Marques et al., 2011). The C-termini of SEPT7 and SEPT6 interacted strongly with a K_D of 15.8 nM that contributes to stabilization of the NC-interface between SEPT6 and SEPT7. Moreover, the C-termini of SEPT2 homodimerized with a K_D of 4 μM. This rather weaker interaction also contributes to the stability of the NC-interface between a pair of SEPT2 in the hexamer (De Almeida Marques et al., 2011). Parallel evidence suggested that the C-termini of Cdc3 and Cdc12 of the yeast septin complex bound each other and assisted in binding to their counterparts from another filament (Bertin et al., 2008). Therefore, it seems that the coiled coil domain of septins functions in maintenance and stability of subunit interaction and filament bundling.

The yeast septin complex of *Saccharomyces cerevisiae* is the best structurally and biochemically characterized septin complex. Five different subunits are expressed during mitosis. The most prominent complex consists of four subunits namely, Cdc12, Cdc11, Cdc10 and Cdc3 arranged as a dimer of heterotetramer with a two-fold rotational symmetry (Bertin et al., 2008). Cdc10 dimerizes to serve as the central hinge of the octamer similar to SEPT2 in the human hexameric complex. But in contrast to SEPT2, Cdc10 is devoid of any coiled coil domains. As mentioned before, in the human octameric septin complex, SEPT9 has no coiled coil and serves as the terminal subunit. On the contrary, in the yeast complex, Cdc10 is the central subunit. The evolutionary significance of this discrepancy is unknown. Cdc3 interacts with Cdc10 via the G-interface and Cdc12 interacting with Cdc3 and Cdc11 resides at the terminal position (Bertin et al., 2008). The yeast septin complex exists as an octamer in a buffer with high ionic content and filament polymerization is initiated at a low salt condition (less than 150 mM NaCl), which facilitates the interaction of a pair of Cdc11 via their NC-interface. The $\alpha 0$ of Cdc11 also plays a significant role in mediating the Cdc11-Cdc11 interaction (Bertin et al., 2008). As mentioned earlier, C-terminal extensions of Cdc3 and Cdc12 bind each other to probably strengthen the NC-interface between them and they subsequently mingle with another pair from the neighboring filament to aid in filament-filament interaction and bundling while the C-terminal extension of Cdc11 is dispensable for filament bundling (Bertin et al., 2008) (Fig. 1.7). Besides, the interaction of coiled coil domains of Cdc3 and

Cdc12 also strengthens the Cdc12-Cdc11 interaction as a result of conformational change in Cdc12 (Bertin et al., 2010). Therefore, a pair of Cdc3-Cdc12 in each octamer serves as a linchpin and functions in filament formation and stability.

In vivo, temperature-sensitive mutations in Cdc3 and Cdc12 are lethal while *cdc10Δ* or *cdc11Δ* cells are viable with more pronounced effects in *cdc11Δ* cells (Frazier et al., 1998). The neck filaments were absent in *cdc10Δ* and *cdc11Δ* cells although septin localized to the neck in *cdc10Δ* cells and retained its function partly at least in localizing Bud4, a protein required to specify bud emergence in budding yeast. This observation suggested that localization of septin is more critical for functionality of septin (Frazier et al., 1998). Yet, it should be noted that interaction partners of Cdc10 that were not examined in that study, might fail to localize to the budding neck to exert their function and localization of Bud4 cannot merely explain the functionality of septin (Frazier et al., 1998). The septin complex purified from *cdc10Δ* and *cdc11Δ* cells failed to polymerize into long filaments at low salt conditions but at high salt, they showed to have undergone slight polymerization to form filaments of ≤ 32 nm (Frazier et al., 1998). However, *in vitro* Cdc10Δ or Cdc11Δ hexamers did not polymerize into filaments under conventional conditions but presence of phosphatidylinositol-4,5-bisphosphate (PIP2) and excess of GTP promoted filament formation (Bertin et al., 2010). Furthermore, septin octamers formed parallel arrays of filaments on PIP2-containing membrane that were connected orthogonally with tiny rods of 36.7 ± 7 nm long and 36.5 ± 5 nm apart to form mesh-like structures (Bertin et al., 2010). The basic amino acids that reside in $\alpha 0$ of Cdc10 play a pivotal role in associating with PIP2-containing membranes and deletion of this motif eliminates binding to PIP2-membranes. Mutations in $\alpha 0$ (K29A, K28A, R25A and H24A) of other subunits of the septin complex reduced the ability of septin to bind to membranes only under condition that normally did not allow filament formation in solution and barely affected the association of septin filaments with the membrane (Bertin et al., 2010). Septin filaments from brain extract also embraced PIP2-containing liposomes and triggered the tubulation of the membrane. Upon binding of septin filaments to the surface of the membrane, they lied in pairs and initiated transformation of membrane into rigid tubules (Tanaka-Takiguchi et al., 2009). However, the possibility that the purified septin was contaminated with other membrane-binding proteins was not ruled out in this study. In fact, PIP2 has broader roles than just organizing septin filaments. Particularly, other proteins involved in septin ring formation and regulation interact with PIP2 as well. Cdc42p, Gic proteins (two of the effectors of Cdc42p), which are involved in early recruitment of septin to the budding neck and Cla4p, a kinase necessary for septin assembly, all interact with PIP2 (Orlando et al., 2008; Bertin et al., 2010).

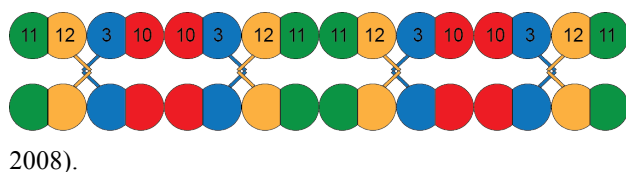


Fig. 1.7. Pairing of the yeast septin filaments.

Filaments associate via the interaction between C-terminal extensions of Cdc3 and Cdc12 (Bertin et al., 2008).

Budding yeast expresses five septins during mitosis, four of which are essential and one is nonessential. The fifth septin encoded by *SHS1* gene been shown to be redundant during mitosis since *shs1Δ* cells are viable (Mino et al., 1998). However mutation in both *cdc10* and *shs1* causes temperature-sensitive lethality (Iwase et al., 2007). Shs1 was shown to replace Cdc11 in the octameric structure to form a novel octamer that polymerizes end-to-end to form circular filaments *in vitro* (Garcia 3rd et al., 2011). Phosphomimetic mutants of Shs1 were shown to have drastic conformational changes ranging from formation of a mesh-like structure to inability to form filaments (Fig. 1.8). It is noteworthy that Shs1 undergoes tremendous phosphorylation among all other septin subunits (Egelhofer et al., 2008). Phosphorylated Shs1 was also shown to exchange and bind nucleotide much faster when compared to unphosphorylated Shs1 and other septin subunits (Vrabioiu et al., 2004). It is possible that Shs1 can turn over GTP much faster than other septin subunits and this activity is enhanced by phosphorylation (Vrabioiu et al., 2004). However, the significance of such interpretation and how nucleotide hydrolysis can influence the septin architecture has not been investigated *in vivo*.

Shs1 possesses unique structural features that distinguish it from other septins. It possesses an extra 31 amino acid insert in the G-domain and a 45-amino acid insert in the C-terminal extension. These extra features might enable Shs1 to adopt different conformations under various conditions yet still holding a great homology to other septins. Besides, other nonessential proteins such as Spa2, Myo1 and Nis1, which are implicated in establishing cell polarity, bind to Shs1 (Iwase et al., 2007; Mino et al., 1998).

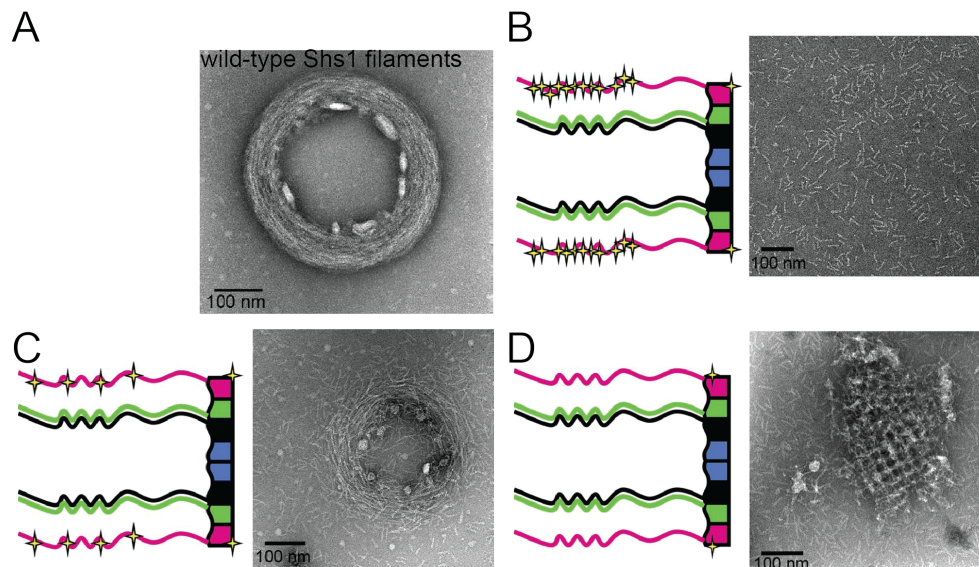


Fig. 1.8. Shs1p-containing septin filaments. (A) A filament, which consists of Shs1, Cdc12, Cdc3 and Cdc10. Phosphomimetic mutations of (B) Shs1 (T6D, T386D, S416D, S441D, and S447D), (C) Shs1 (T6D, T386D, S416D, S441D, S447D, S460D, T462D, S519D, S520D, S521D, S522D, S525D, and S545D) and (D) Shs1 (S259D) cause drastic structural changes (taken from Garcia 3rd et al., 2011).

1.1.3.3) Biochemistry of septin as a GTPase

Despite the structural characterization of the septins and their bound nucleotides, the nature of nucleotide hydrolysis and its effect on the integrity of filaments lags behind. In fact, a few hypotheses have been proposed with respect to the function of nucleotides. One model suggests that nucleotides play a structural role as in α -tubulins. The second model proposes a constant binding and hydrolysis of nucleotides, which ultimately regulates assembly and disassembly of septin filaments like β -tubulins. The last model provides evidence that GTP binding and hydrolysis mediates binding of septin to other proteins. None of these models provide sufficient evidence to generalize a function for nucleotide binding or hydrolysis (Mitchison and Field, 2002).

Canonical GTPases constitute a few domains that make contact with the nucleotide and some amino acids that assist in nucleotide hydrolysis. The first domain is the P-loop with the consensus sequence GXXXXGK(S/T) that surrounds the bound nucleotide in which lysine makes contact with the phosphate group and serine/threonine coordinates Mg^{2+} (Vetter and Wittinghofer, 2001). In septin, an invariant threonine (T52) also contacts the α -phosphate. The second domain is G3 (switch II) with the consensus sequence DXXG. Aspartate of switch II also coordinates Mg^{2+} and glycine interacts with γ -phosphate (Vetter and Wittinghofer, 2001). Another domain is G4 (KXD) that recognizes the base of nucleotide and confers specificity for guanosine. Threonine (T78) of the switch I and glycine (G104) of the switch II of septins also mediate the universal switch mechanism (Sirajuddin et al., 2009). In the crystal structure of the SEPT2, serine (S46) of the P-loop hydrogen bonds with the γ -phosphate and acts in polarizing the attacking water. Arginine (R77) does not bind directly to γ -phosphate but could act as an arginine finger (Sirajuddin et al., 2009). Mutational analyses of human SEPT2 revealed that R77 and S46 played no role in GTP hydrolysis whereas mutation of T78 drastically diminished nucleotide hydrolysis, which suggests its prominent role in hydrolysis of GTP (Sirajuddin et al., 2009). Cdc3 and Cdc11 of the yeast septin complex do not possess an amino acid corresponding to T78 and therefore do not hydrolyze GTP (Fig. 1.9). As mentioned in the previous section, histidine (H158) and aspartate (D104) interact to stabilize the G-interface in the GppNHp-bound SEPT2 dimer and mutation of the corresponding H158 only in Cdc3 caused temperature-sensitivity as it makes a G-interface with Cdc10 (Sirajuddin et al., 2009). Together these data suggest that only Cdc10 and Cdc12 of the yeast septin complex have GTPase activity and Cdc3 is the only subunit, which remains GTP bound (Sirajuddin et al., 2009).

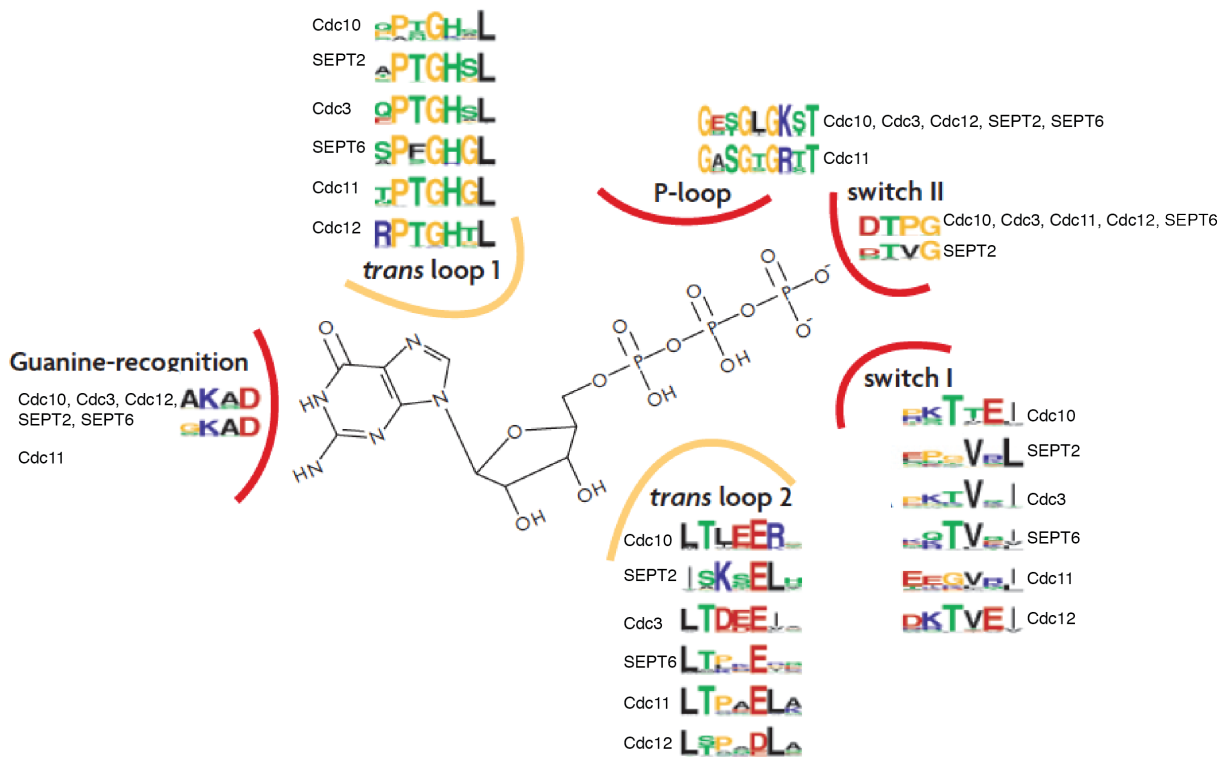


Fig. 1.9. Nucleotide-interacting motifs of human and yeast septins. G4 or guanine-recognition motif confers specificity to guanosine. P-loop contacts phosphate group and coordinates Mg^{2+} . Switch II (G3) contacts γ -phosphate and coordinates Mg^{2+} . The conserved threonine (T78) in switch I is responsible for GTP hydrolysis, which is absent in Cdc3, Cdc11 and SEPT6 group (taken from Weirich et al., 2008).

A comprehensive mutational analysis of the P-loop, G3 and G4 domains in the yeast septin complex showed that all septin subunits could bind to GTP (Nagarj et al., 2008). Furthermore, nucleotide binding was shown to be required for proper function and localization of septins to the cortex. The only other mutants that shared the same phenotype include *cdc24Δ*, *cdc42Δ* and *gic1Δgic2Δ* cells (Iwase et al., 2007). It was also shown that mutations in the P-loop or G4 domain abrogate septin-septin interaction and localization but G3 mutants behaved normally (Nagarj et al., 2008). This points to the previous indication that nucleotides play a structural role rather than a regulatory and nucleotide hydrolysis is not required for septin-septin interaction ruling out the model of β -tubulins filament for assembly and disassembly. Moreover, septins assemble *in vitro* to form stable filaments without the need for nucleotides (Bertin et al., 2008).

Purified *XI*SEPT2 from *Xenopus* was shown to bind and hydrolyze GTP *in vitro* and this hydrolysis assisted in filament formation (Mendoza et al., 2002). The authors showed that addition of GTP but not GDP or ATP led to a very slow binding to the protein, which indicates a possible misfolding of the

bacterially expressed *XI*SEPT2 (Mitchison and Field, 2002). Therefore, it can be concluded that GTP was not the primary cause of filament formation but rather enabled proper protein folding, which then formed a filament *in vitro*. It should be noted that septin filaments usually consist of multiple subunits with a bound nucleotide, which complicates the decipherment of nucleotide's role in filament formation. Nevertheless, the yeast septin complex and the human septin complex form stable filaments independent of nucleotides *in vitro* (Bertin et al., 2008; Kinoshita et al., 2002).

As mentioned earlier, one model suggested a constant binding and hydrolysis of GTP by septin subunits is required for the assembly and function of filaments (Mitchison and Field, 2002). However, it was shown that septins do not turn over GTP in a cell cycle using ¹⁵N-dilution assay. *In vitro*, the binding and exchange of nucleotides were shown to be slow, which is comparable to previous data indicating a very slow GTPase activity of *Drosophila* septins compared to the Ras protein (Vrabioiu et al., 2004; Field et al., 1996; Sprang et al., 1997). The nucleotide exchange rate is the rate-limiting step in septin's GTPase activity. However, it could not be determined by means of biochemical experiments if all septin subunits have the same exchange rate or some bind and hydrolyze nucleotide faster (Vrabioiu et al., 2004). But, the dominant rate of GTP binding is very slow compared to other small GTPases. Moreover, in switch II region of Ras protein superfamily, a glutamine after glycine assists in orientating the water to hydrolyze GTP, which is absent in septin (Vetter and Wittinghofer, 2001).

These data illustrate that nucleotide binding is crucial to maintain structural integrity and functionality of septins whereas GTP hydrolysis of if not all, at least some septins is very slow compared to canonical small GTPases. Thus, the model derived from these studies agrees with the model for α -tubulin for which GTP binding is an absolute structural requirement (Mitchison and Field, 2002). However, it is noteworthy that no conclusive studies have aimed at understanding the function of nucleotides on filaments and how they modify the preassembled filaments.

1.1.3.4) Functions of septin

Unique structural properties of septins including the potential to assemble into filaments, a slow but possibly significant GTPase activity and capability to bind to membrane has made septins appear in many cellular compartments and play a significant role in different processes. Emergence of septins at places in which compartmentalization is demanded and their association with other cytoskeletal proteins have suggested novel and general functions for septins as scaffold and diffusion barrier. Recent studies in budding yeast and also in metazoans have provided a plethora of evidence as how septin can serve these functions. These function and their relevance to diseases is briefly discussed below.

1.1.3.4.1) Diffusion barrier in yeast

Establishment of polarity and asymmetric division of materials between mother and daughter cells have been extensively studied in budding yeast where septin was first discovered. Budding yeast undergoes a closed mitosis during which nuclear membranes remain intact but the genetic material is split between the two cells (Caudron and Barral, 2009). Several lines of evidence point to the existence of a diffusion barrier at different levels, which gives rise to asymmetry. At late G1, a septin ring forms at the budding neck, which interacts with multiple proteins to establish asymmetry. For instance, Cdc5, Elm1, Kin4 and PP2A^{rs1} are among the proteins with different localization and activity in daughter and mother cells, which is attributed to the scaffold and barrier functions of septin (detailed in 1.2) (McMurray and Thorner, 2009b). Moreover, small GTPases including Cdc42p have different localization as well. Cdc42p marks the location where the bud forms and it recruits many proteins to the bud site and therefore creates a molecular gradient in the cell. After bud formation, Cdc42p remains localized in the bud and its back-diffusion into the mother cell is prohibited by septin (Orlando et al., 2011). Moreover, septins can associate with membrane and play a role in membrane and membrane protein segregation. During budding, intracellular membranes including endoplasmic reticulum (ER) are passed to daughter cells along with chromosomes. However, its membrane proteins do not diffuse freely. HMG-CoA reductase (Hmg1p), Sec61 and Sec22 have been shown to be confined in the mother ER in a septin-dependent fashion (Caudron and Barral, 2009).

Aging in yeast is defined by accumulation of extrachromosomal ribosomal DNA circles (ERC) and carbonylated and aggregated proteins in the mother cell. ERCs replicate autonomously along with chromosomes as the cell goes through successive rounds of cell cycle (Caudron and Barral, 2009). ERCs are devoid of centrosomes and therefore do not segregate with chromosomes. Instead, they associate with nuclear pores of the mother cell, which are prevented from diffusing into the bud. Therefore, the septin barrier limits the movement of proteins in the outer nuclear envelope with which ERC associates. In this way, septins ascertain progression of the cell cycle and couple it to aging in budding yeast (Caudron and Barral, 2009).

1.1.3.4.2) Septin in ciliogenesis

The diffusion barrier function of septins in mammalian systems has been highlighted in ciliogenesis, too. Cilia are cellular projections involved in generating movement and sensing signals such as odor and light (Saarikangas et al., 2011). The basic structure of cilia is composed of an axoneme with 9+0 cylindrically arranged microtubules. Although the membrane of cilia is connected to the plasma membrane but a ring of septin present at the base of cilia creates a separate membrane-associated compartment and thereby constraining the movement of membrane proteins within cilia membrane such as components of hedgehog signaling pathway. Septins have been implicated in transport of Golgi vesicles in epithelial

cells (Spiliotis et al., 2008; Kim et al., 2010). Depletion of SEPT2 in mammalian systems resulted in reduced number of cilia by decreasing the vesicle transport and membrane deposition required for ciliogenesis (Saarikangas et al., 2011).

1.1.3.4.3) Septin in nervous system

Multiple cytoskeletal proteins are crucial for functionality and viability of neuronal cells. Dendritic spines are projections that exist on the surface of dendrites involved in processing and storage of information (Saarikangas et al., 2011). Each spine works independently of other spines suggesting membranous and proteinous insulation. Septins especially SEPT7 has been shown to form a ring-like structure at the base of spine and it is an essential factor in spine formation. This observation suggests an analogous function to that of septin in cilia (Cho et al., 2011). Moreover, septins have been implicated in atrophy of Parkinson's disease (discussed in 1.3.4.7). These cumulative evidences imply several roles for septin in the nervous system (Saarikangas et al., 2011).

1.1.3.4.4) Septin in cellular movement

Two distinct properties of septins make them a suitable candidate to be involved in maintenance of membrane rigidity and therefore cell motility. First, septins bind to PIP2 and anchor themselves to the membrane surface and second they interact indirectly with actin. Cell movement requires a forward movement, which depends on actin-driven motility force and retraction in the rear. The molecular machineries involved in the front and the rear are kept apart by means of molecules that confer cell polarity (Saarikangas et al., 2011). For instance, PIP2 is enriched in the rear where septin can bind and provide a scaffold or diffusion barrier to create cell polarity. T-cells, which possess an ability to migrate in an amoeboid-like manner, encode SEPT2, 4, 6, 7, 8, 9 and 11. Knockdown experiments showed that reduction of SEPT7 level induces membrane blebbing, an amoeboid type of cell movement used by leukocyte and cancer cell (Kim et al., 2010). Besides, knockdown of SEPT2 and 11 in HeLa cells caused reduced cortical elasticity (Mostowy et al. 2011). Furthermore, colocalization of septin with actin has suggested a possible role for septin in cell motility. Several lines of evidence show that septin associates via anillin or NM2 with contractile actomyosin in non-muscle cells and focal adhesion to serve as a scaffold for ROCK and CRK binding required for myosin phosphorylation (Joo et al., 2007; Kinoshita et al., 2002; Bowen et al., 2011).

1.1.3.4.5) Septins in vesicle trafficking

Human SEPT4 and the yeast Cdc10 possess a polybasic element in their N-termini that enables them to interact with phosphatidylinositol (Zhang et al., 1999; Bertin et al., 2010). It is speculated that septins might function in vesicle transport machinery in the cell. The rat brain sec6/8 complex coprecipitated with septin filaments containing SEPT7 (Hsu et al., 1998) and SEPT5 with syntaxin-1, a t-SNARE component (Beites et al., 1999). The underlying mechanism by which septin mediates membrane fusion is mediated via modulation of membrane properties such as rigidifying or bending (Caudron and Barral, 2009).

1.1.3.4.6) Septins and other cytoskeletal proteins

Primarily, the cortical capture of microtubule was shown to depend on Cdc12 of the yeast septin complex (Kusch et al., 2002). Besides, microtubules affinity regulated kinases including Hsl1 and Gin4 were shown to localize in a septin-dependent manner and even Gin4 regulated septin ring formation (Gladfelter et al., 2004). In mammalian cells, SEPT2, 3, 6, 7, 9 and 11 were shown to co-precipitate with microtubules (Sakamoto et al., 2008). The polybasic sequence present at the N-terminus of septin probably contributes to the interaction with microtubules especially in the case of polyglutamated microtubules (Spiliotis, 2010). Recent studies suggested that septins use actin (Kinoshita et al., 2002) or microtubules (Sellin et al., 2011b) as template for their assembly. Moreover, SEPT6 and 7 were shown to be required for axon branching in central nervous system by serving as a scaffold for cortactin (Hu et al., 2012). Recently, it was shown that SEPT2 directly bound to CENP-E, a plus-end mitotic motor at the kinetochore or serve as a scaffold for Par1-related kinases to regulate microtubule dynamics (Spiliotis et al., 2005; Kusch et al., 2002).

1.1.3.4.7) Septin in disease

With respect to multiplicity of septin complexes and their functions, mutation or overexpression of each septin gene can be a cause of a disease. One of the prominent diseases caused by mutation of septin is male infertility. It was shown that SEPT4 localized to the annulus of sperm and its targeted disruption led to lack of sperm motility and capacitation (last stage of maturation required for fertility). It seems that a complex of septins are present at the annulus to provide a scaffold for proteins such as DNAJB13 and SLC26A8 required for maturation and motility (Toure et al., 2011).

Probably the hallmark of septin dysfunction is underscored in cancer where septin shows a variety of genetic aberrations. Multiple septin genes including SEPT2, 5, 6, 9 and 11 have been shown to form an in-frame fusion with *MLL* in acute myeloid leukemia. An inherent ability of septins to polymerize and form a chain of *MLL* fusion protein can be the cause of atrophy (Cerveira et al., 2011).

SEPT9 encodes 11 different transcripts and 5 isoforms (Table 1.1). Each transcript is transcribed and translated under specific situations with some transcripts producing a single isoform to ensure its production. *SEPT9_v1* encodes an isoform with the largest N-terminus, which is associated to tumorigenesis. This isoform can enter the nucleus and stabilize the HIF1- α to up-regulate genes related to angiogenesis in prostate cancer (Amir et al., 2006, 2007, 2009, 2010; Grützmann et al., 2008).

Septins have also been shown to promote the formation of α -synuclein in Lewy bodies found in Parkinson's disease. It was proposed that association of *SEPT4* with α -synuclein is protective to self-aggregation and phosphorylation thereby increasing its cytotoxicity (Ihara et al., 2003; 2007). Another dominant autosomal disease caused by mutations in *SEPT9* gene is hereditary neuralgic amyotrophy characterized by nerve damage, muscle atrophy and severe pain (Pellegrino et al., 1996). Furthermore, *SEPT2*, 9 and 11 were shown to participate in phagosome formation containing *Listeria* implying a role for septins in infection biology of obligatory cellular parasites (Huang et al., 2008; Mostowy et al., 2009, 2010 and 2011).

A detailed list of septins, their expression pattern and association to corresponding disease are given in table 1.2.

Septin	Expression	Disease
SEPT1	Lymphocyte, CNS	Alzheimer's disease, leukemia, lymphoma, oral cancer
SEPT2	Ubiquitous	Alzheimer's disease, bacterial infection, brain, liver and renal cancer, von-Hippel-Lindau syndrome
SEPT3	CNS	Alzheimer's disease, brain, cancer, teratocarcinoma
SEPT4	CNS, eye, testes	Alzheimer's disease, Parkinson disease, male infertility, skin, brain, breast, lung, liver, head and neck, urogenital and colon cancer, leukemia, myeloma
SEPT5	Ubiquitous	Parkinson disease, schizophrenia, bipolar disorder, congenital hydrocephalus, leukemia, pancreatic cancer
SEPT6	Ubiquitous	Bipolar disorder, hepatitis C, leukemia
SEPT7	Ubiquitous	Male infertility, brain cancer
SEPT8	CNS, lymphocyte, intestinal track, placenta, eye	Retinal degeneration
SEPT9	Ubiquitous	Hereditary neuralgic amyotrophy, bacterial infection, leukemia, breast, ovarian, colorectal, liver and head and neck cancer, Hodgkin lymphoma
SEPT10	Ubiquitous	
SEPT11	Ubiquitous	Schizophrenia, bipolar disorder, bacterial

		infection, liver cancer, leukemia
SEPT12	Testes, lymphocyte	Male infertility
SEPT14	Testes, CNS	

Table 1.2. Septin, expression pattern and disease (Hall et al., 2012; Saarikangas et al., 2011)

1.1.3.5) Establishment of polarity, cooperation between septin and Cdc42p

Symmetry breaking in budding yeast is a complicated and fairly uncomprehended mechanism that involves polarized accumulation of multiple protein machineries to a certain site in the cell. Selection of the polarization site or “bud site” depends on the internal signals that reside adjacent to the previous bud site known as bud scar (Park and Bi, 2007). Redundant pathways work in parallel to ascertain bud selection and progression through the cell cycle. The first pathway, involves a positive feedback loop between actin and Cdc42p. Actin exists as either a patch or a cable with the earlier being present as branched filaments in the cytoplasm and the later being unbranched and straight filaments nucleated by formin V (Park and Bi, 2007). In polarizing cells, Cdc42p localizes to the bud site and directs the formation of actin cables towards the bud. Actin cables, which are also involved in vesicle transport, transfer more Cdc42p to the bud site to create a positive feedback loop. However, interference with actin function does not abrogate establishment of polarity indicating the presence of another pathway (Slaughter et al., 2009). The second pathway requires multiple GTPases that work in concert to activate Cdc42p locally. First, Bem1 localizes to the bud site next to the previous bud scar and then recruits and activates Cdc24p, a GEF for Cdc42p (Park and Bi, 2007). Bem1 is a protein with multiple binding sites for Cdc42p, Cdc24p and Cla4 (a kinase involved in septin ring dynamics) whose polar localization depends on Cdc42p. This suggests another positive-feedback loop between Cdc42p and Bem1 that leads to polar activation of Cdc42p (Bose et al., 2001 and Butty et al., 2002). Upon binding of Bem1 to Cdc24p, the conformation of the autoinhibitory domain of Cdc24p changes, which leads to its polar activation and consequently activation of Cdc42p. Supporting evidence showed that artificial localization of Cdc24p to the membrane did not promote localized activation of Cdc42p, which illustrates the significance of its interaction with Bem1 (Park and Bi, 2007). On the other hand, another GTPase, called Rsr1 or Bud1 physically interacts with Cdc24p and its simultaneous deletion with Bem1 is lethal implying their redundancy (Park et al., 1997). However, Rsr1 does not act merely as a physical cue since mutation of its GEF (Bud5) and GAP (Bud2) randomizes the bud site selection suggesting that multiple rounds of GTP hydrolysis are required for establishment of polarity and local activation of Cdc42p (Slaughter et al., 2009). Altogether, the biochemical data and mathematical modeling suggest that binary pathways work in concert to deliver more Cdc42p to the bud site but Bem1 captures Cdc42p and this consequently rises the level Cdc42p(GTP). Moreover, GDP-dissociation inhibitor (GDI) of Cdc42p extracts Cdc42p(GDP) from the membrane and diffuses in the cytosol while conversion of Cdc42p(GDP)

to Cdc42p(GTP) decreases its extraction by GDI leading to increased concentration of Cdc42p(GTP) at the incipient bud site (Johnson et al., 2011).

Majority of Cdc42p effectors have been shown to physically interact with septin but Cdc42p either in its GTP or GDP bound states failed to bind to single septin subunits purified from *E. coli* (Versele et al., 2004). Rga1, Rga2 and Bem3 serve as the GAP for Cdc42p and they colocalize with septin as the bud emerges. It was shown that these proteins are required for proper assembly of the septin ring and their overexpression suppressed the septin-defective mutants and some of the Cdc42p mutants (Gladfelter et al., 2002; Caviston et al., 2003). Moreover, many rounds of GTP binding and hydrolysis by Cdc42p is required for initial assembly of the septin ring implying a role for Cdc42p GAPs (Gladfelter et al., 2002). However, it was shown that maintenance of septin at the budding neck is independent of Cdc42p whereas actin polarization and its maintenance require active Cdc42p (Gladfelter et al., 2002). Therefore, a switch mechanism of Ras protein cannot account for septin assembly but rather an EF-Tu-like mechanism for assembly of macromolecules fits to the function of Cdc42p as repeated hydrolysis of the nucleotide is required.

As discussed earlier, activation of Cdc42p and bud selection coincide with activation of mitotic exit network (MEN). MEN components are activated in anaphase after entry of spindle pole body into the bud cell. Cdc42p contributes to activation of MEN in three distinct but redundant ways (Höfken et al., 2004). The first two ways depend on p21-activated kinases Ste20 and Cla4. Ste20 activates mitotic exit directly whereas Cla4 phosphorylates Lte1, a GEF for Tem1, which then activates MEN. Moreover, two structurally similar and functionally redundant proteins called Gic1 and Gic2 (GTPase interacting component) interact with Bub2/Bfa1 complex and inhibit this complex (Höfken et al., 2004). Bub2/Bfa1 acts as a GAP for Tem1 and its inactivation via Gic1 and 2 keeps Tem1 active and promotes MEN activity (Fig. 1.10). Therefore cell uses multiple redundant pathways to ensure successful exit from mitosis coupled to polarity and division (Höfken et al., 2004).

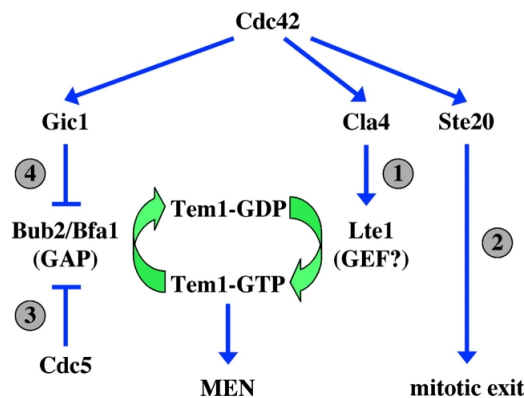


Fig. 1.10. Mitotic exit network (MEN). Cdc42p activates MEN via its several effectors, Gic1, Gic2, Ste20 and Cla4. Gic1 and Gic2 disrupt the Bub2/Bfa1/Tem1 complex formation (taken from Höfken et al., 2004).

Gic proteins were first identified through genetic screening in yeast deficient in budding. Gic1 and Gic2 possess a CRIB domain (Cdc42/Rac-interactive binding), which enables them to bind to the Cdc42p(GTP) and a polybasic region that interacts with PIP2 required for proper localization and function (Orlando et al., 2008; Brown et al., 1997). Gic proteins were implicated to be essential in establishment of polarity and budding initiation. It was shown that overexpression of Gic1 or Gic2 could restore the defects in *bem1Δ* or *bem2Δ* cells whose gene products serve as a scaffold for polarity proteins (Brown et al., 1997). Moreover, *gic1 gic2 rsr1Δ* cells showed synthetic lethality reminiscent of Cdc42p or Cdc24p mutants (Kawasaki et al., 2003). The *gic1 gic2 rsr1Δ* cells were not able to initiate budding while the single mutants could commence the budding. Furthermore, it was shown that Gic2 is required for localization and coupling of Cdc42p(GTP) to Bni1, Spa1 and Bud6 to regulate actin polymerization (Jaquenoud et al., 2000). Therefore, Gic1 and Gic2 constitute a redundant pathway that works in parallel to Rsr1, which both are required for bud site selection, Cdc42p activation and maintenance of polarisome. However, Gic2 is expressed just before bud emergence despite Gic1, which is expressed during the whole cell cycle and is subjected to Cdc42p-dependant degradation immediately after bud formation (Jaquenoud et al., 1997).

It was recently shown that Gic1 and Gic2 are required during early recruitment of septin by Cdc42p to the budding neck (Iwase et al., 2006). Both Gic proteins are downstream effectors of Cdc42p whose disruption impairs septin ring assembly. On the onset of bud formation, Gic1 interacts with Cdc42p to form a cap in the bud without colocalization with septin but changes its localization as the bud grows while Gic2 has a more dispersed localization through bud and neck with a faster turnover (Iwase et al., 2006). In contrast, both Gic1 and Gic2 localize to the bud neck in large buds. These data suggest that although both Gic proteins seem to function redundantly but they might be involved in organizing different septin structures or even at different stages of the cell cycle. Both Gic1 and Gic2 were shown to interact physically with septin (Iwase et al., 2006). Using yeast two-hybrid assay, Gic proteins were shown to bind to Cdc12 and weakly to Cdc11. On the other hand, by immobilizing MBP-Gic on the column, strong interaction with Cdc12 and weak interaction with Cdc3 was detected to both Gic1 and Gic2. Finally, pull-down experiments also revealed co-fractionation of Cdc11, Cdc12 and Cdc3 with Gic proteins (Iwase et al., 2006). These data together showed that all septin subunits except Cdc10 interacted with Gic. It is known that the conformation of subunits changes upon binding to each other or filament formation. Therefore, detection of interaction using purified subunits could result in invalid data. The closest homolog of Gic in human is the Borg family. Borg3 was shown to possess a BD3 domain in its C-termini required for binding to SEPT6 and SEPT7 that mediated aggregation of septin filaments in mouse fibroblast cells (Joberty et al., 2001). Cdc42 negatively regulated this effect by interfering with Borg and septin interaction (Joberty et al., 2001 and Sheffield et al., 2003). This has been the only indication up to now providing evidence that Cdc42 might indirectly regulate septin filament/bundle formation *in vivo*.

Upon selection of the bud site, septins are recruited to the incipient bud site via concerted action of Cdc42p and its effectors Gic1 and Gic2. There are contradictory data with regard to the function of actin in septin recruitment. Some data suggest that septin recruitment takes place independent of actin (Harkins et al., 2001) whereas other data point to an early role for actin as disruption of actin cables with Latrunculin A (LatA) delays septin ring formation (Kadota et al., 2004 and Iwase et al., 2006). How actin contributes to septin ring assembly remains unknown but it can indirectly assist in delivery of Cdc42p to the bud site and directly by delivering septin. At this stage of the cell cycle (early G1), septin exists as an unorganized patch with high exchangeability. But upon establishment of polarity and bud emergence, septins organize into a ring without exchangeability with cytoplasmic pool (frozen state) (Oh and Bi, 2011). Soon after the bud neck grows, septin expands to form a rigid structure known as an “hourglass”. The hourglass structure is composed of septin filaments aligned side-by-side and parallel to the bud axis with a C_2 symmetry (Vrabioiu et al., 2006 and 2007). Concomitant with telophase, the septin hourglass splits into two discrete rings in which septin filaments are orientated perpendicularly to the bud axis (Vrabioiu et al., 2006 and 2007 and DeMay et al., 2011). The septin filaments either in the hourglass or the ring are anisotropic and during transition between these two structures, they become isotropic for a brief time (DeMay et al., 2011). These data highlight that despite the rigidity of each septin structure, they undergo tremendous conformational changes during different stages of cell cycle; first an unorganized patch of filaments or octamers, second a single ring, third an hourglass, fourth two separate rings and finally disassembly into reusable pieces. Additionally, septin filaments confer asymmetry to the cell, which requires an intrinsic polarization of a non-polar filament. Differential localization of proteins either in the bud or the mother cell necessitates polarity of the diffusion barrier. It is still puzzling how septin can maintain polarity while it runs parallel to the bud axis and then undergoes vast structural changes including a 90° rotation (Fig. 1.11).

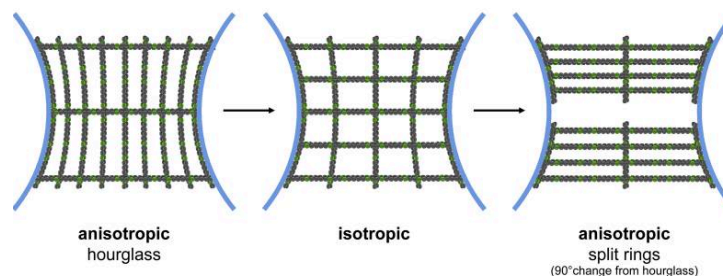


Fig. 1.11. Rotation of septin filament at the budding neck. Primarily, septin filaments are organized in arrays in the hourglass structure that run parallel to the bud axis. After cell separation, septin hourglass splits into two rings, which are perpendicular to the bud axis. Transition to split ring structure follows a brief time of filament isotropy (taken from DeMay et al., 2011).

Post-translational modification of septin is known to regulate their structure and therefore their function and it can account for differential binding of proteins on either side of the bud. It is reasonable to assign a role for phosphorylation concerning the high activity of kinases many of which associate with septin directly. Concomitantly with exit from G1, Shs1 is phosphorylated by Cdc28 and Pho85, which might account for the conformational changes observed *in vitro* (Egelhofer et al., 2008, Garcia 3rd et al., 2011). Later, Cdc3 and Cdc10 are phosphorylated by Cla4, a kinase whose polar localization is dependent on Cdc42p, septin and binding to PIP2 (Versele et al., 2004; McMurray and Thorner, 2009b). Coincident with cytokinesis, Shs1 is phosphorylated by Gin4 on residues different to those modified previously (Mortensen et al., 2002; McMurray and Thorner, 2009b). Ultimately, after cell separation Cdc3 is phosphorylated in a Cdc28-dependent manner promoting disassembly of the inherited septin rings (Tang et al., 2002). Another kinase, Kin4 and its regulator Elm1 were shown to regulate septin ring assembly and to be involved in spindle position checkpoint. These kinases are recruited to the budding neck in a Dma1- and Dma2-dependent fashion. Dma1 and Dma2 are ubiquitin ligases that regulate Elm1 recruitment but do not modify septin itself (Merlini et al., 2012). In fact, Elm1 was shown to confer stability to septin and deletion of PP2A^{Rts1} suppresses the deficiencies of *cla4Δ* cells. Differential association of proteins could also account for establishment of filament polarity. For instance, Gin4 is usually found on the mother side whereas the closely related kinase, Kcc4 exists on the interior of bud side. Bni4, a septin-interacting protein is found only on the exterior of the septin ring (McMurray and Thorner, 2009b). Moreover, septins on the mother side of the hourglass are subject to sumoylation. Cdc3, Cdc11 and Shs1 become sumoylated as the collar appears and it is reverted before hourglass splits into rings (Johnson et al., 1999). Despite the availability of plethora of evidence for post-translational modification of septins, it is not completely perceived how these moieties contribute to polarity of filaments (Gladfelter et al., 2004).

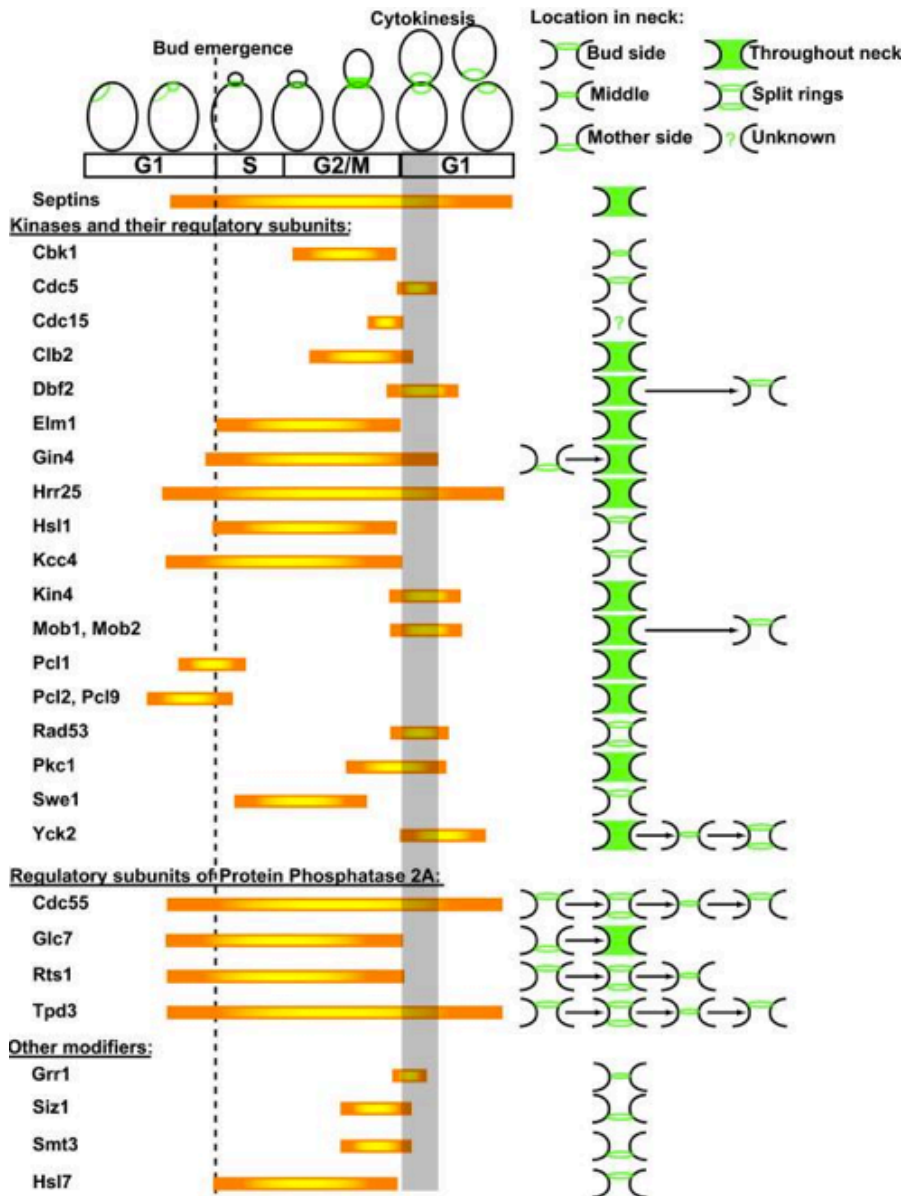


Fig. 1.12. Septin-related kinome of the budding yeast. Various kinases associate with septin during different stages of cell cycle and regulate structure and function of septin (taken from McMurray and Thorner, 2009b).

1.2) Introduction into DHCR7

1.2.1) Cholesterol

Cholesterol in solid form was first identified in 1769 by François Poulletier de la Salle in gallstone and later in 1815 Eugène Chevreul coined the name “cholesterine” (Lecerf et al., 2011). Cholesterol is an organic compound with four sterol rings and a 3- β hydroxyl head group. The human body acquires cholesterol in two different ways that balance each other. First, cholesterol is adsorbed from dietary intake and second it is synthesized mainly in the liver, where it is synthesized in the endoplasmic reticulum of the hepatic cells (Olson, 1998). The excess of cholesterol is excreted in the form of bile acid through the gallbladder but most of the biliary cholesterol is also recycled back in the small intestine through their insertion into chylomicrons (Olson, 1998). In fact, the dietary intake has a little overall impact on the total amount of body cholesterol since the major fraction is synthesized in the body. Disruption of balance between exogenous cholesterol uptake and endogenous cholesterol biosynthesis leads to increased level of plasma cholesterol and low-density lipoprotein (LDL) that ends with thickening of arteries and ultimately atherosclerosis (Lemaire-Ewing et al., 2012). Statins are widely prescribed as a cholesterol-lowering medication. They inhibit HMG-CoA reductase, the first enzyme in the cholesterol biosynthesis pathway (discussed in detail in 1.2.2). However, there are contradictory reviews whether statins can be used for primary prevention for people with high risk to develop cardiovascular diseases (Ray et al., 2010; Onelli et al., 2011).

Cholesterol is one of the most abundant constituents of membranes and plays numerous functions in the cell and body. It serves as the precursor for synthesis of vitamin D and steroid hormones including testosterone, progesterone, estrogen, cortisol and aldosterone (Hanukoglu, 1992). Within the cell, cholesterol is buried in the membranes via the interaction of its hydroxyl group with the charged moieties of phospholipids and its hydrophobic steroid rings with the hydrocarbon chain of other lipids. It has been postulated that cholesterol modulates the fluidity of membranes in a temperature-dependent fashion. In general, increased cholesterol content leads to reduced fluidity at a physiological temperature (Yeagle, 1991). An interesting characteristic of biological membranes is confinement of certain lipids and proteins into discrete domains while retaining its fluidity. Cholesterol is enriched in certain domains called lipid rafts, which play a key role in signal transduction, ion transport across the membrane, organization of cytoskeletal proteins and endocytosis (Bastiaanse et al., 1997; Chichili et al., 2009; Simons and Sampaio, 2011; Staubach and Hanisch, 2011; Lemaire-Ewing et al., 2012).

1.2.2) Cholesterol biosynthesis

The biosynthesis of cholesterol starts with conversion of acetyl-CoA and acetoacetyl-CoA to 3-hydroxy-3-methyl-glutaryl-CoA (C6-backbone) by mitochondrial-associated proteins HMG-CoA synthase 1 (HMGCS1) and HMG-CoA synthase 2 (HMGCS2). HMG-CoA is then reduced to mevalonate by HMG-CoA reductase, which is the first rate limiting step in the cholesterol biosynthesis pathway. HMG-CoA reductase is the target of cholesterol lowering drug family of statins (Endo et al., 1976). In the next step, mevalonate is phosphorylated first by mevalonate kinase (MVK) to mevalonate-5-phosphate and subsequently by phosphomevalonate kinase (PMVK) to produce mevalonate-5-pyrophosphate. Next, Δ^3 -isopentenyl pyrophosphate (C5-backbone) is produced as a result of decarboxylation of mevalonate-5-pyrophosphate catalyzed by mevalonate decarboxylase (MVD). Δ^3 -isopentenyl pyrophosphate is further processed in three enzymatic reactions until two farnesyl pyrophosphates (C15-backbone) are condensed by farnesyl-diphosphate farnesyltransferase (FDFT1) or squalene synthase (SQS) using NADPH as a cofactor to produce squalene (C30-backbone). Squalene synthase is located in the endoplasmic reticulum and could serve as a possible target for inhibition of cholesterol biosynthesis. As a result of inhibition of HMG-CoA reductase, the level of farnesyl pyrophosphate drops, which is a precursor for production of ubiquinone, Heme A and dolichol (Amin et al., 1997; Rozman et al., 2010). Therefore, by inhibiting squalene synthase, cholesterol production is halted while other vital products are produced and utilized by other biochemical pathways (Charlton-Menys et al., 2007). Squalene epoxidase (SQLE) uses NADPH to reduce molecular oxygen to form an epoxide on squalene (Chug et al., 2003). The squalene-2,3-epoxide then undergoes a cyclization to lanosterol by lanosterol synthase (LSS) in a two-step reaction (Dean et al., 1967). Lanosterol is the first compound with recognizable sterol rings in the cholesterol biosynthesis pathway. 14-dimethyl lanosterol is catalyzed by five enzymatic steps involving demethylation, decarboxylation and migration of double bonds in the molecule to zymosterol (C27-backbone). Zymosterol is reduced by 24-dehydrocholesterol reductase (DHCR24) to cholest-8(9)-en-3 β -ol. This cholesterol precursor is modified by 3 β -HSD- Δ^8,Δ^7 -isomerase (also called emopamil-binding protein, EBP) to lathosterol. Sterol C5 desaturase (SC5D) is an enzyme that catalyzes a dehydrogenation reaction introducing a C5-C6 double bond into lathosterol resulting in production of 7-dehydrocholesterol (7-DHC) as a product (Becker et al., 2001 and Brunetti-Pierri et al., 2002). 7-dehydrocholesterol is reduced by 7-dehydrocholesterol reductase (DHCR7) to produce cholesterol. To produce cholesterol another route via desmosterol exists in human cells, which shares the enzymes until lanosterol. Alternatively, lanosterol can be converted into desmosterol in multiple steps and desmosterol is subsequently reduced by 24-dehydrocholesterol reductase (DHCR24) to form cholesterol. DHCR24 is the enzyme that is able to catalyze each intermediate in the desmosterol pathway to the intermediates of 7-dehydrocholesterol pathway in the last four steps (Rozman et al., 2010) (Fig. 1.13).

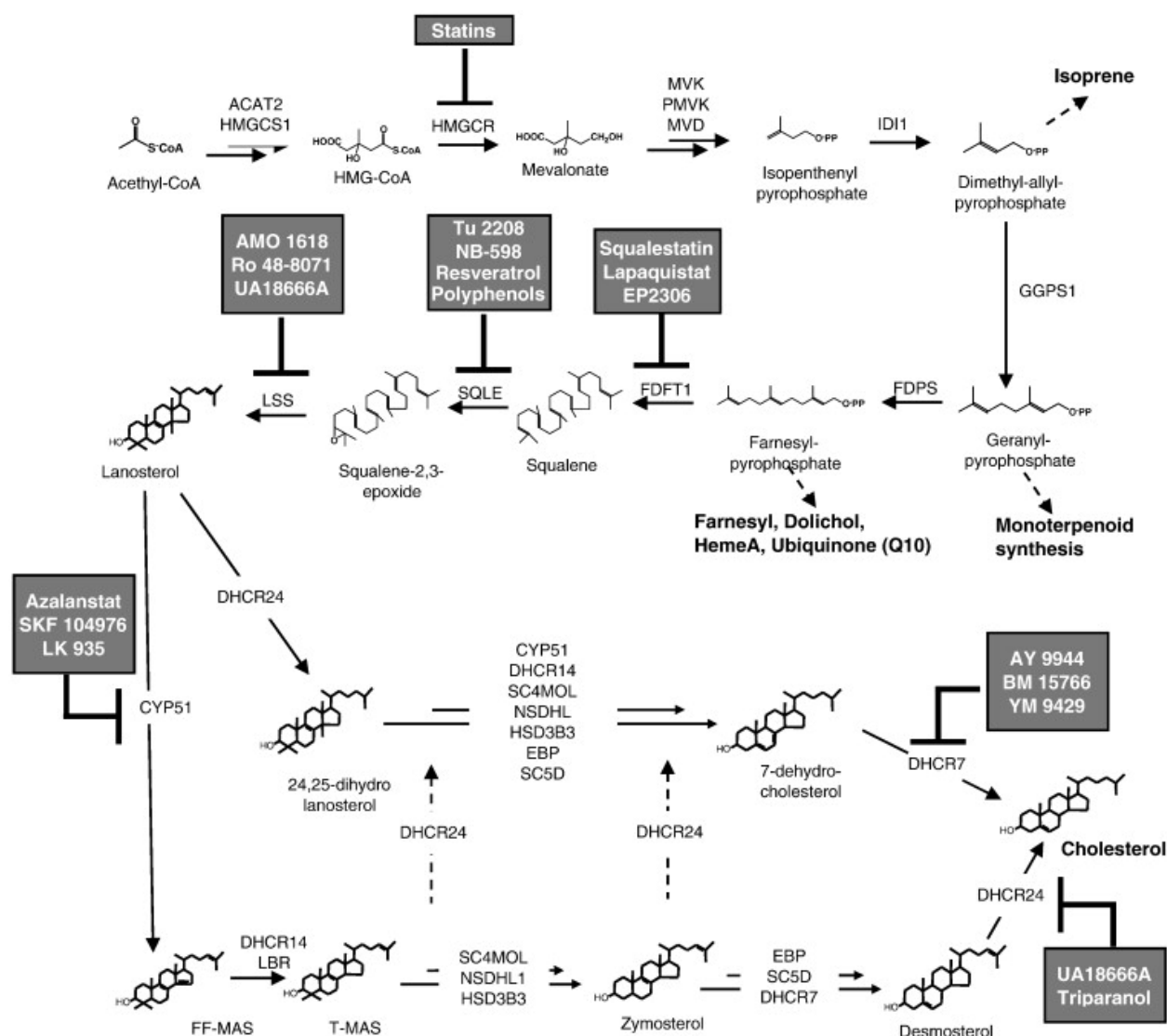


Fig. 1.13. Schematic representation of cholesterol biosynthesis pathway. Inhibitors that block enzymes of the pathways are shown in the grey box (taken from Rozman et al., 2010).

1.2.3) Regulation of cholesterol biosynthesis

Cholesterol uptake and biosynthesis are interdependent and tightly regulated at many levels. Cholesterol biosynthesis is activated when cellular level of free cholesterol drops below a certain concentration. This activation could be due to insufficient cholesterol intake or deficient uptake by LDLR (Espenshade and Hughes, 2007). In either case, a sensory machinery is required that activates and thus upregulates genes related to cholesterol synthesis and uptake. In human cells, a tertiary complex is responsible for sensing cholesterol, which is composed of SREBP (sterol regulatory element binding protein), SCAP (SREBP cleavage activating protein) and Insig (insulin induced gene). SREBP is a transcription factor anchored in ER membrane, which is transported to Golgi apparatus for cleavage and finally to the nucleus to activate

genes of cholesterol biosynthesis pathway and uptake. SCAP and SREBP form a steady complex in the ER membrane. At high cholesterol concentrations, cholesterol binds to SCAP causing conformational changes, which induce Insig binding to SCAP and formation of the tertiary SREBP-SCAP-Insig complex (Brown and Goldstein, 2009). This prevents their transport to the Golgi apparatus. On the other hand, Insig binds to HMG-CoA reductase and assists in its ubiquitination-dependent degradation. This myriad of interactions leads on the one hand to the down-regulation of cholesterol synthesizing genes by retaining SREBP in the ER and on the other hand, halting the cholesterol biosynthesis pathway by degradation of HMG-CoA reductase (Brown and Goldstein, 2009). When cholesterol levels drop below 5% total ER lipid (molar ratio), cholesterol dissociates from SCAP which results in the dissociation of Insig from the complex. SCAP together with SREBP is then packed into COPII vesicles and moves to the Golgi apparatus (Radhakrishnan et al., 2008 and Goldstein et al., 2006). The SCAP dissociates from SREBP in the Golgi apparatus and SREBP is sequentially cleaved by two enzymes namely, SP1 and SP2 to release its nuclear fragment (Brown and Goldstein, 1999). The nuclear fragment of SREBP dimerizes in the cytoplasm and travels to the nucleus to up-regulate many genes including its own, HMG-CoA reductase and DHCR7 (Espenshade and Hughes, 2007; Brown and Goldstein, 2009). Furthermore, free Insig becomes ubiquitinated and degraded to allow HMG-CoA reductase to pursue cholesterol synthesis. As mentioned earlier, HMG-CoA reductase is the rate-limiting enzyme in the cholesterol biosynthesis pathway. This enzyme is inhibited by cholesterol, lanosterol and 7-DHC (7-dehydrocholesterol) at an enzymatic and by Insig at a molecular level (Fritzky et al., 2001; Song et al., 2005). Several compounds of the pathway participate in feedback inhibitory mechanism by direct interaction with the sterol-sensing domain of SCAP, Insig and HMG-CoA reductase. In this manner, the cell guarantees that there is enough cholesterol available by coupling exogenous cholesterol intake with endogenous cholesterol synthesis.

1.2.4) 7-dehydrocholesterol reductase (DHCR7)

This enzyme catalyzes the reduction of the Δ^7 double bond of 7-dehydrocholesterol to produce cholesterol or 7-dehydrodesmosterol to make desmosterol that differs from cholesterol in the presence of a C24–25 double bond in the side chain (Waterham and Wanders, 2001). Tissues such as brain, testis, and exocrine breast can have significant levels of desmosterol in addition to cholesterol and therefore express DHCR7 at higher levels. Deficiency of this enzyme leads to an autosomal disease called Smith-Lemli-Opitz Syndrome (SLOS). Genetics and biochemistry of this enzyme will be discussed in the following sections.

1.2.4.1) Genetics of DHCR7

The *dchr7* gene spans 14,100 base pairs on the 11q12-13 chromosome and contains nine exons (Correa-Cero and Porter, 2005). The first two exons of a 2,786 base pair long mRNA contain the 5'-UTR and the start codon is located in the third exon. The *dchr7* is expressed ubiquitously in all tissues with the highest expression level in liver, brain and testis to meet their need for higher cholesterol levels. Upstream of the *dchr7* promoter, one SRE1/E-box (sterol responsive element), four SP1 sites and two NF-Y sites have been mapped suggesting its up-regulation under sterol starvation by SREBP (Correa-Cero and Porter, 2005). However, alternative splicing in the 5'-UTR of rat *dchr7* can create up to five different isoforms each expressed in a different tissue and age (Lee et al., 2002). This observation highlights that DHCR7 might play broader functions than merely a reductase. In conjunction with this, DHCR7 was postulated to regulate the sonic hedgehog (Shh) pathway (Koide et al., 2006; Tadjuidje and Hollemann, 2006). Two opposing evidences suggested that DHCR7 acts as a positive regulator (Tadjuidje and Hollemann, 2006) and as negative regulator of the Shh pathway (Koide et al., 2006). Although contradictory, it is conceivable that DHCR7 can regulate Sonic hedgehog, which covalently binds to cholesterol in the Golgi apparatus (Tadjuidje and Hollemann, 2006). Furthermore, it was shown that an accumulating concentration of 7-DHC in the cell leads to degradation of HMG-CoA reductase, the rate-limiting enzyme of the cholesterol biosynthesis pathway to add another level of feedback inhibition to the pathway (Honda et al., 1998).

The *dchr7* gene exists in eukaryotes except in yeast, which produces ergosterol instead of cholesterol (Espenshade, 2006). Apart from eukaryotes, three bacterial strains including *Plesiocystis pacifica*, *Coxiella burnettii* and *Legionella longbeachae* own a relatively similar *dchr7* gene. Alignment of the human DHCR7 (hDHCR7) with its bacterial homologs shows that DHCR7 from *P. pacifica* (pDHCR7) has the least homology to others (Fig. 5.5 and 5.6 in supplementary information). Even in terms of length of amino acid sequence, pDHCR7 is much shorter than hDHCR7 and cDHCR7. Moreover, by comparing the sequence alignment it can be noticed that cDHCR7 shares many conserved amino acids with hDHCR7 suggesting structural and functional similarity. It can be deduced that the *dchr7* gene was transferred from the human genome to infectious bacteria during the course of evolution (Chen et al., 2007).

1.2.4.2) Protein structure of DHCR7

The hDHCR7 is a membrane protein with 475 amino acids, which has a predicted molecular weight of 55 kDa (Correa-Cero and Porter, 2005). However, ectopic expression of hDHCR7 tagged with FLAG epitope in COS cells showed a band at 42 kDa (Moebius et al., 1998). The proposed topology of hDHCR7 based on similarity of hydropathy plots of the lamin B receptor and DHCR7 predicted nine transmembrane segments with the N-terminus in the cytoplasm and the C-terminus in the ER lumen (Holmer et al., 1998).

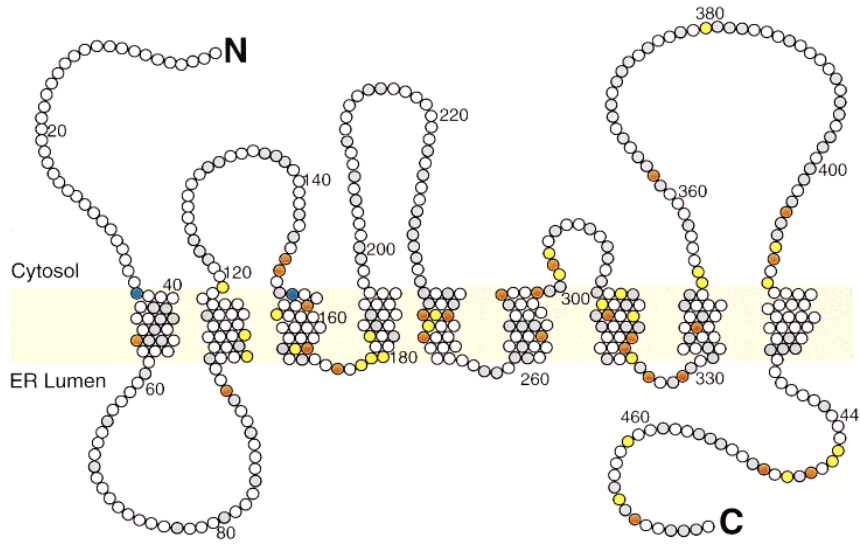


Fig. 1.14. Proposed model of the hDHCR7 topology. The model was calculated based on similarity of hydropathy plots of lamin B receptor and DHCR7. All missense mutations identified in SLOS patients are indicated by colored circles (yellow circle = mutated nonconserved amino acid, orange circle = mutated conserved amino acid, blue circle = stop mutations) (Fritzky et al., 1998

and Witsch-Baumgartner et al., 2001).

DHCR7 contains several motifs including a sterol-sensing domain (amino acids 181-362), sterol reductase 1 motif (amino acids 213-228), sterol reductase 2 motif (amino acids 439-462) and a sterol reductase recognition motif (394-405) (Correa-Cero and Porter, 2005). Sterol reductase 1 (GNFFYNYMMGIEFNPR) and sterol reductase 2 (LLTHRCLRDEHRCASKYGRDWERY) motifs are shared by other sterol reductases involved in ergosterol biosynthesis pathway in yeast such as ERG3, ERG4, ERG24. These motifs have a very conserved sequence among hDHCR7, cDHCR7 and even pDHCR7 suggesting their significance and involvement in reduction. Especially the sterol reductase 2 motif was proposed to be responsible for substrate binding (Fig. 5.5 in supplementary information) (Witsch-Baumgartner et al., 2001). It has been proposed that the sterol reductase recognition motif (LLXSGWWGXXRH) exists among all sterol reductase family members (Lecain et al. 1996). Although the biochemical function of all of these motifs has not been characterized, the majority of missense mutations have been mapped to these motifs underlining their functional significance (Yu and Patel, 2005). A sterol-sensing domain (SSD) with 47% amino acid similarity to that of SCAP has been mapped in hDHCR7 encompassing transmembrane segment 4 to 8. This domain exists also in other proteins, which participate in cholesterol regulatory pathways including HMG-CoA reductase, Insig, Patched, Dispatched, Niemann-Pick C proteins and SCAP. It was recently shown that the sterol-sensing domain of SCAP binds directly to cholesterol *in vitro* (Radhakrishnan et al., 2004) and *in vivo* (Goldstein et al., 2009) followed by conformational changes. It has been reported that in addition to cholesterol lanosterol and probably 7-DHC bind to HMG-CoA reductase to regulate its activity (Honda et al., 1998; Song et al., 2005). A possible function of SSD in DHCR7 could be sensing cholesterol, its product or other sterols as a part of a negative feedback mechanism. On the other hand, proteins with a SSD such as SCAP, Insig

and HMG-CoA reductase bind each other in a cholesterol- and oxysterol-dependent manner. It has not been investigated whether DHCR7 also interacts with Insig to be set for degradation.

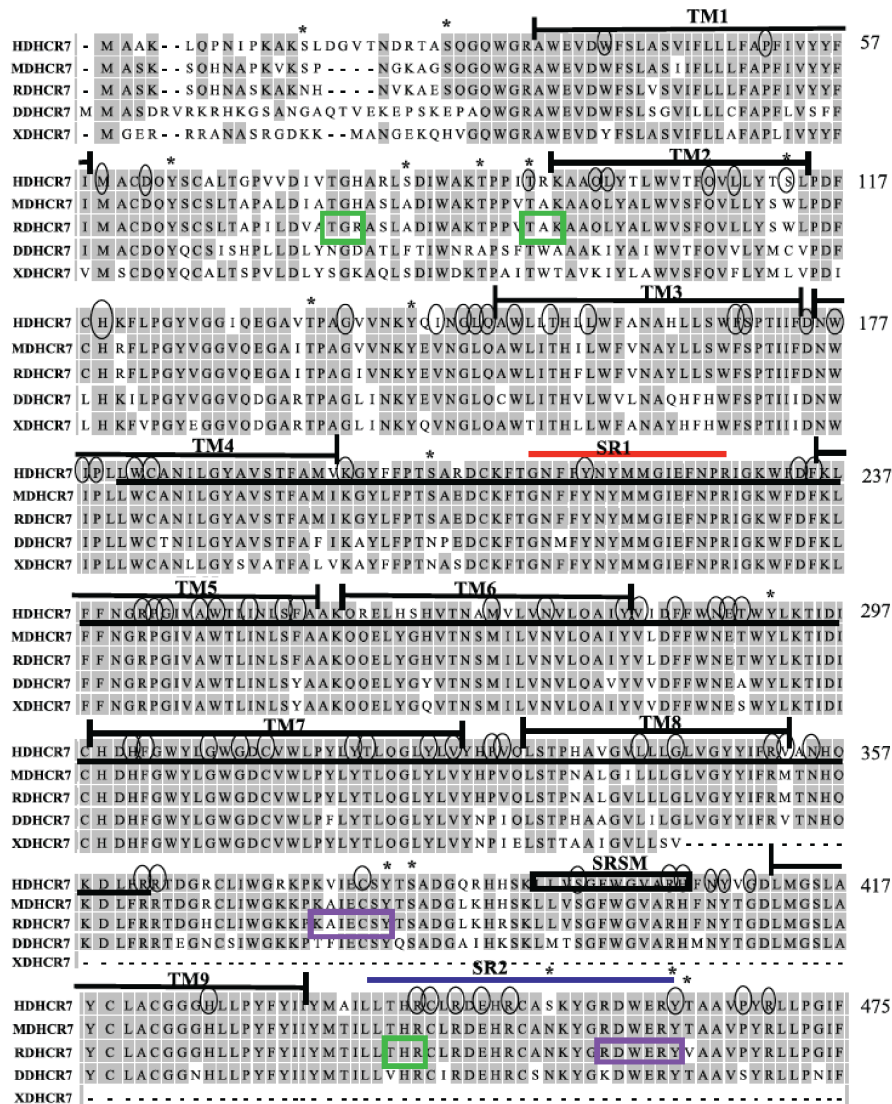


Fig. 1.13. Sequence alignment of motif organization of human, mouse, rat, *Drosophila* and *Xenopus* DHCR7. Sterol reductase 1 and sterol reductase 2 motifs and the SSD are underlined by red, blue and black, respectively. The sterol reductase recognition motif is boxed in black. Potential protein C kinase and tyrosine kinase phosphorylation sites are boxed green and purple, respectively. Numbering is based on human DHCR7 (taken from Correa-Cerro and Porter, 2005). HDHCR7=human, MDHCR7=mouse, RDHCR7=rat, DDHCR7=*Drosophila*, XDHCR7=*Xenopus*.

1.2.4.3) Enzymatic activity of DHCR7

DHCR7 is an ER-resident enzyme that facilitates the removal of a double bond from 7-dehydrocholesterol and 7-dehydrodesmosterol (7-DHD). Although DHCR7 has been shown to be a $\text{NADPH}^+ + \text{H}^+$ -dependent reductase it possesses no NADPH-binding motif. It was previously suggested that P450 oxidoreductase (POR) is required as an electron acceptor and is indispensable for the enzymatic reaction (Nishino et al., 2000). However, it was recently shown that POR is not an essential component of the reduction machinery required for removal of the double bond in 7DHC (Zou et al., 2011). Thus, it still remains to be dissected where NADPH binds to DHCR7 and how electrons are transferred to 7-DHC

or 7-DHD. Nevertheless, DHCR7 has been postulated to be an iron-containing enzyme, which might assist in electron transfer and it has been biochemically proven that iron is required for functionality of the enzyme (Nishino et al., 2000).

Substrate specificity of DHCR7 has been shown to depend on the sterol ring B containing a C7-8 double bond (Shefer et al., 1998). It was shown that DHCR7 could reduce the double bond in 7-dehydroepicholesterol, 7-dehydrositosterol and ergosterol in addition to 7-dehydrodesmosterol and 7-dehydrocholesterol. Conversion of ergosterol to brassicasterol has been used as an assay to evaluate the activity of DHCR7 in SLOS patients (Honda et al., 1998).

1.2.4.4) Disease

Defects of cholesterol biosynthesis comprise multiple disorders. Patients afflicted with these disorders present recurrent febrile attacks and often have malformations, neurological symptoms, psychomotor retardation and a low life expectancy (Hoffmann et al., 1993). Enzyme deficiencies have been implicated in various human inherited diseases: mevalonic aciduria (mevalonate kinase deficiency), Conradi Hünemann Happle syndrome (3β -HSD- Δ^h, Δ^g -isomerase deficiency), desmosterolosis (24-dehydrocholesterol reductase deficiency), lathosterolosis (sterol C5 desaturase deficiency) and Smith-Lemli-Opitz syndrome (7-dehydrocholesterol reductase deficiency) (Hoffmann et al., 1986; Has et al., 2000; FritzPatrick et al., 1998; Waterham et al., 2001; Brunetti-Pierri et al., 2002; Opitz, 1994; Smith, Lemli and Opitz, 1964). The first recognized and most commonly occurring developmental disorders associated with cholesterol synthesizing pathway is Smith-Lemli-Opitz syndrome (SLOS). SLOS is an autosomal recessive disorder caused by mutations in the *dher7* gene resulting in a deficiency of the encoded 7-dehydrocholesterol reductase. In SLOS patients the deficiency of 7-dehydrocholesterol reductase (DHCR7), is characterized by accumulation of 7- and 8-dehydrocholesterol (7-DHC and 8-DHC) (Porter, 2008). Over 90% of patients show a lower level of cholesterol in blood and all body tissues than normal (Irons et al., 1993). SLOS patients show a variety of phenotypes that can range from mild mental retardation and dysmorphism to multiple organ and skeletal malformations. SLOS patients usually have short stature, low body weight and a shorter life expectancy. Cholesterol supplementation is practically not beneficial since cholesterol is not able to pass the brain-blood barrier. However, it has been shown that cholesterol supplementation improved growth and behavior in most patients (Irons et al., 1997; Kelley and Hennekam, 2000). Furthermore, treatment of mildly affected SLOS patients with simvastatin, an HMG-CoA reductase inhibitor, reduced the level of 7DHC and 8DHC to lower the severity of SLOS symptoms associated with high level of 7DHC (Jira et al., 2000 and 2003).

1.3) Methodology

1.3.1) Membrane protein expression and purification

Expression of membrane proteins is a tedious and time-consuming task, which requires tedious optimization. There are multiple expression hosts available such as *E. coli*, *P. pastoris*, insect cells and even mammalian cells chosen depending on the purpose of the experiment (Cox, 2012; Sweich et al., 2012). The most widely used expression host is *E. coli*, which offers many benefits over other expression hosts. The main advantages of *E. coli* include ease of handling, cost efficiency and obtained quantity (Baker et al., 2010). However, expression of human membrane proteins often causes toxicity, the proteins are not folded correctly or are expressed only at minute quantity. Moreover, many eukaryotic proteins are post-translationally modified and require specific machineries for correct folding. Therefore, if bacterial homologs of eukaryotic membrane proteins exist, they are used for expression, crystallization and characterization to gain insight about the function of the protein. To study the function of proteins it is necessary to obtain them in a high concentration and purity for further analysis. In this case the DNA sequence of the protein of interest is cloned into a high-copy number plasmid containing the gene sequence of the *lac* operon, which is then transformed into *E. coli*. As long as the repressor protein is bound to the operator side of the *lac* operon the RNA polymerase is not able to bind and to express the gene, because promoter and operator overlap. By addition of Isopropyl β -D-1-thiogalactopyranoside (IPTG) an analogue of lactose the repressor changes its conformation so that the RNA polymerase can bind to the promoter sequence and expresses the downstream genes. Bacterial homologs of human membrane proteins do not need folding machineries but require to be properly inserted into the membrane. When not properly folded, membrane proteins with large hydrophobic patches partition in insoluble particles known as inclusion bodies. Therefore, it is a necessary step for expression screening to separate the membrane fraction from the cell pellet and the insoluble fraction to realize if the protein of interest has been correctly folded into the membrane (Wagner et al., 2006). After achieving a successful expression condition, membrane proteins need to be solubilized with a detergent. Detergents are amphipathic molecules capable of extracting membrane proteins from lipid bilayer into detergent micelles (Seddon et al., 2004). The detergent micelles consist of a hydrophobic part that covers transmembrane segments of membrane proteins and a hydrophilic part making contact with aqueous solution. The biological lipid bilayer is not homogenous regarding the distribution of its lipids. Therefore, membrane proteins are embedded in environments with different lipids around them. Detergents also have different characteristics and detergent screening is required to find out the optimal detergent to solubilize the protein of interest. Detergents are categorized as anionic, cationic, non-ionic and zwitterionic detergents (Seddon et al., 2004). Ionic detergents contain a head group with a net positive or negative charge and a hydrophobic backbone. The critical micelle concentration (CMC), which defines the minimal concentration at which micelles are formed, is defined for ionic detergents by hydrophobic interactions of

the tail and repulsive force of the head group (Seddon et al., 2004). Sodium dodecyl sulfate and bile acid salts are two examples of ionic detergents, which are considered to be effective in solubilizing membrane proteins but meanwhile denaturing them to some extent. Nonionic detergents contain hydrophilic uncharged head groups of polyoxyethylene or glycosidic groups, which are considered to be very mild detergents preserving the native structure of membrane proteins (Seddon et al., 2004). Examples of this category include n-octyl- β -D-glucopyranoside (OG) and n-dodecyl- β -D-maltoside (DDM), which are widely used for crystallographic purposes. Zwitterionic detergents consist of head groups with both positive and negative charges (Seddon et al., 2004). CHAPS and Fos-cholines are examples of zwitterionic detergents. Fos-choline possesses a choline head group that resembles that of phospholipids especially sphingomyelin. CHAPS is a sulfobetaine derivative of cholic acid, which is an analogue of cholesterol. The CMC of zwitterionic detergents depends on the ionic strength of the solution. For instance CMC of CHAPS declines from 6.41 mM to 4.1 mM in the absence or presence of 1.5 M NaCl, respectively (Chattopadhyay and Harikumar, 1996). As mentioned earlier, there are no conventions as which detergents to use for specific membrane proteins. Normally, a cocktail of detergents is used to find out which detergent is the most potent solubilizer of protein of interest. As soon as the protein is purified, it can be studied using several methods some of which are explained briefly in the next section.

1.3.2) Electron microscopy (EM)

To fully understand the precise function of macromolecules, knowledge about its architecture and spatial organization is required. X-ray crystallography and NMR provide detailed information about the atomic structure of proteins. Crystallization of macromolecules and membrane proteins poses a great challenge, as a large quantity of sample is required and many of the membrane proteins or large protein assemblies are very difficult to crystallize. Furthermore, proteins are usually embedded in buffers that contain constituents different from physiological conditions, which can produce artifacts and physiologically irrelevant structures (Orlova and Saibil, 2011). On the other hand, molecular biology techniques have enabled tracing molecules tagged with fluorophores in the cell. Super-resolution microscopy has reached up to 50-nm resolution providing details of the spatial organization of proteins in the cell. However, tagging of molecules in the cell usually requires overexpression of fusion proteins, which might lead to unwanted localization and thereby false interpretation of their localization and function (Leung and Cheu, 2011). Moreover, fusion proteins do not necessarily own the natural function of the tagged proteins. Electron microscopy (EM) is a suitable technique to cover the gap between X-ray crystallography and fluorescent imaging without compromising the natural features and characteristics of protein machineries. Several methodologies have been developed in order to investigate the structure of macromolecules within or out the cell. The most commonly used method is single particle analysis of purified protein complexes (discussed in 1.3.2.1). In this method, a macromolecule is imaged at different orientations and

later processed to build up its 3D model. Moreover, where purification is not feasible or the dynamics of complexes in the cell are desired to be studied another method known as cryo-electron tomography is used. In this regard, a thin section of the cell is prepared and imaged as it is tilted incrementally (discussed in 1.3.2.2). Later, a 3D model of the ultrastructure within the cell is built from the images. Ultimately, electron microscopy offers the possibility to study the structure of membrane proteins reconstituted in lipid bilayers (discussed in 1.3.2.3).

For large enough macromolecules, cryo-EM is the preferred method to visualize the structure in the hydrated and native environment. The technique benefits from rapid freezing of the sample in liquid ethane to preserve the hydrated state of molecules and prevent ice crystal formation (Orlova and Saibil, 2011). In this regard, a sample is placed on a holey grid, which subsequently is blotted and plunge-frozen in the liquid ethane (-182°C) cooled by liquid nitrogen. Ethane is preferred to liquid nitrogen since the freezing is done at the freezing point of ethane rather than the boiling point of nitrogen and guarantees a rapid freezing of the sample. The disadvantage of this method is that biological samples are prone to disassembly or conformational changes upon high dosage of irradiation. Therefore, a low dosage of electrons ($10\text{-}20\text{ e}^{-}/\text{\AA}^2$) is used to record an image, which consequently decreases the contrast. In order to increase the contrast, many images have to be aligned and averaged using image processing procedures (Orlova and Saibil, 2011). Advancement in instrumentation and image processing have aided in obtaining high-resolution reconstructions of viral particles (up to 3.3 \AA), ribosomes (up to 5.6 \AA) and actomyosin at 8 \AA (Zhang et al., 2010; Bhushan et al., 2011; Behrmann et al., 2012). Some of the routinely used techniques are discussed in the next following sections.

1.3.2.1) Single particle analysis

In order to gain insight into the overall features of a protein complex, a sample is applied to a carbon-coated grid and stained with heavy atom salts such as uranyl formate. The salt covers the grid and surrounding of the protein complex and enhances the contrast (Ohi et al., 2004). However, sometimes stain does not cover the protein surrounding equally leading to loss of information on that side of the complex. Moreover, some proteins have a preferential orientation on the grid. For instance, 50S subunit of ribosome is seen mostly on the crown and the kidney views (Tischendorf et al., 1974). But in general, negatively stained samples are processed by single particle analysis to obtain a 2D reconstruction of the protein complex. This method provides sufficient information about general views of the complex although samples are flattened due to staining and air-drying (Orlova and Saibil, 2011).

The first step in single particle analysis is to select (box) thousands of particles in a way that the center of the box is placed in the center of the particle. In addition, all selected particles are centered before further processing (Frank, 2009). There are two different methods of centering. The first method searches for the center of gravity. In this method, the intensity peaks of the images are calculated to find the center of the

particle mass (Frank, 2006). Then images are shifted to maximize the number of peaks near the center. In the second method, first an average of all particles is generated and then the particles are cross-correlated to the average. The cross-correlation function is used to determine by how much to shift each particle. The particles are then shifted according to the cross-correlation function measurements to become centered (Frank, 2006). Then, a new average is generated and once again particles are shifted according to the average. This iterative process generates many averages and cross-correlations until no significant shift is required and all particles are centered. Once particles have been picked and centered, they need to be aligned, ordered, and classified for the reconstruction. During alignment, particles are placed in the same orientation to facilitate classification. Simply, two particles are just shifted in the x and y axes and rotated relative to each other in the plane of the images (reference-free alignment) or even to a defined template (reference-based alignment) to achieve a certain orientation (Frank, 2006; Orlova and Saibil, 2011). Particle classification involves grouping images that are similar, and separating images that are distinct. Protein particles generally do not lie in one preferred orientation on the carbon film. Therefore, after classification, many class averages are generated, which manifest different views of the protein complex. Furthermore, alignment of particles then has to be done for each class and classification is repeated until no further change is observed (Orlova et al., 2011). Multiple software programs exist for image processing of TEM images including SPIDER, IMAGIC, EMAN and SPARX. In this work we used a newly released image-processing environment called SPARX (single particle analysis for resolution extension). SPARX includes a graphical user interface with an extensive library of Python scripts and a core library of C++ image processing functions that allows integration of libraries from EMAN and *cctbx*. Therefore, SPARX provides its users with a uniform environment with combinatorial algorithms without a need to learn programming language (Hohn et al., 2007).

1.3.2.2) Cryo-electron tomography (cryo-ET)

As mentioned before, cryo-electron tomography (cryo-ET) is the most suitable method when cellular organelles or tissue architecture is studied. Fluorescent microscopy has proven to be a useful tool to study the localization of many proteins in the cell at a resolution of up to 50 Å. However, the number of proteins studied simultaneously is limited due to technical reasons (Leung and Chou, 2011). Moreover, the method does not provide information about the overall architecture of organelles such as chloroplast or mitochondria. Advancement in microscope design and image processing has allowed the development of a method known as cryo-electron tomography from which data can be extrapolated to build up a 3D model of the subject of study. In order to retain the native structure of proteins and organelles within cells, a method for rapid freezing (similar to the method explained in the previous section for cryo-electron microscopy) has been developed to keep the hydrated state of cells (Fridman et al., 2012). This method however suffers from poor contrast and biological samples thicker than 1 µm should be sliced to

sections thinner than the mean free path of electrons to improve visualization. Subsequently, the sample is loaded into the microscope, tilted incrementally perpendicular to the beam axis and imaged at each angle (Fridman et al., 2012). Tilt series are then aligned to a specific frame or a marker such as gold particles and finally a 3D tomogram is calculated using commercially available software.

The quality of the tomogram depends on the angular coverage during data acquisition. In practice, the sample can be tilted to cover 140° , which consists of 70-100 images from which the model is built. However, some information about the structure is missing since the angular coverage can never reach 180° . This phenomenon is known as “missing wedge” that leads to elongation of features along the microscopy axis (Fridman et al., 2012).

In order to maximize the signal-to-noise ratio in cryo electron microscopy a high electron dosage should be used instead of a heavy atom salt. However, biological samples are prone to irradiation damage and since a specific area is imaged many times, a very low electron dosage ($1 \text{ e}^-/\text{\AA}^2$) is used, which limits the contrast (Frank, 2006). Fine details of macromolecules and organelles can be visualized using CET in a range of 15-100 nm closing the gap between X-ray crystallography and fluorescent imaging (Orlova et al., 2011).

When possible, multiple tomograms can be combined to improve the resolution. For instance, sub-tomograms containing a specific complex can be extracted from the tomograms and averaged separately. Nuclear pore complex and endocytosis are two examples studied using sub-tomogram averaging (Kukulski et al., 2012). However, variations in cellular architecture prevent averaging of tomographic volumes.

1.3.2.3) Electron crystallography

Structural studies of membrane proteins hinge on the use of detergents for their purification. Detergents usually remove loosely attached lipids known as annular lipids from the protein. These lipids bind to proteins unspecifically due to van der Waals interaction of acyl chains with hydrophobic patches of transmembrane segments and ionic interaction of lipid head groups with the hydrophilic protein surface (Ubarretxena-Belandia and Stokes, 2012). On the contrary, some lipids interact specifically and therefore bind tightly to the protein. These lipids due to their strong interaction are less flexible and therefore they are resolved in the crystal structure. For instance, cardiolipin binds to cytochrome *c* oxidase and removal of this lipid hampers functionality of the protein (Harrenga et al., 1999). Annular lipids were resolved in the crystal structures of bacteriorhodopsin, aquaporin-0 and V-type Na^+ -ATPase where lipids were tightly packed either in the crystals or in the interior space of protein channels (Lueke et al., 1999; Hite et al., 2008; Murata et al., 2005). Since most of the membrane proteins are purified in detergent micelles using chromatographic steps, they usually lose the necessary lipids and may adopt a different structure or become nonfunctional in the detergent micelle. On the other hand, conditions used for 3D

crystallography trials usually include nonphysiological buffers, which might lead to artifacts in the structure. Therefore, another method known as electron crystallography was developed to reconstitute membrane proteins in a lipid bilayer and study their structures within their natural environment (Henderson, 1975). The study by Henderson and Unwin resolved for the first time an atomic map of bacteriorhodopsin showing α -helices in the membrane. This work was improved by advances in cryogenic sample preparation and computational strategies, which yielded in an atomic structure of bacteriorhodopsin (Henderson et al., 1990). Similar to 3D crystallography, this method entails protein purification, lipid reconstitution, crystal formation, screening, data acquisition and modeling. The first step is to purify the protein of interest using conventional purification protocols in detergent micelles. The choice of a detergent can be a limiting factor in obtaining a well-diffracting crystal (Raunser and Walz, 2009). Some membrane proteins show tendency to be solubilized in certain detergents, which are not suited for crystallography. For instance, SCAP failed to be solubilized in any detergents other than Foscholine®-13, which has never proven successful for crystallography (Ramakrishnan et al., 2004). In principle, different detergents should be screened to determine which one leads to a more homogenous and mono-dispersed peak during gel filtration. In the next step, purified proteins are reconstituted in a lipid bilayer and dialyzed for several days. In this regard, purified membrane proteins are mixed with a variety of lipids at different lipid-to-protein ratios (LPR) measured as mg/mg (Raunser and Walz, 2009). Then, the protein-lipid mixture is dialyzed against a buffer without any detergents or lipids to remove the detergent. Usually, detergents with long acyl chains have a low CMC (critical micelle concentration) and detergents with a short acyl chain have high a CMC. Detergents with low CMC are dialyzed and removed much slower compared to detergents with high CMC (Raunser and Walz, 2009). Therefore, dialysis of these detergents may require a longer time. Alternatively, detergents can be removed using either cyclodextrin or biobeads, which have proven useful for detergents with low CMC (Signorell et al., 2007). The protein starts to be reconstituted into lipids when the detergent reaches its CMC and the remaining of the detergent contributes to fluidity of the bilayer sheet (Raunser and Walz, 2009). A couple of factors can influence formation of a 2D crystal including the type of lipid, LPR, divalent cations, pH, dialysis time, amphiphiles, ligands, inhibitors and temperature (Ubarretxena-Belandia and Stokes, 2012). The advantage of this method versus 3D crystallography is that very minute concentrations of protein (1 mg/ml) are required to set up trials whereas in 3D crystallography trials usually concentrations above 10 mg/ml are required to enhance contacts within crystals. The disadvantages of the method include long time required for sample screening, lack of automated robots for sample preparation, and poor reproducibility of crystals due to error in pipetting, variations in protein preparation and use of different batches of detergent and lipid (Raunser and Walz, 2009).

Once reconstitution is done, results are screened and evaluated by EM. A sheet-like crystal is favored to other types of crystal such as vesicular and tubular crystals (Raunser and Walz, 2009). Vesicles tend to fold upon adsorption to EM grid, which prevents data processing and so far no high-resolution data have

been obtained from tubules. As soon as a suitable crystal is available, a sample is prepared either with negative staining or vitrified to be studied by cryo-EM. Images and diffraction patterns of 2D crystals are recorded at different tilt angles. In fact, the reason for requirement of a large crystal sheet is to minimize the loss of information at high tilt angles. The images and diffraction patterns are subsequently combined to produce an initial model. An advantage of electron crystallography to 3D crystallography is that high-resolution images contain the phases. However, obtaining high-resolution images is a challenging task due to beam-induced movement and lack of flatness in grid support material. In order to solve this problem, an additional layer of carbon has been used on top of the sample (Abeyrathne et al., 2010 and Gonen et al., 2004). However, it has not been investigated how an additional layer of carbon influences proteins with considerably large extra-membranous domains (Rope and Unger, 2012). Recently, a fragment-based phase extension of electron diffraction was applied to achieve high resolution (Wisedchaisri et al., 2011). In this approach, generic alpha helical polyalanine segments were placed into a 0.7 nm reconstruction and phase distribution probabilities were calculated for high-resolution amplitudes obtained from diffraction patterns. Once high-resolution phases were calculated and applied to low-resolution data, a new density map was generated. This iterative process was repeated until no further changes were observed (Wisedchaisri et al., 2011). This method is advantageous over conventional ways of phase extraction from images since obtaining a high-resolution diffraction is not compromised by contrast transfer function (CTF) and sample movements whereas images are adversely affected. Although this method is very tedious to set up and screen but at least a primary model of the membrane protein in its native environment can be produced. By comparing the model obtained from 2D crystallography with functional data, models obtained from 3D crystallography can be validated. Moreover, attempts are required to overcome the hurdles in automating the procedure and acquisition of high-resolution images to improve the obtained resolution from this method.

2) Materials and Methods

2.1) Materials

2.1.1) Chemicals

Chemicals used in this work are listed in Table 2.1.1.

Table 2.1.1: Chemicals.

Name	Source
Acetonitrile	Sigma-Aldrich
Acrylamide/Bisacrylamide	AppliChem
Ammonium peroxodisulfate (APS)	Serva
Ammonium sulfate	AppliChem
Ampicillin	Gerbu
Adenosine triphosphate (ATP)	Sigma-Aldrich
β -Cyclodextrin	Alfa Aesar
β -mercaptoethanole	Serva
Bacto-agar	Roth
Bacto-tryptone	Sigma-Aldrich
BCA reagents	Pierce
BCIP/NBT solution	Roche
Bradford reagent	Roth
Brain polar lipids extract	Avanti polar lipids Inc.
C-flat holey carbon grid	Protochip Inc.
CHAPS	Affimetrix (Anatrace)
Chloramphenicol	Roth
Chloroform	J.T. Baker
Cholesterol	Sigma-Aldrich
Colloidal gold particles	BBInternatioanl
Complete protease inhibitor cocktail	Roche
Coomassie Brilliant Blue	BioMol Feinchem. GmbH
Cyclohexane	J.T. Baker
Cymal-6	Glycon
DDM	Affimetrix (Anatrace)
DLPC	Avanti polar lipids Inc.
DM	Affimetrix (Anatrace)
DMSO	Sigma-Aldrich
DNase I	Roche
DOGS-NTA	Avanti polar lipids Inc.
DOPC	Avanti polar lipids Inc.
DOPG	Avanti polar lipids Inc.

Dried milk powder (fat free)	Sigma-Aldrich
DTE	Sigma-Aldrich
EDTA	Sigma-Aldrich
<i>E. coli</i> polar lipids extract	Avanti polar lipids Inc.
Ethanol (absolute p.a.)	J.T. Baker
Fluoromount	Serva
Fos-choline-12	Affimetrix (Anatrace)
Fos-choline-13	Affimetrix (Anatrace)
Formaldehyde	Sigma-Aldrich
Glucose	Sigma-Aldrich
Glutathione	Roth
Glycerol	Sigma-Aldrich
Guanosine-5'-(β -imino)triphosphate (GppNHp)	Sigma-Aldrich
Guanosine diphosphate	Sigma-Aldrich
Guanosine monophosphate	Sigma-Aldrich
Guanosine triphosphate	Sigma-Aldrich
HCl	J.T. Baker
HEPES	Gerbu Biotechnik GmbH
Holey carbon grids	Agar scientific
Imidazole	Roth
IPTG	Roth
Kanamycin	Gerbu
KCl	Sigma-Aldrich
KH ₂ PO ₄	Sigma-Aldrich
K ₂ HPO ₄	Sigma-Aldrich
Liver polar lipids extract	Avanti polar lipids Inc.
Lysozyme	Sigma-Aldrich
Methanol (absolute p.a.)	J.T. Baker
MgCl ₂	Sigma-Aldrich
MNG-3	Affimetrix (Anatrace)
N ₂ (liquid)	Air Liquid
NaCl	J.T. Baker
NaHCO ₃	Sigma-Aldrich
NaH ₂ PO ₄	Sigma-Aldrich
Na ₂ HPO ₄	Sigma-Aldrich
NaN ₃	Sigma-Aldrich
NaOH	J.T. Baker
NBD-7dehydrocholesterol	Synthesized by group of Dr. Christian Hedberg at MPI Dortmund, Germany
OG	Affimetrix (Anatrace)
Pefabloc	Roth
Phenylmethylsulfonyl fluoride (PMSF)	Sigma-Aldrich
Sodium dodecyl sulfate (SDS)	Boehringer
Tetrabutyl ammonium bromide	Merck

Tetramethylethylen diamine (TEMED)	Serva
Thrombin	Sigma-Aldrich
Tris-HCl	Roth
Triton-X100	Sigma-Aldrich
Tween-20	Calbiochem
Uranyl formate	SP1-chem
X-Gal	Sigma Aldrich
Yeast extract	Roth
Yeast nitrogen base	Roth

2.1.2) Buffers and solutions

All buffers and solutions used in this work are listed below.

General Buffers:

Name	Ingredients
High salt buffer	500 mM NaCl 20 mM Tris-HCl pH 7.5 1 mM MgCl ₂ 1 mM DTE
HPLC buffer	50 mM potassium phosphate pH 6.6 10 mM tetrabutyl ammonium bromide 16% (v/v) ACN
Low salt buffer	100 mM NaCl 20 mM Tris-HCl pH 7.5 1 mM MgCl ₂ 1 mM DTE
Lysis buffer	1 mg/mL Lysozyme 5 mM DTT 50 mM Tris-HCl pH 7.5 0.5 mg/ml Pefabloc
Paraformaldehyde fixation solution	3.6 % (w/v) Formaldehyde in 1x PBS pH 7.5
PBS	2.7 mM KCl 1.7 mM NaH ₂ PO ₄ 10 mM Na ₂ HPO ₄ 137 mM NaCl pH 7.5 with HCl
Solubilization buffer for screening	1% of detergent 20 mM Tris-HCl pH 7.5 300 mM NaCl 10% glycerol

TBS	150 mM NaCl 10 mM Tris pH 7.5 pH 7.5 with NaOH and/or HCl
Uranyl formate staining solution	0.0375 g was added to 5 ml of boiling water and stirred for 5 min. Then 6 μ l of 5 M NaOH was added and stirred for another 5 min

Buffers for purification of Cdc42p

Isolation Buffer 1 (IB1)	TBS 5 mM ATP Complete protease inhibitor (Roche) 2 mM PMSF
Isolation Buffer 2 (IB2)	25 mM Na ₂ PO ₄ pH 7.9 150 mM NaCl 1 mM MgSO ₄ 5 mM DTE 1 mM ATP Complete protease inhibitor (Roche) 2 mM PMSF
Isolation Buffer 3 (IB3)	Isolation Buffer 2 10 mM Glutathione

Buffers for purification of cDHCR7 in Fos-choline13

Solubilization buffer	1% Fos-choline13 50mM Tris-HCl pH 7.5 500 mM NaCl
Binding buffer	0.2% Fos-choline13 50 mM Tris-HCl pH 7.5 500 mM NaCl 10 mM Imidazole
Washing buffer1	0.1% Fos-choline13 300 mM NaCl 50 mM Tris-HCl pH 7.5 30 mM Imidazole
Washing buffer2	0.1% Fos-choline13 300 mM NaCl 50 mM Tris-HCl pH 7.5 50 mM Imidazole

Elution buffer	0.05% Fos-choline13 150 mM NaCl 50 mM Tris-HCl (pH 7.5) 150 mM Imidazole
-----------------------	---

Buffers for purification of hSSD in Fos-choline13

Solubilization buffer	0.5% Fos-choline13 50mM Tris-HCl pH 7.5 700 mM NaCl
Binding buffer	0.2% Fos-choline13 50 mM Tris-HCl pH 7.5 500 mM NaCl 5 mM Imidazole
Washing buffer	0.1% Fos-choline13 300 mM NaCl 50 mM Tris-HCl pH 7.5 20 mM Imidazole
Elution buffer	0.05% Fos-choline13 150 mM NaCl 50 mM Tris-HCl pH 7.5 150 mM Imidazole

Buffers for purification of hDHCR7 in Fos-choline13

Solubilization buffer	1% Fos-choline13 50mM Tris-HCl pH 7.5 500 mM NaCl
Binding buffer	0.2% Fos-choline13 50 mM Tris-HCl pH 7.5 300 mM NaCl 10 mM Imidazole
Washing buffer	0.1% Fos-choline13 300 mM NaCl 50 mM Tris-HCl pH 7.5 30 mM Imidazole
Elution buffer	0.05% Fos-choline13 150 mM NaCl 50 mM Tris-HCl pH 7.5 150 mM Imidazole

Buffers for purification of Gic1

Isolation buffer 1 (IB1)	25 mM NaHPO ₄ pH 7.8 5% glycerol 0.3 M NaCl 1 mM MgCl ₂ 5 mM β-mercaptoethanol 10 mM imidazol Complete protease inhibitors 0.2 mM PMSF
Isolation buffer 2 (IB2)	25 mM NaHPO ₄ pH 7.8 5% glycerol 0.5 M NaCl 1 mM MgCl ₂ 5 mM β-mercaptoethanol 50 mM imidazol 5 mM ATP Complete protease inhibitors 0.2 mM PMSF
Isolation buffer 3 (IB3)	25 mM NaHPO ₄ pH 7.8 5% glycerol 0.3 M NaCl 1 mM MgCl ₂ 5 mM β-mercaptoethanol
Isolation buffer 4 (IB4)	Isolation buffer 3 300 mM imidazole

Buffers for purification of Yeast Septin Complex (YSC)

Isolation Buffer 1 (IB1)	25 mM NaHPO ₄ pH 7.9 5% glycerol 0.3 M NaCl 1 mM MgCl ₂ 5 mM β-mercaptoethanol 6 mM imidazole Complete protease inhibitors (Roche) w/o EDTA 0.2 mM PMSF
Isolation Buffer 2 (IB2)	25 mM NaHPO ₄ pH 7.9 5% glycerol 0.3 M NaCl 0.5 mM MgCl ₂ 5 mM β-mercaptoethanol
Isolation Buffer 3 (IB3)	25 mM NaHPO ₄ pH 7.9 5% glycerol 0.5 M NaCl

	1 mM MgCl ₂ 5 mM β-mercaptoethanol 8 mM imidazole 0.15% Triton X100 Complete protease inhibitors w/o EDTA 0.2 mM PMSF 10 μM GDP, GTP and ATP
Isolation Buffer 4 (IB4)	20 mM HEPES pH 8.0 100 mM NaCl 1 mM MgCl ₂ 5 mM DTE
Isolation Buffer 5 (IB5)	20 mM HEPES pH8.0 500 mM NaCl 1 mM MgCl ₂ 5 mM DTE
Isolation Buffer 6 (IB6)	20 mM Hepes pH 8.0 0.5 M NaCl 1 mM MgCl ₂ 5 mM DTE

Buffer for gel filtration of Cdc42p

Gel filtration buffer	150 mM NaCl 20 mM Tris-HCl pH 7.5 1 mM MgCl ₂ 1 mM DTE 10 μM GDP
------------------------------	---

Buffer for gel filtration of DHCR7

Gel filtration buffer	0.05% Fos-Choline13 150 mM NaCl 20 mM Tris-HCl pH 7.5
------------------------------	---

Buffer for gel filtration of YSC

Gel filtration buffer	500 mM NaCl 20 mM HEPES pH 8 1 mM MgCl ₂ 5 mM DTT
------------------------------	---

Solutions for SDS-PAGE

Stacking gel (5%)	5% acryl-bisacrylamide mix 1.5 M Tris-HCl pH 8.8 10% SDS 10 % APS 0.02% TEMED
Separation gel (15%)	15% acryl-bisacrylamide mix 1.5 M Tris-HCl pH 8.8 10% SDS 10 % APS 0.02% TEMED

Buffers for Western blot

Transfer Buffer	25 mM Tris-HCl pH 7.5 192 mM Glycine 10 % (v/v) MeOH
TBS-TT	250 mM NaCl 10 mM Tris-HCl pH 7.5 0.025 % (v/v) Tween-20 0.1 % (v/v) Triton X-100 pH 7.4 with NaOH and/or HCl
Blocking solution	5 % (w/v) dried milk powder (fat free)
Primary antibody solution	1:4000 <i>mouse</i> -anti-His antibody or 1:500 α -Cdc3 antibody 0.5 % (w/v) dried milk powder in 1x TBS
Secondary antibody solution	1:1000 <i>goat</i> -anti-Mouse or anti-rabbit antibody (coupled to alkaline phosphatase) 0.5 % (w/v) dried milk powder in 1x TBS
Resolving solution	BCIP/NBT

Buffers for Gas Chromatography (GC-MS) sample preparation

Lysis buffer	0.9% NaCl
Injection buffer	Cyclohexane

2.1.3) Media

In Table 2.1.3 all media used in this work are shown. All media were autoclaved or sterile filtered before use.

Table 2.1.3: Media.

Name	Ingredients
LB, for 1 L	1% (w/v) bacto-tryptone (10 g) 0.5% (w/v) yeast extract (5 g) 200 mM NaCl (10 g) ddH ₂ O to 1 L pH 7.0
Insect cell growth medium	TC100 + 10% FCS
Mammalian cell growth medium	DMEM/F12 1:1 (PAN Biotech) 10 % FCS (GIBCO) 1:1000 Penicillin (5,000 U) Streptomycin (5,000 µg) (PenStrep, Invitrogen)
Mammalian delipidated medium, for sterol depletion	DMEM/F12 1:1 (PAN Biotech) 10 % delipidated FCS (PAN Biotech) 50 µM mevastatin (Sigma-Aldrich) 50 µM sodium mevalonate (Sigma-Aldrich)
SD, for 1 L	6.7 g yeast nitrogen base 20 g Bacto-agar ddH ₂ O to 1 L Add 50 mL 40% sterile glucose
SOC, for 1 L	2% (w/v) bacto-tryptone (20 g) 0.5% (w/v) yeast extract (5 g) 10 mM NaCl (0.584 g) 2.5 mM KCl (0.186 g) 10 mM MgCl ₂ (0.952 g) 20 mM glucose (3.603 g) ddH ₂ O to 1 L pH 7.0
TB, for 1 L	1.2% (w/v) bacto-tryptone (12 g) 2.4% (w/v) yeast extract (24 g) 4 mL glycerol 15 mM KH ₂ PO ₄ (2,13 g) 72 mM K ₂ HPO ₄ (12,54 g) ddH ₂ O to 1 L pH 7.0

2.1.4) Bacterial strains, yeast, insect and mammalian cells

The bacterial strains and mammalian cell line used in this work are listed in Table 2.1.4.

Table 2.1.4: Bacterial strains and mammalian cell lines.

Name	Source	Additional information
BL21 Rosetta (DE3) pLysS (<i>E.coli</i>)	Novagen	F ⁻ ompT hsdS _B (R _B ⁻ m _B ⁻) gal dcm λ(DE3 [lacI lacUV5-T7 gene 1 ind1 sam7 nin5]) pLysSRARE (Cam ^R)
DH10EmbacY	Geneva Biotech	Used for Bac-to-Bac system
EGY48	Invitrogen	
HEK-293	MPI Dortmund	Human Embryonic Kidney 293 cell line
OmniMax (<i>E.coli</i>)	Invitrogen	F' {proAB+ lacIq lacZΔM15 Tn10(TetR) Δ(ccdAB)} mcAr Δ(mrr-hsdRMS-mcrBC) φ80(lacZ)ΔM15 Δ(lacZYA-argF) U169 endA1 recA1 supE44 thi-1 gyrA96 reA1 tonA panD
Sf9	Invitrogen	Used for baculovirus production
Sf21	Invitrogen	Used for baculovirus-based expression

2.1.5) Oligonucleotide vectors

All plasmids used for septin, Gic1 and Cdc42p (Table 2.1.5) used in this work were taken from the plasmid bank of the group of Dr. Marian Farkasovsky (Institute of Molecular Biology SAS, Slovak Republic) and emeritus group of Prof. Dr. Alfred Wittinghofer (Max-Planck-Institute of Molecular Physiology, Dortmund). Plasmids used to study DHCR7 were either prepared by me, Sandra Bergbrede or the DPF (Dortmund Protein Facility).

Table 2.1.5: Plasmids

Name	Gene	Additional information	Antibiotic resistance
Golgi marker	RFP-GalT	Coupled to red fluorescent protein	Kan
Peroxisome marker	RFP-PXMP2	Coupled to red fluorescent protein	Amp
p118	GFP_DHCR7 <i>Homo sapiens</i>	N-terminal 6x His, N-terminal GFP	Amp

p285	<i>dchr7</i> from <i>Coxiella bruneei</i>	N-terminal 10x His	Amp	
p286	<i>dchr7</i> from <i>Plesiocystis pacifica</i>	N-terminal 10x His	Amp	
p295	Sterol sensing domain of human <i>dchr7</i>	C-terminal 6x His	Amp	
P455	hDHCR7	N-terminal His tag	Amp	
pEG202	Genes analyzed in Yeast 2-H assay	Yeast two-hybrid assay	Amp	
pGEX4T-1	Cdc42p	GST tag	Amp Cm	&
pFM453	Cdc10 + Cdc11	6x His-Cdc10	Amp	
pFM455	Cdc3 + Cdc12	Cdc3-6x His MBP-Cdc12	Kan	
pFM812	Gic1 (104-314)	His tag	Amp Cm	&
pJG4-5	GAL1 Genes analyzed in Yeast 2-H assay	Yeast two-hybrid assay	Amp	
pFM455	Cdc3 + Cdc12	Cdc3-6x His MBP-Cdc12	Kan	
pSH18-34	LacZ	Yeast two-hybrid assay		

2.1.6) Antibodies

In Table 2.1.6 all commercialized kits used in this work are listed.

Table 2.1.6: Antibodies

Antibody	Manufacturer
Mouse anti-His	Sigma Aldrich
Goat anti-mouse (coupled to alkaline phosphatase)	Calbiochem
Anti-Cdc3	Gift from Michael Knop, DKFZ-ZMBH, Heidelberg, Germany
Anti-Cdc11	Santa Cruz Biotechnology Inc.

Anti-Cdc42p

Santa Cruz Biotechnology Inc.

2.1.7) Consumables

Table 2.1.7: Consumables

Consumable	Manufacturer	Details
3D crystallography kits	Protein crystallography setup	Qiagen
Corning® next generation CrystalEX microplates 3550	Corning Inc.	96-well plates
Amicon ultra-4	Millipore	Cut-off: 10 kDa
Amicon ultra-15	Millipore	Cut-off: 10 kDa
Amylose resin	New England Biolabs	80-mL volume
C18-column	Bischoff chromatography	Prontosil C18 120-5-C18-AQ column
Cell culture flask	BectonDickinson Falcon	75 cm ²
Cell culture plate	BD Biosciences	10 cm
Dialysis bag	Spectrum labs	Cut-off: 12-14 kDa
FuGENE HD	Roche	
Glass slide	Thermo Fisher Scientific	6 x 2 cm
Graduated pipette	Sarstedt	1, 5, 10, 25 mL serological pipette
GSH-sepharose column	QIAGEN	80-mL volume
Insect cell culture bottle	Bellco Glass	
Micropipette tips	Sarstedt	10, 100 µL Biosphere
Micropipette tips (ReFill-System)	Nerbe plus	10 µL, 200 µL, 1250 µL
Ni-NTA column	QIAGEN	50-mL volume
PVDF membrane	Whatman	Polyvinylidene fluoride
Parafilm	Pechiney Plastic Packaging	Parafilm "M"
PD-10 column	GE Healthcare	Desalting column
Qiaprep Spin MiniPrep	Plasmid purification	Qiagen
Q-Sepharose (Hi-Trap)	Amersham	
Reaction tubes	eppendorf	0.5, 1.5, 2.0 mL
Reaction tubes	BectonDickinson Falcon	15 and 50 mL
VivaSpin 500 columns	Sartorius stedim biotech	Cut-off: 10 kDa

2.1.8) Instruments

Table 2.1.8: Instruments

Instrument	Manufacturer	Details
Äkta purifier	GE Healthcare	
Superdex 75 (10/30 GL)	GE Healthcare	
Superdex S200 (16/60)	GE Healthcare	
Superose 12 (10/30 GL)	GE Healthcare	
Sepharyl S400	GE Healthcare	
Analytical balance	Sartorius	
Beckman centrifuges	Beckman	
JA-25.50 rotor		
JLA-8100 rotor		
Ti-50 rotor		
Biological Safety Cabinet	Heraeus Instruments	HS12
Confocal fluorescence Microscope	Leica	DM IRBE - TCS SP2
Objective	Leica	63x Oil, NA: 1.4
Cryo plunge3	Gatan Inc.	
Electron microscope JEM- 1400	JEOL	
Electron microscope JEM- 3200FSC	JEOL	
Freezing Container	Nalgene	Mr. Frosty (-1°C/min)
Gel documentation	Bio-Rad Lab. GmbH	Versadoc
GC-MS	Thermo	Focus GC
Mass spectrometer	Thermo	PolarisQ
Autosampler	CTC Analytics	Liquid
	Sampler A200SE	
Glassware, reusable	Brand and Schott	
High pressure liquid chromatography instrument	Waters	600S, 717 plus, 2487 and 2475
Image film	Kodak	SO163 3.25x4 inch
Incubator	NuAire	CO ₂ AirJacketed
Light microscope	Leitz	Diavert
Objective	Leitz	20/0.32
Objective	Phaco	10/0.25
Magnetic Stirrer	Bellco Biotechnology	Bell-Ennium 5 Position mag. stirr.
Mercury lamp	Leica	HG 50W
Microfluidizer	Microfluidics Corporation	
Micropipettes	Gilson	0.1-2, 2-20, 50-200, 100-1000 µL
Pipette aid	Brand	Accu-jet
Pipette aid	Eppendorf	
Plunge freezing instrument	Gatan Inc.	
Q-sepharose (Hi-Trap)	Amersham	
Sonicator	G. Heinemann	W250
Tabletop Centrifuge	Eppendorf	5810R

Tabletop Centrifuge	Beckman	Allegra X-22R
Tango 3160 drum scanner	Heidelberg AG	
Ultracentrifuge (UC)	Beckman	Beckman Optima TLX
Vortex	Scientific Industries	
Waterbath	Memmert	

2.1.9) Software

Software used in this study for electron microscopy image processing or modeling of EM images:

Amira (Mercury Computer Systems Inc.), IMOD software package, EMAN2, SPARX and UCSF Chimera

Phyre2 server (www.sbg.bio.ic.ac.uk/phyre2/)

Software used in this study for fluorescent image processing:

Fiji with compiled ImageJ Vers. 1.44h

Plug-in: JaCoP Vers. May 2010

2.2) Methods

2.2.1) Expression screening

2.2.1.1) Expression screening in *E. coli*

A 100-ml flask with 30 ml LB medium containing 125 µg/ml ampicillin (w/v) was prepared for an overnight culture. The culture was inoculated using a single clone from a LB agar plate. After overnight incubation, two 1-liter flasks one with 250 ml 2TY medium containing 125 µg/ml ampicillin (w/v) and one with 250 ml TB medium containing 125 µg/ml ampicillin (w/v) were inoculated with 2.5 ml of the pre-culture each. The cultures were grown till the desirable OD₆₀₀ was reached. Then, expression was induced using IPTG (Isopropyl β-D-1-thiogalactopyranoside) and four 70-ml aliquots of each type of media were made and incubated each at 20°C, 25°C, 30°C and 37°C. Samples (15 ml) were taken after 1h, 2h, 3h and overnight. The cells were centrifuged and the resulting cell pellet was stored at -20°C. The cell pellets were lysed and the membrane fraction was solubilized in the solubilization buffer and subjected to western blot to identify the best condition. After finding the best condition in which, protein was expressed to a reasonable quantity, 9 l of media (6 x 1.5 l) in 5-liter flasks was used for a large-scale expression.

2.2.1.2) Expression in insect cells

In order to express full-length hDHCR7-EGFP (in pOPIN vector, Oxford expression technologies), Sf21 cells at exponential growth phase were used. In order to propagate virus, p118 (hDHCR7-EGFP) was transfected along with a BACmid carrying viral genome into Sf9 cells. Virus was harvested after 5-7 days (1-2 days after the highest fluorescent signal was achieved). Virus was further amplified using Sf9 cells at density of 1×10^6 cell/ml for 5-7 days. For expression, Cells were prepared at density of 1×10^6 cell/ml in 3-liter flasks connected to air-supplier on day 0. On day 1, virus was used to initiate the expression. Flasks were covered with aluminum foils to prevent degradation of virus particles by light. After expression screening to achieve optimal MOI and expression longevity, MOI of 1 for 48 hours was found to result in a constant and high level of expression. On day 3, expression level was monitored with fluorescent microscope and cells were subsequently harvested. Alternatively, *hDHCR7* (in pFG vector) was transfected into DH10EmbacY cells. The transformed cells were cultured on plates containing appropriate antibiotic (Amp/Kan) + 10 µg/ml Gent + 10 µg/ml Tet + 0.5 mM IPTG + 400 µg/ml X-Gal. The recombinant plasmid was extracted from white colonies. 0.5×10^6 Sf9 cells were seeded into 6-well plates and transfected with 20 µg of DNA and 10 µl FuGene. The virus was harvested after 2 days. The virus was amplified using 0.5×10^6 cell/ml. In this respect, the cell density was counted every day and maintained at 0.5×10^6 cell/ml until no further cell duplication was achieved. Virus should be normally harvested after 4-5 days. If cells stop growing after addition of virus, defective virus production has occurred and lower amount of virus should be used for amplification. At this time, virus was harvested and stored at 4°C. In order to express the hDHCR7, different concentrations of virus (MOI >1) was used to find out the optimal condition for expression. Fluorescent signal was monitored every day and cells were harvested a day after the highest fluorescent signal was achieved. Moreover, cells should stop dividing after virus addition otherwise virus amplification occurs instead of protein production.

2.2.2) Protein purification

2.2.2.1) Purification of Yeast Septin Complex (YSC)

To express the yeast septins, *E. coli* strain BL21 (DE3) Rosetta (Novagen) was transformed with plasmid pFM455 (carrying the *cdc3* and *cdc12* genes) and pFM453 (carrying *cdc10* and *cdc11* genes). The cells were grown in TB supplemented with ampicillin (50 mg/l), kanamycin (30 mg/l) and chloramphenicol (12.5 mg/l) at 37°C and induced at OD₆₀₀ of 0.6 by addition of 0.4 mM IPTG (1M stock). Following overnight incubation at 28°C, cells were harvested by centrifugation and resuspended in isolation buffer IB1 (25 mM NaHPO₄ pH 7.9, 5% glycerol, 0.3 M NaCl, 1 mM MgCl₂, 5 mM β-mercaptoethanol, 6 mM imidazole, Complete protease inhibitors (Roche) w/o EDTA and 0.2 mM PMSF) and disrupted by a microfluidizer (Microfluidics Co.) and supplemented with 0.1% Triton X100. After centrifugation at

50,000 rpm, the supernatant was applied to a 50-ml (V_i) Ni-NTA-Sepharose (0.5 ml/min) and washed with 300 ml buffer IB3 (25 mM NaHPO₄ pH 7.9, 5% glycerol, 0.5 M NaCl, 1 mM MgCl₂, 5 mM β-mercaptoethanol, 8 mM imidazole, 0.15% Triton X100, protease inhibitors Complete w/o EDTA, 0.2 mM PMSF and 10 μM of GDP, GTP and ATP) and with 100 ml of buffer IB2 (25 mM NaHPO₄ pH 7.9, 5% glycerol, 0.3 M NaCl, 0.5 mM MgCl₂ and 5 mM β-mercaptoethanol). The septin complex was eluted with 250 mM imidazole in buffer IB2. The eluate was diluted 1:1 with 25 mM NaHPO₄ pH 7.9 and 5 mM β-mercaptoethanol and purified further over amylose resin (New England Biolabs, 0.5 ml/min) equilibrated with IB2. Amylose resin was washed with 1 volume of IB2 and eluted with 20 mM maltose in IB2. To the eluate, 4 volumes of 25 mM NaHPO₄ pH 7.9 and 5 mM β-mercaptoethanol were added and MBP was cleaved overnight from the complex by using thrombin at 4°C (5-10 U/ mg protein) and separated from the complex on Q-Sepharose (Hi-Trap, Amersham). Protein was loaded on the column equilibrated with IB4 (20 mM HEPES pH 8.0, 100 mM NaCl, 1 mM MgCl₂ and 5 mM DTE), washed with 5 volumes of IB4 and eluted with IB5 (20 mM HEPES pH 8.0, 500 mM NaCl, 1 mM MgCl₂ and 5 mM DTE). As the last purification step (optional), gel-filtration chromatography using either Superdex 200 or Sephacryl S-400 in IB6 (20 mM HEPES pH 8.0, 0.5 M NaCl, 1 mM MgCl₂ and 5 mM DTE) was performed. Protein was concentrated with centrifugal filter devices Amicon Ultra – 15 (Millipore), divided into aliquots, and stored at –80°C.

2.2.2.2) Purification of Gic1

For the bacterial expression of Gic1 (104-314), plasmid pFM812 (constructed by Dr. Marian Farkasovsky, Institute of Molecular Biology SAS, Slovak Republic) was transformed in *E. coli* strain BL21 (DE3) Rosetta (Novagen). The cells were grown in TB supplemented with ampicillin and chloramphenicol at 37°C and induced at an optical density OD₆₀₀ of 0.6 by addition of 0.2 mM IPTG. After 8 hours at 28°C, cells were harvested by centrifugation and resuspended in isolation buffer IB1 (25 mM NaHPO₄ pH 7.8, 5% glycerol, 0.3 M NaCl, 1 mM MgCl₂, 5 mM β-mercaptoethanol, 10 mM imidazole, Complete protease inhibitors (Roche) and 0.2 mM PMSF) and disrupted by microfluidizer (Microfluidics Co.). Supernatant, after high-speed centrifugation at 50,000 rpm, was applied on a 50-mL (V_i) Ni-NTA-Sepharose (Qiagen), washed with 300 mL buffer IB2 (25 mM NaHPO₄ pH 7.8, 5% glycerol, 0.5 M NaCl, 1 mM MgCl₂, 5 mM β-mercaptoethanol, 50 mM imidazole, 5 mM ATP, Complete protease inhibitors and 0.2 mM PMSF) and with 100 mL of buffer IB3 (25 mM NaHPO₄ pH 7.8, 5% glycerol, 0.3 M NaCl, 1 mM MgCl₂ and 5 mM β-mercaptoethanol). Gic1 (104-314) was eluted with 300 mM imidazole in buffer IB3 and GST was cleaved by using thrombin at 4°C. GST and undigested fusion protein were bound on Glutathione Sepharose (GE Healthcare) and Gic1 (104-314) in flow-through was concentrated and further purified using Superdex S200 (GE Healthcare).

2.2.2.3) Purification of Cdc42p

For the bacterial expression of full-length Cdc42p, plasmid pGEX4T-1 (constructed by Dr. Marian Farkasovsky, Institute of Molecular Biology SAS, Slovak Republic) was transformed in *E. coli* strain BL21 (DE3) Rosetta (Novagen). The cells were grown in TB, supplemented with ampicillin and chloramphenicol at 37°C. expression was initiated at an optical density OD₆₀₀ of 0.6 by addition of 0.25 mM IPTG. After 16 hours at 20°C, cells were harvested by centrifugation and resuspended in isolation buffer IB1 (TBS supplemented with 5 mM ATP, Complete protease inhibitors (Roche) and 0.2 mM PMSF) and disrupted by a microfluidizer (Microfluidics Co.). Supernatant after high-speed centrifugation at 50,000 rpm was applied on a 80-mL (V_t) GSH-Sepharose (Qiagen) equilibrated with IB2 (25 mM Na₂PO₄ pH 7.9, 150 mM NaCl, 1 mM MgSO₄, 5 mM DTT, 1 mM ATP, Complete protease inhibitor (Roche) and 2 mM PMSF) at an 0.5 mL/min. the column was washed with 300 mL of buffer IB2 without protease inhibitor. Cdc42p was eluted from the column using 200 mL buffer IB3 (IB2 with 10 mM Glutathione). GST tag was cleaved using thrombin (200 U) at 4°C. Cdc42p and GST tag were further separated using Superdex S200 (GE Healthcare).

2.2.2.4) Purification of hSSD

In order to express the sterol-sensing domain of the human DHCR7, C43 cells were grown in 2TY medium. The expression was induced at OD₆₀₀ of 0.6 using 0.6 mM IPTG. The temperature was shifted to 25°C and cells were harvested after an overnight incubation. Cells from 9 liters of expression were lysed and centrifuged at 6,000 rpm to remove the cell pellet and unbroken cells. The supernatant was subjected to centrifugation at 40,000 rpm for 1 h to pellet the membrane fraction. The membrane was resuspended in TBS buffer and stripped using 0.2 M urea for 10 minutes and then centrifuged at 40,000 rpm to obtain the membrane. The stripped membrane was resuspended in TBS at a total volume of 50 ml. For small-scale purification, 3 ml of the stripped membrane was solubilized in solubilization buffer (0.5% Fos-choline®-13, 700 mM NaCl and 50 mM Tris-Hcl pH 7.5) in the final volume of 12 ml for 2 hours at 4°C with gentle shaking. The solubilized sample was centrifuged at 35,000 rpm for 30 minutes at 4°C. To the solubilized fraction, 0.8 ml of Ni-NTA beads already calibrated with the binding buffer (0.2% Fos-choline®-13, 500 mM NaCl, 50 mM Tris-HCl pH 7.5 and 5 mM imidazole) was added and incubated at 4°C with gentle agitation for 1 hour. The sample was packed in Econo-Pac chromatography column (BIO-RAD). The beads were washed with 10 ml of binding and washing buffers (0.1% Fos-choline®-13, 300 mM NaCl, 50 mM Tris-Hcl pH 7.5 and 20 mM imidazole) respectively. Protein was eluted with 5 ml of elution buffer (0.05% Fos-choline®-13, 150 mM NaCl, 50 mM Trsi-Hcl pH 7.5 and 150 mM imidazole) and 5 drops per tube was collected. Protein content of fractions was assessed using Bradford assay and protein-rich fractions were mixed and dialyzed to remove the imidazole. The sample was then

concentrated using Amicon column (cut-off of 10 kDa, Millipore) and injected into Superdex 75 (GE Healthcare) for further purification.

For large-scale purification, 15 ml of membrane was used. For solubilization, final volume was adjusted to 50 ml with solubilization buffer. The solubilized fraction was incubated with 4 ml of Ni-NTA beads and 5 mM imidazole. Column was washed with 50 ml of binding and washing buffers each. Protein was eluted with 20 ml of elution buffer and 15 drops per tube was collected.

2.2.2.5) Purification of cDHCR7

The *DHCR7* gene of *C. burnettii* was expressed in *E. coli* strain C43. At OD₆₀₀ of 0.8 cells were induced with 0.6 mM IPTG and the temperature was shifted to 25°C. Cells were harvested after an overnight incubation. Cells from 9 liters of expression were lysed and centrifuged at 6,000 rpm to remove the cell pellet and unbroken cells. The supernatant was subjected to centrifugation at 40,000 rpm for 1h to pellet the membrane fraction. The membrane was resuspended in TBS buffer and stripped using 0.2 M urea for 10 minutes and then centrifuged at 40,000 rpm to obtain the membrane. The stripped membrane was resuspended in TBS in total volume of 50 ml. For small-scale purification, 5 ml of stripped membrane was solubilized in the solubilization buffer (1% Fos-choline®-13, 500 mM NaCl and 50 mM Tris-HCl pH 7.5) in the final volume of 15 ml for 2 hours at 4°C with gentle shaking. The sample was centrifuged at 35,000 rpm for 30 minutes at 4°C. To the solubilized fraction, 1 ml of Ni-NTA beads already calibrated with the binding buffer (0.2% Fos-choline®-13, 500 mM NaCl, 50 mM Tris-HCl pH 7.5 and 10 mM imidazole) was added with 10 mM imidazole and incubated at 4°C with gentle agitation for an overnight. The sample was packed in Econo-Pac chromatography column (BIO-RAD). The beads were washed with 10 ml of binding buffer and washing buffer1 (0.1% Fos-choline®-13, 300 mM NaCl, 50 mM Tris-HCl pH 7.5 and 30 mM imidazole) and 5 ml of washing buffer2 (0.1% Fos-choline®-13, 300 mM NaCl, 50 mM Tris-HCl pH 7.5 and 50 mM imidazole). Protein was eluted with 5 ml of the elution buffer (0.05% Fos-choline®-13, 150 mM NaCl, 50 mM Tris-HCl pH 7.5 and 150 mM imidazole) and 5 drops per tube was collected.

2.2.2.6) Purification of hDHCR7-EGFP

The EGFP-hDHCR7 was expressed in Sf21 cells at a MOI of 1. The cells were harvested after 48-72 h. The cells were lysed and the membrane was prepared and stripped. For small-scale purification, 3 ml of the stripped membrane (membrane obtained from 20-25 liters of expression resuspended in final volume of 50 ml) was solubilized in the solubilization buffer (1% Fos-choline®-13, 500 mM NaCl and 50mM Tris-HCl pH 7.5) in the final volume of 12 ml for 2 hours at 4°C with gentle shaking. The solubilized sample was centrifuged at 35,000 rpm for 30 minutes at 4°C. To the solubilized fraction, 1 ml of Ni-NTA

beads already calibrated with the binding buffer (0.2% Fos-choline®-13, 300 mM NaCl, 50 mM Tris-HCl pH 7.5 and 10 mM imidazole) was added with 10 mM imidazole and incubated at 4°C with gentle agitation for overnight. The sample was packed in Econo-Pac chromatography column (BIO-RAD). The beads were washed with 10 ml of binding and washing buffers (0.1% Fos-choline®-13, 300 mM NaCl, 50 mM Tris-HCl pH 7.5 and 30 mM imidazole). Protein was eluted with 5 ml of the elution buffer (0.05% Fos-choline®-13, 150 mM NaCl, 50 mM Tris-HCl pH 7.5 and 150 mM imidazole) and 5 drops per tube was collected. The protein was dialyzed, concentrated using Amicon column (cut-off of 10 kDa) and injected into Superose 12 (GE Healthcare). The fractions of high UV and fluorescent absorption (emission of 509 nm) were collected.

2.2.3) Cell lysis and membrane stripping

At the end of expression, cells were harvested by centrifugation at 6,000 rpm for 15 minutes at 4°C. The pellet was resuspended in 200 ml of ice-cold 1x TBS and homogenized using a hard brush until no clumps were left. In order to inactivate protease activity, 0.5 ml of a 4.2% PMSF (w/v) stock solution and 2 tablets of protease inhibitor cocktail (Roche) were added. Some DNaseI was added to the solution in order to digest DNA. The solution was passed through the microfluidizer (Microfluidics Corporation) 3 times at 500-600 kPa. After each round 0.5 ml of PMSF stock solution was added. Afterwards the cell debris was removed by centrifugation at 6,000 rpm for 20 minutes at 4°C. The cell debris and unbroken cells were discarded and the supernatant was kept. The resultant supernatant was centrifuged at 40,000 rpm for 1 hour at 4°C to isolate the membrane fraction. The pellet that contained the membranes was resuspended in a glass homogenizer in TBS to final volume of 50 ml. Aliquots of 5-10 mL were frozen in liquid N₂ and stored at -20°C for short time storage or at -80°C for long time storage.

In order to remove membrane-anchored protein, membrane is usually stripped. Resuspended membrane obtained from 9 liters of expression was treated with 200-250 mM urea on ice briefly and subsequently centrifuged at 40,000 rpm for 1 hour at 4°C. A sample of the supernatant containing stripped fraction was taken as a “stripped fraction” to monitor the fraction on western blot. Detection of a band on western blot implies that protein is not properly folded into the membrane. Stripped membrane was resuspended in 1x TBS in final volume of 50 ml.

2.2.4) Solubilization screening

In this study, nine different detergents were tested namely, DDM (n-Dodecyl-β-maltoside), DM (n-decyl-β-maltoside), CHAPS, OG (n-Octyl-β-D-Glucopyranoside), Fos-Choline 12, Fos-Choline 13, MNG-3, Cymal-6 and Triton-X100.

After isolating and resuspending membrane in TBS (final volume of 50 ml), 100 μ l of membrane was used with 200 μ l of solubilization buffer containing respective detergents (1%) and incubated for 2 hour at 4°C. Then, a sample was taken from each detergent and mixed with SDS-loading buffer and named “before solubilization (B)” and the rest was centrifuged at 50,000 rpm for 30 minutes at 4°C. Another sample was taken from the supernatant of each detergent and mixed with SDS-loading buffer and named “after solubilization (A)”. Samples were run on SDS- PAGE followed by western blotting. The detergent that gives the same band density before and after centrifuge is the optimal detergent. In order to optimize the solubilization efficiency, detergent concentration, salt concentration or longevity of solubilization could be altered. Moreover, dilution factor could also lead to a higher yield of the desirable protein. For instance, 300 μ l of solubilization buffer for 100 μ l of hSSD membrane, 200 μ l for 100 μ l of cDHCR7 membrane and 200 μ l for 100 μ l of hDHCR7 membrane were used.

2.2.5) Detergent exchange

One approach to optimize a crystal of a membrane protein is to exchange the detergent to improve the protein-protein contact. In this regard, different detergents namely, Cymal-6, Fos-choline12, DDM and MNG-3 were used using two different approaches.

2.2.5.1) On-column exchange

Proteins, either hSSD or cDHCR7 were solubilized in Fos-Choline13. Then, they were incubated with Ni-NTA according to the protocols described before. Subsequently, Fos-Choline13 was substituted with different detergents in the binding, washing and elution buffers with the same concentration as of Fos-Choline13. After elution, protein content of fractions was assessed using Bradford assay. If detergent exchange fails, the protein precipitates on the column and no protein is detected in Bradford assay.

2.2.5.2) During gel filtration

Another approach to exchange the detergent is to remove the detergent after gel filtration. In this regard, proteins eluted from the gel filtration column were dialyzed with various detergents (1% w/v) for a week. Next, proteins were centrifuged at 13,000 rpm for 10 min to remove the aggregates and supernatant was injected into a gel filtration column and run with a buffer containing the desired detergent. In case of a successful exchange, a mono-dispersed peak is obtained. Otherwise, protein aggregates elute in void volume.

2.2.6) Protein concentration estimation

2.2.6.1) Bradford assay

2 μL of the protein solution was added to 48 μl of ddH₂O and combined with 150 μl of Bradford solution (Roth). This test was done in a 96-well plate (BD Falcon). Elution fractions that did not contain any proteins stayed brownish purple. Fractions with a high protein concentration turned blue. The high-protein-content fractions were pooled for dialysis and gel filtration.

2.2.6.2) BCA

BCA test or Smith assay is used to measure protein quantity precisely. The method is based on reduction of Cu⁺² to Cu⁺¹ by peptide bond. Then two molecules of bicinchoninic acid bind to Cu⁺¹ to produce a purple color, which absorbs light at the wavelength of 562 nm. The BCA protein assay can measure protein concentration between 0.2 to 2 mg/ml. 50 μl of BCA reagent A was mixed with 150 μl BCA reagent B and added to 1 μl of protein of interest. As a control, BSA (bovine serum albumin) was used at known concentrations. The sample was incubated at 37°C for 30 min and adsorption was measured at 562 nm.

2.2.7) Semidenaturing SDS polyacrylamide gel electrophoresis (SDS-PAGE)

In this work the principle SDS polyacrylamide gel electrophoresis (Laemmli, 1970; Shapiro, Vinuela, & Maizel Jr, 1967) was used. However, the samples were not denatured by heating. Therefore the size shown by the protein ladder (PageRuler Prestained Protein Ladder, Fermentas) on the 15% SDS-PAGE does not accurately represent the actual size of the proteins. The electrophoresis was performed in a BIO-RAD system. If Western blotting should be performed afterwards a 6x His Protein ladder (Qiagen) was applied as well. After the run, the gel was stained in a Coomassie Brilliant blue solution and destained overnight in 10% acetic acid. The SDS-PAGE was scanned in a flatbed scanner (Hewlett-Packard).

2.2.8) Western blotting

Western blotting was done using a standard blotting technique (Towbin, Staehelin, & Gordon, 1979). Proteins were transferred in a semi-dry Western blotting chamber (PEQLAB) from a SDS-PAGE gel to a PVDF membrane (Whatman). In order to build a nice stack between the anode and cathode plate 4 filter papers (Whatman) were pre-wetted in transfer buffer. The PVDF membrane was activated for 10 seconds in 100% methanol. The stack was assembled in the following way. Two pre-wetted filter papers were put onto the anode plate, followed by the activated PVDF membrane, the SDS-gel, the other two pre-wetted

filter papers and the cathode plate. The blotting was done at 1 mA/cm^2 for 1 hour and was completed when the prestained protein marker had merged to the membrane. The membrane was transferred to 5% (w/v) milk powder in 1x TBS solution and incubated for 1 hour. After blocking the membrane, it was incubated with the primary anti-His antibody (Sigma) for at least 1 hour at room temperature with gentle agitation. The membrane was washed once with 1x TBS-TT and twice with 1x TBS each time for 10 minutes and then incubated with the secondary antibody (Millipore) for at least 1 hour at room temperature with gentle agitation. After incubation the membrane was washed once with 1x TBS-TT and twice with 1x TBS each time for 10 minutes again. The blot was developed with adding 1 mL of BCIP/NBT solution (Roche) to the membrane. The reaction was stopped after 15 seconds by washing once with 1x TBS. The blot was scanned in a flatbed scanner (Hewlett-Packard).

2.2.9) Preparation of septin filaments

In order to study the septin filaments, $0.3 \mu\text{M}$ of different septin complexes (wild-type, EGFP tagged, Cdc10 Δ , Cdc11 Δ or Cdc10(30-322) mutants) were prepared in a high salt-buffer (500 mM NaCl, 20 mM Tris-HCl pH 7.5 and 1 mM DTE) and dialyzed against a low-salt buffer (100 mM NaCl, 20 mM Tris-HCl pH 7.5 and 1 mM DTE) at 4°C for 16 h. Five times higher molar concentration of Gic1 ($1.5 \mu\text{M}$) was added to the septin octamers either to the septin complex during dialysis or to the filaments. Considering that Gic1 elutes in gel filtration with a size between dimer and trimer and each septin has a pair of Cdc10, the final ratio of Gic1 to Cdc10 is 2.5.

For studies that involved Cdc42p, $0.1 \mu\text{M}$ of the septin octamer with or without $0.5 \mu\text{M}$ of Gic1 were used. Different concentrations of Cdc42p(GDP) and Cdc42p(GppNHp) were added either during dialysis or to the preassembled complexes. Briefly, for the studies, which addressed the binding of Cdc42p(GppNHp) to the septin-Gic1 complex, $0.5 \mu\text{M}$ of Cdc42p was used during dialysis. $5 \mu\text{M}$ of Cdc42p was added to the septin filaments or the septin-Gic1 complex to show the disassembly of the corresponding complexes.

The samples used to examine the effect of nucleotides contained $0.5 \mu\text{M}$ of septin octamers with or without $2.5 \mu\text{M}$ of Gic1. Then varying concentrations of GMP, GDP, GTP and GppNHp were added to the samples (as stated in figure legends) and incubated for 16 h.

For Cryo-electron tomography, $2 \mu\text{M}$ of YSC and $10 \mu\text{M}$ of Gic1 with or without $10 \mu\text{M}$ Cdc42p-GppNHp were dialyzed together for 16 h and plunged (as explained in 2.2.12).

For antibody decoration, $5 \mu\text{l}$ of polyclonal antibodies against Cdc11 (Santa Cruz Biotechnology Inc.) or Cdc3 (a gift from Michael Knop, DKFZ-ZMBH, Heidelberg, Germany) (diluted 1:100) were added to $20 \mu\text{l}$ of a sample containing either septin-Gic1 complex or the septin octamers (generated by GTP, Cdc42p-GDP or both) and incubated overnight at 4°C to allow efficient binding.

2.2.10) Adsorption to lipid monolayer

In order to obtain single-stranded filaments, 30 μl of the samples containing septin complexes were adsorbed to 1 μl of lipid containing 0.5 mg/ml of 1 DOGS-NTA: 3 DOPC and incubated for one hour at 4°C. Then a carbon-coated grid was placed on top the lipidic surface and negatively stained with uranyl formate.

2.2.11) Electron microscopy

Complexes were prepared for electron microscopy by applying them on holey carbon grids (Agar scientific) followed by negative staining with uranyl formate (0.7% wt/vol) as described elsewhere (Ohi et al., 2004). Images of negatively stained samples were recorded with a JEOL JEM 1400 electron microscope equipped with a LaB₆ filament at an acceleration voltage of 120 kV. Images were taken at low dose mode (screen current of 4.5 e⁻/Å²) on Kodak SO163 3.25x4 inch image films at a magnification of 50,000x and a defocus of 1.5 μm . Negatives were scanned with a Tango 3160 drum scanner (Heidelberg AG, Germany) with 2419 dpi resolution to yield a pixel size of 4.5 Å on the specimen level. Alternatively, images were recorded with a 4k x 4k CMOS camera F-416 (TVIPS) at a calibrated magnification of 67,200x, resulting in a pixel size of 2.32 Å/pixel.

2.2.12) Cryo Electron Tomography (cryo-ET)

For cryo-ET of the septin-Gic1p and septin-Gic1p-Cdc42p complexes, 2 μM of YSC and 10 μM of Gic1p with or without 10 μM Cdc42p-GppNHp were used, respectively. The septin-Gic1p and septin-Gic1p-Cdc42p-GppNHp complexes were mixed with 5 nm colloidal gold particles. 4 μl aliquots of each preparation were applied to a glow discharged C-flat holey carbon grid (Protochips Inc.) and plunge-frozen in liquid ethane using a Cryoplunge3 (Gatan Inc.). Images were collected with a JEOL JEM 3200FSC TEM, equipped with an 8k x 8k pixel TVIPS CMOS camera (F-816), at an acceleration voltage of 200 kV and a magnification of 85,470x. An in-column omega energy filter was used to improve image contrast by zero-loss filtering with a slit width of 15 eV. Tilt series were collected at a defocus of ~5 μm , covering the range of ± 60 in 2° increments and a dosage of about 1e⁻/Å² per image. Images were then reduced by 4 x 4 pixel averaging resulting in a pixel size of 7.3 Å. Data were processed using the IMOD software package (Kremer et al., 1996). Gold particles were tracked as fiducial markers to align the stack of tilted images, and tomograms were reconstructed by weighted backprojection. Selected sub-tomograms were segmented using Amira (Mercury Computer 11 Systems Inc.). After low-pass filtering, segmented structures were visualized using Chimera (Pettersen et al., 2004).

2.2.13) Image processing of negatively stained samples

In order to analyze the fine details of septin and Gic1 structures, we boxed either septin filaments or Gic1 particles using boxer (Ludtke et al., 1999 & Frank et al., 1996). The selected particles were windowed into either 128 x 128 or 256 x 256 pixel images for octamers and antibody-labeled samples, respectively. The numbers of particles selected for further processing are listed below.

Samples	Septin particles	Gic1 particles
Septin octamers	4461	-
Septin octamer + α -Cdc11	132	-
Septin octamer + α -Cdc3	199	-
Non-polymerizing septin	1371	-
Non-polymerizing septin + Gic1	2195/ 1282	-
Non-polymerizing septin + Cdc42p(GDP)	1252	-
Septin-Gic1 complex	2228	1471
Septin-Gic1 complex + α -Cdc11	180	-
Septin-Gic1(224-314) complex	1144	1105
Septin(EGFP)-Gic1 complex	3491	3235
Septin(Cdc11 Δ)-Gic1 complex	1971	1561
Septin-Gic1-Cdc42p(GppNHp)	3979	3837
Septin + GTP	3169	-
Septin + GTP + α -Cdc11	188	-
Septin + GTP + α -Cdc3	281	-
Septin + Cdc42p(GDP)	14407	-
Septin + Cdc42p(GDP) + α -Cdc11	142	-
Septin + Cdc42p(GDP) + α -Cdc3	451	-
Septin + Cdc42p(GDP) + GTP	1141	-

All further steps of image processing were performed using the SPARX software package (Hohn et al., 2007). Images were normalized to the same mean and standard deviation and band-pass filtered. Images were then centered, subjected to 2D reference-free rotational alignment (sxali2d) and Kmeans classification (sxx_means), with approximately 100-150 images per class. The images were then further aligned and classified by several rounds of multireference alignment (sxmref_ali2d), where only high quality classes were used as references, followed by k-means classification. Classification was performed within an elongated mask including the respective septin density, expanded by 5 pixels. For analysis of septin + Cdc42p(GDP), non-polymerizing + Gic1 and non-polymerizing + Cdc42p(GDP), density corresponding to septin was masked and the immediate surrounding was left free for classification. For analysis of antibody binding, all members of class averages showing additional density were merged and subjected to further rounds of alignment and classification, with approximately 15-20 images per class.

The characteristic class averages with the lowest intra-class variance were chosen for publication.

2.2.14) Plasmid construction for Yeast two-hybrid assay

Construction of septin's yeast two-hybrid plasmids was done by Dr. Marian Farkasovsky (Institute of SAS, Bratislava, Slovak Republic) (Farkasovsky et al., 2005). Briefly, in order to construct plasmids coding for the LexA and AD fusions with Gic1p fragments of different size, gic1(310-942) (primers GIC1-N3: CCAAGGATCCATGTTCAAAAAAAGGACCTGTTGTCGAGG and GIC1-C1: CCAAGTCGACGGTATTTTCGAGGAGTACTAGTTTC) and gic1(670-942) (primers GIC1-N4: CCAAGGATCCGATTTGGAAATGACCTTGGAAAGAC and GIC1-C1: CCAAGTCGACGGTATTTTCGAGGAGTACTAGTTTC) were amplified by using yeast chromosomal DNA as a template and the Expand High Fidelity PCR system (Roche). The PCR products were digested with BamHI and Sall and fragments were introduced between the BamHI and Sall sites of pEG202 or pJG4-5 vectors. The same PCR products were also used in the construction of expression plasmids pFM812 (gic1(310-942) in pEGST with C-terminal His₆-tag) or pFM562 (gic1(670-942) in pGEX4T-3). All plasmid constructs were confirmed by sequencing.

2.2.15) Yeast two-hybrid assay

Two-hybrid assays were performed using a LexA-based system as previously described (Ausubel et al., 1995). Yeast strain EGY48 was co-transformed with pEG202-based and pJG4-5-based plasmids. Reporter plasmid pSH18-34 was used for quantitative β -galactosidase assay. Three independent isolates of each strain were tested on a minimal medium in absence of leucine or presence of X-gal.

2.2.16) Nucleotide exchange of Cdc42p

Cdc42p is usually GDP bound after purification due its intrinsic GTPase activity. But, in order to exchange GDP to GppNHp or remove residual GTP, 5 mM EDTA (x5 of MgCl₂ concentration in the gel filtration buffer) and 20 times excess of the desired nucleotide to the protein concentration were added to Cdc42p and incubated at room temperature for 2 h. Subsequently, protein was concentrated using Amicon® Ultra-4 Centrifugal Filter with a cut-off of 10 kDa. During the procedure, protein was washed with the gel filtration buffer devoid of EDTA and nucleotide (150 mM NaCl, 20 mM Tris-HCl pH 7.5 and 1 mM MgCl₂).

2.2.17) High Pressure Liquid Chromatography (HPLC)

Septin octamers at a final concentration of 0.6 mg/ml were prepared in a high-salt buffer and dialyzed against a low-salt buffer to allow filament polymerization. Either Cdc42p-GDP or Cdc42p-GppNHp was added to the septin filament at a final concentration of 3 mg/ml and samples were incubated at 4°C. At different time intervals (0h, 1h, 3h and 16h) a sample was taken, boiled at 96°C for 2 minutes and centrifuged at 13,000 rpm for 5 minutes. 25 µl of the supernatant was applied to reversed phase chromatography (C18-column: Prontosil C18 120-5-C18-AQ column, Bischoff chromatography) for separation of GTP from GDP under isocratic conditions (50 mM potassium phosphate pH 6.6, 10 mM tetrabutyl ammonium bromide, 16% (v/v) ACN). Peaks of GTP and GDP were quantified spectrometrically at OD 254 nm.

2.2.18) Analytical gel filtration analysis

To evaluate the binding between Cdc42p to septin (with or without α -Cdc3 antibody), Cdc42p to Gic1-GST and non-polymerizing septin to Gic1-GST the Äkta purifier (GE Healthcare) system with Superdex S200 or Superose 6 (GE Healthcare) was used. In this regard, 1 mg of each desirable protein was mixed together and incubated shortly for 15 minutes to allow binding and the samples were then loaded onto the columns and ran at 0.4 ml/min. In the case of antibody labeling, 4 µl of the α -Cdc3 antibody was mixed with the sample and incubated for 1 h before loading the sample into the column. The fractions containing protein were either precipitated with trichloroacetic acid (TCA) or directly analyzed using EM. In this regard, 1 volume of TCA was added to 4 volumes of protein and incubated at 4°C for 10 minutes. The samples were subsequently centrifuged at 13,000 rpm for 10 minutes. The supernatant was discarded and the pellet was washed with acetone and centrifuged again. The washing was repeated twice and the pellet was resuspended in SDS-loading buffer with β -mercaptoethanol and boiled at 95°C for 5 minutes and analyzed with SDS-PAGE.

2.2.19) Cell culture

For all experiments HEK-293 (ATCC: No. CRL-1573) cells were used. The cells were cultured in the standard mammalian cell growth medium at 37°C in a humidified incubator with 5% (v/v) CO₂ saturation. In order to maintain the cells in culture, they were kept in a 75 cm² cell culture flask (BD Falcon) till they reached 90% confluence. At this density, the cells were passaged. The old growth medium was removed from the flask and the cell layer was briefly rinsed in sterile 1x PBS (pH 7.5). In order to detach the cells from the surface 2 ml of trypsin/EDTA solution (PAN Biotech) was added and the cell suspension was incubated for 1-2 minutes at room temperature. The trypsin was inactivated by adding 10 ml of complete growth medium containing 10% FCS. The resulting cell suspension was gently pipetted up and down

several times that no cell clusters remained in the suspension. Of the suspension, 1 ml was transferred to a new flask containing 12 ml fresh standard mammalian cell growth medium. Following this protocol 90% confluence was reached every 2-3 days. Cells growing at that speed are considered healthy for experiments. However, cells used for experiments were never kept longer than passage 20.

2.2.20) Fluorescence imaging

2.2.20.1) Preparation of HEK cells

HEK-cells do not show a very strong attachment to glass surfaces. If the medium and other solutions are pipetted onto the cover slips and are removed it is always a danger that some cells detach from the cover slip. In order to prevent this problem, poly D/L lysine coated glass cover slips were used. The glass cover slips were kept in ethanol (abs.). After drying, they were transferred to a 6-well plate. Each glass slip was incubated with 400 μ l of a 2 mg/ml poly D/L lysine solution for 30 minutes at room temperature. The surface tension of the solution allowed that the cover slips were wetted completely. After incubation, each slip was briefly rinsed with 2 ml of sterile water. These plates can be stored at 4°C up to 2 month.

For fluorescence imaging, cells were seeded into a 6-well cell culture insert companion plate with lid (BD Falcon) containing a poly D/L Lysin coated cover slip. In each well, 2 ml of standard growth medium was present along with 0.5×10^6 HEK-cells. The cells were incubated for 24 h to attach to the glass cover slip. After attaching to the surface, transfection of HEK-293 cells was done using FuGene (Roche). The transfection was done according the manufacturer's protocol using a 1 μ l FuGene : 0.5 μ g DNA ratio. Before transfection the medium was removed and 1 ml of fresh growth medium without FBS and antibiotics was added.

If needed, 18-20 h after transfection the delipidation of cells was done. The growth medium was removed from all wells and replaced by 1 ml of delipidated medium. For depletion of sterols 50 μ l of 20% β -cyclodextrin (Alfa Aesar) was added to the delipidation culture medium to gain a final concentration of 1% (v/v). The cells were incubated for one hour at 37°C. After incubation with β -cyclodextrin the cells were washed extensively with PBS.

After each individual treatment, the cells were fixed. Fixation was done using 2 ml of a 3.6% PFA (w/v) solution for each well and incubated for 20 minutes at room temperature. Afterwards the cells were rinsed with PBS and the glass slip was mounted with Fluoromount (Serva) upside down onto a glass slide (Thermo Fisher Scientific). The slides were stored in the dark at 4°C to avoid any damage done by light (photobleaching) or heat.

2.2.20.2) Microscopy

We used the Leica SP2 Confocal System (Leica) to visualize the fluorescence of transfected HEK-293 cells. The 63× Plan-Apochromat (numerical aperture, 1.4) oil immersion lens objective used was. GFP was imaged with 488 nm wavelength laser excitation and 505-530 nm band pass emission filter. RFP was imaged with 558 nm laser excitation and 580-650 nm filter. A z-stack of the cells was acquired by moving the focal plane from the bottom to the top of the images cells. The pinhole was set to 1 airy to ensure that the acquired image shows a thin plane of the specimen. This is crucial to state overlapping pixels of different channels as colocalization.

2.2.20.3) Image processing

For the processing of images the software Fiji (<http://pacific.mpi-cbg.de/wiki/index.php/Fiji>) was used. In order to determine the colocalization a plug-in called JACoP (Bolte & cordelieres, 2006) was used.

2.2.21) Measurement of cholesterol

2.2.21.1) Kit to quantify total cholesterol (Axiom diagnostics)

Cholesterol fluid mono-reagent provided by Axiom diagnostics was used to measure “total cholesterol” from eukaryotic cells. Approximately 2×10^6 cells were seeded in 10 cm plates (BD Biosciences) on day 0. Cells were incubated at 37°C overnight to allow them to attach to the plate and grow. After treatment, cells were harvested at different time points with use of trypsin and subsequently centrifuged and washed with 1x PBS once and kept at -20°C till lysed. 0.5 ml of 0.9 % NaCl was added to cells, resuspended and sonicated 1x 15 counts at an output of 3.5 and duty cycle of 10%. 10 µl of lysate from each sample was mixed with 200 µl cholesterol reagent as duplicates and incubated at 37 °C for 10 minutes. As a control, 10 µl of standard cholesterol was also mixed 200 µl cholesterol reagent in parallel. Solutions were transferred into 96-well plates (BD Biosciences) and light absorption at OD₄₉₅ nm was measured with an Omega Ω spectrometer. Total cholesterol was quantified by the following formula:

(Sample absorption ÷ standard absorption) x standard concentration = Cholesterol concentration (mg/dl)

Cholesterol content was normalized to 10^7 cells. Each experiment was performed three times in duplicates and the final cholesterol content was averaged.

2.2.21.2) Gas chromatography

Free sterols reside in the hydrophobic core of membranes. In order to extract them, a hydrophobic solution is required. Chloroform, hexane or cyclohexane satisfy this purpose. Approximately 2×10^6 cells

were seeded in 10 cm plates (BD Biosciences) on day 0. Cells were incubated at 37°C overnight to allow them to attach to the plate and grow. After treatment, cells were resuspended in 0.5 ml of 0.9% NaCl and sonicated 1x15 counts at an output of 3.5 duty cycle 10%. After lysis, 300 µl methanol (100%) and 300 µl chloroform and also 100 µM Stigmasterol (as a recovery standard) were added. The sample was vortexed vigorously and centrifuged at 3000 rpm for 2 minutes to separate the hydrophobic and aqueous phase. The lower inorganic (lower) phase contains sterols. The lower phase was then transferred into a glass vial. This procedure was repeated three times and the extracts were pooled into the same glass vial and dried under gentle stream of N₂. Alternatively, samples can be transferred into microtubes and dried by Speedvac for 10 minutes without heating. Dried sterols were solubilized in 300 µl cyclohexane and injected into a GC-MS instrument.

1 µl of the isolated sterols was injected into a gas chromatography instrument (Focus GC, Thermo) equipped with a mass spectrometer (PolarisQ, Thermo) and an autosampler (CTC Analytical Liquid Sampler A200SE). Chromatographic separation was achieved using HP-5MS column, 30 m, 0.25 mm ID and 0.25 µm film with helium as a carrier gas at 1 ml/min (constant flow). The oven temperature was initiated at 200°C and raised to 270°C at 7°C per min ramp. The split/splitless injector temperature was held at 230°C. The injector was operated in split mode at 10 ml/min. The sterols were identified according to their retention time and standards used to calibrate the system. MS initiation time was 10 min and MS transfer line was 280°C.

Four different ion masses (386 for cholesterol, 412 for stigmasterol, 398 for brassicasterol and 396 for ergosterol) were detected and integrals of peak areas were calculated for each ion. Values were subsequently normalized against the cholesterol concentration under normal condition. Experiments were performed in triplicates and averaged for each point.

2.2.22) 2D crystallography

2D crystallography is a method to study membrane proteins in a lipidic environment. In this method, purified membrane proteins are reconstituted in a lipid bilayer. The protein and lipid both solubilized in detergent are dialyzed for 1-2 weeks against a buffer without any detergents or lipids to remove the detergents. Cyclodextrin and biobeads have also been used to chelate the detergents. Formation of a 2D crystal depends on the type of phospholipids, lipid to protein ratio (LPR), pH, divalent cations and temperature. Trials are usually screened after negatively staining a sample on EM grids. In this work, we used *E. coli* polar lipids, Brain polar lipids, DOPC (1,2-dioleoyl-*sn*-glycero-3-phosphocholine) and DLPC (1,2-Lauroyl-*sn*-Glycero-3-Phosphocholine) solubilized in DDM at a final concentration of 10 mg/ml. 60 µl of the protein (1 mg/ml) was mixed with lipids at LPR of 0.1, 0.25, 0.5, 1 and 1.5. Samples were incubated for 1 h, subsequently transferred to dialysis buttons and covered with dialysis membrane (Cut-off of 12 kDa). Dialysis buttons were dialyzed against a buffer containing 150 mM NaCl and 50 mM

Tris-HCl pH 7.5 for 1-2 weeks at room temperature. 4 μ l of the samples were coated on grids and stained with uranyl formate before EM analysis.

2.2.23) 3D crystallography

3D crystallography is the preferred method in structural biology to study the structure of nucleic acids and proteins. Primarily, crystallographic trials are set up using commercially available kits and each condition is further optimized to obtain well-diffracting crystals. In this work, protein crystallization kits (*JCSG Core I-IV Suite*, *Mb I-II Suite*, *PACT suite* and *Protein Complex Suite*) were used along with 8, 20 and 28 mg/ml of SSD and 6 mg/ml of cDHCR7. 0.1 μ l of protein was mixed with 0.1 μ l of the buffers from the kits using Mosquito robots into Corning® 96-well plates. Plates were incubated at 20°C or 4°C for a period of three weeks and imaged regularly.

2.2.24) NBD-7DHC binding assay

In order to test the binding between 7-DHC and DHCR7, a fluorescently or radiolabeled substrate is needed. Radiolabeled 7-DHC was shown to be unstable since upon UV exposure, it is converted to vitamin D precursor (Batta et al., 1997). NBD-cholesterol has been used in several cases and shown to mimic cholesterol localization and kinetics. Therefore, we synthesized NBD-labeled 7-DHC in collaboration with Dr. Christian Hedberg, MPI for Molecular Physiology, Dortmund, Germany.

We used two different methods to measure the binding between cDHCR7 and NBD-7DHC. We used 0.3 μ M of cDHCR7 and 50 μ M of NBD-7DHC (solubilized in DMSO) in a final volume of 200 μ l of the gel filtration buffer. In the first method, we added the reaction mixture to 0.1 ml Ni-NTA beads calibrated with gel filtration buffer. Then the column was washed with gel filtration buffer extensively to remove the unbound substrate. Then the protein was eluted using gel filtration buffer containing 250 mM imidazole, histidine or EDTA. Fractions were collected as 3-4 drops per microtube. The concentration of the eluted protein was measured with the Bradford assay and fluorescence was measured at emission wavelength of 488 nm and emission of 509 nm using an Omega Ω spectrometer. In the second method, the reaction mixture was added to PD-10 desalting column. The column was washed 10 ml of gel filtration buffer and fractions of 4 drops per microtube were collected. The protein concentration and fluorescence absorbance were measured as explained. As a negative control, BSA (50 μ M) was mixed with NBD-7DHC and subjected to both methods. In case of a negative interaction between NBD-7DHC and BSA fluorescence absorption and Bradford absorption should not overlap whereas as a positive interaction they should overlap.

3) Results

3.1) Results and discussion of septin, Gic1 and Cdc42p

3.1.1) Filament formation and bundling by Gic1

3.1.1.1) Yeast Septin Complex (YSC) structural organization

The Yeast Septin Complex (YSC) is comprised of four subunits that are organized into an octamer with a two-fold rotational symmetry. The complex has been expressed in a bacterial host, which facilitates cellular assembly of the whole complex and high protein yield. In order to bacterially express the yeast septin complex in *E. coli*, two different plasmids were co-transformed into Rosetta cells. The first plasmid carried MBP-Cdc12 (Maltose Binding Protein) and Cdc3 and the second plasmid carried His-Cdc10 and Cdc11. Primarily, the expression of the septin complex was induced in *E. coli* Rosetta cells grown in TB medium at OD₆₀₀ of 0.6 by addition of 0.5 mM imidazole. Then the temperature was shifted to 28°C and cells were harvested after 16 h. Subsequently, the cells from 10 liters of expression were lysed using microfluidizer and centrifuged at 30,000 rpm. The supernatant, which contained the septin complex, was purified using a 50-mL Ni-NTA column. The eluate was further purified using a 20-mL amylose column to capture the MBP-tagged proteins. Next, the eluate was incubated with thrombin to cleave the MBP tag during an overnight dialysis. The septin complex was further purified using either Q-Sepharose Hi-Trap (Amersham) or alternatively Sephadex S200 (GE Healthcare) to reach high purity (Fig. 3.1). Fractions containing all four subunits of the septin complex were pooled, concentrated and used for further analyses.

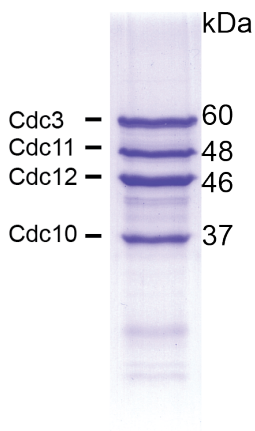


Fig. 3.1. Purification of the Yeast Septin Complex (YSC). The septin complex was expressed in 10 L of *E. coli* cells. Cells were lysed using a microfluidizer and centrifuged at 30,000 rpm for 45 minutes. The supernatant was passed through a 50-mL Ni-NTA column and the eluate was further purified using a 20-mL amylose column. The MBP tag was cleaved with 200U of thrombin overnight. The complex was further purified using a Sephadex S200 column with a buffer containing 500 mM NaCl to keep septin in octameric status as reported previously (Frazier et al., 1998).

The septin complex remains as an octamer in a solution with a high salt content (500 mM NaCl) due to perturbation of interaction in the NC-interface between a pair of Cdc11 of the septin octamers. Initially, a

sample containing the septin octamer was applied on a carbon-coated grid and negatively stained with uranyl formate (Fig. 3.2A). In order to gain more details about the structure, we performed single particle analysis on the septin octamers. In this regard, 4461 particles were picked, aligned and classified by K-means as explained (as explained in 1.3.2.1). Classification of the septin octamer resulted in an exclusive structure with eight subunits aligned in a rod as reported previously (Bertin et al., 2008) (Fig. 3.2B).

A previous study showed that the four mitotic septin subunits are arranged as Cdc11-Cdc12-Cdc3-Cdc10-Cdc10-Cdc3-Cdc12-Cdc11 as a non-polar octamer (Bertin et al., 2008). The authors took advantage of antibody labeling and tagging strategies to identify the position of each subunit in the octamer. However, in some cases the tagging and consequently the localization of subunits were not completely clear. Therefore, in an attempt to localize the position of each subunit in the octamer and also to have a comparative model for future antibody labeling experiments, we used polyclonal antibodies against Cdc3 (Gift from Michael Knop, DKFZ-ZMBH, Heidelberg, Germany) and Cdc11 (Santa Cruz Biotechnology Inc.). In this regard, 5 μ l of each antibody (1:100 dilution) was mixed with 20 μ l of a sample containing the septin octamers and incubated for 16 h at 4°C to allow efficient binding of antibody to the octamers. The antibody against Cdc3 decorated the octamers at a position between the second and the third subunits from the terminal position (Fig. 3.2C). Use of a polyclonal antibody would lead to different binding positions with respect to the location of the C- and N-termini of Cdc3. The C-terminal extension of Cdc3 interacts with the C-terminal extension of Cdc12. Therefore binding of an antibody to the C-termini of Cdc3 would locate the antibody in a position between Cdc3 and Cdc12. Our class average (Fig. 3.2C) showed an extra density in the middle of the second and the third subunit from the top that corroborates the previously published evidence that Cdc3 is the third subunit from the terminal position (Bertin et al., 2008). The antibody against Cdc11 bound to the terminal subunit of the octamer as it can be seen in a representative particle used for further classification (Fig. 3.2D). However, the binding of the antibody to the septin complex was sub-stoichiometric most probably due to the high ionic content of the buffer that is required to keep the septin as an octamer, which was also a challenging task in the earlier work of Nogales and colleagues (Bertin et al., 2008). Therefore, just a few particles could be selected to perform single particle analysis obtaining well-resolved class averages (Fig. 3.2E). In conclusion, our present data are in agreement with the previously published data showing that Cdc10-Cdc10 occupies the central position of the octamer that is flanked by Cdc3 and Cdc12 on both sides and Cdc11 sits at the terminal position (Fig. 3.2F) (Bertin et al., 2008).

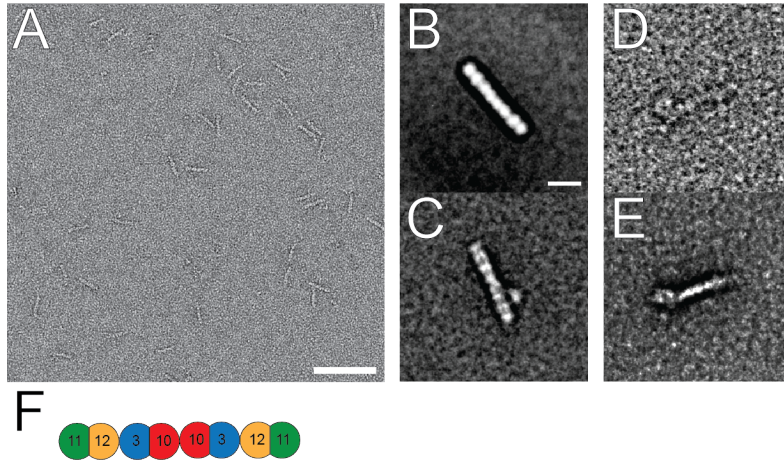


Fig. 3.2. Structure of the septin octamer. (A) A sample of septin octamers was applied onto a carbon-coated grid and negatively stained with uranyl formate. (B) A representative class average of the yeast septin complex showing its octameric structure reconstructed from 4461 particles. (C) A representative class average of the

α -Cdc3 antibody bound to the septin octamer reconstructed from 199 particles. 20 μ l of the octamer was mixed with 5 μ l of α -Cdc3 (1:100) and incubated for 16 h. (D) A particle showing the bound α -Ccd11 antibody at the terminal position of the octamer. (E) A representative class average of the α -Cdc11 antibody bound to the septin octamer reconstructed from 132 particles. (F) A model that depicts the organization of septin subunits in an octamer. Scale bar in A is 100 nm and in B is 10 nm.

3.1.1.2) Filament formation and enhancement of bundling by Gic1

The septin complex readily undergoes polymerization at a salt concentration below 100 mM. Polymerization of octamers is mediated via the interaction of two Cdc11s that leads to formation of a new NC-interface among the connected octamers (Bertin et al., 2008 and McMurray et al., 2011). Initially, a septin complex tagged with EGFP on the C-terminus of Cdc3 of the septin complex was used to facilitate monitoring of filament formation with a fluorescence microscope. In order to obtain straight and long filaments, the octamers were dialyzed against a low-salt buffer for 16 h at 4°C. The optimal concentration to obtain extended filaments without excessive bundling was found to be 0.3 μ M (Fig. 3.3A).

Gic1 and Gic2 are the effectors of Cdc42p, which are involved in early recruitment of septin and actin to the budding neck (Iwase et al., 2006). It was previously shown that Gic proteins could physically interact with septin but the precise significance and possible conformational changes of this interaction remained elusive (Iwase et al., 2006). In order to study the interaction between Gic1 and septin, we expressed Gic1 (104-314) in *E. coli* Rosetta cells by inducing cells with 0.2 mM IPTG when they reached the OD₆₀₀ of 0.2. The temperature was then shifted to 28°C and cells were harvested after 8 h. Cells were lysed and centrifuged at 50,000 rpm and the supernatant was passed through a 50-ml Ni-NTA column. The eluate was mixed with thrombin and incubated at 4°C overnight to cleave the GST tag. The protein was subjected to Glutathione sepharose to capture the GTS tag and undigested proteins. The eluate of the Glutathione column was injected to Sephadex S200 column to further purify Gic1 (104-314) (from hereon referred to as Gic1 otherwise stated). The protein eluted at a molecular weight of approximately

50 kDa, which corresponds to a molecular weight of a dimer (predicted molecular weight of Gic1 (104-314) is 23 kDa) (Fig. 3.3A and B). In order to examine the possible binding of Gic1 to septin and its possible effect on filament conformation, different concentrations of Gic1 were dialyzed together with the septin octamers. We observed with use of a fluorescence microscope that filament formation and bundling was extremely enhanced when Gic1 was used in excess (Fig. 3.3D). Therefore, we sought to study the details of filament bundling by Gic1 protein by EM to gain more insights into the features of the structure and binding pattern that led to a seemingly discrepant structure. In this regard, the optimal concentration of the septin complex (0.3 μM) was dialyzed with varying concentrations of Gic1 to find out the optimal concentration of Gic1 that results in bundling of filaments. We observed that the septin filaments formed extended arrays with the inter-filamentous connections (Fig. 3.4A). As reported previously, binding of C-termini of pairs of Cdc3 and Cdc12 are an absolute prerequisite to filament pairing. Whereas, binding of C-terminal extensions of pairs of Cdc11 is dispensable for this process but however present in the filaments prepared in this work (Bertin et al., 2008). At equimolar concentration, filaments appeared to have formed bundles around some particles but they were still dispersed (Fig. 3.4B). As the molar concentration of Gic1 was raised to five times the concentration of the septin octamers, a peculiar structure formed that resembled a railway (Fig. 3.4D). This structure resulted from binding of at least two filaments to round Gic1 particles that stacked on top of each other to form a bundle.

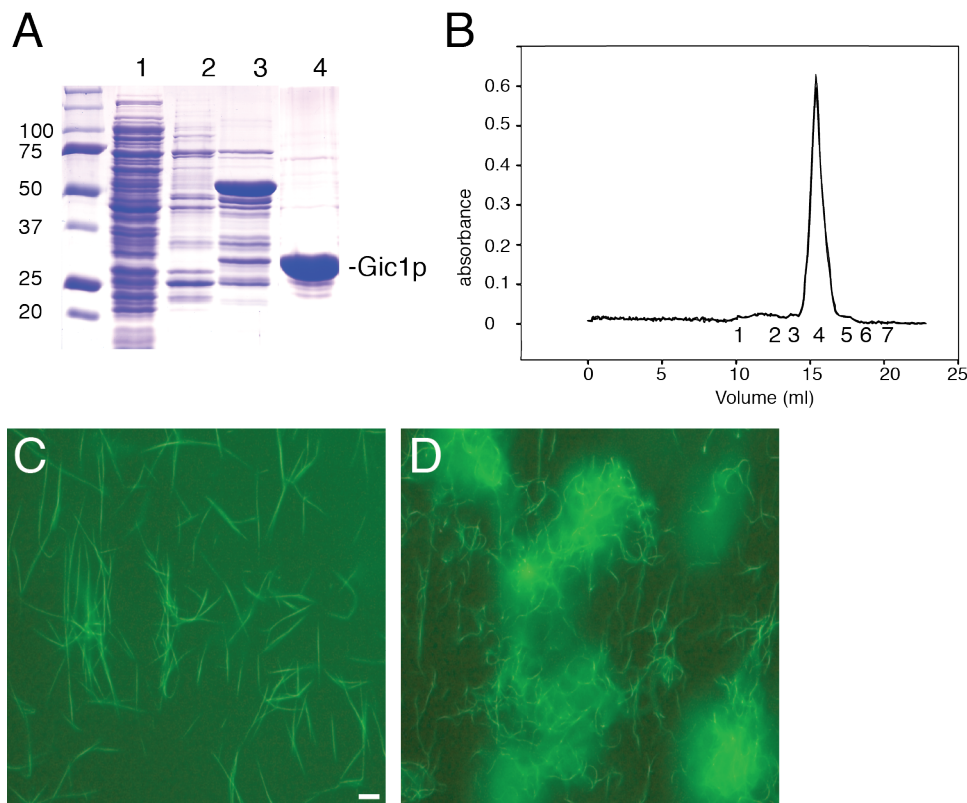


Fig. 3.3. Purification of Gic1 (104-314) and Bundling of septin-EGFP complex by Gic1. (A)

Purification of Gic1 (104-314). Band (1) corresponds to Ni-NTA flow-through, (2) Ni-NTA wash, (3) Ni-NTA elution and (4) elution from gel filtration and cleavage with precision protease.

(B) Gel filtration chromatogram of Gic1 (104-314) using Sephadex S200. The calculated molecular weight of Gic1

(104-314) is approximately 23 kDa and the protein elutes at 50 kDa suggesting a dimeric-trimeric ratio. Protein standards used include (1) ferritin (440 kDa); (2) aldolase (158 kDa); (3) conalbumin (75 kDa); (4) ovalbumin (43 kDa); (5) carbonic anhydrase (29 kDa); (6) RNase A (13.7 kDa); (7) aprotinin (6.5 kDa). 0.3 μM of septin-EGFP was dialyzed against a low-salt buffer (0.1 M NaCl) at 4°C for 16 h (C) without or (D) with 1.5 μM of Gic1. A droplet of the complexes was applied on a cover slip and observed with fluorescent microscope. Scale bar in C is 0.5 μm .

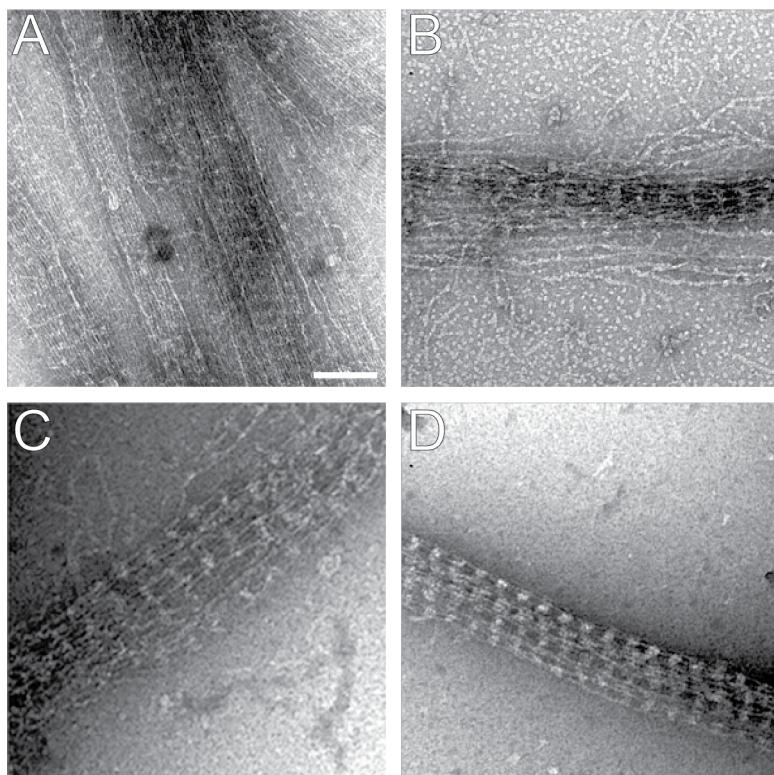


Fig. 3.4. Formation of a railway structure by the septin octamers and Gic1. 0.3 μM of the septin complex was dialyzed (A) without Gic1, (B) with 0.3 μM of Gic1, (C) 0.6 μM of Gic1, and (D) with 1.5 μM of Gic1 against a low-salt buffer (0.1 M NaCl) at 4°C for 16 h. Scale bar is 100 nm.

The structure of the septin-Gic1 complex showed excessive bundling of filaments. In order to obtain singular filaments, a lipidic mixture of 1 DOGS-NTA: 3 DOPC was used. DOGS-NTA is coupled to Ni^{+2} beads to bind to His tag of both septin and Gic1. Prerequisite to single particle analysis, 1 μl of the lipid monolayer was placed on top of a 30 μl protein sample and incubated at 4°C for 1 h to allow complete adsorption of the complex to the lipidic surface (Fig. 3.5). The integrity of the septin-Gic1 complex remained intact after adsorption to the lipid monolayer. To analyze the septin and Gic1 complex, two different sets of particles were selected. The first set focused on the septin filaments between two Gic1 cross-bridges and the second focused in the middle of the Gic1 cross-bridges. 2228 particles of septin and 1471 particles of Gic1 cross-bridges were picked, aligned using multi-reference alignment and classified by K-means. Representative class averages of the septin-Gic1 complex showed that a Gic1 cross-bridge had a density of ~ 10 nm, which bound to two subunits of the septin complex. Moreover, the Gic1 cross-

bridges were separated from each other by six subunits of the septin complex (Fig. 3.5C and 3.5D). The recurring pattern of 2-6-2 could result from binding of Gic1 to a Cdc10-Cdc10 dimer in the middle of the octamers or to a dimer of Cdc11-Cdc11 at the end of the octamers, which would be separated by six subunits (Fig. 3.5E and 3.5F). Therefore, further studies were required to resolve the binding site of Gic1.

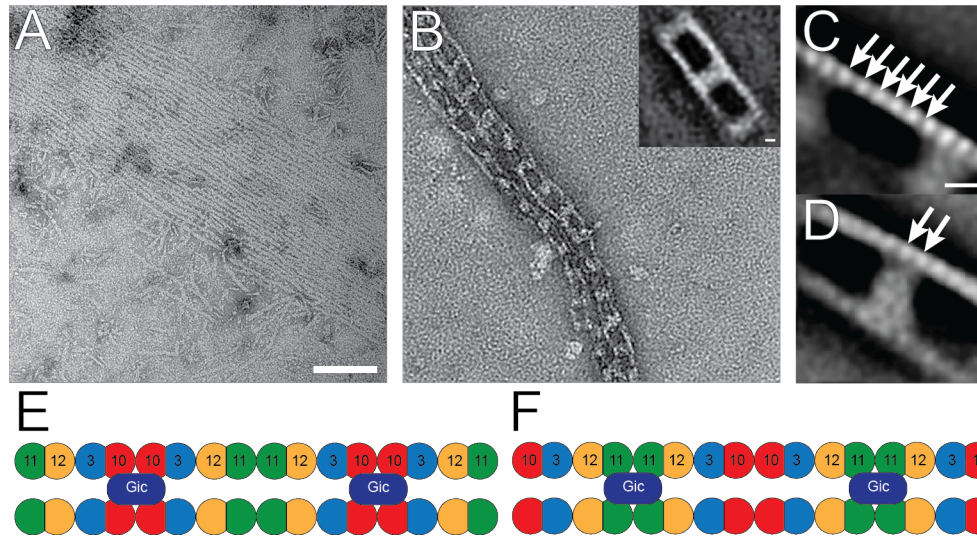


Fig. 3.5. Septin filaments with Gic1 protein on a lipid monolayer and the railway structure. 0.3 μM of the septin complex (A) without or (B) with 1.5 μM Gic1 were mixed and dialyzed against a low-salt buffer (0.1 M NaCl) at 4°C for 16 h. Then 30 μl of each sample was adsorbed to 1 μl of 0.5 mg/mL of 1 DOGS-NTA: 3 DOPC for 1 h at 4°C. A carbon-coated grid (not glow-discharged) was placed on top of the lipidic surface and the samples were stained with uranyl formate. The inset in (B) shows the overall structure of the septin-Gic1 complex. (C) A class average of the septin complex obtained from 2228 particles. Arrows show the six septin subunits between Gic1 cross-bridges. (D) A representative class average of Gic1 obtained from 1471 particles. Arrows show that Gic1 cross-bridges bind to two septin subunits. (E) A model showing a possible binding of Gic1 particle to Cdc10 dimer. (F) A model for binding of Gic1 to Cdc11 dimer. Scale bar in A is 100 nm and in C and inset of B are 10 nm.

3.1.1.3) Time-dependent binding of Gic1 to septin filaments

The railway structure of the septin-Gic1 complex resulted from co-dialysis of the septin octamers and Gic1 for nearly 16 h. We then asked whether Gic1 could bind to the pre-assembled septin filaments or if it only could bind to septin octamers to act as a bundling factor during filament formation. In order to answer this question, appropriate concentration of Gic1 was added to pre-assembled septin filaments and a sample was taken at different time points to check for the presence of the railway structure. We observed that Gic1 started to bind to the septin filaments as soon as 2 minutes but the formation of a neat railway structure was fulfilled after an overnight incubation (Fig. 3.6D). Therefore, Gic1 does not serve as

an essential factor for bundling of filaments during the course of filament formation but rather acts as a bridge between filaments to either stabilize the filaments or serve as a platform for other proteins to execute their functions.

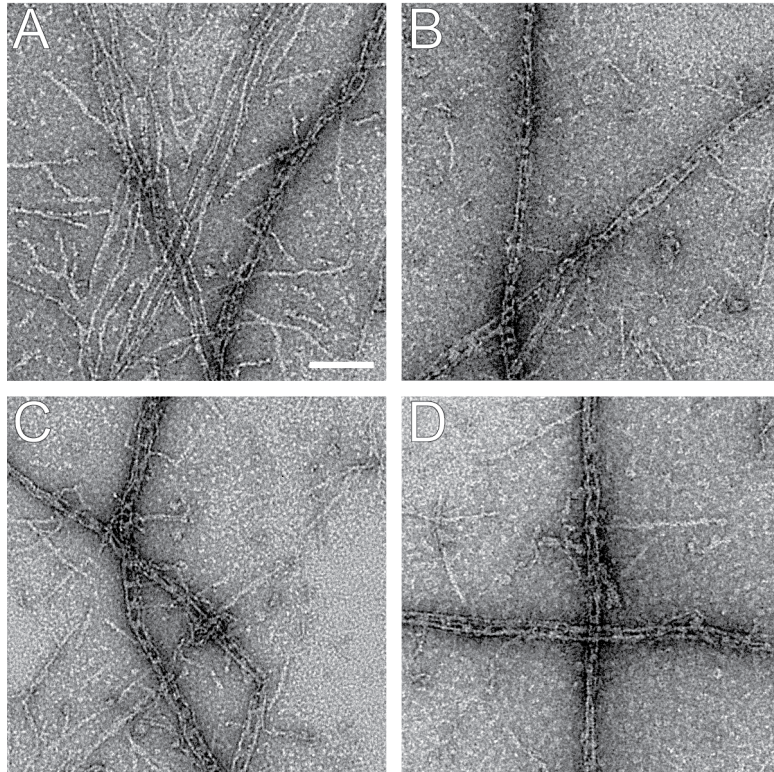


Fig. 3.6. Time-dependent binding of Gic1 to septin filament. 0.3 μM of the septin complex was dialyzed against a low-salt buffer, then 1.5 μM Gic1 was added and samples were taken after (A) 2 minutes, (B) 15 minutes, (C) 1 h and (D) 16 h. Scale bar is 100 nm.

3.1.1.4) Analysis of binding site of Gic1 using an α -Cdc11 antibody

Previously, it was shown that Gic1 bound to Cdc12 and partially to Cdc3 using *in vitro* binding assay (Iwase et al., 2006). In that study, authors used purified single subunits of the septin complex. The method neglects that upon binding of subunits to each other, they undergo conformational changes, which can alter their binding properties. Our preliminary data ruled out the previous model for binding to Cdc12 and Cdc3, as it would lead to a structure with only two subunits between Gic1 particles. We concluded from our data that Gic1 either binds to Cdc10 dimers or Cdc11 dimers but we could not distinguish between these two binding sites. Therefore, in order to identify the binding site, we used a polyclonal antibody against Cdc11. At first, the septin-Gic1 complex was prepared by overnight dialysis and then 20 μl of the complex was incubated with 5 μl of the antibody (1:100 dilution) for 16 h. Then the sample was adsorbed to a lipid monolayer and used for single particle analysis. An extra density between the two Gic1 cross-bridges was seen in the raw images (inset of Fig. 7A) and in the class averages (Fig. 3.7B).

This observation suggests that Cdc11 is located between two Gic1 cross-bridges and therefore Gic1 binds to Cdc10 dimers. A model for the binding of the antibody to Cdc11 is represented in Fig. 3.7D.

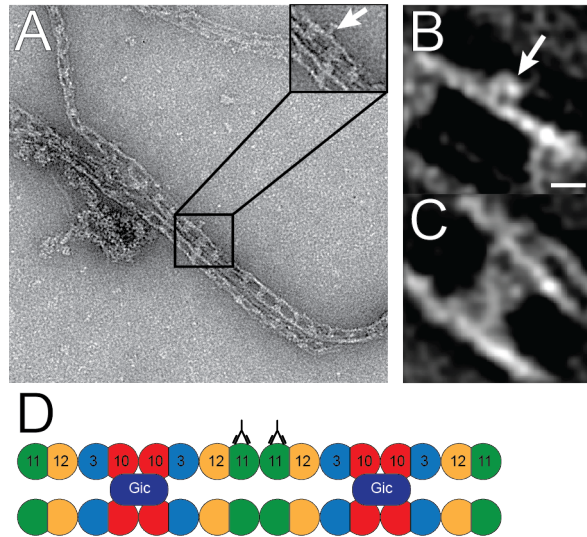


Fig. 3.7. Septin-Gic1 complex decorated with α -Cdc11 antibody. (A) The septin-Gic1 complex was prepared as described before. 20 μ l of the complex was mixed with 5 μ l of polyclonal α -Cdc11 antibody (1:100) and incubated for 16 h. In the inset, bound antibody to septin filament is shown at a higher focus. (B) and (C) show the class averages of septin with the bound antibody to Cdc11 in the middle of the filament obtained from 180 particles and Gic1 from left to right respectively. (D) A model showing the binding of α -Cdc11 antibody to the septin-Gic1 complex. Scale bar in A is 100 nm and in B is 10 nm.

3.1.1.5) Analysis of septin-EGFP filaments

We previously used EGFP tagged septin filaments to show the bundling effect of Gic1 on septin filaments (Fig. 3.3). We dialyzed septin-EGFP together with Gic1 to locate the binding site of Gic1 on septin filament. Filaments were prepared, adsorbed to lipid monolayer and analyzed with electron microscope as described before. We observed that EGFP tag did not cause any irregularities in the structure of the filaments or the complex as compared to wild-type complex (Fig. 3.8B). Evidently, we did not see two separate densities on the filaments corresponding to EGFP and Gic1 cross-bridges. Instead, there was a single density covering a mass equal to four septin subunits that was bigger when compared to Gic1 cross-bridges in the wild-type complex (compare Fig. 3.8D with Fig. 3.5D). Moreover, class averages showed that only four subunits separated the Gic1 cross-bridges (Fig. 3.8C). Since the C-termini of septin subunits bind each other and face the interior space between filaments, it is expected that EGFP molecules, which are C-terminally tagged to Cdc3 to form a density between filaments like Gic1 cross-bridges. A single density (Fig. 3.8D) is indicative of the presence of Cdc3-EGFP next to the Gic1 cross-bridges. As Cdc3 is an immediate neighbor of Cdc10 and flanks it, this observation corroborates our previous evidence that Gic1 binds to Cdc10 (Fig. 3.8E).

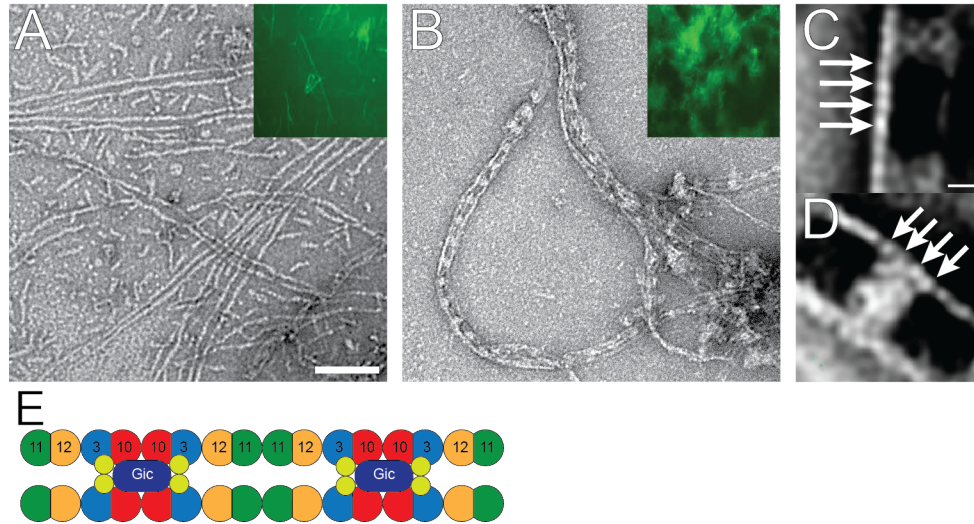


Fig. 3.8. Septin-EGFP filaments with Gic1. (A) 0.3 μM of septin-EGFP filaments and (B) 0.3 μM of septin-EGFP and 1.5 μM of Gic1 complex were dialyzed against a low-salt buffer. (C) A class average of septin-EGFP obtained from 3491 particles. Arrows indicate the four septin subunits that separate the Gic-EGFP particles. (D) A class average of Gic1-EGFP obtained from 3235 particles. Arrows point at four septin subunits bound to a Gic1-EGFP particle. (E) Shows a model of septin-EGFP and Gic1 in which the extra density corresponding to EGFP is depicted around Gic1. Scale bar in A is 100 nm and in C is 10 nm.

3.1.1.6) Analysis of Cdc10 Δ and Cdc11 Δ filaments

It was previously shown that filaments purified from *cdc10 Δ* and *cdc11 Δ* cells are shorter than wild-type filaments (Frazier et al., 1998). However, another study showed that in the absence of Cdc10 or Cdc11 filaments formed in the presence of lipidic surface and excess of GTP (Bertin et al., 2008 and 2010). We prepared septin hexamers devoid of either Cdc11 or Cdc10. We, however, observed that in the absence of Cdc10 or Cdc11 filaments formed after overnight dialysis albeit inefficiently (Fig. 3.9A and 3.9C). Interestingly, when Gic1 was included during dialysis, it was not able to bind to Cdc10 Δ septin filaments while it still bound to Cdc11 Δ septin filaments and they together formed the railway structure, which indicates the requirement of Cdc10 for binding of Gic1 to the septin complex (Fig. 3.9D). Moreover, filament (complex) formation of Cdc11 Δ filaments was enhanced in the presence of Gic1, which pinpoints to a novel function for Gic protein as a stabilizing factor for septin filaments (see sections 3.1.1.10, 3.1.2.2 and 3.1.4.1).

Representative class averages obtained from single particle analysis of Cdc11 Δ septin filaments are shown in Fig. 3.9E and F. The measured distance between two Gic1 cross-bridges was nearly 20 nm, which corresponds approximately to the mass of four subunits that is shorter than the distance in the wild-

type septin-Gic1 complex shown in Fig. 3.5C. The shorter distance indicates the absence of Cdc11 dimers and once again binding of Gic1 to Cdc10 (Fig. 3.9G).

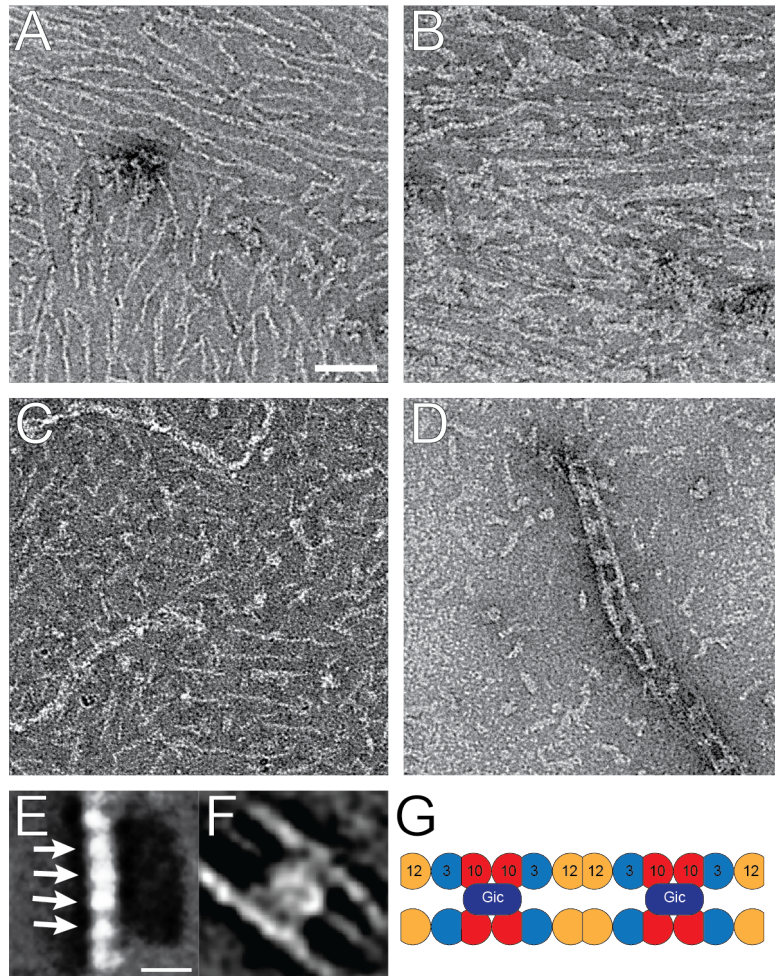


Fig. 3.9. Septin filaments devoid of Cdc10 or Cdc11 with Gic1 protein.

(A) 0.3 μM septin(Cdc10Δ) without Gic1, (B) 0.3 μM septin(Cdc10Δ) with 1.5 μM Gic1, (C) 0.3 μM septin(Cdc11Δ) without Gic1, (D) 0.3 μM septin(Cdc11Δ) with 1.5 μM Gic1 protein were prepared as described before. (E) and (F) show the class averages of septin(Cdc11Δ) and Gic1 obtained from 1971 and 1561 particles respectively. Arrows point at the four septin subunits between Gic1 particles. (G) A model derived from septin(Cdc11Δ) with Gic1 complex. Scale bar in A is 100 nm and E is 10 nm.

To this end, we showed that Gic1 binds to septin filaments and they together form a distinct structure that resembled a railway. Our microscopic results excluded the existing model for binding of Gic1 to Cdc12 (Iwase et al., 2006) and we showed that Gic1 bound to Cdc10 dimers. However, we needed to complement our *in vitro* data with *in vivo* data to corroborate our binding model.

3.1.1.7) Yeast-two hybrid assay confirms *in vitro* data

Yeast two-hybrid assay is a technique routinely used in molecular biology to investigate the interaction between DNA and protein or protein and protein. The yeast two-hybrid assay is based on the virtue of interaction between the DNA binding domain and activation domain of eukaryotic transcription factors. When the activation domain is located in close proximity to the DNA binding domain, the transcription of

the desired gene is switched on. In this system, usually a mutant yeast strain deficient in one biochemical pathway (usually an amino acid or nucleic acid) is utilized. When plasmids carrying the interactors are transferred into this strain, cells survive in medium lacking the product of the pathway.

Plasmids are designed to produce a fusion protein composed of the DNA-binding domain fragment and a protein known as bait. The other plasmid carries the activation domain fragment fused to another protein called prey. Upon interaction between bait and prey proteins, the activation domain and DNA binding domains are brought in close proximity and transcription of the reporter gene is switched on. If the two proteins do not interact, transcription of the reporter gene will not be activated. In this way, a successful interaction between the fused proteins is linked to a change in the cell phenotype.

In furtherance of our microscopic data, we performed yeast-two hybrid assay to investigate the interaction partner of Gic1 *in vivo* (experiments were done by our collaboration partner Marian Farkasovsky). Yeast cells were transformed with plasmids encoding Gic1 (116-314) or Gic1 (224-314) and each septin subunit as bait and prey respectively. Cells were cultivated either in the presence of X-Gal or in the absence of leucine. Upon a positive interaction, colonies that contained Gic1 and its interaction partner could grow in the absence of leucine or turn blue in the presence of X-Gal as a result of interaction between bait and prey. Our results clearly showed a positive interaction between both Gic1 (116-314) and Gic1 (224-314) and only Cdc10 (Fig. 3.10). Interaction of Gic1 with Cdc10 in the cell complemented our observations obtained from *in vitro* experiments. However, our result contradicts the previous yeast two-hybrid results (Iwase et al., 2006), which could be due to genetic background of yeast strains used.

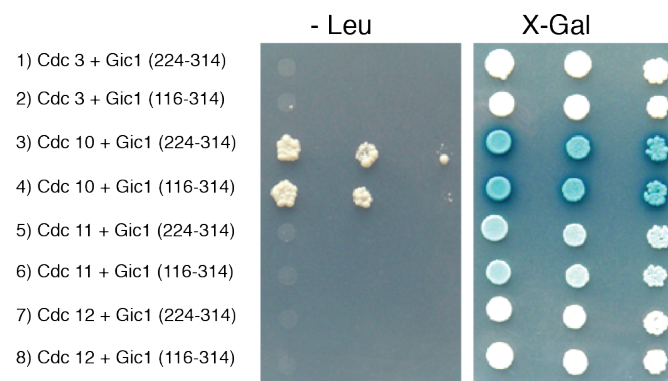


Fig. 3.10. Yeast two-hybrid assay. Plasmids carrying different septin subunits were co-transformed into yeast along with a plasmid carrying either Gic1 (224-314) or Gic1 (116-314) as described in materials and methods. Sample 1 and 2 correspond to Cdc3, sample 3 and 4 to Cdc10, sample 5 and 6 to Cdc11, sample 7 and 8 to Cdc12 plus Gic1 (224-314) and Gic1 (116-314) respectively (Courtesy of Dr. Marian Farkasovsky).

to Cdc12 plus Gic1 (224-314) and Gic1 (116-314) respectively (Courtesy of Dr. Marian Farkasovsky).

3.1.1.8) C-terminus of Gic1 is the septin-binding domain

The closest homologues of Gic1 in *homo sapiens* are proteins of the Borg family. It was shown that the Borg3 causes filament bundling in human cell lines. This effect was exerted by the BD3 domain in the C-terminal region of Borg3. This finding prompted us to uncover which part of Gic1 is responsible for

septin binding and formation of the railway structure. Gic1 and 2 contain a CRIB (Cdc42/Rac interactive binding) domain on their N-termini, which is responsible for binding to Cdc42p. The Gic1 used in previous experiments encompassed the middle and C-terminal region of the protein (amino acids 104-314). In the yeast two-hybrid assay we observed a positive interaction between Gic1 (224-314) and Cdc10. Therefore, we expressed and purified the C-terminus of Gic1 (224-314) to examine its effect on filament bundling of the yeast septin. We observed that Gic1 (224-314) and septin formed similar structures to the railway structure (Fig. 3.11). However, class averages of the Gic1 (224-314) cross-bridges showed that Gic1 (224-314) formed a thinner density compared to Gic1 (104-314) cross-bridges (Fig. 3.11D) but the distance between filaments did not change. Altogether, these data suggest that like the BD3 domain of Borg3, the C-terminus of Gic1 is responsible for septin binding and bundling while the middle part confers rigidity to Gic1 cross-bridges and the N-terminus binds Cdc42p and PIP2.

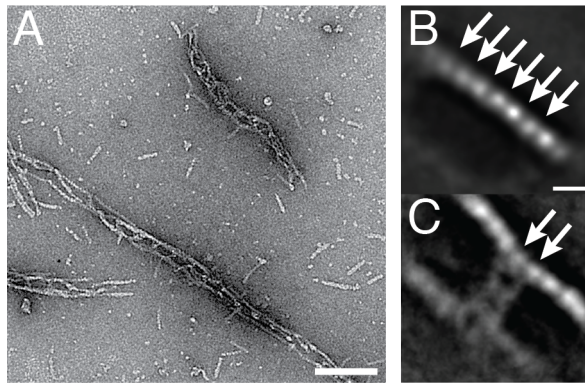


Fig. 3.11. C-terminus of Gic1 (amino acids 224-314) is the septin-binding domain. (A) 0.3 μM of the septin octamers was dialyzed with 1.5 μM of Gic1 (224-314) for 16 h at 4°C. (B) Representative class average of septin and (C) Gic1 (224-314) of the septin-Gic1 (224-314) complex obtained from 1144 and 1105 particles respectively. Scale bar in A is 100 nm and in B is 10 nm.

3.1.1.9) Binding of Gic1 to filaments vs. octamers

In an attempt to map the domain of Cdc10 that interacts with Gic1, we deleted the first 29 amino acids of Cdc10 that hampers polymerization of septin octamers. It was shown that this deletion interferes with Cdc10-Cdc10 interaction making septin tetramers or inside-out octamers when dialyzed against a low-salt buffer (Bertin et al., 2010). We performed single particle analysis on Cdc10 Δ (30-322)(R134A) septin and we confirmed the presence of tetramers and octamers (Fig. 3.12B and C). However, when Cdc10 Δ (30-322)(R134A) septin was dialyzed with Gic1, an extra density appeared on top of both tetramers and octamers in the class averages (Fig. 3.12E and F). This density that corresponds to Gic1 implies that Gic1 does not require the first 29 amino acids of Cdc10 for binding. This finding was also corroborated using analytical gel filtration, which showed the presence of Gic1-GST in the same fraction with the non-polymerizing septin (Fig. 3.12G). Moreover, we used another non-polymerizing septin with two deletions in Cdc10 Δ (30-322)(309-322) and another deletion in Cdc11 Δ (298-425) as a complementary experiment (Fig. 3.12H-I).

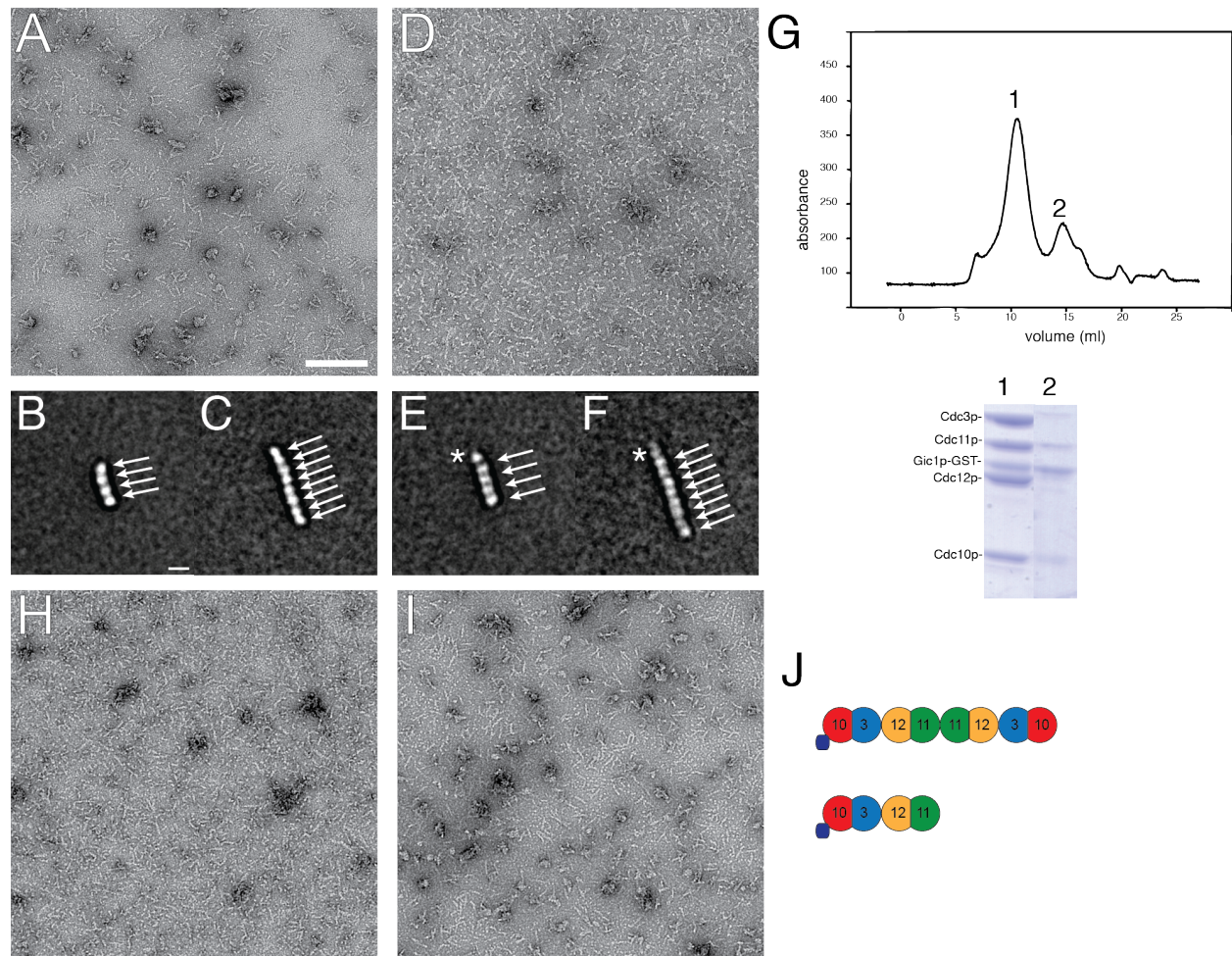


Fig. 3.12. Non-polymerizing septin with Gic1. (A) 0.3 μ M Cdc10 Δ (30-322)(R134A) septin was prepared for EM analysis. (B) and (C) show the class averages of Cdc10 Δ (30-322)(R134A) non-polymerizing septin. Classification resulted in two different populations constituting tetramer and octamer obtained from 1371 particles. (D) 0.3 μ M Cdc10 Δ (30-322)(R134A) was dialyzed with 1.5 μ M Gic1 for 16 h. (E) and (F) show the class averages of Cdc10 Δ (30-322)(R134A) non-polymerizing septin and Gic1 that resulted in a tetramers with an extra density on top (Cdc10) and inside-out octamers with an extra density on top (Cdc10) obtained from 2195 and 1282 particles respectively. (G) 1 mg of Cdc10 Δ (30-322)(R134A) septin was mixed with 1 mg of Gic1-GST, incubated for 15 min and injected into Superose 6 (GE Healthcare). Lane 1 shows a band corresponding to Gic1-GST, which shows binding of Gic1 to non-polymerizing septin. (H) 0.3 μ M Cdc11 Δ (298-425)Cdc10 Δ (30-322)(309-322) septin alone or (I) with 1.5 μ M Gic1 were prepared as described earlier. (J) Two model showing the binding of Gic1 to Cdc10 Δ (30-322) septin. Scale bar in A is 100 nm and in B is 10 nm.

We calculated homology models of Cdc3, Cdc10, Cdc11 and Cdc12 using SEPT2 structure (PDB 2QA5) as a reference to identify the conserved regions among different septin subunits. Interestingly, we found that the N-terminal region of Cdc10 is the least conserved region when we examined the NC-interface in

Cdc10-Cdc10 (Fig. 3.13). Therefore, it is expected that this region could confer specificity for binding of Gic1 to Cdc10 among septin subunits. Nevertheless, binding of Gic1 to Cdc10 Δ (30-322) septin is not impaired and seems to be still specific among septin subunits.

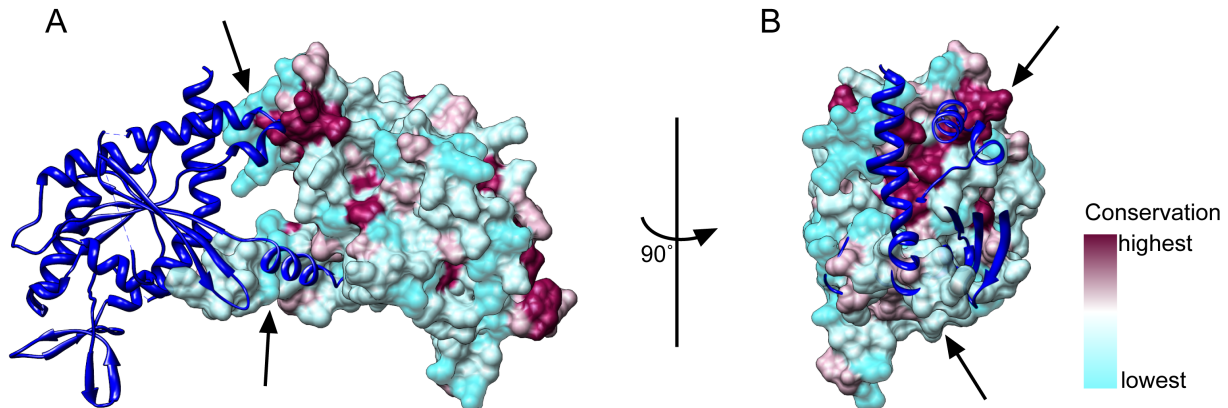


Fig. 3.13. Conservation of the NC-interface between Cdc3, Cdc10, Cdc11 and Cdc12. (A) side view and (B) end-on view of the NC-interface between two Cdc10 septins. Homology models of Cdc3, Cdc10, Cdc11 and Cdc12 were calculated using Phyre2 (Kelley and Sternberg, 2009) and SEPT2 structure (2QA5) as a model. The sequences of all septin subunits were aligned using ClustalW (Larkin et al., 2007). Arrows indicate the N- and C-termini of the Cdc10 (Courtesy of Dr. Stefan Raunser).

3.1.1.10) Gic1 confers resistance to septin filaments against high salt

Salt concentrations above 150 mM disrupt the NC-interface between a pair of Cdc11 and keeps septin in the octameric form. Interestingly, when we added Gic1 to the septin octamer in high salt, they polymerized into filaments and the railway complex formed (Fig. 3.14A). Furthermore, when a buffer containing high salt concentration was added to the septin-Gic1 complex, the integrity of the complex was not perturbed (Fig. 3.14B). This observation suggests that binding of Gic1 to Cdc10 dimers confers some conformational changes on the overall structure of each septin subunits making specifically the Cdc11-Cdc11 NC-interface resistant to the effect of high salt. Therefore, this finding provided another evidence that Gic1 acts as a stabilizer of the septin filaments.

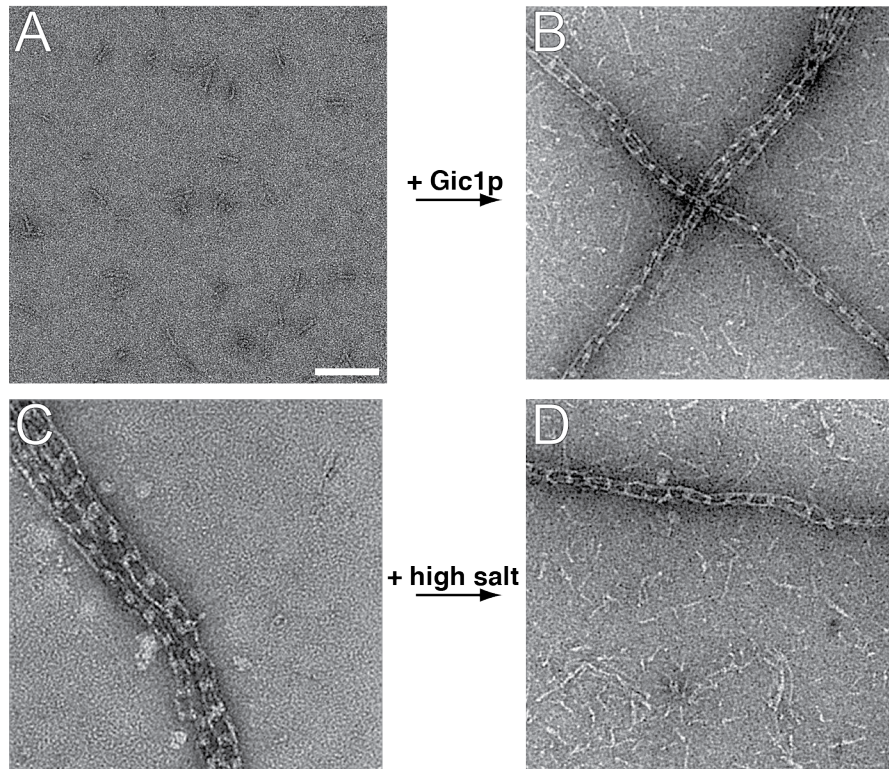


Fig. 3.14. Gic1 confers resistance against high salt. **(A)** 1.5 μM of Gic1 was added to 0.3 μM of the septin octamers in high salt buffer and they were dialyzed against a buffer containing 500 mM NaCl for 16 h. **(B)** the septin-Gic1 complex was prepared as described earlier. Then, the salt concentration was raised to 500 mM NaCl and incubated for 16 h. Scale bar is 100 nm.

3.1.2) Cdc42p regulates assembly of septin filaments

3.1.2.1) Cdc42p(GDP) enhances disassembly of the filaments

Cdc42p is the master regulator of cell polarity in yeast and human. It was shown that Cdc42 negatively regulated bundling of septin filament induced by Borg3 in mammalian cells (Joberty et al., 2001). This observation prompted us to ask whether the yeast Cdc42p can have similar effects on the yeast septin filaments as well. In this regard, we expressed Cdc42p in *E. coli* cells at OD₆₀₀ 0.6 by using 0.2 mM IPTG. The temperature was shifted to 20°C and cells were harvested after 16 h. The protein was purified via GSH-sepharose column (detailed in 2.2.2.3). The protein was eluted with 10 mM glutathione and the GST tag was cleaved using thrombin. The cleaved protein was concentrated and injected into Superdex 75 (10/30 GL) column (GE Healthcare) for further purification (Fig. 3.15).

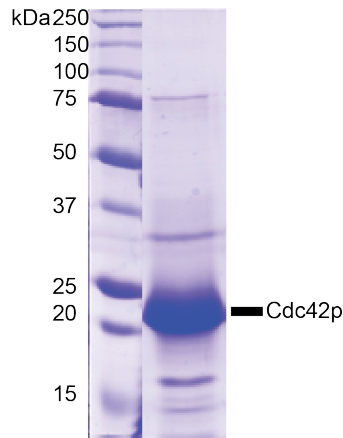


Fig. 3.15. Purification of Cdc42p. The Cdc42p was expressed in 10 L of *E. coli* cells. Cells were lysed with microfluidizer and centrifuged at 30,000 rpm for 45 minutes. The supernatant was passed through an 80-mL GSH-Sepharose column. The bound protein was eluted with 10 mM glutathione and 200 U of thrombin was added for cleavage of GST tag and dialyzed overnight. Sample was then concentrated and injected into Superdex 75 (10/30 GL) column (GE Healthcare).

In order to analyze the effect of Cdc42p on septin filaments, it needed to be in either GDP- or GppNHp-bound states. Usually, G-proteins are GDP-bound after purification due to their intrinsic GTPase activity. But to assure that majority of proteins have the desired nucleotide, excess of the desired nucleotides (over 100 times to the protein concentration) and EDTA were added to the protein and incubated for 2 h at room temperature. The protein was then applied to desalting column (PD-10) to remove the residual EDTA and unbound nucleotides or alternatively, it was concentrated and washed with a buffer devoid of any nucleotides using VivaSpin 500 column. The nucleotide content of the samples was controlled using HPLC to assure of the nucleotide exchange.

In order to examine the effect of Cdc42p on septin filaments, Cdc42p(GDP) and Cdc42p(GppNHp) were either added to the septin octamers during filament polymerization or to the pre-assembled filaments. First, we dialyzed excess (50 times higher than septin concentration) of Cdc42p(GDP) and Cdc42p(GppNHp) with the septin octamers. Surprisingly, we did not detect any filaments in the sample containing Cdc42p(GDP) whereas filaments comparable to the wild-type filaments were seen in the sample containing Cdc42p(GppNHp) (Fig. 3.16).

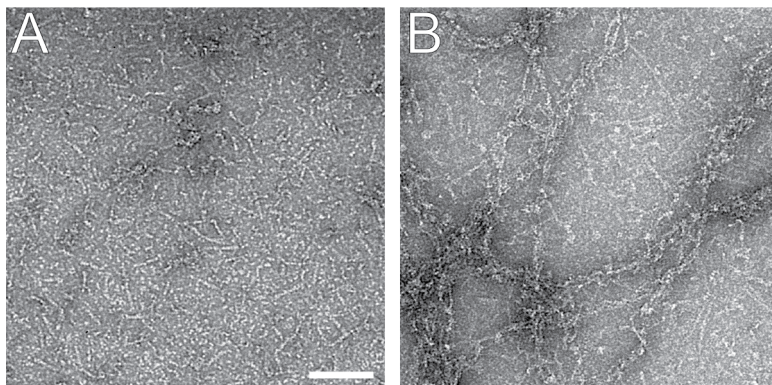


Fig. 3.16. Co-dialysis of Cdc42p and the septin octamers. 0.1 μ M of the septin octamer and 5 μ M of (A) Cdc42p(GDP), or (B) Cdc42p(GppNHp) were dialyzed together against a low-salt buffer. Samples were taken after 16h. Scale bar is 100 nm.

Next, both Cdc42p(GDP) and Cdc42p(GppNHp) were added to the pre-assembled filaments to check if Cdc42p(GDP) only prevents filament formation or it also disassembles the filaments. We observed that excess of Cdc42p(GDP) started to break the filaments as soon as 15 minutes and this process was almost complete after an hour (Fig. 3.17C). But to reach full breakage of all filaments, samples were incubated for 16 h. On the contrary, Cdc42p(GppNHp) had no effects on the filaments even after an overnight course of incubation (Fig. 3.17F). This indicates that Cdc42p(GDP) has a very high affinity for binding to septin and upon binding, it triggers the disassembly of the septin filaments in a time-dependent manner whereas Cdc42p(GppNHp) has a very low affinity to bind to septin.

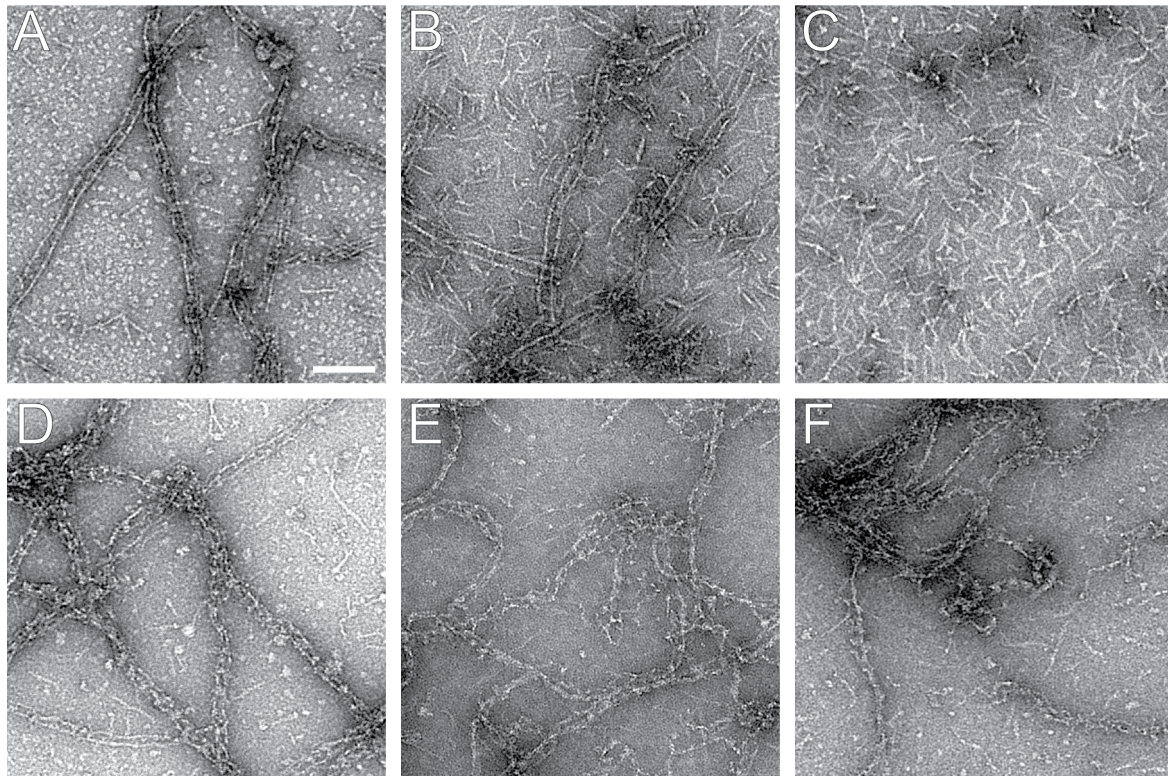


Fig. 3.17. Time-dependent disassembly of septin filaments by Cdc42p(GDP). 0.1 μ M of the septin octamers was dialyzed against a low-salt buffer. Then, either 5 μ M of Cdc42p(GDP) or Cdc42p(GppNHp) was added to the filaments. Samples were taken after 2 minutes (**A** and **D**), 15 minutes (**B** and **E**) and 1 h (**C** and **F**). Scale bar is 100 nm.

In order to find out the critical concentration at which Cdc42p(GDP) could break the filaments, different concentrations of both Cdc42p proteins were added to septin filaments and incubated for 16 h. We observed that at 10 times higher molar concentration, Cdc42p(GDP) could not bind and disassemble the septin filaments (Fig. 3.18A). As the concentration was raised to 30 times above septin concentration,

Cdc42p(GDP) bound to the filaments but it was still below the effective concentration to execute full disassembly of the filaments (Fig. 3.18C). But, at 50 times the septin concentration, Cdc42p(GDP) could exert its effect to disassemble the filaments into smaller pieces (Fig. 3.18D). The need for high concentration of Cdc42p is in agreement with its biological function that Cdc42p accumulates at the budding site. Therefore, a high concentration of Cdc42p is present at a location where septin is present to keep it as an unorganized patch of most likely octamers or filaments undergoing constant assembly and disassembly.

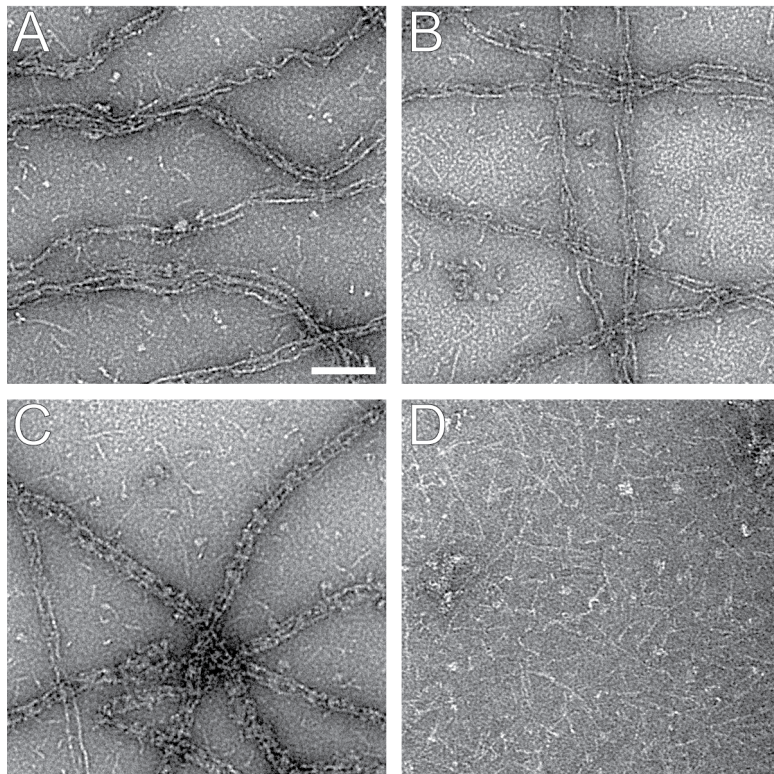


Fig. 3.18. Concentration-dependent disassembly of septin filaments by Cdc42p(GDP). 0.1 μ M of the septin octamers was dialyzed against a low-salt buffer. (A) 1 μ M, (B) 2 μ M, (C) 3 μ M and (D) 5 μ M of Cdc42p(GDP) was added to the filaments and samples were taken after 16h. Scale bar is 100 nm.

Moreover, we used a mutant Cdc42p-T17N, which is always locked in a GDP bound state to supplement our previous finding that Cdc42p(GDP) caused the disassembly of filaments. Expectedly, we observed that Cdc42p-T17N disassembled the filaments after an overnight incubation with pre-assembled septin filaments (Fig. 3.19).

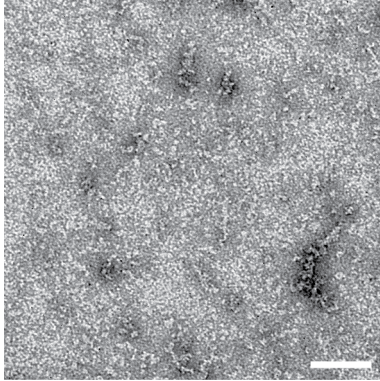


Fig. 3.19. Cdc42p-T17N disassembles the septin filaments. 0.1 μM of septin octamer was dialyzed against a low-salt buffer. 25 μM of Cdc42p-T17N was added to the filaments and a sample was taken after 16h. Scale bar is 100 nm.

3.1.2.2) Addition of Gic1 to broken septin filaments restores the railway structure

Before the onset of budding, in early G1, Cdc42p exists in its GDP-bound state. As the cycle proceeds, it becomes GTP-bound and recruits proteins required for budding including septin and Gic1. During early G1 septin prevails as octamers in the cytoplasm. The mechanism by which septins are kept in octameric form is unknown. We observed that Cdc42p in its GDP-bound state could disassemble the septin filaments. Our studies unveiled a new function of Cdc42p and provided a clue that Cdc42p(GDP) maintains septins as an octamer and as it becomes GTP-bound it recruits septin to the budding neck along with Gic1 to form the railway structure. Hence, it inspired us to speculate that addition of Gic1 to the Cdc42p-broken septin should restore the filament/railway formation capability. In this respect, we added Gic1 to the sample containing disassembled septin and Cdc42p(GDP) or Cdc42p(GppNHp). Expectedly, after an overnight incubation, the railway structure was reconstituted in both samples (Fig. 3.20). This observation highlights two points; first, Gic1 and Cdc42p(GDP) bind to the same area and compete for binding to promote filament assembly or disassembly, respectively and second, Gic1 has a higher affinity to septin compared to Cdc42p(GDP).

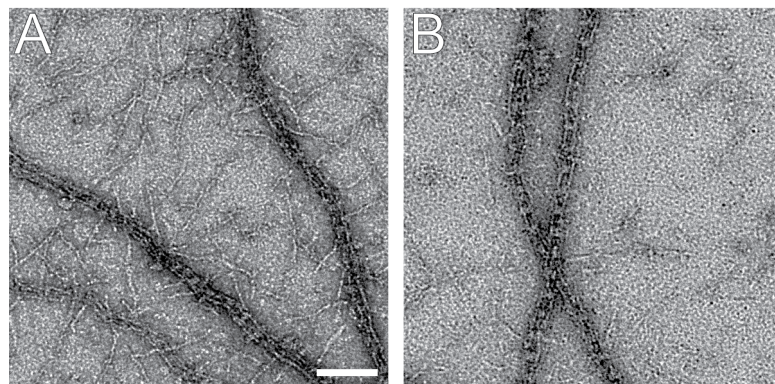


Fig. 3.20. Addition of Gic1 restores the railway structure. 0.1 μM of septin octamers was dialyzed against a low-salt buffer. Then, 0.5 μM of Cdc42p(GDP) or Cdc42p(GppNHp) were added to the filaments and incubated for 16 h. Afterwards, 1.5 μM of Gic1 was added to the sample containing (A)

septin and Cdc42p(GDP) and (B) septin and Cdc42p(GppNHp) and incubated for 16 h. Scale bar is 100 nm.

3.1.2.3) Mechanism of disassembly

Breakage of the septin filaments by Cdc42p unveils a previously unknown regulatory mechanism. *In vitro*, upon addition of Gic1 to Cdc42p-broken septin sample they formed the septin-Gic1 complex. Thus, the underlying mechanism of disassembly should not perturb the structural integrity of the septin octamers. In order to find out the mechanism, first we mixed the septin octamers with either Cdc42p(GDP) or Cdc42p(GppNHp) and injected the samples into Superdex S200 column. Samples were precipitated with trichloroacetic acid and analyzed on SDS-PAGE (experiments performed by Dr. Marian Farkasovsky). We observed that Cdc42p(GDP) but not Cdc42p(GppNHp) remained bound to the septin octamer, which indicates that its binding to a certain subunit of septin caused the dissociation of the filaments (Fig. 3.21).

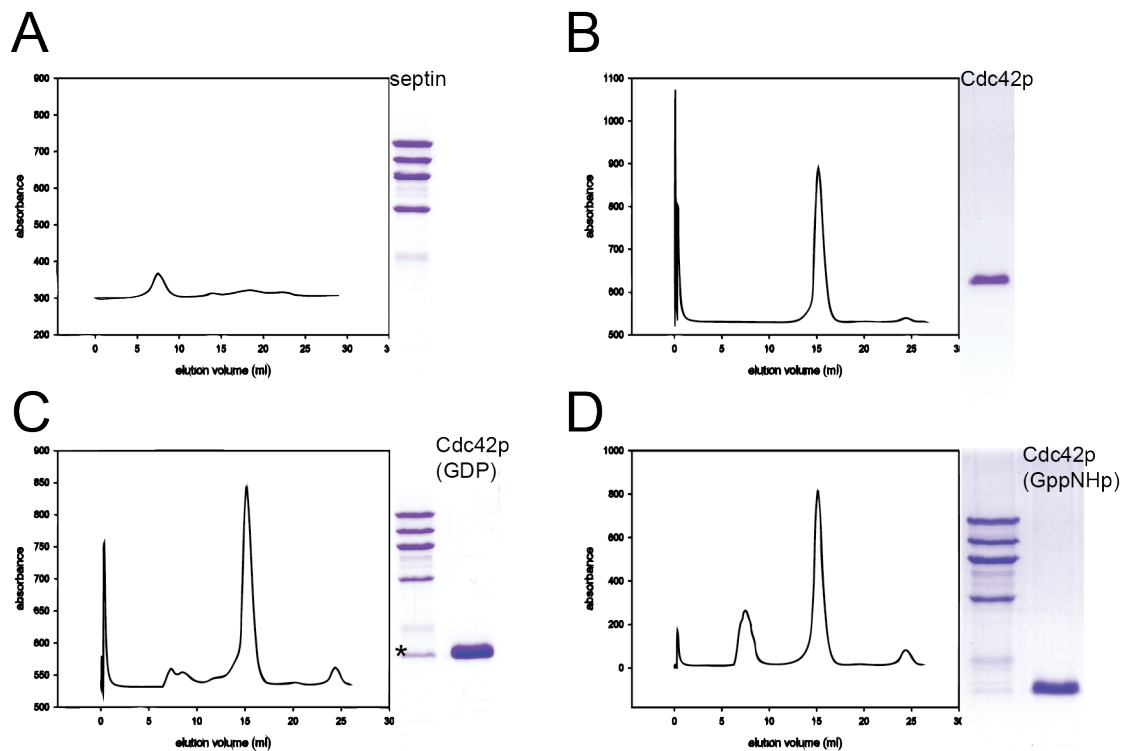


Fig. 3.21. Gel filtration analysis of Cdc42p with the septin octamer. (A) 1 mg of the septin octamer, (B) 1 mg of Cdc42p(GDP), (C) 1 mg of the septin octamer with 1 mg of Cdc42p(GDP) and (D) 1 mg of the septin octamer with 1 mg of Cdc42p(GppNHp) were injected into the Superdex S200 column (GE Healthcare). Samples were precipitated with trichloroacetic acid and analyzed with SDS-PAGE. Asterisk in (C) shows Cdc42p(GDP) and septin together in the same fraction.

Furthermore, single particle analysis was performed on a sample that contained Cdc42p-broken septin. We observed that the majority of fragments generated by Cdc42p(GDP) were octamers (Fig. 3.22A). However, by masking the septin octamer and focusing on the immediate surrounding of septin for classification, we could obtain class averages that showed an obvious extra density around the septin octamer, which indicates the presence of Cdc42p(GDP) on the tip of the octamers (Fig. 3.22B and 3.22C). The same sample was incubated with α -Cdc11, α -Cdc3 and α -Cdc42p polyclonal antibodies (1:100 dilution) for an overnight to identify the breakage point. We showed that α -Cdc3 antibody labeled the sub-terminal subunit (Fig. 3.22D) and α -Cdc11 antibody bound to the central position (Fig. 3.22E). A few of the particles showed a hexameric structure and α -Cdc3 antibody labeled them on the top position (Fig. 3.22F and G). This observation implies that Cdc42p(GDP) binds to an area around Cdc10-Cdc10 interface and triggers the disassembly of septin filaments at the central hinge of octamers that leads to generation of an octamer that constitutes two halves of the septin octamers (Fig. 3.22H). Notably, in a few particles, binding of Cdc42p(GDP) to Cdc10 led to their dissociation from the octamers generating hexamers with no extra density.

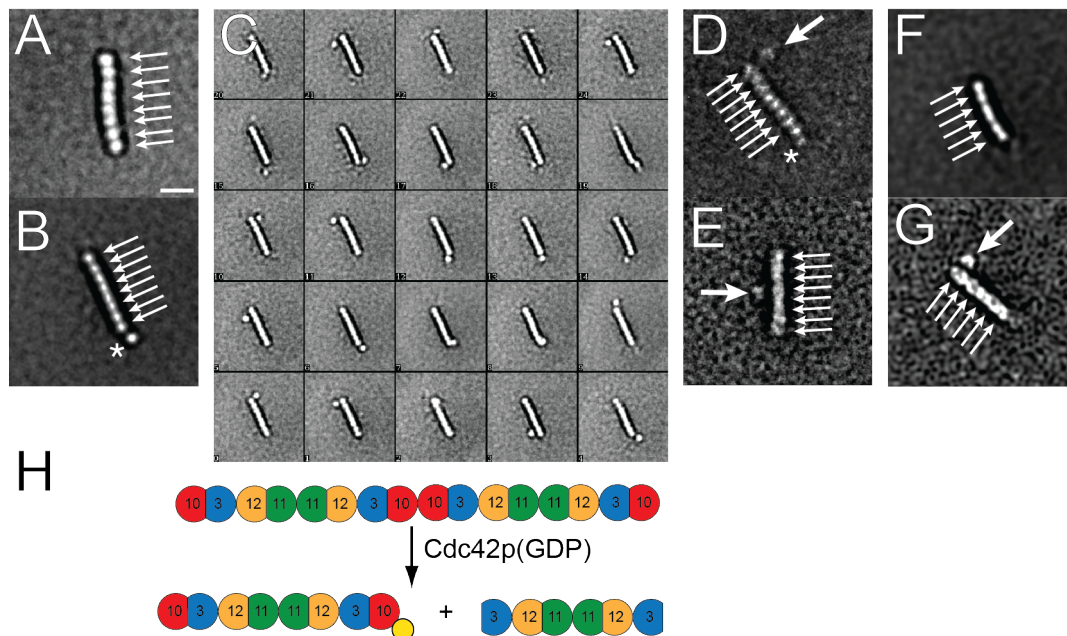


Fig. 3.22. Cdc42p(GDP) disassembles the septin filament at Cdc10-Cdc10 interface. (A) A class average of broken septin filaments by Cdc42p(GDP) (prepared as explained in the legend of Fig. 3.17D) obtained from 14407 particles. (B) A class average of broken septin filaments by Cdc42p(GDP), which showed a small density at the end of the octamers that corresponds to Cdc42p(GDP). 14407 particles were classified after masking the septin and leaving the surrounding free. (C) An overview of all classes generated after masking the septin and focusing on the immediate surrounding of septin. 20 μ L of the same sample was mixed with 5 μ L of either (D) α -Cdc3 or (E) α -Cdc11 antibodies (1:100) and incubated for 16 h. The class averages were obtained from 451 and 142 particles

respectively. **(F)** A class average of broken septin filaments by Cdc42p(GDP), which showed a hexameric structure obtained from a subset of 14407 particles used for **(A)**. **(G)** Hexameric structures labeled with α -Cdc3 antibody obtained from a subset of 451 particles used for **(D)**. **(H)** A model representing the breakage mechanism of septin by Cdc42p(GDP). Thin arrows indicate the septin subunits and the thick arrow points to antibody. Asterisk shows the Cdc42p(GDP) bound to Cdc10. Scale bar is 10 nm.

The α -Cdc42p antibody did not bind to the octamers probably due to weak binding affinity and very few numbers of particles that still had Cdc42p(GDP) bound to the octamers. Yet, use of a proper mask during classification, antibody labeling and gel filtration analysis illustrated a mechanistic function for Cdc42p(GDP) that binds around the Cdc10-Cdc10 dimer and breaks the interaction in the NC-interface and remains bound to Cdc10. Upon addition of Gic1, it competes with Cdc42p(GDP) for binding to Cdc10 and as it has a higher affinity for septin, it binds to Cdc10 and connects two octamers to restore the filaments (Fig. 3.20).

To identify the binding site of Cdc42p(GDP) on Cdc10, we mixed the non-polymerizing Cdc10 Δ (30-322)(R134A) septin with Cdc42p(GDP) and injected into the Superose 6 column (GE Healthcare). The proteins eluted separately suggesting that Cdc42p(GDP) requires the first 29 amino acids of Cdc10 to bind (Fig. 3.23A). Single particle analysis also showed the presence of tetramers and octamers as expected without any extra densities (Fig. 3.23C and D). This finding suggests that Cdc42p(GDP) requires the first 29 amino acids of Cdc10 for binding. However, we showed that Gic1 competes with Cdc42p(GDP) for binding to Cdc10 and does not require the first 29 amino acids of Cdc10. Therefore, the binding site of Gic1 should partly overlap with Cdc42p(GDP).

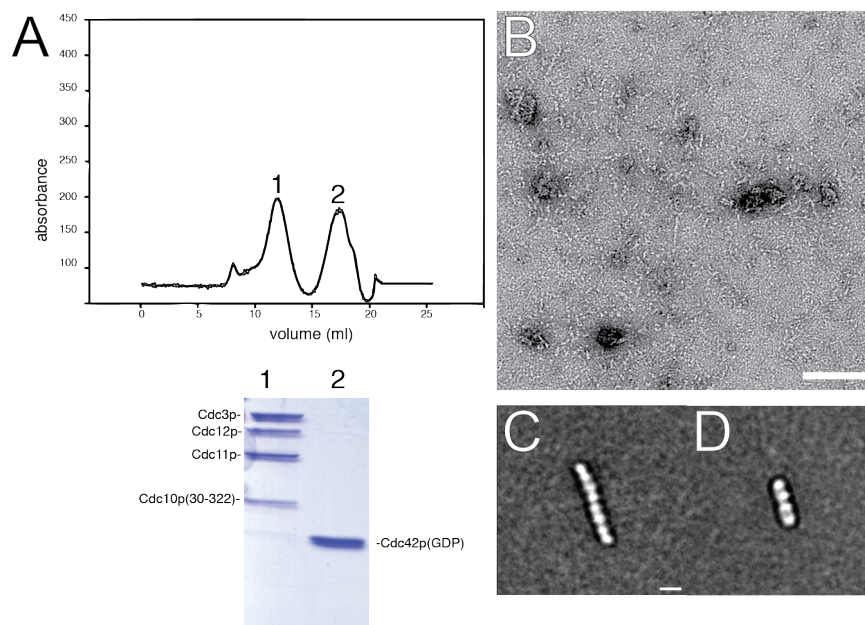


Fig. 3.23. Cdc42p(GDP) binds to the N-terminus of Cdc10. **(A)** 1 mg of Cdc10 Δ (30-322)(R134A) septin was mixed with 1 mg of Cdc42p(GDP) and injected into Superose 6 (GE Healthcare). The 1st peak corresponds to Cdc10 Δ (30-322)(R134A) septin and the 2nd peak to the unbound Cdc42p(GDP). **(B)** A sample was prepared for EM from the

1st peak and single particle analysis was performed. (C) and (D) show the octameric and tetrameric structures obtained from 1252 particles. Scale bar in B is 100 nm and in C is 10 nm.

By all means, it could not be ruled out that Cdc42p(GDP) would act as a GAP (GTPase Activating Protein) for septin. The only septin subunit, which is GTP-bound is Cdc3. Therefore, we hypothesized that as Cdc42p(GDP) binds in the proximity of Cdc10-Cdc3 interface, it could trigger a GTPase activity on Cdc3. As a result of such activity, the structural changes upon hydrolysis of GTP would be transferred to an immediate NC-interface, which, in this case, is Cdc10-Cdc10 interface. Accordingly, septin filaments were prepared as explained before and either Cdc42p(GDP) or Cdc42p(GppNHp) were added to the filaments. At 0 h and 16 h a sample was taken, boiled, centrifuged and injected into C18 column to examine the nucleotide content of septin in a long span of time. In order to assess the changes of nucleotide level, we monitored decrease of GTP as excess of Cdc42p(GDP) could hinder a reasonable judgment of increase of GDP. However, the low content of GTP in septin filaments complicated a proper detection of GTP drop but still enough to draw a conclusion whether Cdc42p(GDP) can act as a GAP. The HPLC analyses did not show any changes of the nucleotide content over 16 hours of reaction time (Fig. 3.24).

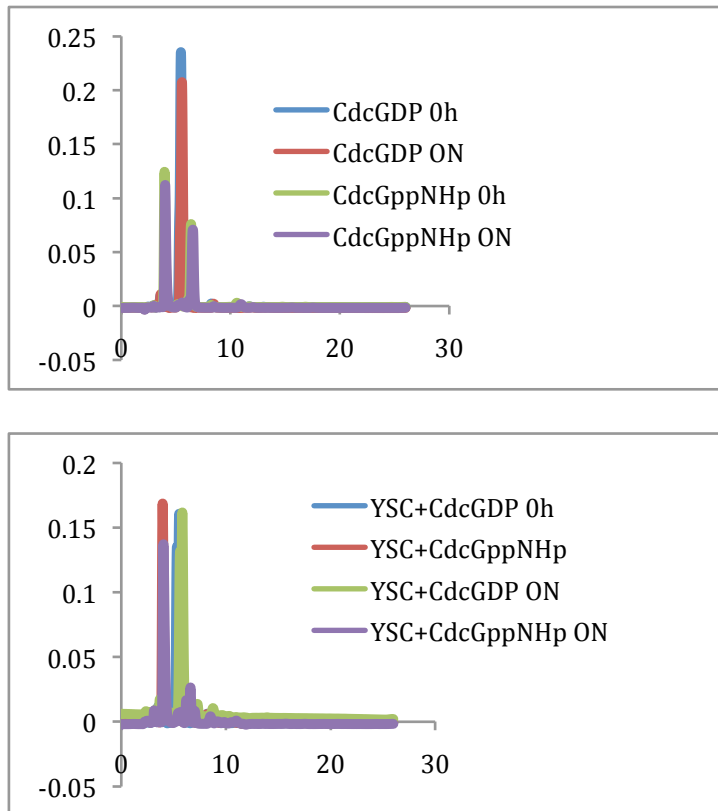


Fig. 3.24. HPLC analysis on the effect of Cdc42p on the YSC. 0.3 μ M of YSC was prepared as explained before. Then, 3 μ M of Cdc42p(GDP) was added to the filaments. 25 μ l of the the samples were taken at 0 h and 16 h, boiled and centrifuged at 13000 rpm for 5 minutes and the supernatant was injected into C-18 column. Samples were run under isocratic conditions (50 mM potassium phosphate pH 6.6, 10 mM tetrabutyl ammonium bromide, 16% (v/v) ACN) for separation of GTP from GDP. Upper chart corresponds to control samples of either Cdc42p(GDP) or Cdc42p(GppNHp) at 0 h or 16 h. Lower chart corresponds to mixture of the Cdc42p and YSC.

This observation could be explained by the facts that firstly, Cdc3 does not have an intrinsic GTPase activity and Cdc42p(GDP) is not able to activate or assist in this activity. Secondly, addition of Gic1 restores the filament formation, which indicates that the integrity of septin subunits is maintained. Therefore, changes in the nucleotide content cannot be a valid explanation and disassembly can be reasonably explained by binding of Cdc42p(GDP) to Cdc10.

3.1.3) Cdc42p(GppNHp) mechanistically regulates the septin-Gic1 complex

3.1.3.1) Cdc42p(GppNHp) but Cdc42p(GDP) binds to Gic1

Septin filaments serve as a scaffold for many proteins to localize themselves to the proper site to execute their function required for cytokinesis. To achieve this, some proteins bind to the septin filaments and serve as a platform for other proteins to get connected to the septin filaments. For instance, Bni5p binds to septin and myosin II to connect actomyosin complex to the septin (lee et al., 2002 and Fang et al., 2010). Gic2 was shown to interact with Cdc42p(GTP) via its CRIB (Cdc42/Rac interactive binding domain) domain located in its N-terminus (Orlando et al., 2008). We hypothesized that Gic1 could also serve as a platform for other proteins including Cdc42p to perform its function. In this regard, we mixed equal amounts of Gic1 with either Cdc42p(GDP) or Cdc42p(GppNHp) and injected them into Superdex S200 column. We observed that Cdc42p(GDP) and Gic1 eluted separately whereas Gic1 and Cdc42p(GppNHp) formed a binary complex and they co-eluted together (Fig. 3.25), which indicates binding between Cdc42p(GppNHp) and its effector, Gic1 at a molecular level.

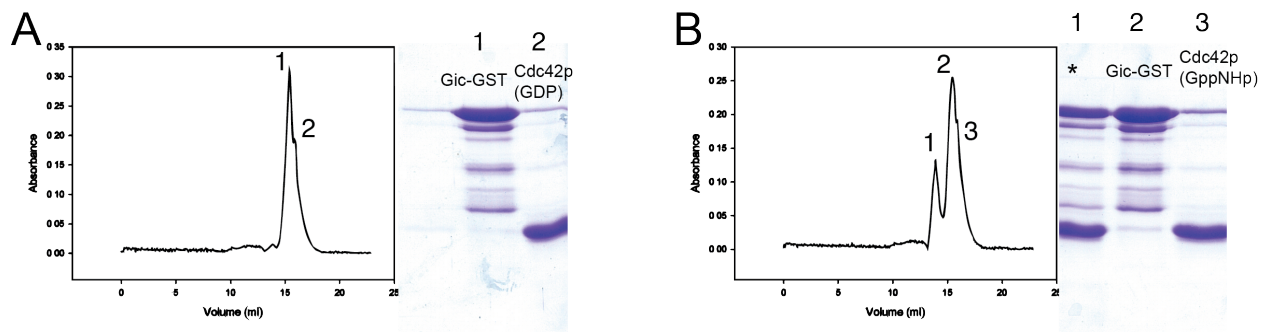


Fig. 3.25. Gel filtration analysis of binding between Gic1 and Cdc42p(GppNHp). 1mg of Gic1-GST was mixed with either (A) 1 mg of Cdc42p(GppNHp) or (B) 1 mg of Cdc42p(GDP) and injected into Superdex S200 column (GE Healthcare). Asterisk in (B) corresponds to an extra peak detected during gel filtration, which shows the binding between Cdc42p(GppNHp) and Gic1-GST.

We dialyzed septin and Gic1 with either Cdc42p(GppNHp) or Cdc42p(GDP) (equimolar to Gic1 concentration) together. In both samples, the railway structure formed but in the sample containing

Cdc42p(GppNHp), the Gic1 particle seemed to have a larger density (compare the insets in Fig. 3.26A and 3.26B). Hence, we picked the respective particles and performed single particle analysis. The representative class averages of the septin-Gic1-Cdc42p(GppNHp) complex depicted that the distance between two Gic1 cross-bridges was shorter with only four subunits in between and also the mass of Gic1 cross-bridges covered four subunits, which is due to the presence of Cdc42p(GppNHp) next to Gic1 (Fig. 3.26C and 3.26D). It should be noted that in the sample containing Cdc42p(GDP), the railway structure formed since Gic1 overcomes the effect of Cdc42p(GDP) and has a higher affinity to septin.

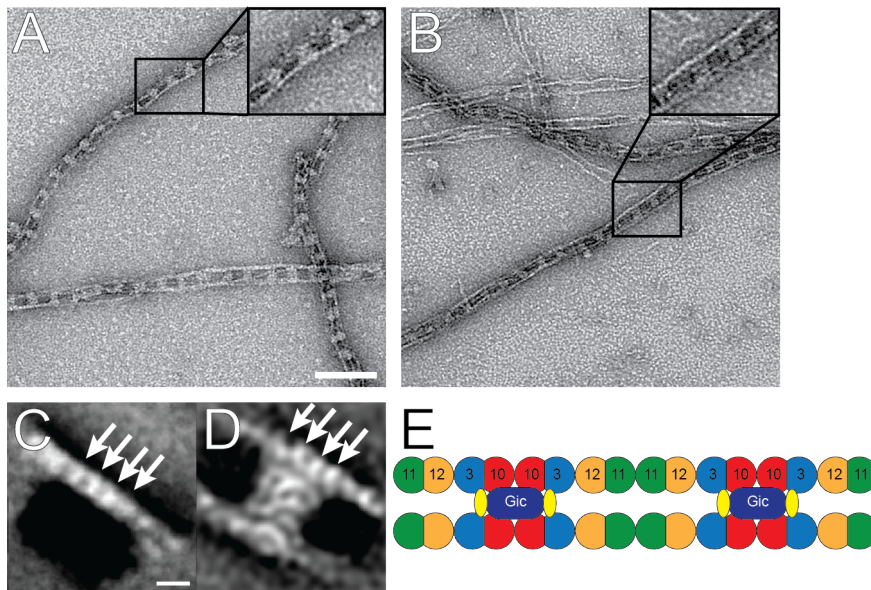


Fig. 3.26. Cdc42p(GppNHp) binds to Gic1. 0.1 μM of the septin octamers and 0.5 μM of Gic1 were dialyzed with 0.5 μM of either (A) Cdc42p(GppNHp) or (B) Cdc42p(GDP). Insets show a focused area around Gic1 cross-bridges. (C) A representative class average of septin in the septin-Gic1-Cdc42p(GppNHp) complex obtained from 3979 particles. (D) A class average of Gic1-Cdc42p(GppNHp) particle from the septin-Gic1-Cdc42p(GppNHp) complex obtained from 3837 particles. (E) A model that depicts the presence of Cdc42p(GppNHp) next to Gic1. Scale bar in A is 100 nm and in D is 10 nm.

3.1.3.2) The septin-Gic1 complex disassembles at high concentration of Cdc42p(GppNHp)

Our results showed that Gic1 is a binding partner for Cdc42p(GppNHp) and could theoretically serve as a platform for Cdc42p binding. The local concentration of Cdc42p at the budding neck is known to increase by its constant delivery as the cell cycle proceeds (Orlando et al., 2010). Therefore, it prompted us to examine the effect of higher concentrations of Cdc42p on the septin-Gic1 railway structure as Cdc42p(GDP) also needed to pass a threshold concentration to exert its effect on the septin filaments. In

this regard, the septin-Gic1 complex was prepared as described before and then we added excess (x10 of Gic1 concentration) of either Cdc42p(GDP) or Cdc42p(GppNHp) to the complex. Cdc42p(GDP) did not perturb the integrity of the complex since it does not bind to Gic1 and besides, Cdc10 (binding site of Cdc42p) is occupied by Gic1. On the contrary, Cdc42p(GppNHp) disassembled the septin-Gic1 complex in a time- and concentration-dependent manner. Cdc42p(GppNHp) bound to Gic1 and formed aggregates and as a result of a possible tension that they exert on filaments, they broke the filaments into smaller but still filamentous fragments (Fig. 3.27 and 3.28). Disassembly of the septin-Gic1 complex initiated as soon as 15 minutes and after an hour was almost complete but to achieve full disassembly, samples were incubated for 16 h. Our observation unveils a new mechanistic regulation of septin filaments by Cdc42p. In fact, in telophase Cdc42p relocates to the neck where Gic1 and septin are present. At this stage, cytokinesis is fulfilled with the help of actomyosin and septin rings disassemble. The fragmented septin is reused in the next round of cell cycle to make new septin rings. We showed that Cdc42p(GppNHp) could bind to Gic1 and upon binding, it broke apart the septin-Gic1 complex. In this way, the fragments generated by Cdc42p(GppNHp) can mix with the newly synthesized septin to make octamers composed of old and new septin (McMurray et al., 2009). It should be noted that other post-translational modifications and regulatory mechanisms such as sumoylation that control septin assembly and disassembly are neglected in this study.

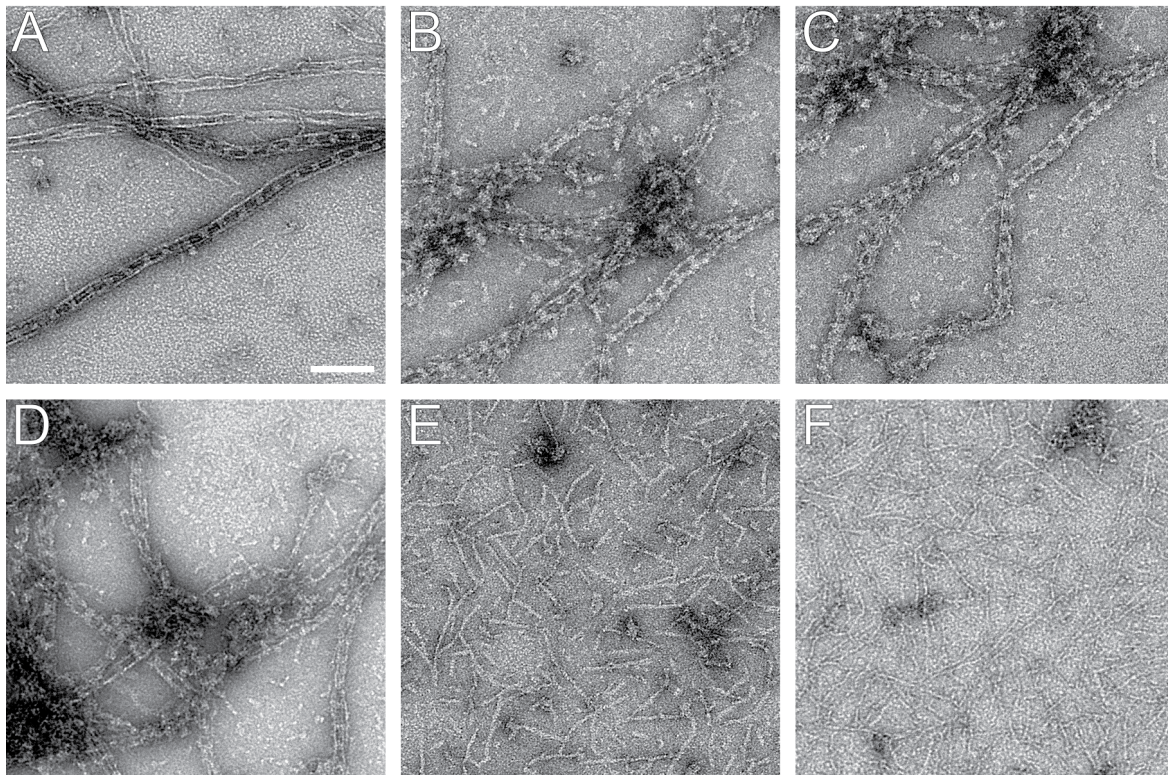


Fig. 3.27. Time-dependent disassembly of the septin-Gic1 complex by Cdc42p(GppNHp). 0.1 μ M of septin octamer was dialyzed with 0.5 μ M of Gic1. 5 μ M of either Cdc42p(GDP) or Cdc42p(GppNHp) was added to the

complex and samples were taken after 2 minutes (**A** and **D**), 15 minutes (**B** and **E**), 1 h (**C** and **F**). Scale bar is 100 nm.

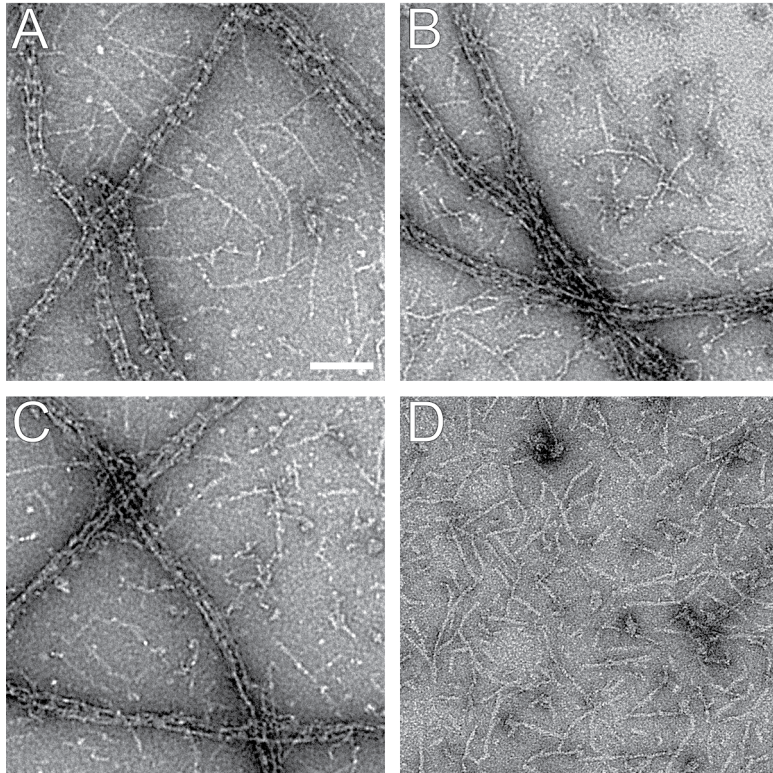


Fig. 3.28. Concentration-dependent disassembly of the septin-Gic1 complex by Cdc42p(GppNHp). 0.1 μ M of septin octamer was dialyzed with 0.5 μ M of Gic1. Then (**A**) 0.25 μ M, (**B**) 0.5 μ M, (**C**) 2 μ M and (**D**) 5 μ M of Cdc42p(GppNHp) was added and samples were taken after 16 h. Scale bar is 100 nm.

As a control, we used Gic1 (224-314), which lacks the N-terminus and its central domain containing the CRIB domain to show that binding of Cdc42p to Gic1 causes the disassembly of the septin-Gic1 complex. We prepared the septin-Gic1 (224-314) complex. Then, low and high concentrations of Cdc42p(GDP) and Cdc42p(GppNHp) were added to the complex and incubated for 16 h. As expected, addition of either Cdc42p(GDP) or Cdc42p(GppNHp) at low or high concentration did not perturb the septin-Gic1 (224-314) complex (Fig. 3.29). Our data substantiated once again that binding of Cdc42p(GppNHp) to Gic1 is mediated via the CRIB domain of Gic1. The interaction of Gic1 to Cdc42p(GppNHp) is favored upon septin that results in a mechanistic tension on the septin filaments. Our results are in full agreement with the previously reported mode of action for the human Cdc42 that assisted in relieving the filament bundling caused by Borg3 (Joberty et al., 2001).

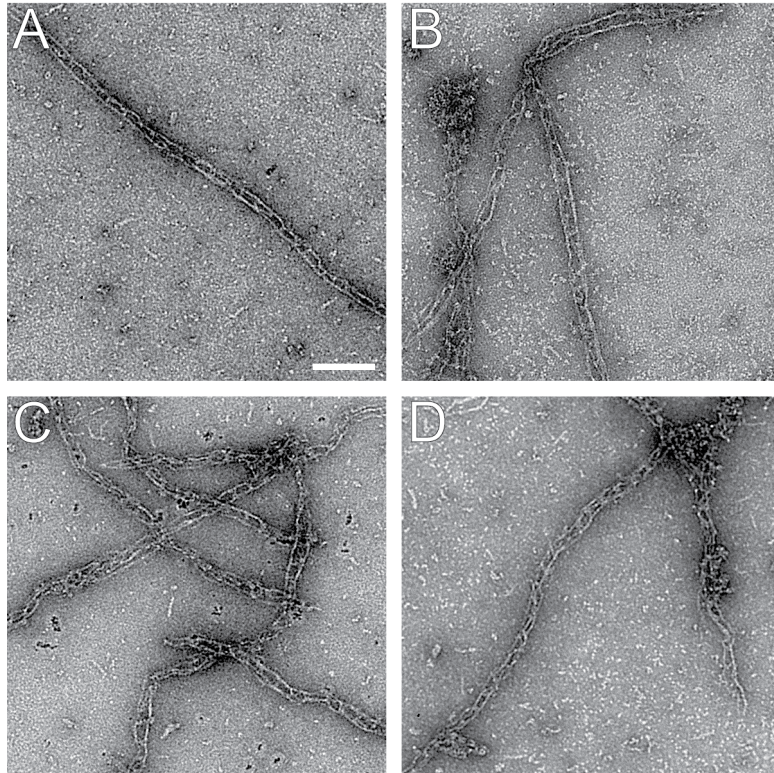


Fig. 3.29. Cdc42p(GppNHp) or Cdc42p(GDP) do not disturb the septin-Gic1 (224-314) complex. 0.1 μ M of septin octamer was dialyzed with 0.5 μ M of Gic1 (224-314). Then either 0.5 μ M of (A) Cdc42p(GDP) or (C) Cdc42p(GppNHp), or 5 μ M of (B) Cdc42p(GDP) or (D) Cdc42p(GppNHp) were added and incubated for 16 h. Scale bar is 100 nm.

1.3.3.3) Simultaneous addition of Gic1 and Cdc42p to filaments

In order to evaluate the binding affinity between septin, Gic1, Cdc42p(GppNHp) and Cdc42p(GDP), Gic1 was mixed with either Cdc42p(GppNHp) or Cdc42p(GDP) and then added to the septin filaments. In the sample containing Gic1 and Cdc42p(GDP), the railway structure formed since Gic1 does not bind to Cdc42p(GDP) and Cdc42p could not also disassemble the septin-Gic1 complex as Cdc10 was occupied by Gic1 (Fig. 3.30A). It indicates that Gic1 has a higher affinity than Cdc42p(GDP) to bind to septin. In the other sample, Gic1 and Cdc42p(GppNHp) formed a binary complex and when added to the septin filaments, they did not bind to the filament (Fig. 3.30B). However, in some areas, a punctuate pattern of the railway could be seen. This observation shows that Cdc42p(GppNHp) is the preferred binder of Gic1 than the septin.

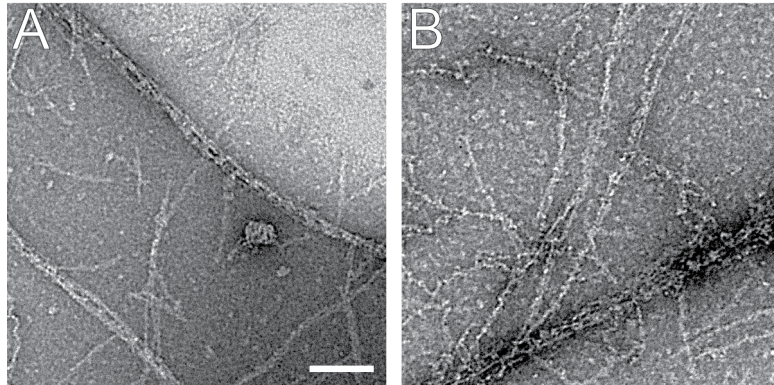


Fig. 3.30. Simultaneous addition of Gic1 and Cdc42p. 0.1 μM of the septin octamer was dialyzed against a low-salt buffer. 0.5 μM of Gic1 and either (A) 5 μM Cdc42p(GDP) or (B) 5 μM of Cdc42p(GppNHp) were mixed and incubated for 1h then added to the filaments for 16 h. Scale bar is 100 nm.

3.1.4) Effect of nucleotides on septin filaments

3.1.4.1) GTP destabilizes the filaments but not the septin-Gic1 complex

A few studies have been performed that targeted understanding the function of nucleotides in septins (Mitchison et al., 2002; Vrabioiu et al., 2004; Sirajuddin et al., 2009; Nagaraj et al., 2008). These studies suggest that nucleotides play a structural role rather than regulatory in septins. Moreover, the turnover of nucleotides is quite slow during a round of cell cycle (Vrabioiu et al., 2004). Therefore, at least some septins, if not all, appear to have a very weak GTPase activity, which is due to a very slow nucleotide exchange rate (Vrabioiu et al., 2004). In fact, Cdc3 and Cdc11 of the yeast septin complex do not have a threonine (T78) required for nucleotide hydrolysis (Sirajuddin et al., 2009). Thus, only Cdc12 and Cdc10 are able to hydrolyze GTP to GDP. Among septin subunits only Cdc3 is bound to GTP and all others are GDP-bound, which is in agreement with an evidence showing that septins have a 3:1 GDP to GTP ratio after purification (Sirajuddin et al., 2009). But, data concerning the effect of nucleotide exchange and its effect on filaments are missing. In order to gain insight about the effect of nucleotides on filaments, we added excess of GTP to the septin filaments and incubated them for 16 h. GTP started to disassemble the filaments at 200 times above the septin concentration (it should be considered that each septin octamer has 8 nucleotides). As the nucleotide concentration rose to 2000 times above the septin concentration, disassembly reached fulfillment (Fig. 3.31E). Moreover, GppNHp had a similar effect on the filaments (Fig. 3.31F).

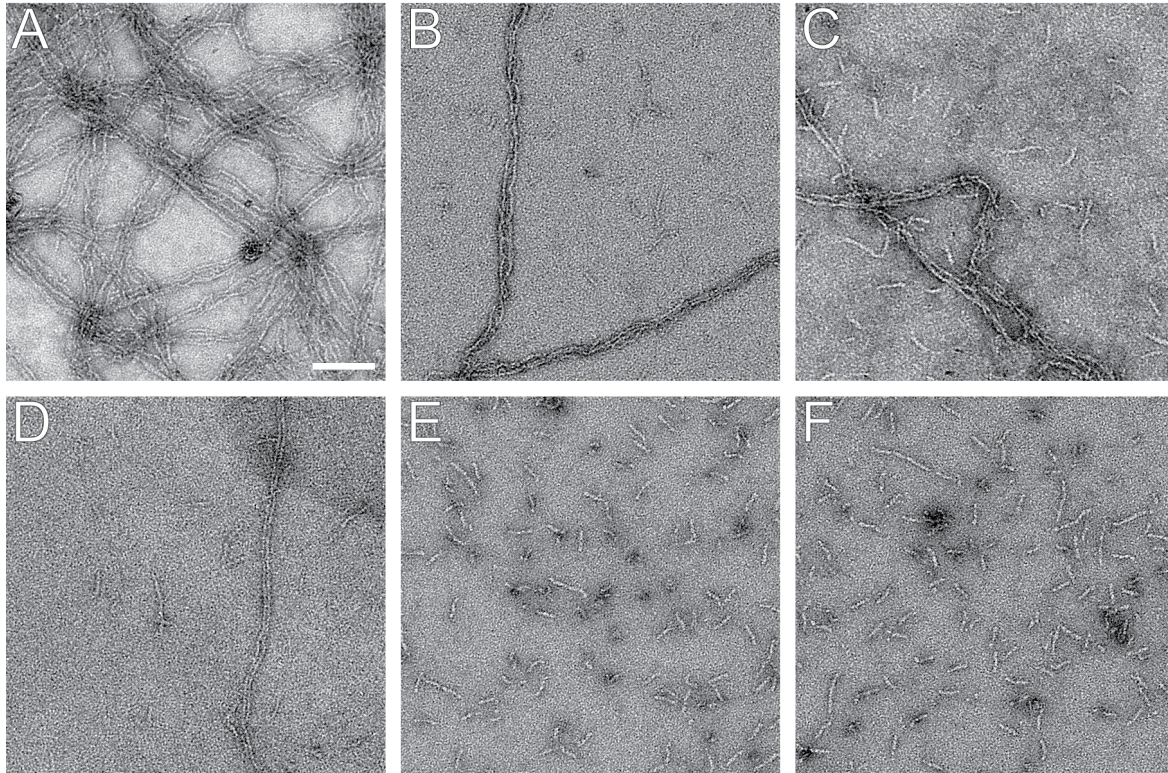


Fig. 3.31. GTP disassembles the septin filaments. 0.5 μ M of the septin octamers was dialyzed against a low-salt buffer. Then (A) 0.01 mM, (B) 0.05 mM, (C) 0.5 mM, (D) 1 mM, (E) 4 mM GTP or (F) 4 mM GppNHp was added to the filaments and sample were incubated for 16 h. Scale bar is 100 nm.

The mechanism of breakage does not involve hydrolysis of GTP but rather an exchange of GDP to GTP since GppNHp had similar effects on the septin filaments compared to GTP. Cdc11, Cdc12 and Cdc10 are the possible candidates for exchange of GDP to GTP as Cdc3 was proposed to be GTP-bound (Sirajuddin et al., 2009). Cdc11 is the only GDP-bound subunit, which does not have an intrinsic GTPase activity. It was shown that upon binding of GppNHp to the human SEPT2, conformational changes are transferred to the N-terminus of the protein and thereby affect the NC-interface (Sirajuddin et al., 2009). Thus, nucleotide exchange in Cdc11 could perturb the NC-interface in Cdc11-Cdc11 dimers and lead to dissociation of octamers. Accordingly, we used polyclonal antibodies against Cdc3 and Cdc11 to show the breakage point of septin filaments to confirm our hypothesis. In agreement with our hypothesis, we observed that α -Cdc3 antibody labeled the septin octamers in the sub-terminal position (Fig. 3.32A) and the α -Cdc11 antibody labeled the octamers on the terminal position (Fig. 3.32B). Therefore, our model (Fig. 3.32C) provides the first evidence regarding the regulatory function of nucleotides on septin filaments.

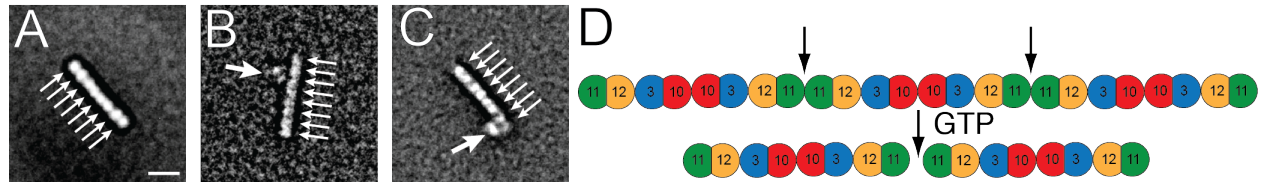


Fig. 3.32. GTP disassembles septin filaments at Cdc11-Cdc11 interface. 0.5 μM of the septin octamers was dialyzed against a low-salt buffer to prepare filaments. Then, 4 mM of GTP was added and incubated for 16 h. Subsequently, 5 μl of either anti-Cdc3 or anti-Cdc11 antibodies (1:100) were added to 20 μl of the septin sample. **(A)** A class average of GTP-broken septin obtained from 3169 particles **(B)** A class average of GTP-broken septin with $\alpha\text{-Cdc3}$ antibody obtained from 188 particles. **(C)** A class average of GTP-broken septin with $\alpha\text{-Cdc11}$ antibody obtained from 281 particles. Thin arrows point to septin subunits and thick arrows to antibody. **(D)** A model that represents the breakage point of septin filaments upon addition of GppNHp or GTP. Scale bar is 10 nm.

Increase of the local concentration of GTP at the budding neck through budding could destabilize filaments as a result of nucleotide exchange in Cdc11. We asked whether presence of Gic1 could have any contrary effects on filament stability as it does against Cdc42p. We answered this question in two different experiments. First, we added Gic1 to GTP-broken septin octamers and incubated them for 16 h. We observed that addition of Gic1 could partially restore the filament and the railway formation (Fig. 3.33A). Second, we added excess of GTP to the septin-Gic1 complex and we noticed that GTP could not destabilize the complex (Fig. 3.33B). This finding underscores the stabilizing role of Gic1, which upon binding to Cdc10 confers conformational changes to the subunits of the filaments that prohibits the exchange of nucleotide in Cdc11 (see also 3.1.1.6 and 3.1.1.10).

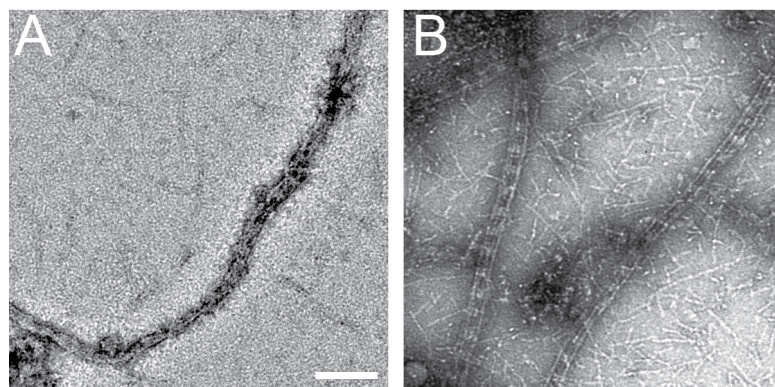


Fig. 3.33. Gic1 counteracts the effect of GTP. **(A)** 0.5 μM of septin octamers was dialyzed to form filaments and 4 mM of GTP was mixed for 16 h. Subsequently, 2.5 μM of Gic1 was added and incubated for another 16 h. **(B)** 0.5 μM of the septin octamers and 2.5 μM of Gic1 were mixed and dialyzed. Then, 4 mM of GTP was added and incubated for

16 h. scale bar is 100 nm.

3.1.4.2) GDP and GMP have no effects on filaments or septin-Gic1 complex

In parallel to previous experiments, we examined the effect of other nucleotides on either septin filaments or the septin-Gic1 complex. In this regard, excess of GDP or GMP were mixed with either septin filaments or the septin-Gic1 complex and the samples were incubated for 16 h. Surprisingly, neither of the nucleotides could destabilize the septin or the septin-Gic1 architecture (Fig. 3.34). It is intriguing that excess of GDP could not either replace the GTP present in Cdc3 or in case of an exchange, it did not cause any conformational irregularities and the filaments remained intact. This observation points to the peculiar structural features of the G3, G4 and the P-loop of Cdc3 that accommodate only GTP in the nucleotide binding pocket of the protein and once bound, it cannot be hydrolyzed or replaced.

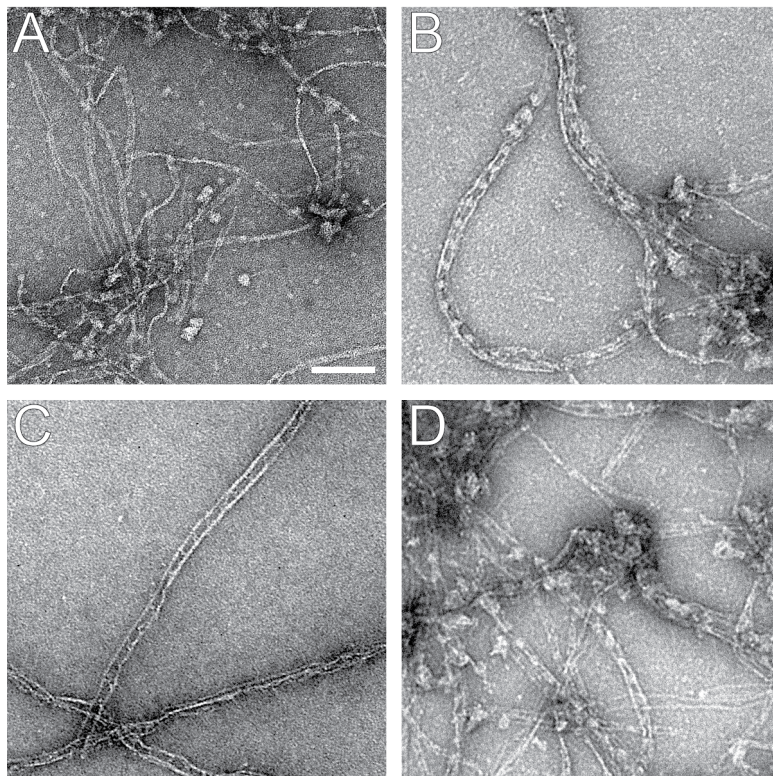


Fig. 3.34. GDP and GMP do not disassemble the septin filaments or septin-Gic1 complex. 0.5 μ M of the septin octamers was dialyzed without or with 2.5 μ M of Gic1 to prepare septin filaments and septin-Gic1 complex. 4 mM of GDP was mixed with (A) septin filaments or (B) septin-Gic1 complex and incubated for 16 h. 4 mM of GMP was added to (C) septin filaments or (D) septin-Gic1 complex and incubated for 16 h. Scale bar is 100 nm.

3.1.4.3) Cdc42p(GDP) and GTP generate tetramers together

We showed that Cdc42p(GDP) and GTP disassemble the septin filaments at Cdc10 and Cdc11 NC-interface respectively (Fig. 3.22 and 3.31). In order to have a combinatorial effect, first we disassembled the septin filament with GTP at the Cdc11-Cdc11 interface. Next, we dialyzed GTP out and added Cdc42p(GDP) and incubated the octamers for 16 h. By taking advantage of single particle analysis, we showed that a combination of GTP and Cdc42p(GDP) generated a tetramer with an extra density on top that corresponds to Cdc42p(GDP) bound to Cdc10 (Fig. 3.35). A minority of particles depicted a trimeric structure that resulted from dissociation of Cdc10 from the octamer, which when combined with GTP-

breakage at Cdc11 would make a trimer (Fig. 3.35C). This result complements our previous antibody labeling experiments suggesting two different points of action for Cdc42p and GTP.

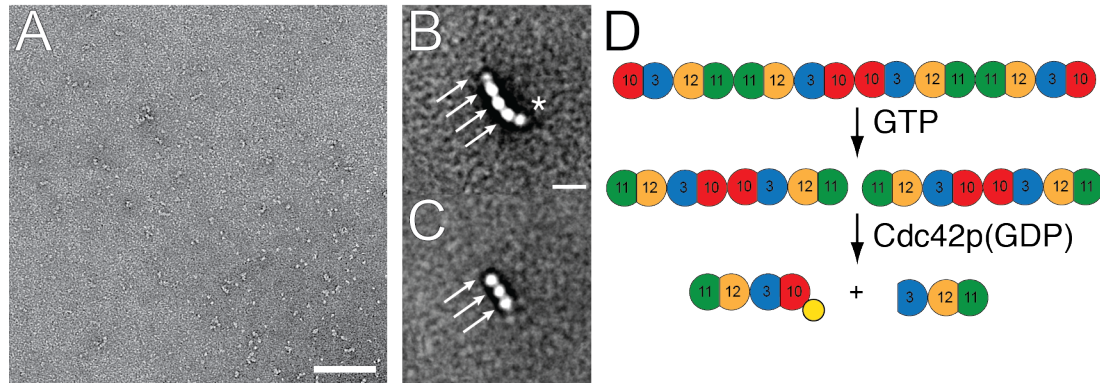


Fig. 3.35. Cdc42p(GDP) and GTP disassemble the septin filaments to make tetramers. (A) 0.1 μM of the septin octamers was dialyzed for 16 h and then 800 μM of GTP was added and incubated for another 16 h. Next, GTP was dialyzed out for a few hours and subsequently 5 μM of Cdc42p(GDP) was added and incubated for 16 h. (B) A class average showing a tetrameric structure with an extra density bound on top obtained from 1141 particles. (C) A class average showing a trimeric structure obtained from a subset of 1141 particles used for (B). Arrows indicate the septin subunits and the asterisk points to Cdc42p(GDP). Scale bar in A is 100 nm and in B is 10 nm.

3.1.5) Cryo-Electron Tomography (CET) of septin filaments

We dialyzed the septin octamer and Gic1 to prepare the railway structure. Samples were mixed with colloidal gold particles (1:1) and 4 μl was applied on a grid and plunge frozen in liquid ethane. Subsequently, tilt series were recorded from -60° to $+60^\circ$ with 2 degrees increment using JEM3200 electron microscope. Gold particles were used as a marker to align the tilt images and the structures were reconstructed using IMOD. Serial slices extracted from 3D tomograms clearly revealed mass densities of septin and Gic1. The densities were assigned manually to the corresponding proteins using Amira program (Fig. 3.36). In this regard, minimal densities were chosen and assigned in order to avoid inclusion of noise into the final reconstruction. Finally, segmented structures were low-pass filtered and visualized using UCSF Chimera.

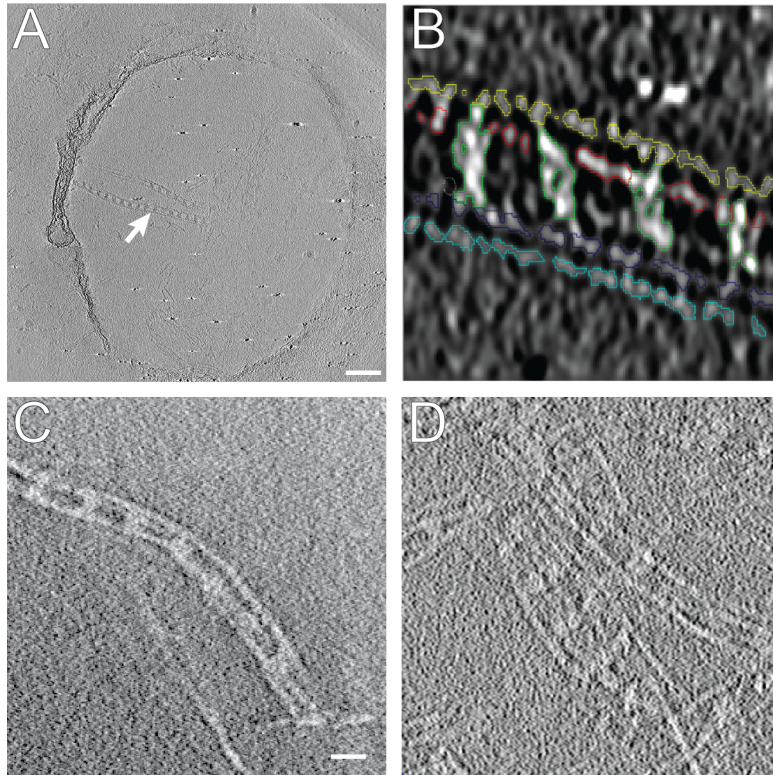


Fig. 3.36. Cryo electron tomography of the septin-Gic1 complex. (A) A representative cryo-EM image of the septin-Gic1 complex. Arrow indicates the septin-Gic1 complex. (B) Segmentation of the septin-Gic1 complex with Amira program. Densities were assigned to different filaments and Gic1 with different colors. (C) and (D) Show the extracts from tomograms that manifest the flexibility and bending of the septin-Gic1 complex. In (D) the ability of the septin-Gic1 complex to form mesh-like structure is seen. Scale bar in A is 100 nm and in B is 10 nm. (Courtesy of Dr. Christos Gastogiannis and Dr. Oliver Hofnagel).

In order to reconstruct the 3D structure of the septin-Gic1, we chose an area in which septin-Gic1 ran parallel to the tilt axis so the final reconstruction showed the least missing wedge. However, due to flexibility and bending of the septin filaments, averaging multiple structures into a single high-resolution structure was not feasible. Our 3D structures showed that Gic1 cross-bridges could interact with varying numbers of filaments ranging from four to six (Fig. 3.37). The septin-Gic1 complex is organized in a way that many filaments anchor themselves to the central Gic1 ensemble with an apparent molecular weight of 700-800 kDa. In fact, Gic1 elutes as a dimer with a molecular weight of 50 kDa from a gel filtration column. If a dimer binds to a single of Cdc10 then at least 12 Gic1 dimers are required to bridge six septin filaments, which correspond to a molecular weight of 600 kDa. However, at the limited resolution of our reconstruction these measurements can vary greatly. Furthermore, Gic1 ensembles both in our 2D class averages and 3D reconstructions are not well resolved, suggesting that its flexibility and variable number of Gic1 proteins present in each Gic1 cross-bridge.

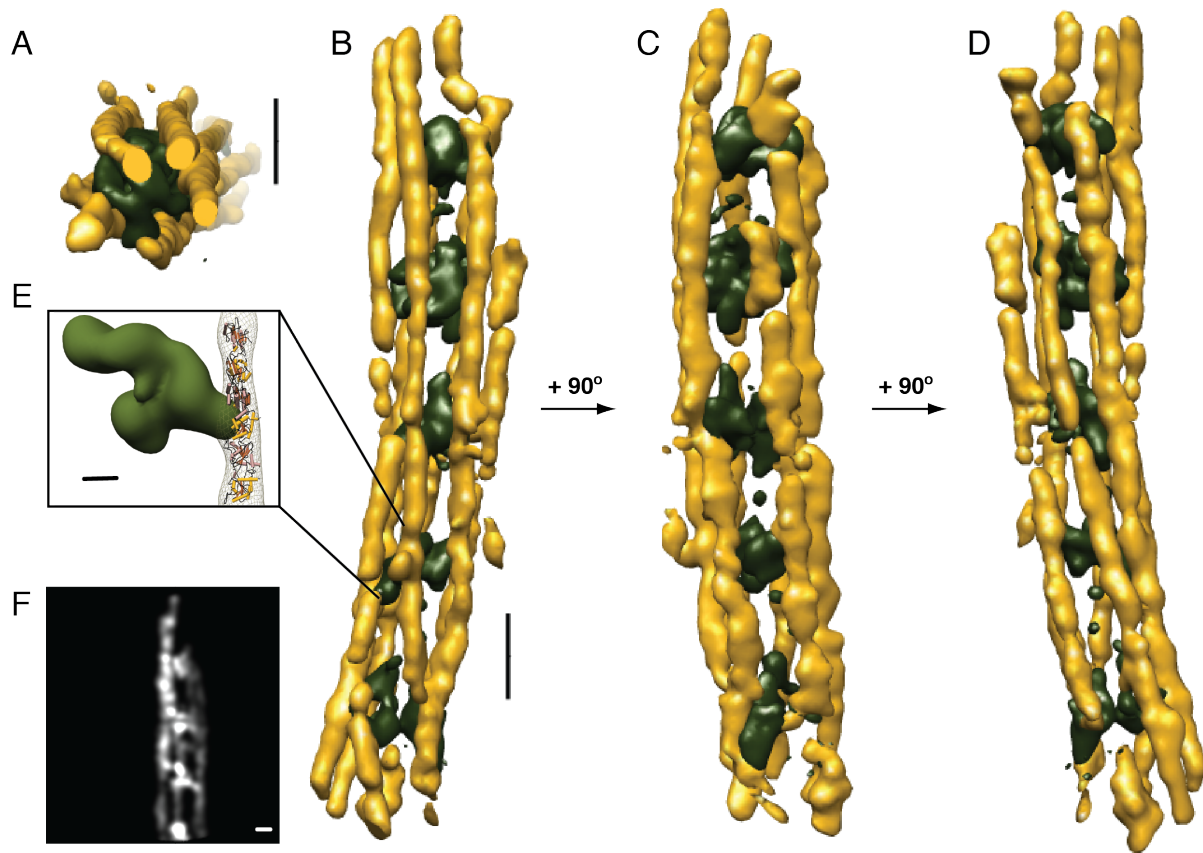


Fig. 37. 3D models obtained from Cryo-ET of septin-Gic1. 2 μ M of the septin octamers was dialyzed with 10 μ M of Gic1 for 16 h. 3D models were reconstructed using IMOD and Amira after selection of an area of interest. **(A)** Top view of the septin-Gic1 complex. **(B, C and D)** The full structure of the septin-Gic1 complex rotated by 90° at each view. **(E)** Fitting of the human crystal structure into the septin filaments, which shows the binding of Gic1 to an area equal to two septin subunits. **(F)** Back projection of the 3D model of the septin-Gic1 complex. Scale bar in A and B is 200 nm, in E is 5 nm and in F is 1 nm.

In a parallel experiment, equimolar concentration of Cdc42p(GppNHp) was also dialyzed along with the rest of the complex members to obtain the tertiary complex of septin-Gic1-Cdc42p(GppNHp). In the presence of Cdc42p(GppNHp), Gic1 ensembles had a bigger density due to the presence of Cdc42p(GppNHp) next to Gic1 (compare Fig. 3.37E and 3.38E). This observation confirms our previous result from the negatively stained sample that Gic1-Cdc42p(GppNHp) binds to an area that covers the mass of four septin subunits. We fitted the crystal structure of the human septin into our 3D model and observed that Gic1 binds to an area equal to two septin subunits and Gic1-Cdc42p(GppNHp) binds to four (Fig. 3.38E). The apparent size of Gic1-Cdc42p(GppNHp) is roughly 1.2 MDa suggesting a stoichiometry of 2:1 between Gic1 and Cdc42p(GppNHp), respectively.

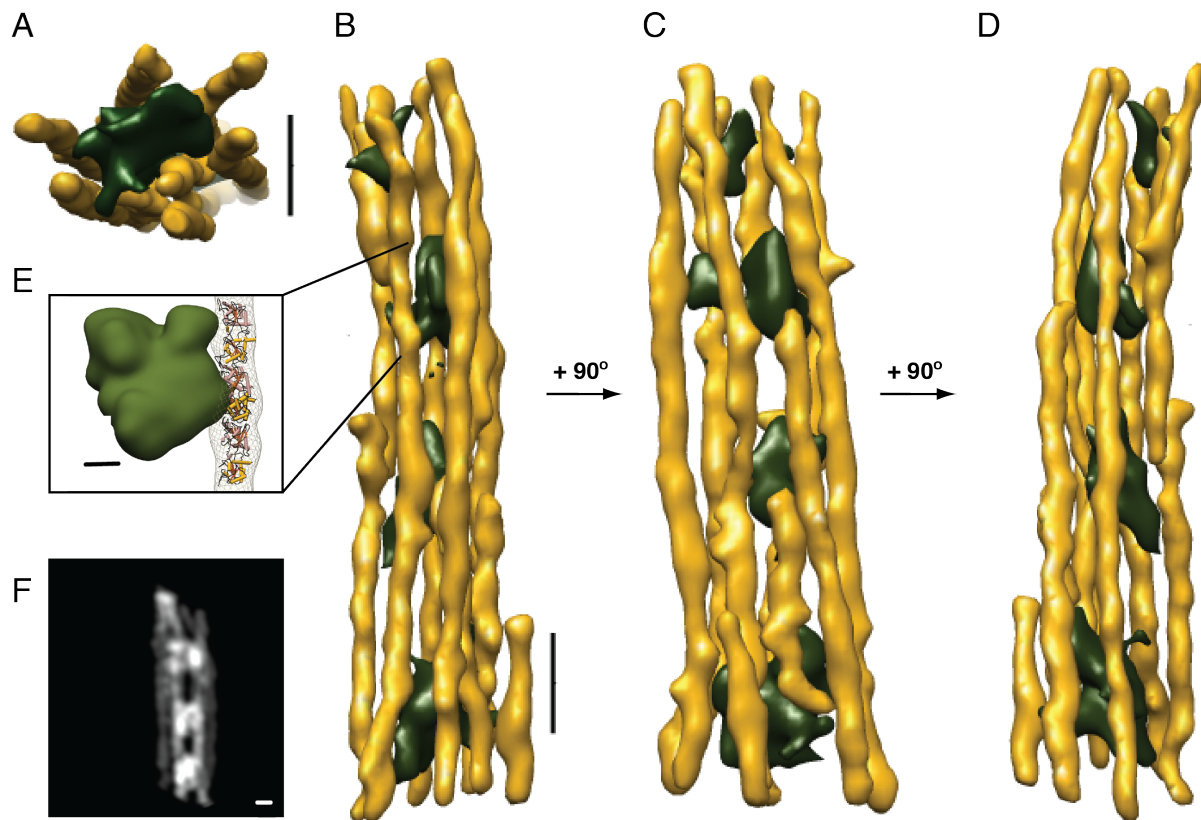


Fig. 38. 3D models obtained from Cryo-ET of septin-Gic1 + Cdc42p(GppNHp). 2 μ M of the septin octamers was dialyzed with 10 μ M of Gic1 and Cdc42p(GppNHp) for 16 h. 3D models were reconstructed using IMOD and Amira after selection of an area of interest. **(A)** Top view of the septin-Gic1-Cdc42p(GppNHp) complex. **(B, C and D)** The full structure of the septin-Gic1-Cdc42p(GppNHp) complex rotated by 90° at each view. **(E)** Fitting of the human crystal structure into the septin filaments, which shows the binding of Gic1-Cdc42p(GppNHp) to an area equal to four septin subunits. **(F)** Back projection of the 3D model of the septin-Gic1-Cdc42p(GppNHp) complex. Scale bar in A and B is 200 nm, in E is 5 nm and in F is 1 nm.

An inherent property of septin filaments is flexibility and rigidity. Septin filaments require flexibility to wrap around the membrane and also rigidity to serve as a scaffold (Gilden et al., 2012; Spiliotis et al., 2012). The 3D reconstructions also showed a high degree of flexibility both for septin filaments and Gic1 ensembles, which hindered averaging multiple reconstructions to achieve a higher resolution. There were several spectacular features visible in our reconstructions. First, septin filaments with different sizes bound to Gic1 ensembles at varying positions and ran parallel to the axis of the complex (Fig. 39A and C). Second, at random positions, filaments swapped their binding to a particular Gic1 ensemble but yet connected to other Gic1 ensembles (Fig. 3.39A). Another interesting feature of the septin-Gic1 complex

pertains to the filament bending. Filaments could bypass the binding to a Gic1 ensemble while still stretched in the same direction without any connections to Gic1 ensembles (Fig. 3.39A, D and E). These features suggest that Gic1 performs an anchoring function to hold filaments together at a certain position and does not compromise the inherent flexibility of the septin filaments. Furthermore, some filaments connected only to other septin filaments in the complex without binding to Gic1 (Fig. 3.39E). Finally, in some cases filaments splayed out along the axis of the complex (Fig. 39.B and F). This observation shows that Gic1 has multiple binding sites for septin filaments as such filaments can diverge along the axis of the complex. In fact, filament replacement and divergence of filament route both together originate from multiplicity of binding sites present in Gic1 ensembles. Altogether, varying number of filaments with different sizes can be brought together by different numbers of Gic1 proteins to form a multi-filamentous structure, which possesses both rigidity and flexibility suitable for wrapping around membrane and scaffolding for other proteins including even other cytoskeletal proteins.

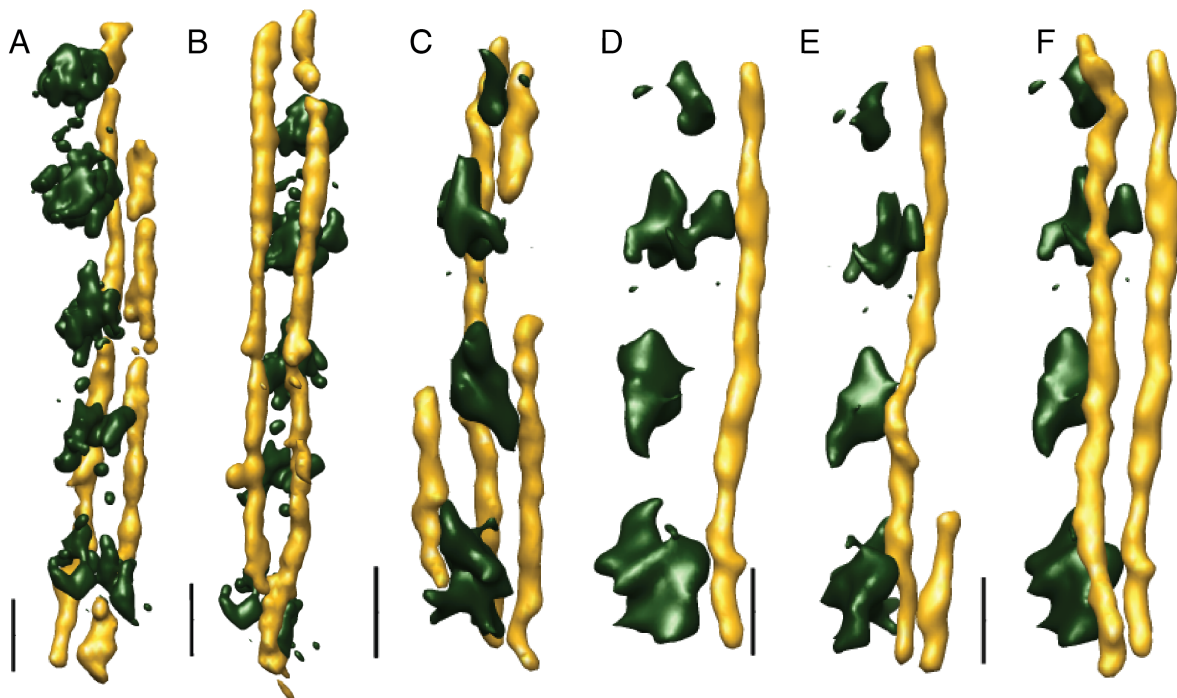


Fig. 3.39. Flexibility of filaments in the septin-Gic1 \pm Cdc42p(GppNHp) complexes. (A) A view of the septin-Gic1 3D model showing replacement of filaments for binding to the second top Gic1 ensemble. (B) A view of the septin-Gic1 3D model showing attachment of filaments at the most bottom Gic1 ensemble. (C) A view of the septin-Gic1-Cdc42p(GppNHp) complex 3D model showing truncated filaments. (D) A view of the septin-Gic1-Cdc42p(GppNHp) complex 3D model showing that a filament bypasses binding to a Gic1 ensemble. (E) A view of the septin-Gic1-Cdc42p(GppNHp) 3D model showing that a filament is connected to the complex by binding to another filament and not to Gic1. (F) A view of the septin-Gic1-Cdc42p(GppNHp) 3D model showing that filaments spray out as they connect to higher Gic1-Cdc42p(GppNHp) ensemble. Scale bar in is 20 nm.

Our study provided three major questions with an answer about the function of septin using electron microscopy. The first question concerns the mechanism by which septin polymerization into filaments is prohibited when it is not needed before the onset of cytokinesis. A mechanism like microtubule catastrophe cannot account for prevention of filament formation since septins form non-polar filaments composed of octamers with a two-fold symmetry. Another mechanism could engage a capping protein that binds to Cdc11 and therefore prevents filament formation. But so far, no proteins have been assigned to undertake this task. Therefore, the most plausible way should involve a protein that cuts septin filaments constantly and it is inactivated as the cell receives a signal to initiate cell division. We showed that two parallel mechanisms function to prevent septin polymerization. First, high concentration of GTP prohibits Cdc11-Cdc11 interaction (Fig. 40A) and Cdc42p(GDP) but not Cdc42p(GppNHP) interferes with Cdc10-Cdc10 interaction (Fig. 40B). Therefore, two distinct populations of octamer (Cdc11-GDP) and tetramer (Cdc11-GTP) exist in the cell (Fig. 40C). Remarkably, this regulatory function of nucleotide with respect to septin higher-order structure formation contradicts the general notion that nucleotides play a structural role (Mitchison et al., 2002). We showed by taking advantage of antibody labeling and analysis of nonpolymerizing septin that Cdc42p(GDP) requires the first 29 amino acids of Cdc10 to bind to Cdc10 to prevent polymerization. This new function of Cdc42p explains how septin is retained in the octameric form or in unorganized patches of filaments that go through constant assembly and disassembly before the onset of cell cycle, early in G1. In fact, Cdc42p(GDP) also interacts with Msb3 and Msb4, two Rab GTPase activating proteins involved in regulation of polarisome (Tchegerepine et al., 2005). Previously, it was shown that septin recruitment to the bud neck was hampered in *gic* mutant at non-permissive temperatures (Iwase et al., 2006). But, at permissive temperature, septin ring formed at the neck suggesting that Gic1 and Gic2 are not the single proteins involved in recruitment but rather they confer stability to the septin filaments. Our data proposes that Cdc42p(GDP) rather than Gic proteins recruits septin octamers or tetramer (depending on the nucleotide state of Cdc11) to the bud neck directly by binding to septin (Fig. 40E). As soon as Cdc42p becomes GTP-bound, it dissociates from the septin and allows septin-Cdc11(GDP) to polymerize into filament whereas septin-Cdc11(GTP) remains as an octamer.

Cdc42p(GTP) recruits more proteins including Gic1 and Gic2. Previously, it was shown that Borg3 (homologue of yeast Gic1) could lead to filament bundling in a mammalian cell line (Joberty et al., 2001). Cdc42p(GTP) and Gic1 form a binary complex and subsequently bind to the septin octamers and assist in polymerization independent of the nucleotide state of Cdc11 (Fig. 40E). We showed the presence of Cdc42p(GTP) next to Gic1 both in our 2D class averages and in the 3D reconstruction. It was previously shown that Cdc42p undergoes many rounds of GTP binding and hydrolysis (Gladfelter et al., 2002). However, it was proposed that Cdc42p is required for the establishment of a stable ring but once formed, they are maintained independently of Cdc42p. Upon GTP hydrolysis, Cdc42p(GDP) dissociates from the

septin-Gic1 complex and participates in another round of septin recruitment leaving the railway structure at the budding neck (Fig. 40F and G). We observed in our 2D class averages that the septin-Gic1 complex have a regular pattern such that Gic1 cross-bridges two filaments by binding to two septin subunits and leaving six subunits in between. However, the 3D reconstruction obtained from cryo-electron tomography showed that Gic1 forms a large complex constituting of approximately 24 Gic1 proteins that attach to up to six filaments. However, in contrast to previous evidence, we showed that Gic1 binds to Cdc10 the central linchpin of the octamers. As a matter of fact, Gic1 fills in the only space among septin filaments, which is devoid of C-terminal extensions and both Gic1 and Cdc10 guarantee anchorage of the complex to the membrane via interaction with PI(4,5)P2 (Orlando et al., 2008; Bertin et al., 2010).

It is known that the concentration of Cdc42p increases in the bud via its constant transport to the budding neck and its diffusion back to the mother is inhibited by septin (Orlando et al., 2011). Moreover, the localization of Gic1, Cdc42p and Rgal (GAP for Cdc42p) changes from the bud tip to the neck in telophase, which highlights the requirement of Cdc42p to terminate the abscission. Therefore, as the concentration of Cdc42p(GppNHp) was raised to ten times higher than Gic1, it started to bind and take Gic1 out of the septin-Gic1 complex and thereby destabilized the septin filaments (Fig. 40H). Septins are usually incorporated into a new ring in the next cell cycle (Younghoon et al., 2010). Although there are multiple post-translational modifications that might influence the structure of septin (Garcia et al., 2011) but this effect of Cdc42p was previously unknown. By means of this mechanism, Cdc42p can generate short fragments composed of “old octamers” that upon mixing with the newly synthesized septin can reconstitute octamers containing old and new septin subunits as suggested by previous studies (McMurray et al., 2009).

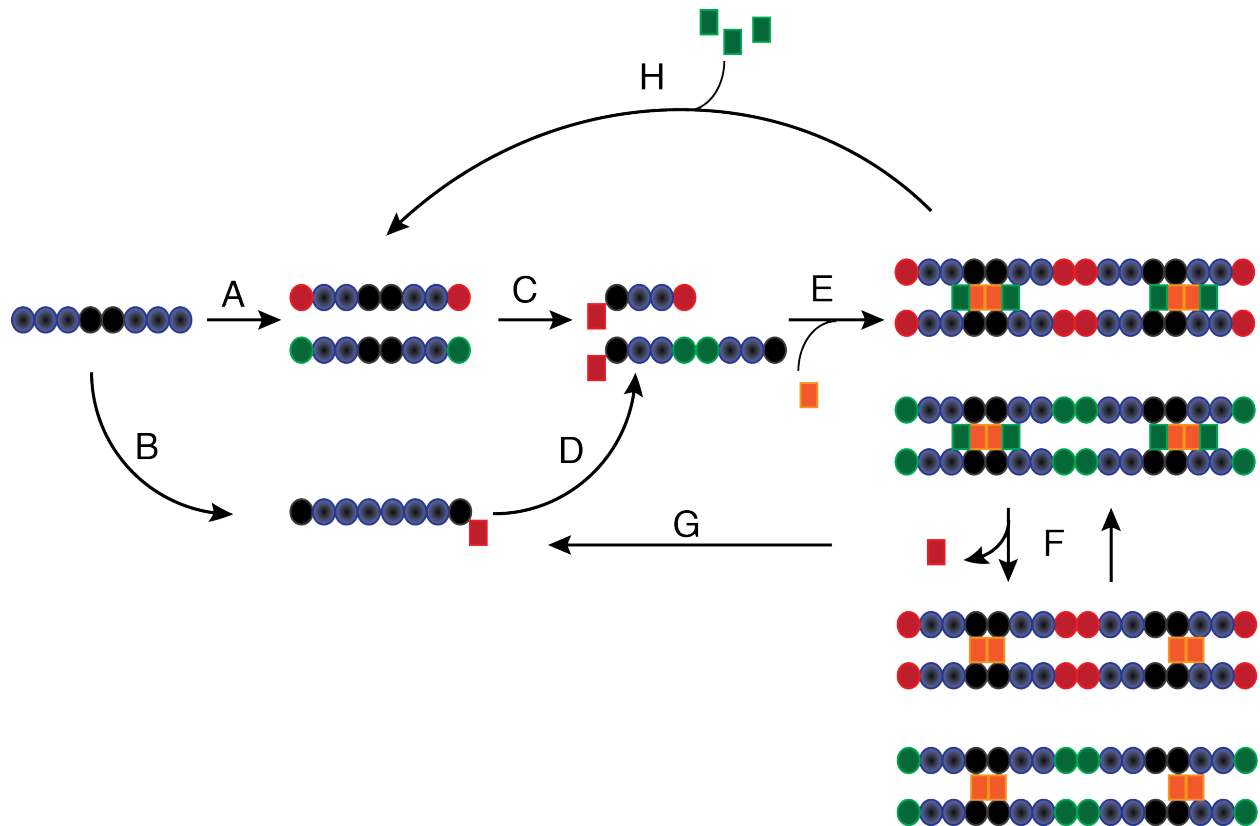


Fig 40. Model for septin recruitment, ring formation and disassembly. (A) Cdc11 is either GDP bound allowing filament polymerization or GTP bound preventing filament polymerization. (B) Cdc42p(GDP) disassemble septin at the Cdc10-Cdc10 interface generating inside-out octamer. (C and D) Dependent on the nucleotide state septins, Cdc42p(GDP) can generate octamer (Cdc11-GDP) or tetramer (Cdc11-GTP). (E) As soon as Cdc42p becomes GTP bound, it allows filament polymerization of septin(Cdc11-GDP) and recruits Gic1 to the budding neck (septin(Cdc11-GTP) remains as an octamer). Gic1 scaffolds and stabilizes septin filaments independent of their nucleotide state and forms septin-Gic1-Cdc42p(GTP) filament cables that are used for building the septin ring. (F) Cdc42p(GTP) is not necessary for the stability of the filaments cables and upon GTP hydrolysis, it dissociates from the septin-Gic1 complexes. (G) Cdc42p(GDP) takes part in recruitment of more septin octamer or tetramer to the bud site. (H) During cell division the local concentration of Cdc42p(GTP) increases by the constant delivery of Cdc24p. This leads to a dissociation of the septin-Gic1-Cdc42p(GTP) filament cables and the septin ring disassembles. Septins are depicted as blue circles (Cdc3 and Cdc12), black circle (Cdc10), red circle (Cdc11-GDP) and green circle (Cdc11-GTP). Gic1 is depicted as orange rectangle. Cdc42p(GTP) and Cdc42p(GDP) are depicted as green and red rectangles, respectively.

3.2) Results of DHCR7

The *dhcr7* gene exists in eukaryotes except in yeast, which produces ergosterol instead of cholesterol. The only bacterial strains with a homologous gene to *dhcr7* are *Plesiocystis pacifica*, *Coxiella burnettii* and *Legionella longbeachae*. In this work, we endeavored to express and purify the *dhcr7* from *C. burnettii*, *P. pacifica* and the sterol-sensing domain of the human *dhcr7* in *E. coli*. The human *dhcr7* was expressed in the insect cell line Sf21.

3.2.1) Expression and purification of DHCR7

3.2.1.1) Purification of hSSD

It was previously reported that some cholesterol-binding proteins including DHCR7, SCAP, NPC1 and HMG-CoA reductase contain a so-called sterol sensing domain. The putative human SSD contains 182 amino acids (181-362), which encompasses five trans-membrane domains. The corresponding gene was cloned in pOPINE2 vector with a non-cleavable C-terminal His-tag. In order to find out the optimal condition at which the protein was reasonably expressed, we tried different media, cell lines, OD₆₀₀, IPTG concentrations, temperatures and expression times (Fig. 3.41). The hSSD (p295 in AG Raunser plasmid data bank) was transformed into the *E. coli* strain C43 and cells were grown in 2TY medium. The expression was induced at OD₆₀₀ of 0.6 using 0.6 mM IPTG. The temperature was then shifted to 25°C and cells were harvested after an overnight incubation (Fig. 3.41C).

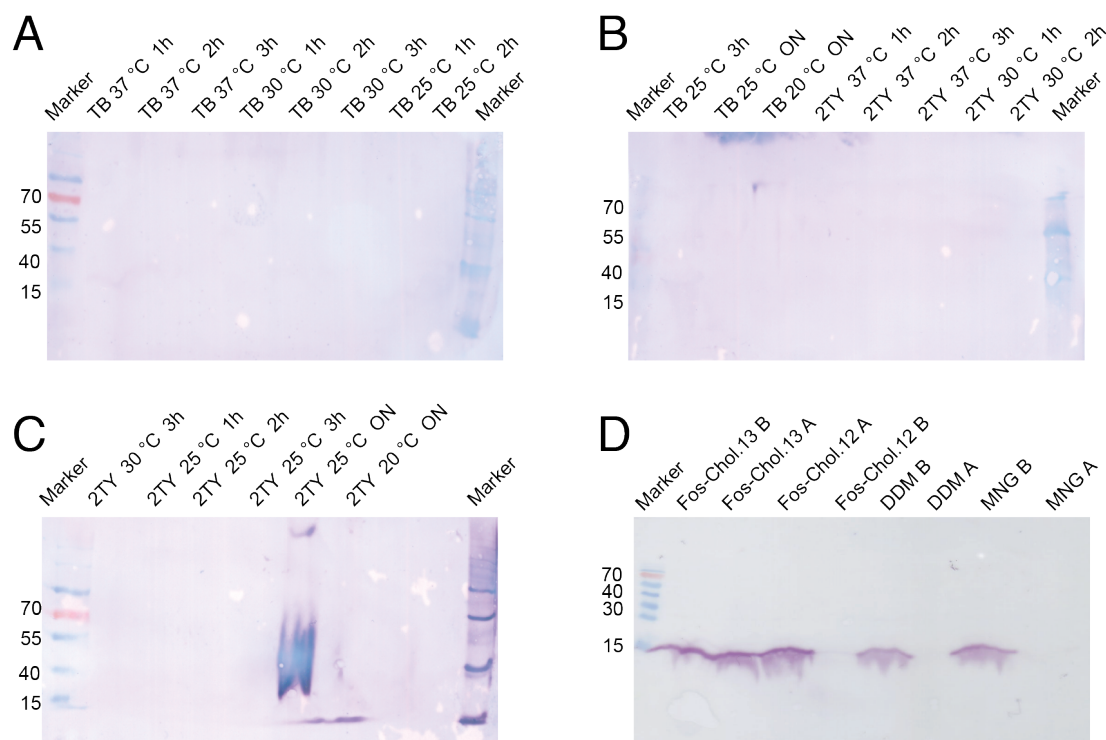


Fig. 3.41. Expression and solubilization screening of hSSD. (A-C) The p295 was transformed into C43 strain and cells were cultured in either TB or 2TY medium. When cells reached the OD_{600} of 0.6, 0.6 mM IPTG was added. Cells were incubated at 37°C, 30°C, 25°C and 20°C and a sample was taken from each condition after 1, 2, 3 or 16 hours. The cells were lysed in lysis buffer (1 mg/ml Lysozyme, 5 mM DTT, 50 mM Tris-HCl pH 7.5 and 0.5 mg/ml Pefabloc) and sonicated 2-3 times for 20 counts at an output of 3.5 and duty cycle 10%. The cell lysate was centrifuged at 10,000 rpm for 10 min and the supernatant was further centrifuged at 50,000 rpm for 1 h. The membrane pellet was solubilized in solubilization buffer (1% DDM, 500 mM NaCl and 50 mM Tris-HCl pH 7.5) and subjected to western blot analysis. (D) hSSD was expressed at the optimal condition (OD_{600} of 0.6, 0.6 mM IPTG, 2TY medium, 25°C for 16 h) in 9 liters. The membrane was prepared and resuspended in TBS to the final volume of 50 ml. 100 μ l of the membrane was solubilized using different detergents (Fos-choline®-13, Fos-choline®-12, DDM and MNG-3) at final concentration of 1%, 700 mM NaCl and 50 mM Tris-HCl pH 7.5 in a total volume of 400 μ l. The samples were centrifuged after 2 h of incubation at 4°C. A sample was taken before (A) and after (B) centrifugation and solubilization was evaluated by western blotting.

In order to purify the hSSD, the membrane was stripped using 0.2 M urea for a short time to strip off membrane-anchored proteins and also proteins loosely attached to the membrane due to their hydrophobic domains. The stripped membrane (from 9 liters) was resuspended in TBS in a final volume of 50 ml. The detergent solubilization screening revealed that 0.5% Fos-choline®-13 along with 700 mM salt is the most efficient detergent to completely solubilize hSSD (Fig. 3.41D). The stripped membrane was solubilized in the solubilization buffer for 2 h. The solubilized fraction was mixed with 0.8 ml of Ni-NTA and 5 mM imidazole and incubated for 1 h at 4°C. The beads were subsequently washed with 10 ml of

binding and washing buffers, respectively. The protein was eluted with 5 ml of elution buffer. The eluate was first dialyzed to remove imidazole, then concentrated and injected into Superdex 75 (GE Healthcare) for further purification using a gel filtration buffer containing 0.05% Fos-choline®-13 (Fig. 3.42C and D). The chromatogram showed that protein eluted as two separate peaks corresponding to dimeric and monomeric states (Fig. 3.42E). In fact the micelle size of Fos-choline®-13 was estimated to be 25 kDa. Therefore together with the monomeric and the dimeric hSSD a molecular weight of 42 and 59 kDa is expected, respectively.

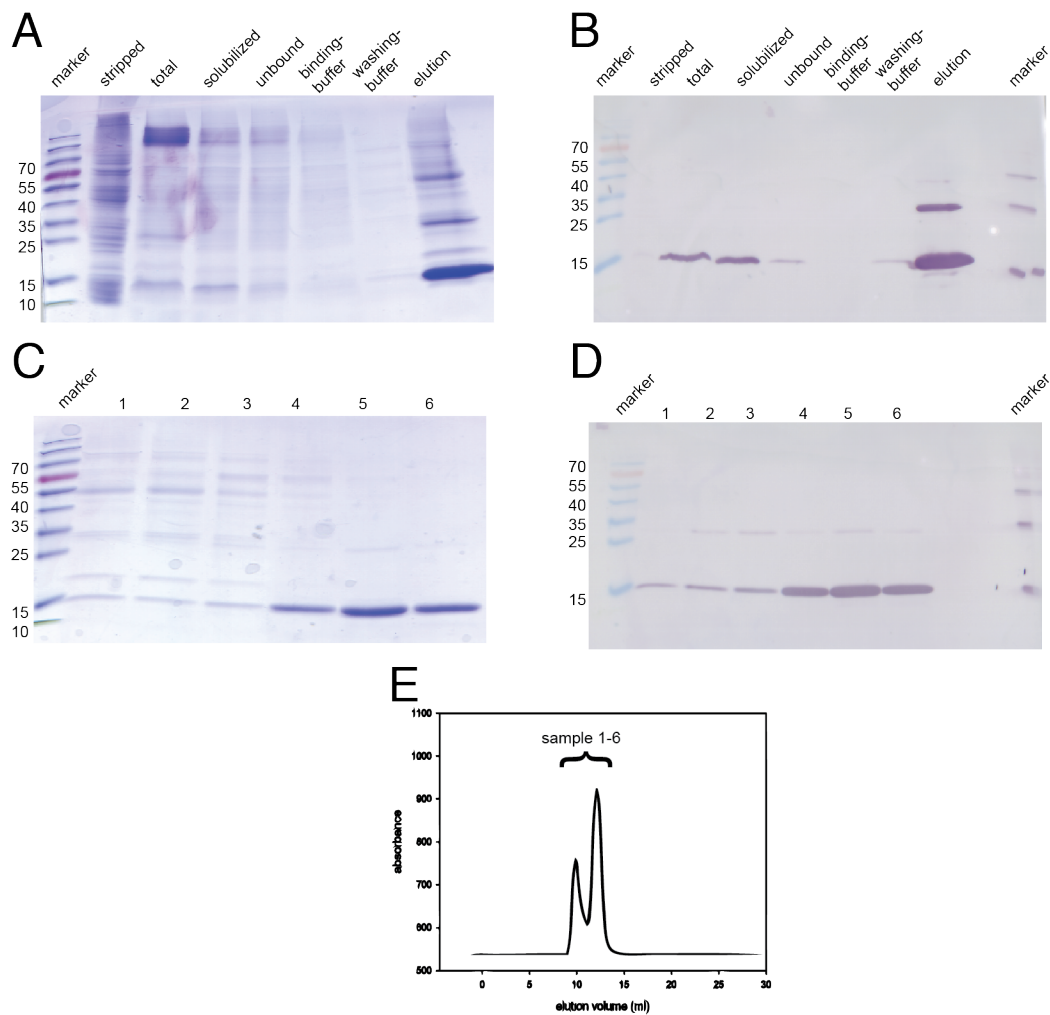


Fig. 3.42. Purification of hSSD. Membrane was stripped with 0.2 M urea, centrifuged at 50,000 rpm and resuspended up to 50 ml TBS. 3 ml of the membrane was solubilized in solubilization buffer (0.5% Fos-choline®-13, 700 mM NaCl and 50 mM Tris-HCl pH 7.5) in a final volume of 12 ml. To the solubilized fraction, 0.8 ml of Ni-NTA and 5 mM imidazole was added and incubated for 2 h at 4°C. The beads were packed into columns (BIO-RAD) and washed with 10 ml binding buffer (0.2% Fos-choline®-13, 500 mM NaCl, 50 mM Tris-HCl pH 7.5 and 5 mM Imidazole) and 10 ml washing buffer (0.1% Fos-choline®-13, 300 mM NaCl, 50 mM Tris-HCl pH 7.5 and 20

mM imidazole). Protein was eluted using 5 ml elution buffer (0.05% Fos-choline®-13, 150 mM NaCl, 50 mM Tris-HCl pH 7.5 and 150 mM imidazole) and samples were collected as 4 drops per microtube. The protein content was evaluated with Bradford assay. The fractions containing protein were pooled, concentrated and injected into Superdex 75 (GE Healthcare). **(A-B)** Show the SDS-PAGE and the corresponding Western blot after Ni-NTA purification. **(C-D)** Show the SDS-PAGE and the corresponding Western blot after gel filtration. **(E)** Shows the chromatogram of gel filtration.

3.2.1.2) Purification of cDHCR7

The closest homologue of human *dhcr7* gene exists in *C. burnettii*. *Coxiella burnettii* is an obligatory intracellular parasite that infects pulmonary cells. The gene was probably transferred laterally from human to the infectious organism, which during the course of evolution was modified. However, it is unknown whether the organism uses this gene during infection. The corresponding gene was cloned into pOPINE vector with a cleavable N-terminal His-tag (p285 in plasmid databank of AG Raunser). The cDHCR7 was transformed into C43 cells and grown in 2TY or TB until they reached OD₆₀₀ of 0.8. Then, cells were induced with 1 mM IPTG to start the expression. Different temperatures were screened but all conditions tested showed a reasonable expression of cDHCR7 (Fig. 3.43A-C). Therefore, OD₆₀₀ and IPTG concentration were varied to optimize the expression. Finally, the best expression was achieved in TB medium at OD₆₀₀ of 0.8 using 0.6 mM IPTG at 25°C for 16 h (Fig. 3.43D). Subsequently, different detergents were used to solubilize cDHCR7. Similar to hSSD, Fos-choline®-13 along with 500 mM NaCl could completely solubilize the protein in 2 h (Fig. 3.44E-F).

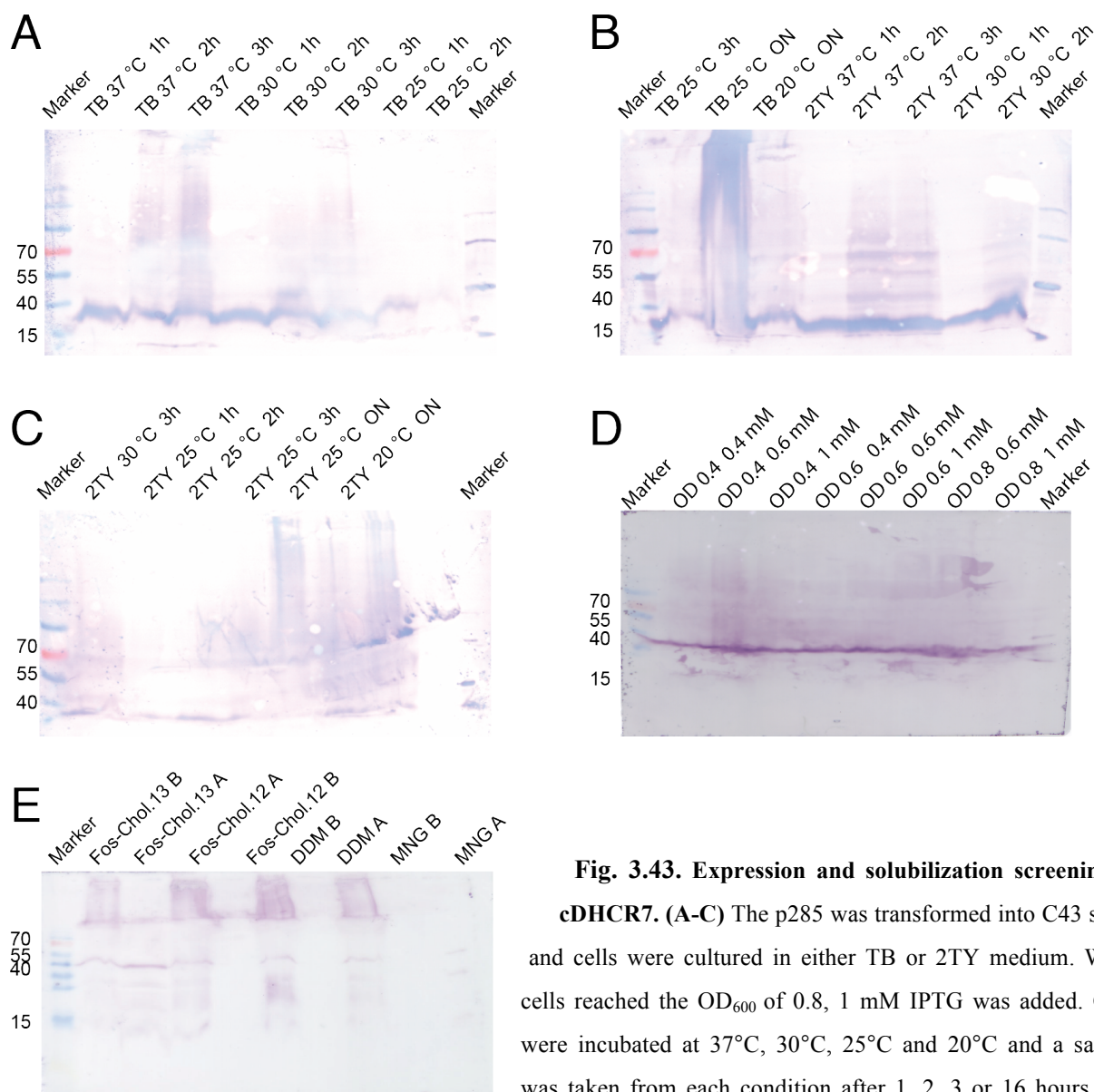


Fig. 3.43. Expression and solubilization screening of cDHCR7. (A-C) The p285 was transformed into C43 strain

and cells were cultured in either TB or 2TY medium. When cells reached the OD_{600} of 0.8, 1 mM IPTG was added. Cells were incubated at 37°C, 30°C, 25°C and 20°C and a sample was taken from each condition after 1, 2, 3 or 16 hours. The

cells were lysed in lysis buffer (1 mg/ml Lysozyme, 5 mM DTT, 50 mM Tris-HCl pH 7.5 and 0.5 mg/ml Pefabloc) and sonicated 2-3 times for 20 counts at an output of 3.5 and duty cycle 10%. The cell lysate was centrifuged at 10,000 rpm for 10 min and the supernatant was further centrifuged at 50,000 rpm for 1 h. the membrane pellet was solubilized in solubilization buffer (1% DDM, 500 mM NaCl and 50 mM Tris-HCl pH 7.5) and subjected to Western blot analysis. (D) The expression was optimized using 2TY medium at varying OD_{600} and IPTG concentration. (E) cDHCR7 was expressed at the optimal condition (OD_{600} of 0.8, 0.6 mM IPTG, TB medium, 25°C for 16 h) in 9 liters. The membrane was prepared and resuspended in TBS to the final volume of 50 ml. 100 μ l of the membrane was solubilized using different detergents (Fos-choline®-13, Fos-choline®-12, DDM, DM, Cymal-6 and MNG-3 at final concentration of 1%), 500 mM NaCl and 50 mM Tris-HCl pH 7.5 in a total volume of 300 μ l. The samples were centrifuged after 2 h of incubation at 4°C. A sample was taken before (A) and after (B) centrifugation and solubilization was evaluated by Western blotting.

The cDHCR7 was solubilized using a solubilization buffer containing 1% Fos-choline®-13 and 500 mM NaCl. To the solubilized fraction, 1 ml Ni-NTA beads already calibrated with binding buffer was added and then incubated for 1 h at 4°C. As evaluated from western blot analysis, the binding of cDHCR7 to the Ni-NTA beads was not efficient and even an overnight incubation with did not improve the binding. This suggests that the detergent micelle covers the His-tag to some extent, which renders its accessibility to Ni²⁺ (Fig. 3.44B, lane 3). The beads were washed with 10 ml binding buffer and washing buffer1 and 5 ml washing buffer2. The protein was eluted with 5 ml elution buffer and the protein content of fractions was assayed with Bradford test (Fig. 3.44A-B). Superose 12 (GE Healthcare) was used to further purify the protein (Fig. 3.44C-D). The chromatogram showed a peak corresponding to a monomer at a molecular size of 60-65 kDa (the expected molecular weight of cDHCR7 is 43 kDa but it runs at 35 kDa in semi-denaturing SDS-PAGE).

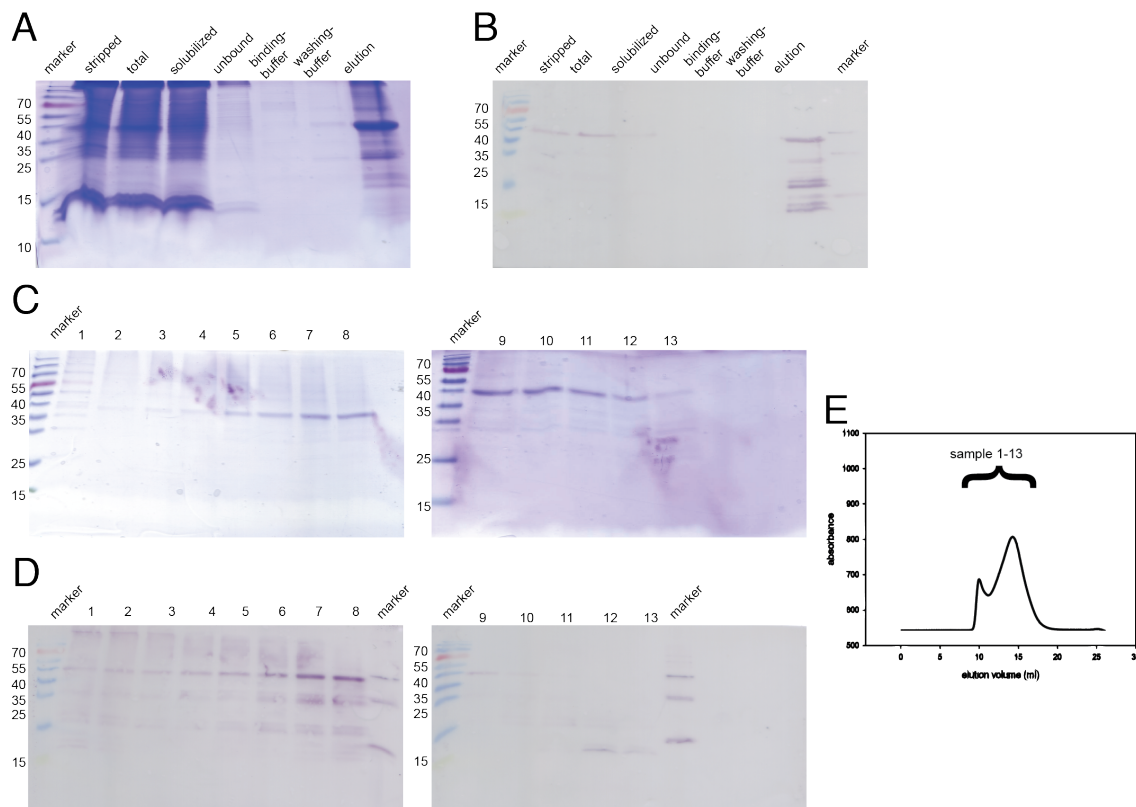


Fig. 3.44. Purification of cDHCR7. Membrane was stripped with 0.2 M urea, centrifuged at 50,000 rpm and resuspended in 50 ml TBS. 4 ml of the membrane was solubilized in solubilization buffer (1% Fos-choline®-13, 500 mM NaCl and 50mM Tris-HCl pH 7.5) in a final volume of 12 ml. To the solubilized fraction, 1 ml of Ni-NTA and 10 mM imidazole was added and incubated for 2 h at 4°C. The beads were packed into columns (BIO-RAD) and washed with 10 ml binding buffer (0.2% Fos-choline®-13, 300 mM NaCl, 50 mM Tris-HCl pH 7.5 and 10 mM imidazole), 10 ml washing buffer1 (0.1% Fos-choline®-13, 300 mM NaCl, 50 mM Tris-HCl pH 7.5 and 30 mM imidazole) and 5 ml of washing buffer2 (0.1% Fos-choline®-13, 300 mM NaCl, 50 mM Tris-HCl pH 7.5 and 50 mM imidazole). Protein was eluted using 5 ml elution buffer (0.05% Fos-choline®-13, 150 mM NaCl, 50 mM Tris-

HCl pH 7.5 and 150 mM imidazole) and samples were collected as 4 drops per microtube. The protein content was evaluated with Bradford assay. The fractions containing protein were pooled, concentrated and injected into Superdex 75 (GE Healthcare). **(A-B)** SDS-PAGE and the corresponding Western blot after Ni-NTA purification. **(C-D)** SDS-PAGE and the corresponding Western blot after gel filtration. **(E)** Chromatogram of gel filtration.

In order to cleave the His-tag to reduce protein flexibility and improve crystallography, 0.6 mg precision protease was added to 1 mg of cDHCR7 and incubated overnight at 4°C. The protein was applied to Ni-NTA beads to capture the cleaved His-tag and precision protease. The beads were washed to collect the cleaved cDHCR7 and eluted with an imidazole-containing buffer to evaluate if cleavage was successful. Unfortunately, most of the cDHCR7 remained bound to His-tag suggesting that His-tag was not accessible to the protease, which was also problematic during binding to Ni-NTA beads (Fig. 3.45).

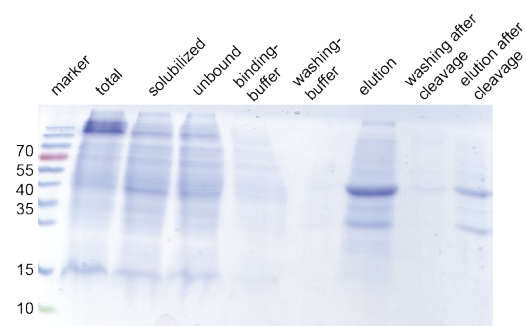


Fig. 3.45. His-tag cleavage using precision protease.

cDHCR7 was first purified as explained earlier (indicated on top the SDS-PAGE as before). Then, 0.6 mg precision protease was added to 1 mg of cDHCR7 and incubated for an overnight at 4°C. The protein was added to 1 ml Ni-NTA beads and incubated for 1h. The column was washed with 10 ml of gel

filtration buffer to wash the cleaved cDHCR7. Then the precision protease and the uncleaved cDHCR7 were eluted using 150 mM imidazole. A sample was taken from each fraction and subjected to SDS-PAGE analysis.

There are only two examples of membrane protein crystal structures using Fos-choline®-14 suggesting the unsuitability of Fos-choline detergents for membrane protein crystallization (Wang et al., 2008 and Bass et al., 2002). Therefore, we attempted to exchange Fos-choline®-13 to other detergents such as DDM, Fos-choline®-12 and MNG-3 using two different approaches. In the first approach, cDHCR7 was solubilized in Fos-choline®-13 and bound to Ni-NTA beads but the binding, washing and elution buffers contained the exchanging detergent instead of Fos-choline®-13. The protein precipitated on the column and did not elute suggesting failure in detergent exchange. In the second approach, the protein was eluted from the gel filtration column using Fos-choline®-13 and dialyzed in the exchanging detergent (1% detergent) for a week. Then, the protein was centrifuged and injected into Superose 12 (GE Healthcare) and run with a buffer containing the exchanging detergents. If detergent exchange is successful, a mono-dispersed peak is seen in the chromatogram otherwise protein either precipitates after centrifugation or elutes in the void volume. None of the detergents tested could exchange Fos-choline®-13 and the protein precipitated after dialysis. Fos-choline®-13 has a very low CMC, which makes it very difficult to dialyze

and exchange it with another detergents. Moreover, it has a very long acyl chain that covers a large surface of the protein making it unsuitable for crystallography.

3.2.1.3) Purification of hDHCR7

Mammalian membrane proteins are not easily expressed in bacterial hosts to reasonable quantities. Moreover, post-translational modifications required for functionality of proteins are also absent in prokaryotes. Therefore, the preferred host of expression is baculovirus-driven expression in insect cells. We tried to express different constructs of DHCR7 in *E. coli* strains including C43, C41 and BL21, but none was successful. Then, we used hDHCR7-EGFP in the pOPINE vector (p118, plasmid data bank of group of Dr. Raunser) along with a BACmid carrying essential genetic elements used to produce baculovirus. We transfected the Sf9 cells with p118 and the BACmid carrying the viral genome and virus was collected after 5-7 days. The virus was further amplified in Sf21 cells at a very low MOI to ensure amplification in 4-5 days. If high MOI of virus is used at this stage, expression rather than amplification is achieved and no virus amplification occurs. Sf21 cells were infected with the virus at an MOI of 1 and cells were harvested after 48 h when the fluorescent signal was high (Fig. 3.45A). The cells were lysed and solubilization screening with different detergents was performed. When semi-denaturing SDS-PAGE is used the conformation of EGFP is conserved and the fluorescent signal can be used instead of Western blotting (Fig. 3.46B). Fos-choline®-13 and to a lower extent DDM showed the most optimal solubilization capability (Fig. 3.46B). Cholesterol and supposedly cholesterol binding proteins reside in special compartments in the membrane known as lipid rafts. Sphingomyelin has a favorable interaction with cholesterol and co-localizes with cholesterol within the raft (Barenholz, 2004). Structural similarity between sphingomyelin and Fos-choline®-13 makes this detergent the best candidate to solubilize cholesterol binding proteins to preserve their near-native structure and function as it was previously shown to be the only functional detergent to solubilize SCAP and Insig (Radhakrishnan A et al., 2004 and 2007).

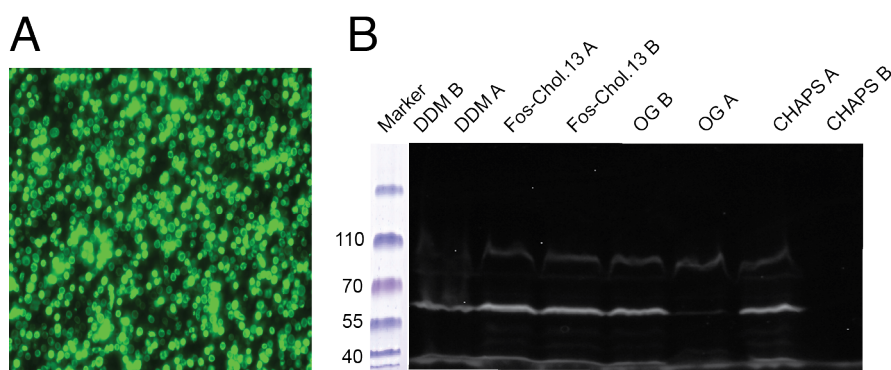


Fig. 3.46. Expression and solubilization of hDHCR7.

(A) The hDHCR7-EGFP (p118) was expressed in Sf21 cells (density of 1×10^6 cells/ml) with an MOI ≥ 1 for 48-72 h until the fluorescent signal was high and cell growth stopped. (B) The membrane of 20-25 liters of cells were resuspended in the final

volume of 50 ml and 100 μ l was used in 300 μ l of solubilization buffer containing Fos-choline®-13, Fos-choline®-12, DDM, DM and Triton X-100. The samples were taken before (A) and after (B) centrifugation.

The hDHCR7-EGFP was expressed in 20-25 liters of cells at 1×10^6 cell/ml density with $\text{MOI} \geq 1$. The membrane (from 20-25 liters) was extracted and 3 ml was solubilized in Fos-choline®-13 with 500 mM NaCl for 2h at 4°C (in a final volume of 12 ml). The solubilized fraction was mixed with 1 ml Ni-NTA and incubated for 2 h at 4°C. The Ni-NTA beads were washed with 10 ml binding and washing buffers respectively. The protein was eluted with 5 ml of elution buffer and the fluorescent signal was used to monitor the protein quantity of fractions. The eluate was dialyzed to remove the imidazole used for elution. The protein was injected into Superose 12 for further purification and both UV and fluorescence (excitation: 488 nm, emission: 509) were used to identify the fraction containing hDHCR7-EGFP (Fig. 3.47A-B). The protein eluted as a monomer from the gel filtration column (Fig. 3.47C). The expected molecular weight of hDHCR7-EGFP is 82 kDa but it ran at approximately 55 kDa in semi-denaturing SDS-PAGE.

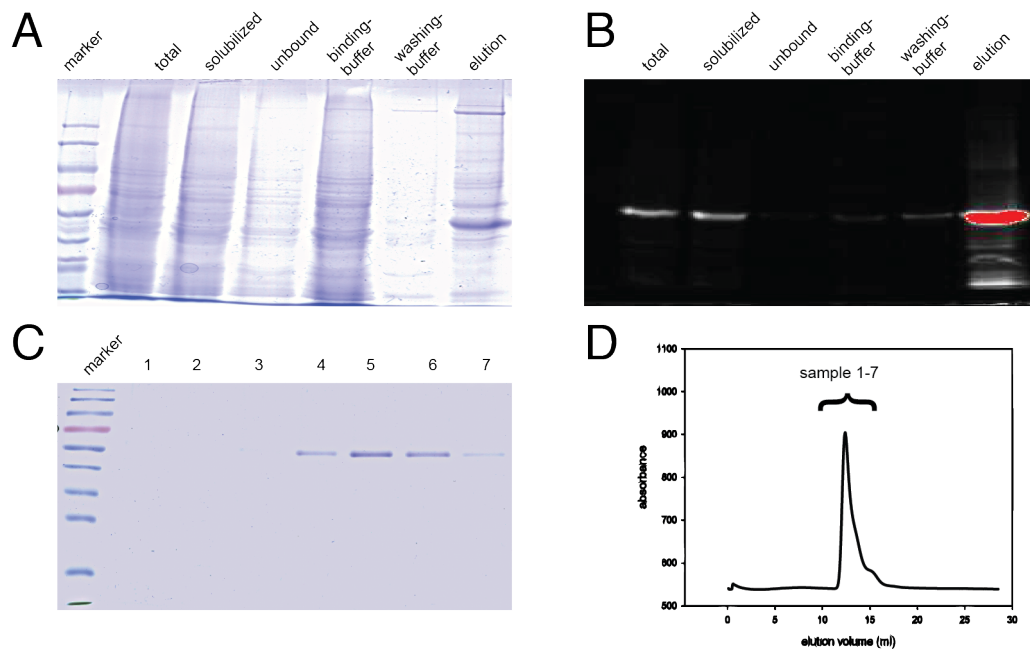


Fig. 3.47. Purification of hDHCR7. The membrane from 20-25 liters of Sf21 cells was prepared and stripped with 0.2 M urea. 3 ml of the stripped membrane was solubilized in solubilization buffer (1% Fos-choline®-13, 500 mM NaCl and 50mM Tris-Hcl pH 7.5) in the final volume of 12 ml for 2 hours at 4°C. to the solubilized fraction 1 ml Ni-NTA and 10 mM imidazole was added and incubated for 2 h at 4°C. the beads were packed into Econo-chromatography columns (BIO-RAD) and washed with 10 ml binding buffer (0.2% Fos-choline®-13, 300 mM NaCl, 50 mM Tris-Hcl pH 7.5 and 10 mM imidazole) and 10 ml washing buffers (0.1% Fos-choline®-13, 300 mM

NaCl, 50 mM Tris-Hcl pH 7.5 and 30 mM imidazole). Protein was eluted with 5 ml of the elution buffer (0.05% Fos-choline®-13, 150 mM NaCl, 50 mM Tris-Hcl pH 7.5 and 150 mM imidazole). The eluate was dialyzed, concentrated and injected into Superose 12 (GE Healthcare). **(A-B)** SDS-PAGE and the corresponding fluorescence image after Ni-NTA purification. **(C)** SDS-PAGE and the corresponding fluorescence image after gel filtration. **(D)** Chromatogram of gel filtration.

3.2.2) Binding of NBD-7DHC to cDHCR7

Different methodologies have been developed in order to measure the binding constants and kinetics of cholesterol binding to various proteins. In this regard either radiolabeled or fluorescently tagged sterols are required. In the classical experiment, the sterol-binding protein is purified and adsorbed to a membrane with no affinity to sterols. Upon addition of radiolabeled sterols to the membrane and vigorous washing, the binding between radiolabeled sterols and sterol binding proteins can be quantitatively measured using scintillation counting. This method has been used to characterize P450 and NPC1 (Xie et al., 2009, Infante et al., 2008 and Mast and Pikuleva, 2005). Another approach that measures the binding in a semi-quantitative manner takes advantage of Ni-NTA followed by simple purification steps. This method has been used to analyze membrane proteins purified in detergent micelles including SCAP and Insig (Radhakrishnan et al., 2004 and 2007). This method suffers from the lag phase between the stop-point of the reaction (loading on the Ni-NTA column) until the measurement is done. Therefore, precise and quantitative measurements cannot be obtained using this method. However, the authors showed that binding between cholesterol and SCAP was saturated at nearly 4 hours, which does not seem to be reasonable for a sensor protein. As mentioned earlier, SCAP was purified in Fos-choline®-13 detergent micelle, which necessitated reconstitution of cholesterol into the same detergent micelle, too. The fusion of micelles and insertion of cholesterol into the micellar environment was the rate-limiting step in this method. Other methods including use of a small gel filtration and acetone precipitation to denature and precipitate the protein-sterol have been used (Okamura et al., 1999 and Ko et al., 2003). The first method again provides semi-quantitative and imprecise binding constants and the second method denatures the protein complex, which both are not suitable for fast and quantitative kinetic measurements.

It was reported that radiolabeled 7-DHC was unstable due to its intrinsic convergence to vitamin D precursor upon UV irradiation (Batta et al., 1997). NBD labeled cholesterol was shown to be a useful tool to investigate the function and localization of cholesterol both *in vitro* and *in vivo* (Faletrov et al., 2012 and Maxfield et al., 2012). Therefore, we synthesized NBD tagged 7-DHC in order to characterize DHCR7 (synthesized by Dr. Christian Hedberg, MPI for Molecular Biology, Germany). We approached this issue using Ni-NTA and gel filtration columns. First, 0.6 μ M of cDHCR7 solubilized in Fos-choline®-13 was mixed with 50 μ M NBD-7DHC solubilized in DMSO and incubated for different time-points. Then, the reaction mixture was applied on 0.1 ml Ni-NTA beads packed in a column and washed

vigorously to remove the unbound substrate. The protein was eluted from the column using gel filtration buffer containing 250 mM imidazole and fractions of 4 drops per microtube were collected. The protein content of fractions was assayed using Bradford assay and fluorescence was measured using Ω Omega spectrometer at a wavelength of 509 nm (excitation: 488 nm). If the protein and the substrate interacted, then the fluorescent intensity would overlap with the protein intensity. The method was not successful for two reasons. First, NBD-7DHC bound to the filter used at the bottom of the chromatographic column (BIO-RAD). Even though extensively washed before elution, but the eluted protein never showed reliable and constant fluorescence absorption. On the other hand, the measured fluorescent value corresponded to a value below 1 μ M while fluorescence absorption of NBD was linear in a 1-100 μ M range. Furthermore, imidazole has a similar structure to NBD and at sub-micromolar range shows similar fluorescent absorption. Alternatively, either histidine or EDTA was used to elute the protein. Histidine showed the same fluorescent absorption like imidazole and the protein did not elute with EDTA completely. Therefore, this method failed to provide a reliable measurement for many reasons. First, absorption of NBD-7DHC was linear in a micromolar range, which is relatively a high concentration regarding kinetics measurements. Second, protein elution was only successful with imidazole, which shows a very similar absorption to NBD at low concentrations. Third, the bound and unbound substrate could not be distinguished in this method.

As an alternative method, we used desalting column (PD-10) to separate the bound and unbound substrate since we could not distinguish between them in the Ni-NTA column. PD-10 column separates molecules smaller than 5 kDa from bigger molecules. Therefore, NBD-7DHC with a molecular weight of around 700 Da can theoretically be separated from proteins. The reaction mixture was applied on a PD-10 column, washed with 10 ml gel filtration buffer and fractions of 4 drops per microtube were collected. As a control, BSA (bovine serum albumin) was used as a non-binder to 7DHC to examine if substrate-protein separation can be achieved using this method. Thus, 0.6 μ M of BSA was mixed 50 μ M NBD-7DHC and applied on PD-10 column. The protein and fluorescence were measured as explained. Unfortunately, BSA with NBD-7DHC or cDHCR7 with NBD-7DHC always co-eluted in the same fraction and separation was not successful.

We solubilized NBD-7DHC in DMSO to measure its binding to a Fos-choline®-13-solubilized protein. One solution to our failure would be to solubilize NBD-7DHC in Fos-choline®-13, which shares the same micellar properties as the protein. However, radiolabeled cholesterol was not reconstituted in Fos-choline®-13 micelles above 25 μ M concentration (Radhakrishnan et al., 2004), which complicates experimentation in minute concentrations, lower than sensitivity of NBD-7DHC fluorescent measurement. The other solution is to use a radiolabeled molecule rather than NBD tagged and adsorb the protein on a charged membrane rather than to a purification column. But experimentation requires extreme care to prevent exposure to UV irradiation to prevent molecular conversion to vitamin D.

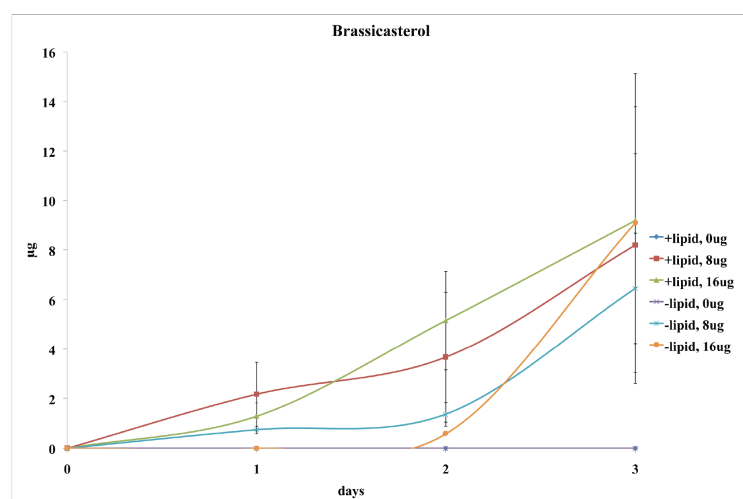
3.2.3) *In vivo* reductase assay

DHCR7 reduces 7-DHC with an unknown mechanism since the double bond (C7-8) of the sterol ring is located in the hydrophobic core of the membrane and electron transfer from solution (NADPH, H^+) to membrane should occur in order to reduce 7-DHC. Contradictory data exist regarding the requirement of cytochrome P450 (POR) as a binder to NADPH since DHCR7 does not have an NADPH-binding domain (Nishino et al., 2000 and Zou et al., 2011). Assuming that binding between DHCR7 and 7-DHC (detergent micelle fusion) is a slow process and POR is required for electron transfer, establishment of an *in vitro* reduction assay is a very complicated task and requires a NADPH regeneration system consisting of glucose-6-phosphate and glucose-6-phosphate reductase since NADPH decays in faster than 30 minutes (Ness et al., 1987). NADPH oxidation cannot be measured spectroscopically in a quantitative manner but the presence of the NADPH regeneration system impedes this method. Moreover, oxidation can occur without actual 7DHC reduction due to its tendency to get oxidized. But the substrate (cholesterol) production can be measured using GC-MS or HPLC-MS methods (Amaral., et al. 2010). This method, however, cannot provide quantitative measures of reductase activity but only proves that the purified protein is functional. Since we did not succeed in establishing a reliable binding assay between cDHCR7 and 7-DHC, we tried to establish an *in vivo* reductase assay. Previously, it was shown that normal human and patient (DHCR7-deficient) cells are able to convert ergosterol to brassicasterol to serve as a functional assay to evaluate severity of DHCR7 mutations (Ginat et al., 2004). Ergosterol is the homologue of cholesterol in yeast with similar sterol rings to cholesterol and brassicasterol is a plant sterol, both of which do not exist in human cells. In this regard, 1×10^6 HEK-293 cells were seeded into 10-cm culture dishes and 8 or 16 μg of ergosterol (40 or 80 μl from a 200 $\mu\text{g}/\text{ml}$ solubilized in ethanol) was added to medium containing normal or delipidated serum and incubated for 1, 2 and 3 days. Cells were subsequently lysed in 0.9% NaCl and mixed with ethanol and chloroform (1:1) and stigmasterol (100 μM) as a recovery standard. The organic phase was isolated and dried under N_2 stream. Dried sterols were resuspended in cyclohexane and injected into a GC-MS instrument. Cholesterol, brassicasterol and stigmasterol were measured as triplicates for each time-point and values were normalized against the cholesterol concentration in the condition with normal serum and no ergosterol (Fig. 3. 48). We observed that HEK-293 cells converted ergosterol to brassicasterol within 3 days up to an average of 8 μg and 6 μg for samples given 8 μg ergosterol in lipidated and delipidated serum, respectively. 9 μg and 15 μg of brassicasterol were detected in lipidated and delipidated samples respectively, which were given 16 μg ergosterol. On the other hand, cholesterol production sank due to oversaturation of cells with high concentration of ergosterol that replaced the natural substrate of DHCR7. Interestingly, in delipidated medium, cholesterol reduction and brassicasterol production were stronger compared to the lipidated medium. At first glance, this observation is puzzling since in the absence of exogenous cholesterol, the SREBP pathway is up-regulated to transcribe genes involved in cholesterol production and uptake including DHCR7. Therefore, it is expected that the cholesterol level increases within 3 days. But, since

DHCR7 is saturated with ergosterol, 7-DHC accumulates in the cells and most probably takes part in a feedback inhibitory mechanism to degrade HMG-CoA reductase as also suggested by others (Fritzky et al., 2001 and Honda et al., 1998). However, the biochemical details of the 7-DHC mediated proteolysis of HMG-CoA reductase has not been elucidated. Furthermore, brassicasterol can theoretically bind to SCAP and suppress the SREBP pathway due to its structural similarity to cholesterol.

The reductase assay provides an invaluable tool to investigate the functionality of DHCR7 and its mutants in the cell. The atrophy of SLOS depends on specific DHCR7 mutations. Some patients show more severe symptoms than others. Using *dhcr7^{-/-}* cells (obtained from human patients, Dr. Porter, NIH, USA) and transfection with different mutants, residues important for sterol binding and reduction can be identified when complemented with structural studies. Furthermore, our methodology needs to be improved in future due to imprecision in the measurements that led to huge error bars.

A



B

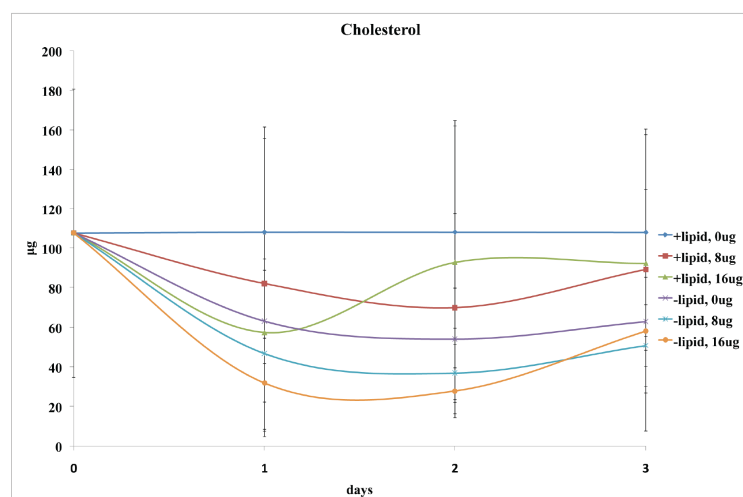


Fig. 3.48. Reduction of ergosterol to brassicasterol in HEK-293 cells.

1×10^6 HEK-293 cells were seeded into 10-cm culture dishes and incubated for an overnight to attach to plates. Then, 0, 8 or 16 μg of ergosterol (from a 200 $\mu\text{g}/\text{ml}$ solution in ethanol) was added to medium containing normal serum or delipidated serum. Cells were incubated for 1-3 days. Cells were lysed in 0.5 ml of 0.9% NaCl and sonicated once for 20 counts at an output of 3.5 and duty cycle 10%. To the lysate, 100 μM of stigmasterol, 300 μl ethanol and 300 μl chloroform were added, vortexed vigorously and centrifuged at 3,000 rpm for 3 min. the organic (lower) phase was transferred to a glass vial and dried under gentle N_2 stream. Dried sterols were resuspended in 300 μl cyclohexane and injected into GC-MS. Each time-point represents a mean value of a triplicate and normalized against cholesterol concentration in the condition with normal serum and no ergosterol. (A) A graph

showing brassicasterol produced within 3 days of experiment. **(B)** A graph showing changes in cholesterol level within 3 days.

3.2.4) 2D crystallography of cDHCR7

We used commercially available kits (*JCSG Core I-IV Suite*, *Mb I-II Suite*, *PACT suite* and *Protein Complex Suite* from QIAGEN) to test whether both hSSD (8, 20 and 28 mg/ml) and cDHCR7 (6 mg/ml) form a crystal. None of the conditions tested at 4°C or 20°C led to formation of a crystal. Fos-choline®-13 has a relatively long acyl chain, which makes it likely unsuitable for crystallography. However, two structures have been reported using Fos-choline®-14 (Wang et al., 2008 and Bass et al., 2002). But, both cDHCR7 and hSSD have very short extra-membranous domains, which renders protein contact when embedded in large acyl-chain detergents.

cDHCR7 (1 mg/ml) was used to set up 2D crystallography trials with *E. coli* polar lipids, brain polar lipids, 1,2-didodecanoyl-sn-glycero-3-phosphocholin (DLPC) and 1,2-dioleoyl-sn-glycero-3-phosphocholin (DOPC) in a lipid-to-protein ratio (LPR) of 1, 0.5 and 0.3. Samples were dialyzed for a week and analyzed using EM (Fig. 3.49). In the primary trial, DOPC at LPR of 1 formed very nice liposomes that contained the protein (Fig. 3.48D). Therefore, we further optimized this condition at LPR of 1 and dialyzed the protein against buffers with pH ranging from 4 to 6 for two weeks (Fig. 3.49E-F). The crystals showed a weak but yet significant diffraction pattern (Fig. 3.49G). In both conditions, very small crystals were present, which require further optimization to grow them bigger suitable for recording images at high tilt angles. Our results can serve as a platform for further optimization and improvements. In future studies, protein quality, cationic additives, temperature, pH and LPR should be fine-tuned. The His-tag is a relatively flexible sequence of 10 histidines, which might prevent crystal contacts and preferably, it should be cleaved before crystallography trials are set up. The cDHCR7 used in this study contained a His-tag since it could not be cleaved with precision protease due to its inaccessibility to the enzyme (as explained in 3.2.1.2). Therefore, constructs can be designed to include a sequence before the cleavage site to make it more accessible to precision protease. On the other hand, Fos-choline®-13 has a very low CMC, which makes it very difficult to be exchanged by any other detergents. We also failed to exchange this detergent (explained in 3.2.1.2). However, using minute concentrations of lipids especially DOPC that led to formation of a crystal may improve the later lipid reconstitution and crystal formation.

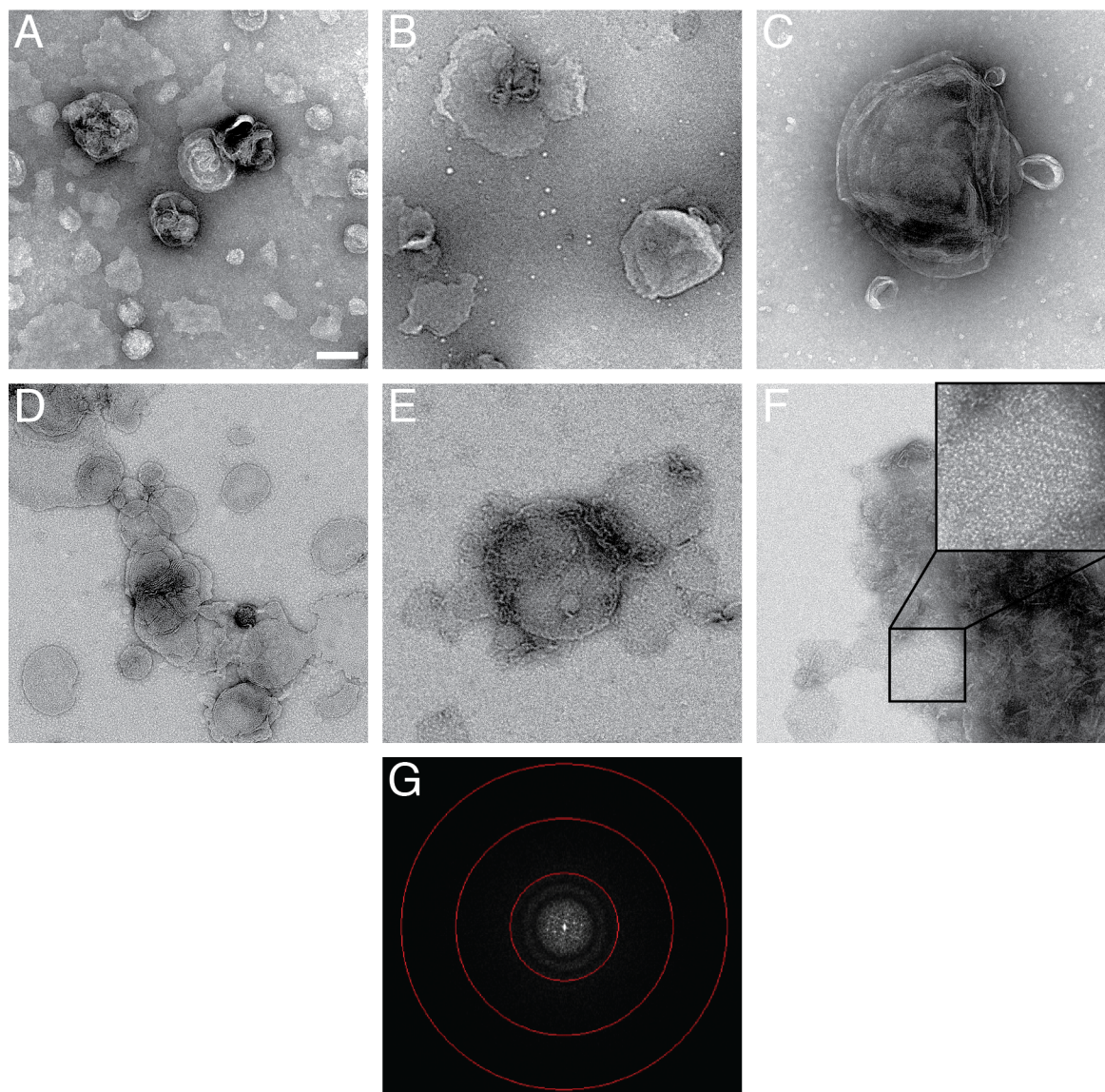


Fig. 3.49. 2D crystallography of cDHCR7. 60 μ l of cDHCR7 purified in Fos-choline®-13 (1/mg/ml) was mixed with (A) *E. coli* polar lipids, (B) brain polar lipids, (C) DLPC and (D) DOPC at final lipid-to-protein ratio of 1:1 and incubated for 1h in dark. Samples were placed in dialysis button, covered with a dialysis bag (Cut-off: 12-14 kDa) and dialyzed for 1 week in Tris-HCl buffer (pH: 7.5). (E-F) cDHCR7 was mixed with DOPC at LPR of 1:1 and dialyzed for 2 weeks against a buffer with pH 6 and 4 respectively.

3.2.5) Localization of hDHCR7-EGFP in HEK-293 cell

DHCR7 localizes to the endoplasmic reticulum (ER) where it synthesizes cholesterol (Correa-Cerro and Porter, 2005). Recent evidence showed that an independent pathway synthesizes cholesterol in peroxisomes where it seemed to be dependent on DHCR7 (Weinhofer, et al., 2006). On the other hand, many proteins including those involved in cholesterol synthesis such as SCAP and SREBP are known to

be transported to the Golgi (Caldas and Herman, 2003 and Nohturfft, et al., 1999). Therefore, we studied the localization of DHCR7 fused to EGFP in HEK-293 cells using a Golgi marker, GalT fused to RFP (Mackenzie et al., 1999) and a peroxisome marker, PXMP2 fused to RFP (Rokka, et al., 2009).

3.2.5.1) Co-localization of DHCR7 with Golgi marker

The HEK293 cells were transfected with plasmids carrying DHCR7-EGFP and GalT-RFP under normal conditions where lipidated serum was used. The cells were imaged 24 h post transfection using a Leica microscope and collecting images at emission ranges of 505-530 nm for EGFP and 580-650 nm for RFP. The cells showed a very significant co-localization as the overlay of RFP and EGFP channels suggested (Fig. 3.50C). the overlay of images at this resolution does not necessarily indicate a meaningful co-localization. Therefore, the intensity of both channels are plotted against each other. The x-axis indicates the red channel (Ch1) with the intensity ranging from 1 to 255 (8-bit grey scale values) and the green channel (Ch2) is displayed on the y-axis with the same values. Each pixel of the channel is compared to the pixel of the other channel at the same position and the so-called pixel-pairs are plotted in the scatter plot. The areas in the scatter plot that appear in pure red or green represent pixel pairs in which one pixel has a much higher intensity than the other one. Those parts of images are not considered as colocalization of the two proteins. The area that appears in yellow represents colocalized pixels and therefore colocalized proteins in the overlay (Fig. 3.50D). In the red-green correlation plot, pixel pairs with a high frequency are shown in white and pairs with a low frequency in purple (Fig. 3.50E). The red-green correlation plot indicates that areas with high intensity in the green channel co-localize with areas of low intensity in the red channel forming white areas in the plot. On the other hand, areas of high red intensity co-localizes with low-intensity areas of the green channel. This pattern does not reflect co-localization but rather results from diffusion of channels at this limited resolution. However, a significant yellow-colored area is seen in the scatter plot suggesting co-localization of DHCR7 and GalT in the Golgi apparatus. This is further verified by the Pearson's and Mander's coefficients (Table 3.1). The Pearson's coefficient indicates the strength of the linear relationship of two values and ranges from -1 to 1. Values around zero from -0.3 to 0.3 are specified to have little or no association. In the case of colocalization studies, this means that both fluorophores have no spatial relationship, as their maxima occur on different points pixels. A Pearson's coefficient of 1 represents total colocalization. Negative values are interpreted that one signal suppresses the other. The Pearson's coefficient only leads to a reliable value when the same amount of pixels is present in both channels. In order to gain a more precise value, the Mander's coefficients M_1 and M_2 were calculated. The Mander's coefficients M_1 is defined as the ratio of the summed intensities of pixels from the red channel in which the intensity of the green channel is above zero divided to the total intensity in the red channel. M_2 is defined conversely for green. The M_1 coefficient corresponding to red channel shows 92% localization of the red channel with the green

channel meaning that at 92% of the Golgi apparatus where GalT-RFP is located DHCR7 is also present (Table 3.1).

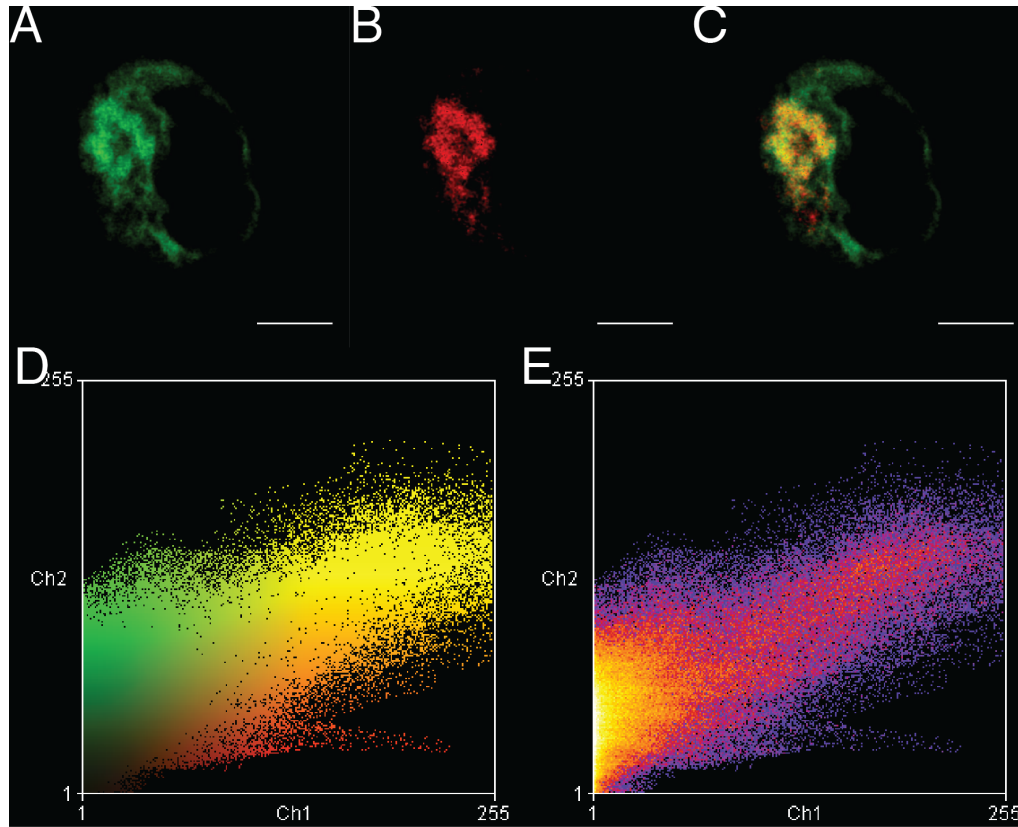


Fig. 3.50. Co-localization of DHCR7-EGFP and GalT under normal conditions. Examples of confocal fluorescence images of HEK293 cells transiently transfected with DHCR7 (EGFP shown in green) and Golgi marker GalT (RFP shown in red). Specimens shown in this figure were kept in standard growth medium before fixation. **(A)** Shows EGFP labeled DHCR7, **(B)** shows RFP labeled GalT (Golgi marker). In **(C)**, a merged image of both channels is displayed. Scale bar represents 5 μ m. The intensities in the “red-green correlation plot” image represent the actual color of the pixels in the image. The scatter plot in **(D)** represents the frequency of pixels that display those particular red/green values. **(E)** Hot colors indicate high frequency of pixel pairs.

Table 3.1: Calculated coefficients for colocalization of DHCR7 and GalT under standard growth conditions.

Conditions	Pearson's coefficient r_p	Mander's coefficient M_1	Mander's coefficient M_2
Standard growth conditions	0.553 ± 0.095	0.924 ± 0.009	0.516 ± 0.080

In a parallel experiment, we tested whether cholesterol depletion via β -methyl-cyclodextrin has an effect on the localization of DHCR7. In this regard, cells were treated with 1% β -methyl-cyclodextrin for 1 h before fixation. In order to confirm that β -methyl-cyclodextrin has removed a considerable fraction of cholesterol, a total cholesterol detection kit (axiom diagnostics) was used. The images showed co-localization of DHCR7 with GalT and the Pearson's and Mander's coefficients showed a significant co-localization comparable to normal cells (Fig. 3.51A-E). However, the Mander's coefficient showed only 83% co-localization for the red channel, which is smaller than the Mander's coefficient calculated for normal cells (92%). This discrepancy results from the smaller size of the Golgi apparatus in the cells imaged in these experiments, which could result from treatment with β -methyl-cyclodextrin and subsequent cholesterol depletion (Table 3.2). Yet, the Mander's coefficient suggests a meaningful colocalization of DHCR7 with GalT. This novel observation shows a significant localization of DHCR7 in both ER and Golgi apparatus independent of cellular cholesterol content.

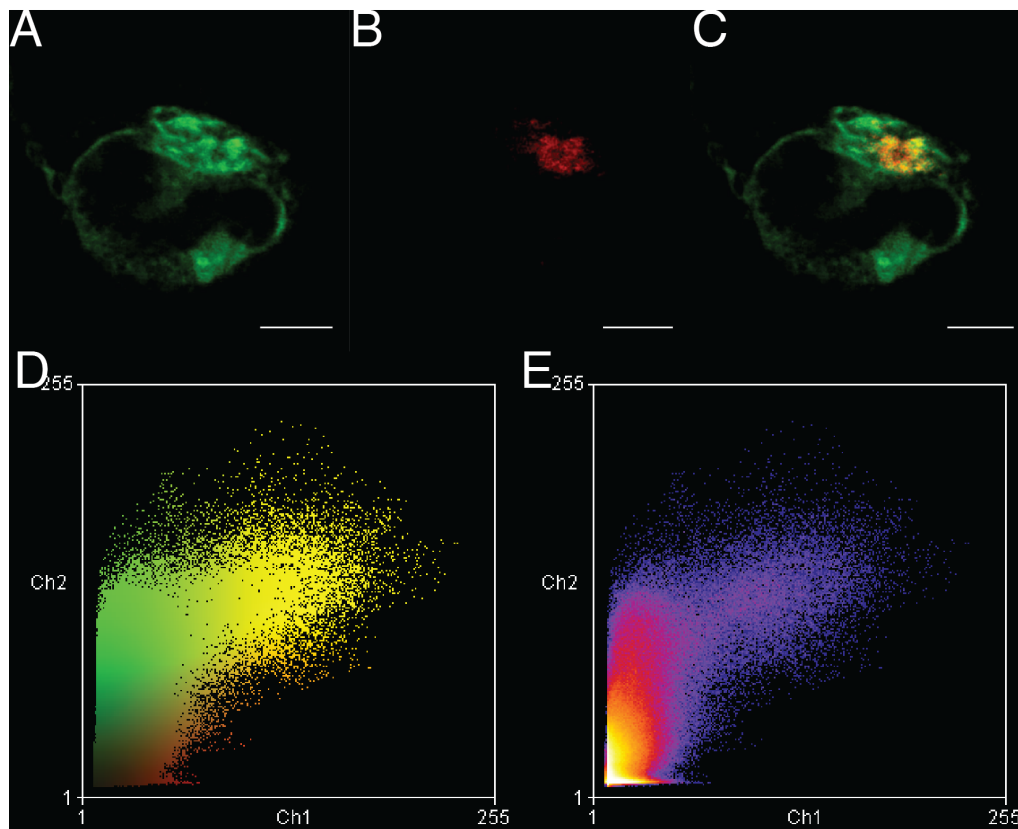


Fig. 3.51. Co-localization of DHCR7-EGFP and GalT after 1 h treatment with β -methyl-cyclodextrin. Examples of confocal fluorescence images of HEK293 cells transiently transfected with DHCR7 (EGFP shown in green) and Golgi marker GalT (RFP shown in red) and treated with β -methyl-cyclodextrin for 1 h. Specimens shown in this figure were incubated for 1 h in delipidated medium containing 1% β -methyl-cyclodextrin before fixation.

(A) Shows EGFP labeled DHCR7, (B) shows RFP labeled GalT (Golgi marker). In (C), a merged image of both channels is displayed. Scale bar represents 5 μm . The intensities in the “red-green correlation plot” image represent the actual color of the pixels in the image. The scatter plot in (D) represents the frequency of pixels that display those particular red/green values. (E) Hot colors indicate high frequency of pixel pairs.

Table 3.2: Calculated coefficients for colocalization of DHCR7 and GalT after treatment with β -methyl-cyclodextrin.

Conditions	Pearson's coefficient r_p	Mander's coefficient M_1	Mander's coefficient M_2
Treated for 1h with β -methyl-cyclodextrin	0.572 ± 0.185	0.835 ± 0.105	0.396 ± 0.075

3.2.5.2) Co-localization of DHCR7 with peroxisome marker

As it was previously reported that an independent cholesterol synthesis pathway exist in peroxisome (Weinhofer, et al., 2006), we examined the localization of DHCR7 and a peroxisome marker PXMP2 in HEK-293 cells under normal and delipidated conditions. Cells in both states showed no co-localization with the peroxisome marker (Fig. 3.52) and scatter plots could not be calculated due to lack of co-localization in the cells examined. The Pearson's coefficients and Mander's coefficients indicated no co-localization either (Table 3.3). Also the distribution of pixels is not equal in both channels at all. The calculated Pearson's coefficients of DHCR7 and PXMP2 show values that support the hypothesis shown in the images. Pearson's coefficients with a value close to zero indicate no co-localization. This is further confirmed by the Mander's coefficients M_1 and M_2 as they have values around 0.2, which indicates no co-localization either.

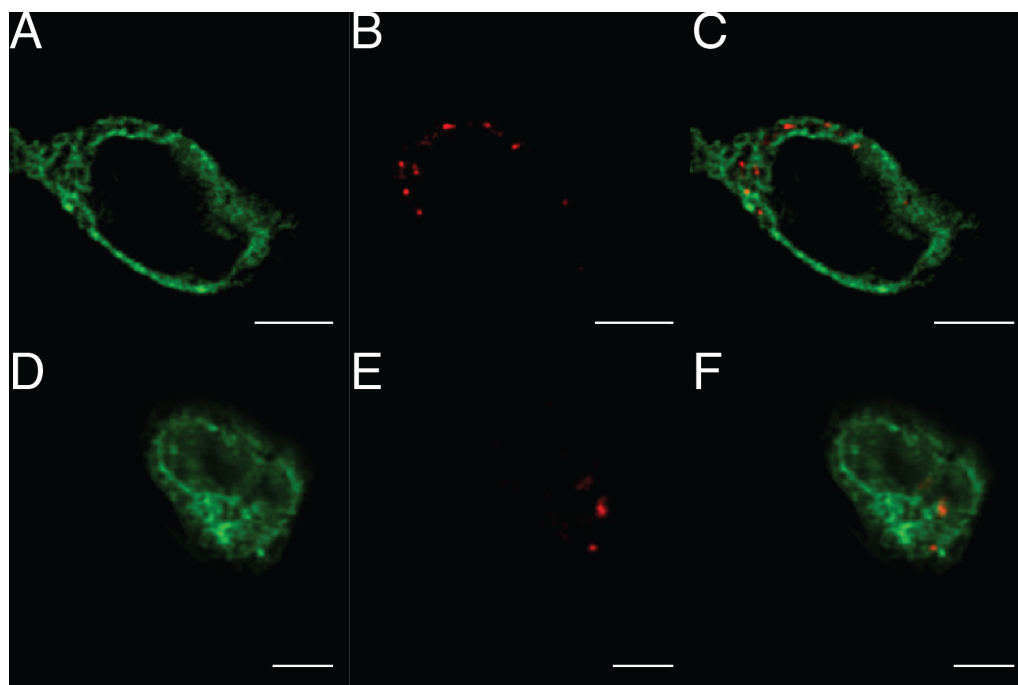


Fig. 3.52. Co-localization of DHCR7-EGFP and PXMP2 under normal and delipidated conditions. Examples of confocal fluorescence images of HEK293 cells transiently transfected with DHCR7 (EGFP shown in green) and Golgi marker PXMP2 (RFP shown in red). Specimens shown in this figure were kept in standard growth medium before fixation. **(A and D)** EGFP labeled DHCR7 under normal and delipidated condition, respectively. **(B and E)** RFP labeled PXMP2 (peroxisome marker) under normal and delipidated condition, respectively. **(C and F)** Merged image of both channels. Scale bar represents 5 μm .

Table 3.6: Calculated coefficients for colocalization of DHCR7 and PXMP2.

Conditions	Pearson's coefficient	Mander's coefficient	Mander's coefficient
	r_p	M_1	M_2
Standard growth conditions	0.098 ± 0.173	0.218 ± 0.086	0.105 ± 0.059
Treated for 1h with β -methyl-cyclodextrin	0.016 ± 0.151	0.224 ± 0.054	0.142 ± 0.096

Our localization studies showed that DHCR7 localizes to Golgi apparatus considerably under normal and delipidated conditions as measured by Mander's coefficient. However, overexpression of proteins might lead to unwanted localization since the original compartment where the protein should localize becomes

saturated. In this case, DHCR7-EGFP could be transported to the Golgi apparatus if the ER is saturated but the significance of this localization is puzzling. On the other hand, it is not known if DHCR7 has functionality or some other regulatory functions in the Golgi apparatus such as interaction with Sonic hedgehog (Shh). However, it was shown that another enzyme involved in post-squalene cholesterol biosynthesis pathway known as NSDHL (NADPH steroid dehydrogenase-like) traffics through the Golgi apparatus, which is required for its localization in the ER and lipid droplets (Caldas et al., 2003). Therefore, further studies are needed to investigate if the same mechanism applies to DHCR7. Furthermore, co-localization of DHCR7 in lipid droplets was not investigated in this study, which could raise more questions regarding the functionality of DHCR7 and possible cholesterol production in compartments other than ER.

Our studies did not show any co-localization of DHCR7 and the peroxisome marker. This observation was validated using Mander's coefficient. Previous data suggested independent cholesterol biosynthesis in peroxisomes mediated via HMG-CoA reductase. In the last decade, accumulating evidence suggested that another isoform of HMG-CoA reductase exists in peroxisome. A recent study showed that in mammals there is a single gene, which could be targeted to peroxisome (Breitling et al., 2002). At least under the conditions we tested with HEK-293 cells, no localization of DHCR7 to peroxisomes could be detected. But, further studies using an endogenous promoter and cell lines more suited for cholesterol or lipid production such as hepatic cells are needed.

Structure-based drug design hinges on the precise knowledge of the structure of proteins. In our studies we aimed to study the structure and function of DHCR7 the ultimate enzyme in the cholesterol biosynthesis pathway. Therefore, revealing the molecular architecture of DHCR7 can provide the platform for future drug development to cure arteriosclerosis. The first step in structure determination is protein purification. We expressed and purified DHCR7 from human, *Coxiella burnettii* and the sterol-sensing domain of the human DHCR7 using *E. coli* and baculovirus-based expression system. We failed to express and purify the DHCR7 from *Plesiocystis pacifica*. Fos-choline®-13 solubilized all of the expressed proteins most efficiently. The structural resemblance between Fos-choline®-13 and sphingomyelin probably is the underlying reason since cholesterol (and cholesterol-binding proteins) and sphingomyelin reside adjacent to each other in the membrane. Long acyl chain of Fos-choline®-13 covers a huge surface of the purified proteins, which hampers the accessibility of the cleavage site between the DHCR7 and the His-tag. Therefore, we could not cleave the His-tag after purification, which conferred flexibility to the protein and thus prevented an efficient crystal formation. Introduction of a rigid linker between the His-tag and the cleavage site might improve the accessibility of the Precession enzyme to the cleavage site. In order to determine the structure of DHCR7, we used 3D and 2D crystallographic methods. 2D crystallography is advantageous to 3D crystallography since the membrane protein is reconstituted in a lipid bilayer. Our preliminary crystal set-up of DHCR7 from *Coxiella burnettii* led to

formation of a very small crystal. To obtain data for processing, a crystal bigger than 1 μm is desired, from which data can be acquired during tilting. In this regard, His-tag cleavage, use of different lipids, addition of cations and varying temperature might improve the crystals. Besides, Fos-choline®-13 has a very low CMC, which is not easily substituted by the lipids. Thus, it is required to test more detergents for solubilization of the proteins to enhance crystal contact. Alternatively, inclusion of minute concentration of lipids and using lipidic cubic phase might improve the further crystallization (Boudker et al., 2007).

We tried to characterize the function of DHCR7 using NBD-tagged 7-DHC (synthesized by Dr. Christian Hedberg). We used either a Ni-NTA-based method or gel-filtration to assess the binding between DHCR7 and its substrate. We however, failed to detect the binding due to technical reasons (explained in 3.2.2). The reason for failure could be that the substrate was solubilized in DMSO rather than the detergent. Solubilization in the same detergent or reconstitution in liposome could enhance the binding assay under the conditions we tested (Ramakrishnan et al., 2004). Alternatively, radiolabeled 7-DHC can be used to measure more quantitatively, which demands its synthesis. Furthermore, we established an assay to measure the reductase activity in the cells using ergosterol as a substrate and GC-MS as detection instrument. This method although unquantitative, can serve as an important tool to identify the vital residues for substrate binding and reductase function. This requires first, improvement of the methodology and use of a more sensitive instrument as very large error bars were observed. Second, *dhcr7*^{-/-} cell lines obtained from SLOS patients that need to be transfected with different *dhcr7* mutants. Combination of *in vitro* and *in vivo* approaches were used in this study to reveal the structural and functional properties of DHCR7. However, our results provided very preliminary insights and need to be improved in future.

4) References

- Abeyrathne, P.D., Chami, M., Pantelic, R.S., Goldie, K.N., and Stahlberg, H. (2010). Preparation of 2D crystals of membrane proteins for high-resolution electron crystallography data collection. *Methods Enzymol.* 481:25-43
- Alushin, G., and Nogales, E. (2011). Visualizing the kinetochore architecture. *Curr Opin Struct Biol.* 21(5):661-9
- Amaral, C., Gallardo, E., Rodrigues, R., Pinto Leite, R., Quelhas, D., Tomaz, C., and Cardoso, M.L. (2010). Quantitative analysis of five sterols in amniotic fluid by GC-MS: application to the diagnosis of cholesterol biosynthesis defects. *J Chromatogr B Analyt Technol Biomed Life Sci.* 878(23):2130-6
- Amin, D., et al. (1997). RPR 107393, a potent squalene synthase inhibitor and orally effective cholesterol-lowering agent: comparison with inhibitors of HMG-CoA reductase. *Journal of Pharmacology and Experimental Therapeutics.* 281(2), 746
- Amir, S. et al. (2006). MSF-A interacts with hypoxia-inducible factor-1 α and augments hypoxia-inducible factor transcriptional activation to affect tumorigenicity and angiogenesis. *Cancer Res.* 66: 856–866
- Amir, S. et al. (2009). SEPT9_v1 up-regulates hypoxia-inducible factor 1 by preventing its RACK1-mediated degradation. *J Biol Chem.* 284: 11142–11151
- Amir, S., Golan, M., and Mabeesh, N.J. (2010). Targeted knockdown of SEPT9_v1 inhibits tumor growth and angiogenesis of human prostate cancer cells concomitant with disruption of hypoxia-inducible factor-1 pathway. *Mol Cancer Res.* 8: 643–652
- Ausubel, F.M. et al. (1995). *Current Protocols in Molecular Biology*, John Wiley and Sons, Ltd., New York, NY
- Baker, M. (2010). Making membrane proteins for structures: a trillion tiny tweaks. *Nature Methods.* 7(6), 429-434
- Barenholz, Y. (2004). Sphingomyelin and cholesterol: from membrane biophysics and rafts to potential medical applications. *Subcell Biochem.* 37:167-215
- Barral, Y. and Kinoshita, M. (2008). Structural insights shed light onto septin assemblies and function. *Curr Opin Cell Biol.* 20(1):12-8
- Barral, Y., and Mansuy, M.I. (2007). Septins: cellular and functional barriers of neuronal activity. *Curr Biol.* 17(22):R961-3
- Bartsch, I. et al. (2010). Human endothelial and platelet septin SEPT11: cloning of novel variants and characterisation of interaction partners. *Thromb Haemost.* 104: 1201–1210

-
- Bass, R.B., Strop, P., Barclay, M., and Rees, D.C. (2002). Crystal Structure of Escherichia coli MscS, a Voltage-Modulated and Mechanosensitive Channel. *Science*. 298(5598):1582-7
 - Bastiaanse EM, Höld KM, and Van der Laarse A. (1997). The effect of membrane cholesterol content on ion transport processes in plasma membranes. *Cardiovasc Res*. 33(2):272-83
 - Batta, A.K., Salen, G., Tint, G.S., Honda, A., and Shefer, S. (1997). Synthesis of [3 alpha-3H]7-dehydrocholesterol via stable tritiated 4-phenyl-1,2,4-triazoline-3,5-dione derivative. *Steroids*. 62(11):700-2
 - Beck, M., Förster, F., Ecke, M., Plitzko, J.M., Melchior, F., Gerisch, G., Baumeister, W., and Medalia, O. (2004). Nuclear pore complex structure and dynamics revealed by cryoelectron tomography. *Science*. 306(5700):1387-90
 - Becker, K., Csikos, M., Horvath, A., and Karpati, S. (2001). Identification of a novel mutation in 3 hydroxysteroid 8 7 isomerase in a case of Conradi–Hünemann–Happle syndrome. *Experimental dermatology*. 10(4), 286-289
 - Behrmann, E., Müller, M., Penczek, P.A., Mannherz, H.G., Manstein, D.J., and Raunser, S. (2012). Structure of the rigor actin-tropomyosin-Myosin complex. *Cell*. 150(2):327-38
 - Beites, C.L., Xie, H., Bowser, R., Trimble, W.S. (1999). The septin CDCrel-1 binds syntaxin and inhibits exocytosis. *Nat Neurosci*. 2(5):434-9
 - Bertin, A. et al. (2008). Saccharomyces cerevisiae septins: supramolecular organization of heterooligomers and the mechanism of filament assembly. *Proc Natl Acad Sci U S A*. 105(24):8274-9
 - Bertin, A. et al. (2010). Phosphatidylinositol-4,5-bisphosphate promotes budding yeast septin filament assembly and organization. *J Mol Biol*. 404(4):711-31
 - Bhushan, S., Hoffmann, T., Seidelt, B., Frauenfeld, J., Mielke, T., Berninghausen, O., Wilson, D.N., and Beckmann, R. (2011). SecM-stalled ribosomes adopt an altered geometry at the peptidyl transferase center. *PLoS Biol*. 9(1):e1000581
 - Bloom, J., and Cross, F.R. (2007). Multiple levels of cyclin specificity in cell-cycle control. *Nat Rev Mol Cell Biol*. 8(2):149-60
 - Bolte, S., and Cordelieres, F. (2006). A guided tour into subcellular colocalization analysis in light microscopy. *Journal of microscopy*. 224(3), 213-232
 - Bose, I., Irazoqui, J.E., Moskow, J.J., Bardes, E.S., Zyla, T.R., and Lew, D.J. (2001). Assembly of scaffold-mediated complexes containing Cdc42p, the exchange factor Cdc24p, and the effector Cla4p required for cell cycle-regulated phosphorylation of Cdc24p. *J Biol Chem*. 276(10):7176-86
 - Botstein, D., Chervitz, S.A., and Cherry, J.M. (1997). Yeast as a model organism. *Science*. 277(5330):1259-60

-
- Boudker O, Ryan RM, Yernool D, Shimamoto K, Gouaux E. (2007). Coupling substrate and ion binding to extracellular gate of a sodium-dependent aspartate transporter. *Nature*. 25;445(7126):387-93
 - Bowen, J.R., Hwang, D., Bai, X., Roy, D., and Spiliotis, E.T. (2011). Septin GTPases spatially guide microtubule organization and plus end dynamics in polarizing epithelia. *J Cell Biol*. 194(2):187-97
 - Bowie, J. (2005). Solving the membrane protein folding problem. *Nature* 438(7068), 581-589
 - Breitling, . and Krisans, S.K. (2002) A second gene for peroxisomal HMG-CoA reductase? A genomic reassessment. *J Lipid Res*. 43(12):2031-6
 - Bretscher, M., & Munro, S. (1993.) Cholesterol and the Golgi apparatus. *Science*. 261(5126), 1280-1281
 - Brown, D., and London, E. (1998). Functions of lipid rafts in biological membranes. *Annual Review of Cell and Developmental Biology*. 14(1), 111-136
 - Brown, J.L., Jaquenoud, M., Gulli, M.P., Chant, J., and Peter, M. (1997). Novel Cdc42-binding proteins Gic1 and Gic2 control cell polarity in yeast. *Genes Dev*. 11(22):2972-82
 - Brown, M.S., and Goldstein, J.L. (1999). A proteolytic pathway that controls the cholesterol content of membranes, cells, and blood. *Proc Natl Acad Sci U S A*. 96(20):11041-8
 - Brown, M.S., and Goldstein, J.L. (2009). Cholesterol feedback: from Schoenheimer's bottle to Scap's MELADL. *J Lipid Res*. 50 Suppl:S15-27
 - Brunetti-Pierri, et al. (2002). Lathosterolosis, a Novel Multiple-Malformation/Mental Retardation Syndrome Due to Deficiency of 3 [beta]-Hydroxysteroid-[Delta] 5-Desaturase. *The American Journal of Human Genetics*. 71(4), 952-958
 - Butty, A.C., Perrinjaquet, N., Petit, A., Jaquenoud, M., Segall, J.E., Hofmann, K., Zwahlen, C., and Peter, M. (2002). A positive feedback loop stabilizes the guanine-nucleotide exchange factor Cdc24 at sites of polarization. *EMBO J*. 21(7):1565-76
 - Caballero, B. (2007). The global epidemic of obesity: An overview. *Epidemiologic reviews*. 29, 1-5
 - Caldas, H., and Herman, G. (2003). NSDHL, an enzyme involved in cholesterol biosynthesis, traffics through the Golgi and accumulates on ER membranes and on the surface of lipid droplets. *Human molecular genetics*. 12(22), 2981
 - Caudron, F., Barral, Y. (2009). Septins and the lateral compartmentalization of eukaryotic membranes. *Dev Cell*. 16(4):493-506
 - Caviston, J.P., Longtine, M., Pringle, J.R., and Bi, E. (2003). The role of Cdc42p GTPase-activating proteins in assembly of the septin ring in yeast. *Mol Biol Cell*. 14(10):4051-66.

-
- Cerveira, N., Bizarro, S., and Teixeira, M.R. (2011). MLL–SEPTIN gene fusions in hematological malignancies. *Biol Chem.* 392: 713–724
 - Chacko, A.D. et al. (2005). SEPT9_v4 expression induces morphological change, increased motility and disturbed polarity. *J Pathol.* 206: 458–465
 - Chacko, A.D., McDade, S.S., Chanduloy, S., Church, S.W., Kennedy, R., Price, J., Hall, P.A., and Russell, S.E. (2012). Expression of the SEPT9_i4 isoform confers resistance to microtubule-interacting drugs. *Cell Oncol (Dordr).* 35(2):85-93
 - Charlton-Menys, V., and Durrington, P. (2007). Squalene synthase inhibitors: clinical pharmacology and cholesterol-lowering potential. *Drugs.* 67(1), 11-16
 - Chattopadhyay, A., and Harikumar, K. (1996). Dependence of critical micelle concentration of a zwitterionic detergent on ionic strength: implications in receptor solubilization. *FEBS letters.* 391(1-2), 199-202
 - Chen, K.C., Calzone, L., Csikasz-Nagy, A., Cross, F.R., Novak, B., and Tyson, J.J. (2004). Integrative analysis of cell cycle control in budding yeast. *Mol Biol Cell.* 15(8):3841-62
 - Chen, L., Wang, G., and Zhang, H. (2007). Sterol biosynthesis and prokaryotes-to-eukaryotes evolution. *Biochemical and biophysical research communications.* 363(4), 885-888
 - Chichili GR, Rodgers W. (2009). Cytoskeleton-membrane interactions in membrane raft structure. *Cell Mol Life Sci.* 66(14):2319-28
 - Cho, S.J. et al. (2011). Septin 6 regulates the cytoarchitecture of neurons through localization at dendritic branch points and bases of protrusions. *Mol Cell.* 32: 89–98.
 - Chugh, A., Ray, A., and Gupta, J. (2003). Squalene epoxidase as hypocholesterolemic drug target revisited. *Progress in lipid research.* 42(1), 37-50
 - Cid, V.J., Jiménez, J., Molina, M., Sánchez, M., Nombela, C., and Thorner, J.W. (2002). Orchestrating the cell cycle in yeast: sequential localization of key mitotic regulators at the spindle pole and the bud neck. *Microbiology.* 148(Pt 9):2647-59
 - Correa-Cerro, L., and Porter, F. (2005). 3 [beta]-Hydroxysterol [Delta] 7-reductase and the Smith-Lemli-Opitz syndrome. *Molecular genetics and metabolism.* 84(2), 112-126
 - Cox, M.M. (2012). Recombinant protein vaccines produced in insect cells. *Vaccine.* 30(10):1759-66
 - Cross, F.R., Buchler, N.E., and Skotheim, J.M. (2011). Evolution of networks and sequences in eukaryotic cell cycle control. *Philos Trans R Soc Lond B Biol Sci.* 366(1584):3532-44
 - Csikász-Nagy, A., Palmisano, A., and Záborszky, J. (2011). Molecular network dynamics of cell cycle control: transitions to start and finish. *Methods Mol Biol.* 761:277-91

-
- Davidson, M. (2007). Squalene synthase inhibition: a novel target for the management of dyslipidemia. *Current atherosclerosis reports*. 9(1), 78-80
 - De Almeida Marques, I., Valadares, N.F., Garcia, W., Damalio, J.C., Macedo, J.N., de Araújo, A.P., Botello, C.A., Andreu, J.M., and Garratt, R.C. (2008). Septin C-terminal domain interactions: implications for filament stability and assembly. *Cell Biochem Biophys*. 62(2):317-28
 - Dean, P., de Montellano, P., Bloch, K., and Corey, E. (1967). A soluble 2, 3-oxidosqualene sterol cyclase. *J Biol Chem*. 242(12), 3014
 - DeMay, B.S., Bai, X., Howard, L., Occhipinti, P., Meseroll, R.A., Spiliotis, E.T., Oldenbourg, R., and Gladfelter, A.S. (2011). Septin filaments exhibit a dynamic, paired organization that is conserved from yeast to mammals. *J Cell Biol*. 193(6):1065-81
 - Diaspro, A. (2002). Confocal and two-photon microscopy: foundations, applications, and advances: *Wiley-Liss, New York*
 - Do, R., Kiss, R., Gaudet, D., and Engert, J. (2009). Squalene synthase: a critical enzyme in the cholesterol biosynthesis pathway. *Clinical genetics*. 75(1), 19-29
 - Egelhofer, T.A., Villén, J., McCusker, D., Gygi, S.P., and Kellogg, D.R. (2008). The septins function in G1 pathways that influence the pattern of cell growth in budding yeast. *PLoS One*. 3(4):e2022
 - Endo, A., Kuroda, M., and Tusija, Y. (1976). ML-336, ML-236B and ML-236C, New Inhibitors of Cholesterologenesis Produced by *Penicillium citrinum*. *J Antibiot (Tokyo)*. 29, 1346-1348
 - Espenshade, P.J. (2006). SREBPs: sterol-regulated transcription factors. *J Cell Sci*. 119(Pt 6):973-6
 - Espenshade, P.J., and Hughes, A.L. (2007). Regulation of sterol synthesis in eukaryotes. *Annu. Rev. Genet*. 41: 401–27
 - Faletrov, Y.V., Bialevich, K.I., Edimecheva, I.P., Kostsin, D.G., Rudaya, E.V., Slobozhanina, E.I., Shkumatov, V.M. (2012). 22-NBD-cholesterol as a novel fluorescent substrate for cholesterol-converting oxidoreductases. *J Steroid Biochem Mol Biol*. 134C:59-66
 - Farkasovsky, M., Herter, P., Voss, B., and Wittinghofer, A. (2005). Nucleotide binding and filament assembly of recombinant yeast septin complexes. *Biol Chem*. 386: 643-56
 - Field, C.M., al-Awar, O., Rosenblatt, J., Wong, M.L., Alberts, B., and Mitchison, T.J. (1996). A purified *Drosophila* septin complex forms filaments and exhibits GTPase activity. *J Cell Biol*. 133(3):605-16
 - Fields, S., and Johnston, M. (2005). Cell biology. Whither model organism research?. *Science*. 307 (5717): 1885–6
 - Frank, J. et al. (1996). SPIDER and WEB: Processing and visualization of images in 3D electron microscopy and related fields. *J Struct Biol*. 116(1):190–199

-
- Frank, J. (2006). Three-Dimensional Electron Microscopy of Macromolecular Assemblies: Visualization of Biological Molecules in Their Native State.
 - Frank, J. (2009). Single-particle reconstruction of biological macromolecules in electron microscopy-30 years. *Q Rev Biophys.* 42(3):139-58
 - Frazier, J.A. et al. (1998). Polymerization of purified yeast septins: evidence that organized filament arrays may not be required for septin function. *J Cell Biol.* 143(3):737-49
 - Fridman, K., Mader, A., Zwerger, M., Elia, N., and Medalia, O. (2012). Advances in tomography: probing the molecular architecture of cells. *Nat Rev Mol Cell Biol.* 13(11):736-42
 - Fitzky, B., et al. (1998). Mutations in the 7-sterol reductase gene in patients with the Smith–Lemli–Opitz syndrome. *Proceedings of the National Academy of Sciences of the United States of America.* 95(14), 8181
 - Firtzky et al., (2001). 7-Dehydrocholesterol-dependent proteolysis of HMG-CoA reductase suppresses sterol biosynthesis in a mouse model of Smith-Lemli-Opitz/RSH syndrome. *J Clin Invest.* 108(6):905-15
 - FitzPatrick, D., et al. (1998). Clinical phenotype of desmosterolosis. *American Journal of Medical Genetics Part A.* 75(2), 145-152
 - Fujishima, K., Kiyonari, H., Kurisu, J., Hirano, T., and Kengaku, M. (2007). Targeted disruption of Sept3, a heteromeric assembly partner of Sept5 and Sept7 in axons, has no effect on developing CNS neurons. *J Neurochem.* 102(1):77-92
 - Garcia, G. 3rd., Bertin, A., Li, Z., Song, Y., McMurray, M.A., Thorner, J., and Nogales, E. (2011). Subunit-dependent modulation of septin assembly: budding yeast septin Shs1 promotes ring and gauze formation. *J Cell Biol.* 195(6):993-1004
 - Ginat, S., Battaile, K.P., Battaile, B.C., Maslen, C., Gibson, K.M., and Steiner, R.D. (2004). Lowered DHCR7 activity measured by ergosterol conversion in multiple cell types in Smith-Lemli-Opitz syndrome. *Mol Genet Metab.* 83(1-2):175-83
 - Gladfelter, A.S., Bose, I., Zyla, T.R., Bardes, E.S., and Lew, D.J. (2002). Septin ring assembly involves cycles of GTP loading and hydrolysis by Cdc42p. *J Cell Biol.* 156(2):315-26
 - Gladfelter, A.S., Zyla, T.R., Lew, D.J. (2004). Genetic interactions among regulators of septin organization. *Eukaryot Cell.* 3(4):847-54
 - Goldstein, J.L., DeBose-Boyd, R.A., and Brown, M.S. (2006). Protein sensors for membrane sterols. *Cell.* 124(1):35-46
 - Gonen, T., Sliz, P., Kistler, J., Cheng, Y., and Walz, T. (2004). Aquaporin-0 membrane junctions reveal the structure of a closed water pore. *Nature.* 429:193-197

-
- Grützmann, R. et al. (2008). Sensitive detection of colorectal cancer in peripheral blood by septin 9 DNA methylation assay. *PLoS One*. 3: e3759
 - Hall, P.A. and Russell, S.E. (2012). Mammalian septins: dynamic heteromers with roles in cellular morphogenesis and compartmentalization. *J Pathol*. 226:287-299
 - Hanukoglu, I. (1992). Steroidogenic enzymes: structure, function, and role in regulation of steroid hormone biosynthesis. *J Steroid Biochem Mol Biol*. 43 (8): 779–804
 - Harkins, H.A., Pagé, N., Schenkman, L.R., De Virgilio, C., Shaw, S., Bussey, H., and Pringle, J.R. (2001). Bud8p and Bud9p, proteins that may mark the sites for bipolar budding in yeast. *Mol Biol Cell*. 12(8):2497-518
 - Harrenga, A., and Michel, H. (1999). The cytochrome c oxidase from *Paracoccus denitrificans* does not change the metal center ligation upon reduction. *J Biol Chem*. 274:33296–99
 - Hartwell, L.H. (1973). Synchronization of haploid yeast cell cycles, a prelude to conjugation. *Exp Cell Res*. 76(1):111-7
 - Has, C., et al. (2000). The Conradi-Hunermann-Happle syndrome (CDPX2) and emopamil binding protein: novel mutations, and somatic and gonadal mosaicism. *Human molecular genetics*. 9(13), 1951
 - Henderson, R. (1975). The structure of the purple membrane from *Halobacterium halobium*: analysis of the X-ray diffraction pattern. *J Mol Biol*. 93:123-138
 - Henderson, R., Baldwin, J.M., Ceska, T.A., Zemlin, F., Beckmann, E., and Downing, K.H. (1990). Model for the structure of bacteriorhodopsin based on high-resolution electron cryo-microscopy. *J Mol Biol*. 213:899-929
 - Herskowitz, I. (1988). Life cycle of the budding yeast *Saccharomyces cerevisiae*. *Microbiol Rev*. 52(4): 536–553
 - Hite, R.K., Gonen, T., Harrison, S.C., and Walz, T. (2008). Interactions of lipids with aquaporin-0 and other membrane proteins. *Pflugers Arch*. 456:651–61
 - Hiyoshi, H., et al. (2000). Effect of ER-27856, a novel squalene synthase inhibitor, on plasma cholesterol in rhesus monkeys: comparison with 3-hydroxy-3-methylglutaryl-CoA reductase inhibitors. *Journal of Lipid Research*. 41(7), 1136
 - Hoffmann, G., et al. (1993). Clinical and biochemical phenotype in 11 patients with mevalonic aciduria. *Pediatrics*. 91(5), 915
 - Hoffmann, G., Gibson, K., Brandt, I., Bader, P., Wappner, R., and Sweetman, L. (1986). Mevalonic aciduria—an inborn error of cholesterol and nonsterol isoprene biosynthesis. *New England Journal of Medicine*. 314(25), 1610-1614

-
- Hohn, M. et al. (2007). SPARX, a new environment for Cryo-EM image processing. *J Struct Biol.* 157(1):47-55
 - Holmer, L., Pezhman, A., and Worman, H. (1998). The Human Lamin B Receptor/Sterol Reductase Multigene Family* 1. *Genomics.* 54(3), 469-476
 - Honda, M., Tint, G.S., Honda, A., Nguyen, L.B., Chen, T.S., Shefer, S. (1998). 7-Dehydrocholesterol down-regulates cholesterol biosynthesis in cultured Smith-Lemli-Opitz syndrome skin fibroblasts. *J Lipid Res.* 39(3):647-57
 - Hotz, M., Lengefeld, J., and Barral, Y. (2012a). The MEN mediates the effects of the spindle assembly checkpoint on Kar9-dependent spindle pole body inheritance in budding yeast. *Cell Cycle.* 11(16):3109-16
 - Hotz, M., Leisner, C., Chen, D., Manatschal, C., Wegleiter, T., Ouellet, J., Lindstrom, D., Gottschling, D.E., Vogel, J., and Barral, Y. (2012b). Spindle pole bodies exploit the mitotic exit network in metaphase to drive their age-dependent segregation. *Cell.* 148(5):958-72
 - Höfken, T., and Schiebel, E. (2004). Novel mitotic exit by Cdc42 effectors Gic1 and Gic2. *J Cell Biol.* 164(2):219-31
 - Hsu, S.C., Hazuka, C.D., Roth, R., Foletti, D.L., Heuser, J., and Scheller, R.H. (1998). Subunit composition, protein interactions, and structures of the mammalian brain sec6/8 complex and septin filaments. *Neuron.* 20(6):1111-22
 - Hu, Q. et al. (2010). A septin diffusion barrier at the base of the primary cilium maintains ciliary membrane protein distribution. *Science.* 329: 436–439
 - Hu, J. et al. (2012). Septin-driven coordination of actin and microtubule remodeling regulates the collateral branching of axons. *Curr Biol.* 22(12):1109-15
 - Huang, Y.W. et al. (2008). Mammalian septins are required for phagosome formation. *Mol Biol Cell.* 19: 1717–1726
 - Ihara, M., Tomimoto, H., Kitayama, H., Morioka, Y., Akiguchi, I., Shibasaki, H., Noda, M., and Kinoshita, M. (2003). Association of the cytoskeletal GTP-binding protein Sept4/H5 with cytoplasmic inclusions found in Parkinson's disease and other synucleinopathies. *J Biol Chem.* 278(26):24095-102
 - Ihara, M. et al. (2005). Cortical organization by the septin cytoskeleton is essential for structural and mechanical integrity of mammalian spermatozoa. *Dev Cell.* 8: 343–352
 - Ihara, M. et al. (2007). Sept4, a component of presynaptic scaffold and Lewy bodies, is required for the suppression of alpha-synuclein neurotoxicity. *Neuron.* 53(4):519-33

-
- Ikemoto, N., Kitagawa, S., Nakamura, A., and Gergely, J. (1968). Electron microscopic investigations of actomyosin as a function of ionic strength. *J Cell Biol.* 39(3):620-9
 - Infante, R.E., Radhakrishnan, A., Abi-Mosleh, L., Kinch, L.N., Wang, M.L., Grishin, N.V., Goldstein, J.L., and Brown, M.S. (2008). Purified NPC1 protein. Binding of cholesterol and oxysterols to a 1278-amino acid membrane protein. *J Biol Chem.* 283(2):1064-75
 - Irons, M., Elias, E., Salen, G., Tint, G., and Batta, A. (1993). Defective cholesterol biosynthesis in Smith-Lemli-Opitz syndrome. *Lancet.* 341(8857), 1414
 - Irons, M., et al. (1997). Treatment of Smith-Lemli-Opitz syndrome: results of a multicenter trial. *American Journal of Medical Genetics Part A.* 68(3), 311-314
 - Iwase, M. et al. (2006). Role of a Cdc42p effector pathway in recruitment of the yeast septins to the presumptive bud site. *Mol Biol Cell.* 17(3):1110-25
 - Iwase, M., Lou, J., Bi, E., and Toh-e, A. (2007). Shs1 plays separable roles in septin organization and cytokinesis in *Saccharomyces cerevisiae*. *Genetics.* 177(1):215-29
 - Jaquenoud, M., Gulli, M.P., Peter, K., and Peter, M. (1997). The Cdc42p effector Gic2p is targeted for ubiquitin-dependent degradation by the SCFGrr1 complex. *EMBO J.* 17(18):5360-73
 - Jaquenoud, M., and Peter, M. (2000). Gic2p may link activated Cdc42p to components involved in actin polarization, including Bni1p and Bud6p (Aip3p). *Mol Cell Biol.* 20(17):6244-58
 - Jira, P., et al. (2000). Simvastatin: a new therapeutic approach for Smith-Lemli-Opitz syndrome. *The Journal of Lipid Research.* 41(8), 1339
 - Jira, P., Waterham, H., Wanders, R., Smeitink, J., Sengers, R., and Wevers, R. (2003). Smith Lemli Opitz Syndrome and the DHCR7 Gene. *Annals of human genetics.* 67(3), 269-280
 - Joberty, G. et al. (2001). Borg proteins control septin organization and are negatively regulated by Cdc42. *Nat Cell Biol.* 3(10):861-6
 - Johnson, E.S., and Blobel, G. (1999). Cell cycle-regulated attachment of the ubiquitin-related protein SUMO to the yeast septins. *J Cell Biol.* 147(5):981-94
 - Johnson, J.M., Jin, M., and Lew, D.J. (2011). Symmetry breaking and the establishment of cell polarity in budding yeast. *Curr Opin Genet Dev.* 21(6):740-6
 - Joo, E., Surka, M.C., and Trimble W.S. (2007). Mammalian SEPT2 is required for scaffolding nonmuscle myosin II and its kinases. *Dev Cell.* 13(5):677-90
 - Kadota, J., Yamamoto, T., Yoshiuchi, S., Bi, E., and Tanaka, K. (2004). Septin ring assembly requires concerted action of polarisome components, a PAK kinase Cla4p, and the actin cytoskeleton in *Saccharomyces cerevisiae*. *Mol Biol Cell.* 15(12):5329-45

-
- Kawasaki, R., Fujimura-Kamada, K., Toi, H., Kato, H., and Tanaka, K. (2003). The upstream regulator, Rsr1p, and downstream effectors, Gic1p and Gic2p, of the Cdc42p small GTPase coordinately regulate initiation of budding in *Saccharomyces cerevisiae*. *Genes Cells*. 8(3):235-50
 - Kelley, R., and Hennekam, R. (2000). The Smith-Lemli-Opitz syndrome. *Journal of Medical Genetics*. 37(5), 321
 - Kelley, L.A., and Sternberg, M.J. (2009). Protein structure prediction on the Web: a case study using the Phyre server. *Nat Protoc*. 4(3):363-71.
 - Kim, S.K. et al. (2010). Planar cell polarity acts through septins to control collective cell movement and ciliogenesis. *Science*. 329(5997):1337-40
 - Kim, M.S., Froese, C.D., Estey, M.P., and Trimble, W.S. (2011). SEPT9 occupies the terminal positions in septin octamers and mediates polymerization-dependent functions in abscission. *J Cell Biol*. 28;195(5):815-26
 - Kinoshita, M., Field, C.M., Coughlin, M.L., Straight, M.F., and Mitchison, T.J. (2002). Self and actin-templated assembly of mammalian septins. *Dev Cell*. 3(6):791-802
 - Kinoshita, M. (2006). Diversity of septin scaffolds. *Curr Opin Cell Biol*. 18(1):54-60
 - Ko, D. C., Binkley, J., Sidow, A., and Scott, M. P. (2003). The integrity of a cholesterol-binding pocket in Niemann-Pick C2 protein is necessary to control lysosome cholesterol levels. *Proc. Natl. Acad. Sci. USA*. 100: 2518–2525
 - Koide, T., Hayata, T., and Cho, K.W. (2006). Negative regulation of Hedgehog signaling by the cholesterologenic enzyme 7-dehydrocholesterol reductase. *Development*. 133(12):2395-405
 - Kollman, .JM., Merdes, A., Mourey, L., and Agard, D.A. (2011). Microtubule nucleation by γ -tubulin complexes. *Nat Rev Mol Cell Biol*. 12(11):709-21
 - Kostic, C., and Shaw, P.H. (2000). Isolation and characterization of sixteen novel p53 response genes. *Oncogene*. 19(35):3978-87
 - Kremer, J.R., Mastronarde, D.N., and McIntosh, J.R. (1996). Computer visualization of three-dimensional image data using IMOD. *J Struct Biol*. 116(1):71-6
 - Krishnan, R., Pangilinan, F., Lee, C., Spencer, F. (2000). *Saccharomyces cerevisiae* BUB2 prevents mitotic exit in response to both spindle and kinetochore damage. *Genetics*. 156(2):489-500
 - Kukulski, W., Schorb, M., Kaksonen, M., and Briggs, J.A. (2012). Plasma membrane reshaping during endocytosis is revealed by time-resolved electron tomography. *Cell*. 150(3):508-20
 - Kusch, J., Meyer, A., Snyder, M.P., Barral, Y. (2002). Microtubule capture by the cleavage apparatus is required for proper spindle positioning in yeast. *Genes Dev*. 16(13):1627-39

-
- Laemmli, U. (1970). Cleavage of structural proteins during the assembly of the head of bacteriophage T4. *Nature*. 227(5259), 680-685.
 - Larkin, M.A., et al. (2007). Clustal W and Clustal X version 2.0. *Bioinformatics*. 23(21):2947-8
 - Lecain, E., Chenivresse, X., Spagnoli, R., and Pompon, D. (1996). Cloning by metabolic interference in yeast and enzymatic characterization of *Arabidopsis thaliana* sterol 7-reductase. *Journal of Biological Chemistry*. 271(18), 10866
 - Lee, J.N., Bae, S.H., and Paik, Y.K. (2002). Structure and alternative splicing of the rat 7-dehydrocholesterol reductase gene. *Biochim Biophys Acta*. 1576(1-2):148-56
 - Leipe, D.D., Wolf, Y.I., Koonin, E.V., and Aravind, L. (2002). Classification and evolution of P-loop GTPases and related ATPases. *J Mol Biol*. 317(1):41-72
 - Lemaire-Ewing S, Lagrost L, Néel D. (2012.) Lipid rafts: a signalling platform linking lipoprotein metabolism to atherogenesis. *Atherosclerosis*. 221(2):303-10
 - Leung, B.O., and Chou, K.C. (2011). Review of super-resolution fluorescence microscopy for biology. *Appl Spectrosc*. 65(9):967-80
 - Lew, D.J. (2003). The morphogenesis checkpoint: how yeast cells watch their figures. *Curr Opin Cell Biol*. 15(6):648-653
 - Lindsey, R., and Momany, M. (2006). Septin localization across kingdoms: three themes with variations. *Curr Opin Microbiol*. 9: 1-7
 - Ludtke, S.J., Baldwin, P.R., and Chiu, W. (1999). EMAN: Semiautomated software for high resolution single-particle reconstructions. *J Struct Biol*. 128(1):82-97
 - Luecke, H., Schobert, B., Richter, H.T., Cartailler, J.P., Lanyi, J.K. (1999). Structure of bacteriorhodopsin at 1.55 °A resolution. *J Mol Biol*. 291:899-911
 - Lukyanova, N., Baldwin, S.A., and Trinick, J. (2008). 3D reconstruction of mammalian septin filaments. *J Mol Biol*. 8;376(1):1-7
 - Mackenzie, J., Jones, M., and Westaway, E. (1999). Markers for trans-Golgi membranes and the intermediate compartment localize to induced membranes with distinct replication functions in flavivirus-infected cells. *Journal of virology*. 73(11), 9555
 - Marilini, L., and Piatti, S. (2011). The mother-bud neck as a signaling platform for the coordination between spindle position and cytokinesis in budding yeast. *Biol Chem*. 392(8-9):805-12
 - Mast, N., and Pikuleva, I.A. (2005). A simple and rapid method to measure cholesterol binding to P450s and other proteins. *J Lipid Res*. 46(7):1561-8

-
- Maxfield, F.R., and Wüstner, D. (2012). Analysis of cholesterol trafficking with fluorescent probes. *Methods Cell Biol.* 108:367-93.
 - McMurray, Thorner, J.W. (2009). Reuse, replace, recycle. Specificity in subunit inheritance and assembly of higher-order septin structures during mitotic and meiotic division in budding yeast. *Cell Cycle.* 8(2):195-203
 - McMurray, Thorner, J.W. (2009b). Septins: molecular partitioning and the generation of cellular asymmetry. *Cell Div.* 4:18
 - Mendoza, M., Hymann, A.A., and Glotzer, M. (2002). GTP binding induces filament assembly of a recombinant septin. *Curr Biol.* 12(21):1858-63
 - Merlini, L., Fraschini, R., Boettcher, B., Barral, Y., Lucchini, G., and Piatti, S. (2012). Budding yeast dma proteins control septin dynamics and the spindle position checkpoint by promoting the recruitment of the Elm1 kinase to the bud neck. *PLoS Genet.* 8(4):e1002670
 - Mino, A., Tanaka, K., Kamei, T., Umikawa, M., Fujiwara, T., and Takai, Y. (1998). Shs1p: a novel member of septin that interacts with spa2p, involved in polarized growth in *Saccharomyces cerevisiae*. *Biochem Biophys Res Commun.* 251(3):732-6
 - Mitchison, T.J., and Field, C.M. (2002). Cytoskeleton: what does GTP do for septins? *Curr Biol.* 12(22):R788-90
 - Moebius, F., Fitzky, B., Lee, J., Paik, Y., and Glossmann, H. (1998). Molecular cloning and expression of the human 7-sterol reductase. *Proceedings of the National Academy of Sciences of the United States of America.* 95(4), 1899
 - Mostowy, S. et al. (2009). Septin 11 restricts InlB-mediated invasion by *Listeria*. *J Biol Chem.* 284: 11613–11621.
 - Mostowy, S. et al. (2010). Entrapment of intracytosolic bacteria by septin cage-like structures. *Cell Host Microbe.* 8: 433–444
 - Mostowy, S., and Cossart, P. (2011). Autophagy and the cytoskeleton: new links revealed by intracellular pathogens. *Autophagy.* 7: 780–782.
 - Murata, T., Yamato, I., Kakinuma, Y., Leslie, A.G., and Walker, J.E. (2005). Structure of the rotor of the V-Type Na⁺-ATPase from *Enterococcus hirae*. *Science.* 308:654–59
 - Nagaraj, S., Rajendran, A., Jackson, C.E., and Longtine, M.S. (2008). Role of nucleotide binding in septin-septin interactions and septin localization in *Saccharomyces cerevisiae*. *Mol Cell Biol.* 28(16):5120-37
 - Nagata, K., Asano, T., Nozawa, Y., and Inagaki, M. (2004). Biochemical and cell biological analyses of a mammalian septin complex, Sept7/9b/11. *J Biol Chem.* 279(53):55895-904

-
- Ness, G.C., Pendleton, L.C., and Pendleton, A.S. (1987). Loss of NADPH during assays of HMG-CoA reductase: implications and approaches to minimize errors. *Lipids*. 22(6):409-12
 - Nishino, H., Ishibashi, T. (2000). Evidence for requirement of NADPH-cytochrome P450 oxidoreductase in the microsomal NADPH-sterol Delta7-reductase system. *Arch Biochem Biophys*. 374(2):293-8
 - Nohturfft, A., DeBose-Boyd, R., Scheek, S., Goldstein, J., and Brown, M. (1999). Sterols regulate cycling of SREBP cleavage-activating protein (SCAP) between endoplasmic reticulum and Golgi. *Proceedings of the National Academy of Sciences of the United States of America*. 96(20), 11235
 - Novak, B., Tyson, J.J., Gyorffy, B., and Csikasz-Nagy, A. (2007). Irreversible cell-cycle transitions are due to systems-level feedback. *Nat Cell Biol*. 9(7):724-8
 - Oh, Y., and Bi, E. (2011). Septin structure and function in yeast and beyond. *Trends Cell Biol*. 21(3):141-8
 - Ohi, M., Li, Y., Cheng, Y., and Walz, T. (2004). Negative staining and image classification—Powerful tools in modern electron microscopy. *Biol Proc Online*. 6:23–34
 - Okamura, N., S. et al. (1999). A porcine homolog of the major secretory protein of human epididymis, HE1, specifically binds cholesterol. *Biochim. Biophys. Acta*. 1438: 377–387
 - Opitz, J. (1994). RSH/SLO (“Smith Lemli Opitz”) syndrome: Historical, genetic, and developmental considerations. *American journal of medical genetics*. 50(4), 344-346
 - Orlando, K. et al. (2008). Regulation of Gic2 localization and function by phosphatidylinositol 4,5-bisphosphate during the establishment of cell polarity in budding yeast. *J Biol Chem*. 283(21):14205-12
 - Orlando, K. and Guo, W. (2009). Membrane organization and dynamics in cell polarity. *Cold Spring Harb Perspect Biol*. 1(5):a001321
 - Orlando, K. et al. (2011). Exo-endocytic trafficking and the septin-based diffusion barrier are required for the maintenance of Cdc42p polarization during budding yeast asymmetric growth. *Mol Biol Cell*. 22(5):624-33
 - Orlova, E.V., Saibil, (2011). Structural analysis of macromolecular assemblies by electron microscopy. *Chem Rev*. 111(12):7710-48
 - Ormo, M., Cubitt, A., Kallio, K., Gross, L., Tsien, R., and Remington, S. (1996). Crystal structure of the *Aequorea victoria* green fluorescent protein. *Science (Washington)*. 273(5280), 1392-1392
 - Ostermeier, C., and Michel, H. (1997). Crystallization of membrane proteins. *Curr Opin Struct Biol*. 7(5), 697-701

-
- Pan, F. et al. (2007). Analysis of septins across kingdoms reveals orthology and new motifs. *BMC Evol. Biol.* 7, 103
 - Park, H.O., Bi, E., Pringle, J.R., and Herskowitz, I. (1997). Two active states of the Ras-related Bud1/Rsr1 protein bind to different effectors to determine yeast cell polarity. *Proc Natl Acad Sci U S A.* 94(9):4463-8
 - Park, H.O., and Bi, E. (2007). central role of small GTPases in the development of cell polarity in yeast and beyond. *Microbiol Mol Biol Rev.* 71(1):48-96
 - Pellegrino, J.F. et al. (1996). Mapping of hereditary neuralgic amyotrophy (familial brachial plexus neuropathy) to distal chromosome 17q. *Neurology.* 46: 1128–1132.
 - Pettersen, E.F. et al. (2004). UCSF Chimera--a visualization system for exploratory research and analysis. *J Comput Chem.* 25(13):1605-12
 - Popot, J., and Engelman, D. (1990). Membrane protein folding and oligomerization: the two-stage model. *Biochemistry.* 29(17), 4031-4037
 - Porter, F.D. (2008). Smith-Lemli-Opitz syndrome: pathogenesis, diagnosis and management. *Eur J Hum Genet.* 16(5):535-41
 - Radhakrishnan, A., Sun, L.P., Kwon, H.J., Brown, M.S., and Goldstein, J.L. (2004). Direct binding of cholesterol to the purified membrane region of SCAP: mechanism for a sterol-sensing domain. *Mol Cell.* 15(2):259-68
 - Radhakrishnan, A., Ikeda, Y., Kwon, H.J., Brown, M.S., and Goldstein, J.L. (2007). Sterol-regulated transport of SREBPs from endoplasmic reticulum to Golgi: oxysterols block transport by binding to Insig. *Proc Natl Acad Sci U S A.* 104(16):6511-8
 - Radhakrishnan, A., Goldstein, J.L., McDonald, J.G., and Brown, M.S. (2008). Switch-like control of SREBP-2 transport triggered by small changes in ER cholesterol: a delicate balance. *Cell Metab.* 8(6):512-21
 - Raunser, S., and Walz, T. (2009). Electron crystallography as a technique to study the structure on membrane proteins in a lipidic environment. *Annual review of biophysics.* 38, 89-105
 - Roberti, R., et al. (2002). Cloning and expression of sterol 14 reductase from bovine liver. *European Journal of Biochemistry.* 269(1), 283-290
 - Rokka, A., et al. (2009). Pxmp2 is a channel-forming protein in Mammalian peroxisomal membrane. *PLoS one.* 4(4), 5090
 - Pope, C.R., and Unger, V.M. (2012). Electron crystallography--the waking beauty of structural biology. *Curr Opin Struct Biol.* 22(4):514-9

-
- Rudolph, M.G. et al. (1998.) The Cdc42/Rac Interactive Binding Region Motif of the Wiskott Aldrich Syndrome Protein (WASP) Is Necessary but Not Sufficient for Tight Binding to Cdc42 and Structure Formation. *J Biol Chem.* 273: 18067–18076
 - Saarikangas, J., Barral, Y. (2011). The emerging functions of septins in metazoans. *EMBO rep.* 2(11):1118-26
 - Sakamoto, T., Uezu, A., Kawauchi, S., Kuramoto, T., Makino, K., Umeda, K., Araki, N., Baba, H., Nakanishi, H. (2008). Mass spectrometric analysis of microtubule co-sedimented proteins from rat brain. *Genes Cell.* 13(4):295-312
 - Sandrock, K., Bartsch, I., Bläser, S., Busse, A., Busse, E., and Zieger, B. (2011). Characterization of human septin interactions. *Biol Chem.* 392(8-9):751-61
 - Scott, M. et al. (2005). Multimodality expression profiling shows SEPT9 to be over-expressed in a wide range of human tumours. *Oncogene.* 24: 4688–4700.
 - Seddon, A.M., Curnow, P., Booth, P.J. (2004). Membrane proteins, lipids and detergents: not just a soap opera. *Biochim Biophys Acta.* 1666(1-2):105-17
 - Sellin, M.E. et al. (2011). Deciphering the rules governing assembly order of mammalian septins. *Mol Biol Cell.* 22: 3152–3164.
 - Sellin, M.E., Holmfeldt, P., Stenmark, S., and Gullberg, M. (2011b). Microtubules support a disk-like septin arrangement at the plasma membrane of mammalian cells. *Mol Biol Cell.* 22(23):4588-601
 - Sellin, M.E., Stenmark, S., and Gullberg, M. (2012). Mammalian SEPT9 isoforms direct microtubule-dependent arrangements of septin core heteromers. *Mol Biol Cell.* 23(21):4242-55
 - Shaner, N., Steinbach, P., and Tsien, R. (2005). A guide to choosing fluorescent proteins. *Nature Methods.* 2(12), 905-909
 - Shapiro, A., Vinuela, E., and Maizel Jr, J. (1967). Molecular weight estimation of polypeptide chains by electrophoresis in SDS-polyacrylamide gels. *Biochemical and biophysical research communications.* 28(5), 815.
 - Shefer, S., Salen, G., Honda, A., Batta, A.K., Nguyen, L.B., Tint, G.S., Ioannou, Y.A., and Desnick, R. (1998). Regulation of rat hepatic 3beta-hydroxysterol delta7-reductase: substrate specificity, competitive and non-competitive inhibition, and phosphorylation/dephosphorylation. *J Lipid Res.* 39(12):2471-6
 - Sheffield, P.J., Oliver, C.J., Kremer, B.E., Sheng, S., Shao, Z., and Macara, I.G. (2003). Borg/septin interactions and the assembly of mammalian septin heterodimers, trimers, and filaments. *J Biol Chem.* 278(5):3483-8

-
- Shimomura, O., Johnson, F., and Saiga, Y. (1962). Extraction, purification and properties of aequorin, a bioluminescent protein from the luminous hydromedusan, *Aequorea*. *Journal of cellular and comparative physiology*. 59(3), 223-239
 - Signorell, G.A., Kaufmann, T.C., Kukulski, W., Engel, A., and Remigy, H.W. (2007). Controlled 2D crystallization of membrane proteins using methyl-beta-cyclodextrin. *Journal of structural biology*. 157:321–328
 - Siller, K.H., and Dou, C.Q. (2009). Spindle orientation during asymmetric cell division. *Nat Cell Biol*. 1, 365 - 374
 - Silverman-Gavrila, R.V., and Silverman-Gavrila, L.B. (2008). septins: new microtubule interacting partners. *ScientificWorldJournal*. 13;8:611-20
 - Simons, K., and Ikonen, E. (1997). Functional rafts in cell membranes. *Nature*. 387(6633), 569-572
 - Simons, K., and Ikonen, E. (2000). How cells handle cholesterol. *Science*. 290(5497), 1721
 - Simons K, Sampaio JL. (2011). Membrane organization and lipid rafts. *Cold Spring Harb Perspect Biol*. 3(10):a004697
 - Simons, K., and Toomre, D. (2000). Lipid rafts and signal transduction. *Nature Reviews Molecular Cell Biology*. 1(1), 31-39
 - Sirajuddin, M., Farkasovsky, M., Hauer, F., Kühlmann, D., Macara, I.G., Weyand, M., Stark, H., and Wittinghofer, A. (2007). Structural Insight into filament formation by mammalian septins. *Nature*. 449(7160):311-315
 - Sirajuddin, M., Farkasovsky, M., Zent, E., and Wittinghofer, A. (2009). GTP-induced conformational changes in septins and implications for function. *Proc Natl Acad Sci U S A*. 106(39):16592-7
 - Slaughter, B.D., Smith, S.E., and Li, R. (2009). Symmetry breaking in the life cycle of the budding yeast. *Cold Spring Harb Perspect Biol*. 1(3):a003384
 - Smith, D., Lemli, L., and Opitz, J. (1964). A newly recognized syndrome of multiple congenital anomalies**. *The Journal of pediatrics*. 64(2), 210-217
 - Song, S., Grenfell, T.Z., Garfield, S., Erikson, R.L., and Lee, K.S. (2000). Essential function of the polo box of Cdc5 in subcellular localization and induction of cytokinetic structures. *Mol Cell Biol*. 20(1):286-98
 - Song, B.L., Javitt, N.B., and DeBose-Boyd, R.A. (2005). Insig-mediated degradation of HMG CoA reductase stimulated by lanosterol, an intermediate in the synthesis of cholesterol. *Cell Metab*. 1(3):179-89
 - Spiliotis, E.T., Kinoshita, M., and Nelson, W.J. (2005). A mitotic septin scaffold required for Mammalian chromosome congression and segregation. *Science*. 307(5716):1781-5

-
- Spiliotis, E.T. et al. (2008). Epithelial polarity requires septin coupling of vesicle transport to polyglutamylated microtubules. *J Cell Biol.* 180: 295–303.
 - Sprang, S.R. (1997). G protein mechanisms: Insights from structural analysis. *Annu Rev Biochem.* 66:639-78
 - Staubach S, Hanisch FG. (2011). Lipid rafts: signaling and sorting platforms of cells and their roles in cancer. *Expert Rev Proteomics.* 8(2):263-77
 - Stegmeier, F., Visintin, R., and Amon, A. (2002). Separase, polo kinase, the kinetochore protein Slk19, and Spo12 function in a network that controls Cdc14 localization during early anaphase. *Cell.* 108(2):207-20
 - Strömstedt, M., Rozman, D., and Waterman, M. (1996). The Ubiquitously Expressed Human CYP51 Encodes Lanosterol 14 [alpha]-Demethylase, a Cytochrome P450 Whose Expression Is Regulated by Oxysterols. *Archives of biochemistry and biophysics.* 329(1), 73-81
 - Studier, F., and Moffatt, B. (1986). Use of bacteriophage T7 RNA polymerase to direct selective high-level expression of cloned genes* 1. *J Mol Biol.* 189(1), 113-130
 - Sudo, K., et al. (2007). SEPT9 sequence alternations causing hereditary neuralgic amyotrophy are associated with altered interactions with SEPT4/SEPT11 and resistance to Rho/Rhotekin-signaling. *Hum Mutat.* 2007; 28: 1005–1013.
 - Swiech, K., Picanço-Castro, V., and Covas, D.T. (2012). Human cells: new platform for recombinant therapeutic protein production. *Protein Expr Purif.* 84(1):147-53
 - Tadjuidje, E., and Hollemann, T. (2006). Cholesterol homeostasis in development: the role of *Xenopus* 7-dehydrocholesterol reductase (Xdhcr7) in neural development. *Dev Dyn.* 235(8):2095-110
 - Tada, T. et al. (2007). Role of septin cytoskeleton in spine morphogenesis and dendrite development in neurons. *Curr Biol.* 17: 1752–1758
 - Tanaka-Takiguchi, Y., Kinoshita, M., and Takiguchi, K. (2009). Septin-mediated uniform bracing of phospholipid membranes. *Curr Biol.* 27;19(2):140-5
 - Tang, C.S., and Reed, S.I. (2002). Phosphorylation of the septin cdc3 in g1 by the cdc28 kinase is essential for efficient septin ring disassembly. *Cell Cycle.* 1(1):42-9
 - Tcheperegine SE, Gao XD, Bi E. (2005). Regulation of cell polarity by interactions of Msb3 and Msb4 with Cdc42 and polarisome components. *Mol Cell Biol.* 25(19):8567-80.
 - Tischendorf GW, Zeichhardt H, Stöffler G. (1974). Location of proteins S5, S13 and S14 on the surface of the 30S ribosomal subunit from *Escherichia coli* as determined by immune electron microscopy. *Mol Gen Genet.* 134(3):209-23

-
- Toure, A., Rode, B., Hunnicutt, G.R., Escalier, D., and Gacon, G. (2011). Septins at the annulus of mammalian sperm. *Biol Chem.* 392(8-9):799-803
 - Towbin, H., Staehelin, T., and Gordon, J. (1979). Electrophoretic transfer of proteins from polyacrylamide gels to nitrocellulose sheets: procedure and some applications. *Proceedings of the National Academy of Sciences of the United States of America.* 76(9), 4350
 - Ubarretxena-Belandia, I., and Stokes, D.L. (2012). Membrane protein structure determination by electron crystallography. *Curr Opin Struct Biol.* 22(4):520-8
 - VanAken, T., Foxall-VanAken, S., Castleman, S., and Ferguson-Miller, S. (1986). Alkyl glycoside detergents: Synthesis and applications to the study of membrane proteins. *Methods in Enzymology.* 125, 27-35
 - Versele, M., and Thorner, J. (2004). Septin collar formation in budding yeast requires GTP binding and direct phosphorylation by the PAK, Cla4. *J Cell Biol.* 164(5):701-15.
 - Vetter, I.R., and Wittinghofer, A. (2001). The guanine nucleotide-binding switch in three dimensions. *Science.* 294(5545):1299-30
 - Vrabioiu, A.M., Gerber, S.A., Gygi, S.P., Field, C.M., and Mitchison, T.J. (2004). The majority of the *Saccharomyces cerevisiae* septin complexes do not exchange guanine nucleotides. *J Biol Chem.* 279(4):3111-8
 - Vrabioiu, A.M., and Mitchison, T.J. (2006). Structural Insights into yeast septin organization from polarized fluorescence microscopy. *Nature.* 443(7110):466-9
 - Vrabioiu, A.M., and Mitchison, T.J. (2007). Symmetry of septin hourglass and ring structures. *J Mol Biol.* 372(1):37-49
 - Wagner, S., Bader, M., Drew, D., and de Gier, J. (2006). Rationalizing membrane protein overexpression. *TRENDS in Biotechnology.* 24(8), 364-371
 - Wang, W., Black, S.S., Edwards, M.D., Miller, S., Morrison, E.L., Bartlett, W., Dong, C., Naismith, J.H., and Booth, I.R. (2008). The Structure of an Open Form of an E. coli Mechanosensitive Channel at 3.45 Å Resolution. *Science.* 321(5893):1179-83
 - Waterham, H., and Wanders, R. (2000). Biochemical and genetic aspects of 7-dehydrocholesterol reductase and Smith-Lemli-Opitz syndrome. *Biochimica et Biophysica Acta (BBA)-Molecular and Cell Biology of Lipids.* 1529(1-3), 340-356
 - Waterham, H., et al. (2001). Mutations in the 3 β -hydroxysterol D24-reductase gene cause desmosterolosis, an autosomal recessive disorder of cholesterol biosynthesis. *Am J Hum Genet.* 69, 685-694

-
- Weinhofer, I., Kunze, M., Stangl, H., Porter, F., and Berger, J. (2006). Peroxisomal cholesterol biosynthesis and Smith-Lemli-Opitz syndrome. *Biochemical and biophysical research communications*. 345(1), 205-209
 - Weirich, C.S., Erzberger J.P., and Barral, Y. (2008). The septin family of GTPases: architecture and dynamics. *Nat Rev Mol Cell Biol*. 16(4):493-506
 - Wilcox, C., Feddes, G., Willett-Brozick, J., Hsu, L., DeLoia, J., and Baysal, B. (2007). Coordinate up-regulation of TMEM 97 and cholesterol biosynthesis genes in normal ovarian surface epithelial cells treated with progesterone: implications for pathogenesis of ovarian cancer. *BMC cancer*. 7(1), 223
 - Wild, A.C., Yu, J.W., Lemmon, M.A., and Blumer, K.J. (2004). The p21-activated protein kinase-related kinase Cla4 is a coincidence detector of signaling by Cdc42 and phosphatidylinositol 4-phosphate. *J Biol Chem*. 279(17):17101-10
 - Wisedchaisri, G., and Gonenm T. (2011). Fragment-based phase extension for three-dimensional structure determination of membrane proteins by electron crystallography. *Structure*. 19:976-987
 - Witsch-Baumgartner, M., Löffler, J., and Utermann, G. (2001). Mutations in the human DHCR7 gene. *Human Mutation*. 17(3), 172-182
 - Xie, Y. et al. (2007). The GTP-binding protein Septin 7 is critical for dendritic branching and dendritic-spine morphology. *Curr Biol*. 17, 1746-1751
 - Xie, X., Brown, M.S., Shelton, J.M., Richardson, J.A., Goldstein, J.L., and Liang, G. (2009). Amino acid substitution in NPC1 that abolishes cholesterol binding reproduces phenotype of complete NPC1 deficiency in mice. *Proc Natl Acad Sci U S A*. 108(37):15330-5.
 - Yagi, M. et al. (1998). Structure and expression of the human septin gene HCDCREL-1. *Gene*. 212: 229–236.
 - Yeagle, P.L. (1991). Modulation of membrane function by cholesterol. *Biochimie*. 73(10):1303-10
 - Yu, H., and Patel, S. (2005). Recent Insights into the Smith–Lemli–Opitz syndrome. *Clinical genetics*. 68(5), 383-391
 - Yu, Y., Chipot, C., Cai, W., and Shao, X. (2006). Molecular dynamics study of the inclusion of cholesterol into cyclodextrins. *J. Phys. Chem. B*. 110(12), 6372-6378
 - Zachariae, W., and Nasmyth, K. (1999). whose end is destruction: cell division and the anaphase-promoting complex. *Genes Dev*. 13, 2039-2058
 - Zent, E., Vetter, I., and Wittinghofer, A. (2011). Structural and biochemical properties of Sept7, a unique septin required for filament formation. *Biol Chem*. 392(8-9):791-7

-
- Zhang, J., Kong, C., Xie, H., McPherson, P.S., Grinstein, S., and Trimble, W.S. (1999). Phosphatidylinositol polyphosphate binding to the mammalian septin H5 is modulated by GTP. *Curr Biol.* 9(24):1458-67
 - Zhang, X., Jin, L., Fang, Q., Hui, W.H., and Zhou, Z.H. (2010). 3.3 A cryo-EM structure of a nonenveloped virus reveals a priming mechanism for cell entry. *Cell.* 141(3):472-82
 - Zheng, Y., Bender, A., and Cerione, R.A. (1995). Interactions among proteins involved in bud-site selection and bud-site assembly in *Saccharomyces cerevisiae*. *J Biol Chem.* 270(2):626-30
 - Zieger, B. et al. (2000). Characterization and expression analysis of two human septin genes, PNUTL1 and PNUTL2. *Gene.* 261: 197–203
 - Zou, L., Li, L., Porter, T.D. (2011). 7-Dehydrocholesterol reductase activity is independent of cytochrome P450 reductase. *Steroid Biochem Mol Biol.* 127(3-5): 435–438

5) Supplementary information

5.1) Protein sequence of septin subunits

P-loops, Switch I regions, Switch II regions and G4 domains are colored yellow, red, cyan and green respectively.

Cdc10:

MDPLSSVQPASYVGFDTITNQIEHRLKKGKFQFNIMVVGQSGLGKSTLINTLFASHLIDSATGDDI
SALPVTKTTEMKISTHTLVEDRVRLNINVIDTPGFGDFIDNSKAWEPVKYIKEQHSQYLRKELTA
QRERFITDTRVHAILYFLQPNGKELSRDLVVEALKRLTEIANVIPVIGKSDTLTLDERTEFRELIQNEF
EKYNFKIYPYDSEELTDEEELNRSVRSIIPFAVVGSENEIEINGETFRGRKTRWSAINVEDINQCD
FVYLREFLIRTHLQDLIETTSYIHYEGFRARQLIALKENANSRSSAHMSSNAIQR

Cdc3:

MSLKEEQVSIKQDPEQEERQHDQFNDVQIKQESQDHDGVDSQYTNGTQNDDSERFEAAESDVK
VEPGLGMGITSSQSEKQVLPDQPEIKFIRRQINGYVGFANLPKQWHRRSIKNGFSFNLLCVGPDG
IGKTLMKTLFNNDIEANLVKDYEEELANDQEEEEGQEGHENQSQEQRHKVKI KSYESVIEEN
GVKLNLNVIDTEGFGDFLNNDQKSWDPIIKEIDSRFDQYLDAENKINRHSINDKRIHACL YFIEPT
GHYKPLDLKFMQSVYEKCNLIPVIAKSDILTDEEILSFKKTIMNQLIQSNIELFKPPIYSNDDAENS
HLSERLFSSLPYAVIGSNDIVENYSGNQVRGRSYPWGVIEVDNDNHSDFNLLKNLLIKQFMEELK
ERTSKILYENYRSSKLAKLGKQDNSVFKEFDPISKQQEEKTLHEAKLAKLEIEMKTVFQQKVSEK
EKKLQKSETELFARHKEMKEKLTQQLKALEDKKKQLELSINSASPNVNHSPVPTKKKGFRLR

Cdc11:

MSGIIDASSALRKRKHLKRGITFTVMIVGQSGSGRSTFINTLCGQQVVDSTTILLPTDTSTEIDLQ
LREETVELEDDEGVKQLNVIDTPGFGDSDLNPSFEEISDYIRHQYDEILLEESRVRNPRFKDGRV
HCCLYLINPTGHGLKEIDVEFIRQLGSLVNIIPVIGKSDSLTRDELKLNKKLIMEDIDRWNLPIYNFP
FDEDEISDEDYETNMYLRLTLLPFAIIGSNEVYEMGGDVG TIRGRKYPWGILDVEDSSISDFVILRN
ALLISHLHDLKNYTHEILYERYRTEALSGESVAAESIRPNLTKLNGSSSSSTTRRNTNPFKQSNNI
NNDVLNPASDMHGQSTGENNETYMTREEQIRLEEERLKA FEERVQQELLLKRQELLQREKELRE
IEARLEKEAKIKQEE

Cdc12:

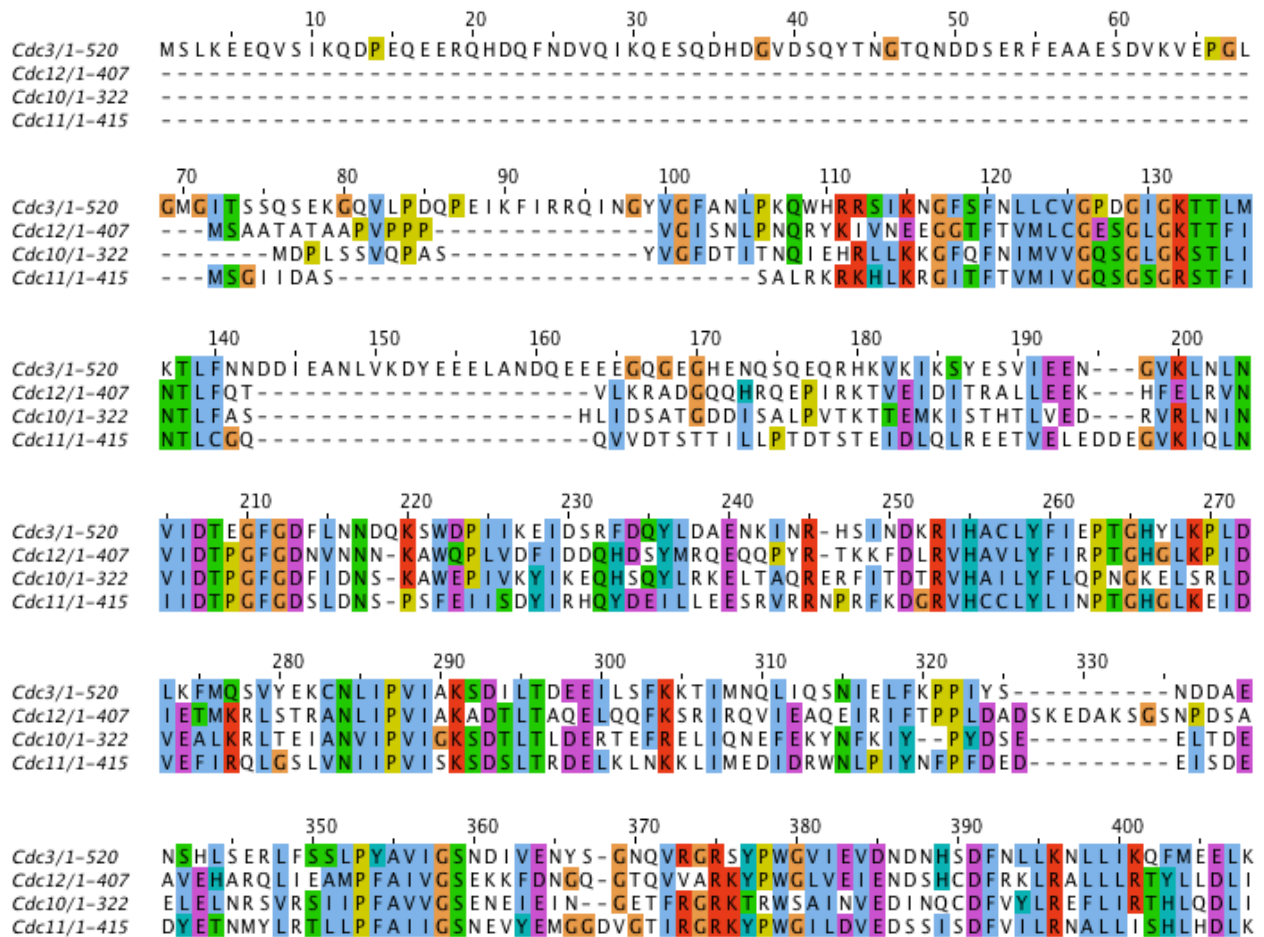
MSAATATAAPVPPVPGISNLPNQRKYIVNEEGGTFTVMLCGESGLGKTFINTLFQTVLKRADGQ
QHRQEPIRKTVEIDITRALLEEKHFELRVNVIDTPGFGDNVNNKAWQPLVDFIDDQHDSYMRQE
QQPYRTKKFDL RVHAVLYFIRPTGHGLKPIDIETMKRLSTRANLIPVIAKADTLTAQELQQFKSRI
RQVIEAQEIRIFTPPLDADSKEDAKSGSNPDSAAVEHARQLIEAMPFAIVGSEKKFDNGQGTQVV
ARKYPWGLVEIENDSHCDFRKL RALLRLTYLLDLISTTQEMHYETYRRLRLEGHENTGEGNEDF

TLPAIAPARKLSHNPYKKEENALKKYFTDQVKAEQFRQWEQNIVNERIRLNGDLEEIQGKVK
KLEEQVKSLLQVKKSHLK

Shs1:

MSTASTPPINLFRKKKEHKRGITYTMLLC**GPAGTGTKT**AFANNLLETKIFPHKYQYGKSNASISSNP
EVKVIAPTKVVSFNSKNGIPSYVSEFDPMRANLEPGITITSTSLELGGNKDQGKPEMNE**DDTVFFN**
LIMTHGIGENLDDSLCSEEVMSYLEQQFDIVLAEETRIKRNPRFEDTRVHVALYFIEPTGHGLREV
DVELMKSISKYTNVLPITRADSFTKEELTQFRKNIMFDVERYNVPIYKFEVDPEDDDLESMEENQ
ALASLQPFIAITSDTR**DSEG**RYVREYPWGIISIDDDKISDLKVLKNVLFGSHLQEFKDTTQNLLYEN
YRSEKLSSVANAAEEIGPNSTKRQSNAPLSNFASLISTGQFNSSQTLANNLRADTPRNQVSGNFKE
NEYEDNGEHDSAENEQEMSPVRQLGRE**KQE**NENLIRSIKTESSPKFLNSPDLPERTKLRNISETPV
YVLRHERILARQQKLEELEAQSARELQKRIQELERKAHELKLREKLINQNKLNQSSSSINSLQOST
RSQIKKNDTYTDLASIASGRD

5.2) Alignment of Cdc3, Cdc10, Cdc11 and Cdc12

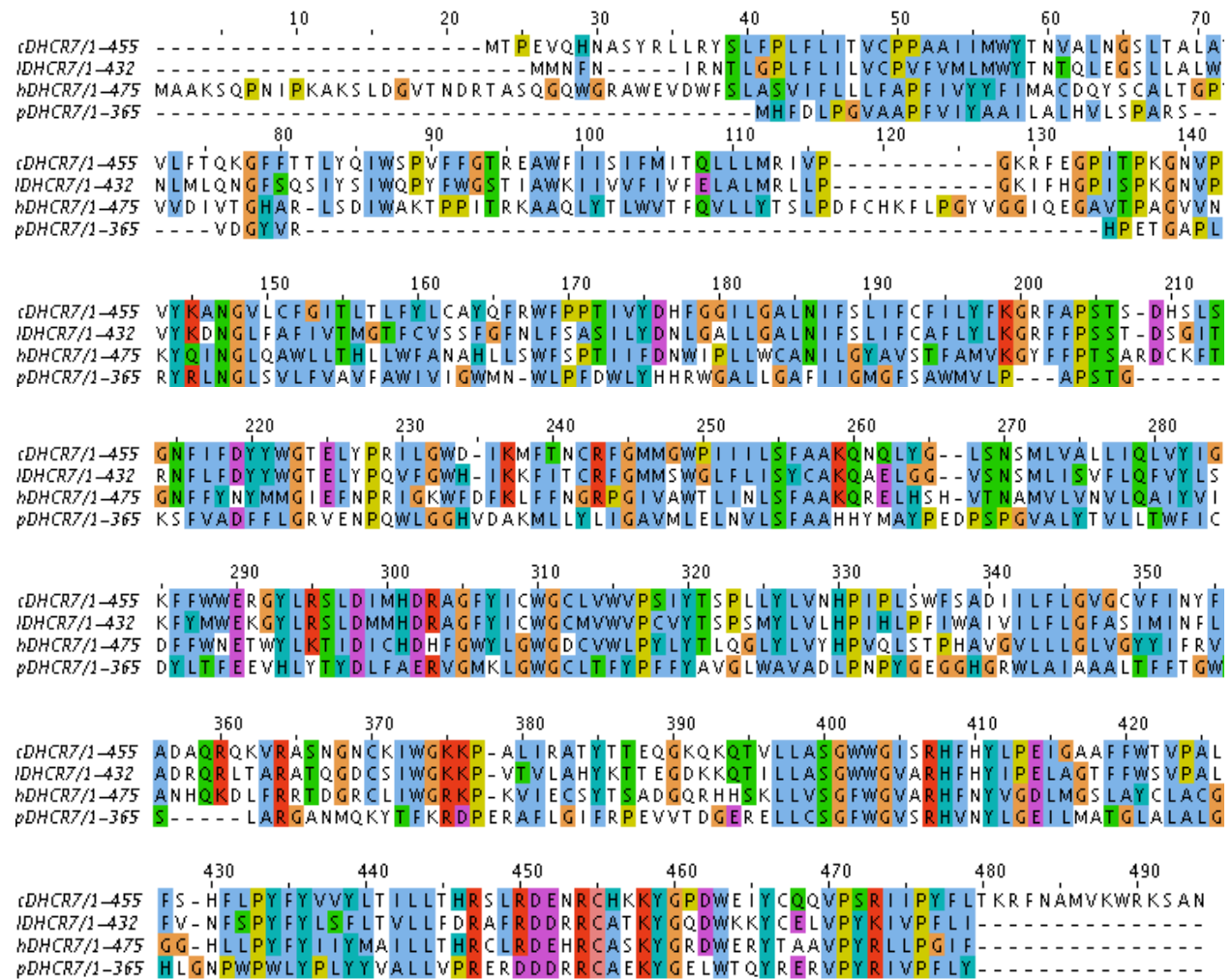


GNPWPWLYPLYVALLVPRERDDRRCAEKYGELWTQYRERVPYRIVPFLY

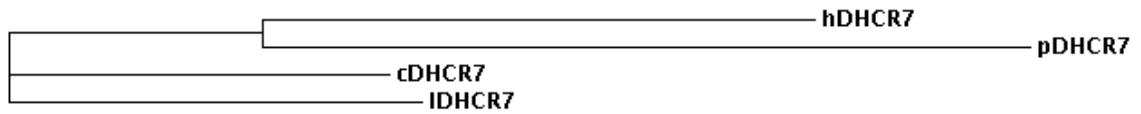
IDHCR7:

MMNFNIRNTLGPLFLILVCPVFMMLMWYTNTQLEGSLALWNLMLQNGFSQSIYSIWQPYFWGS
 TIAWKIIVFVIFELALMRLLPKGFHGPISPKGNVPVYKDNGLFAFIVTMGTFCVSSFGFNLFASAI
 LYDNLGALLGALNIFSLIFCAFLYLKGRFFPSSTDSGITRNLFDYIWGTTELYPQVFGWHIKKFITC
 RFGMMSWGLFLISYCAKQAEELGGVSNMMLISVFLQFVYLSKPYMWEKGYLRSLDMMHDRAGF
 YICWGCMMVWPCVYTPSMYLVLHPIHLPFIWAIVILFLGFASIMINFLADRQRLTARATQGDCSI
 WGKKPVTVLAHYKTTEGDKKQTILLASGWWGVARHFHYIPELAGTFFWVSPALFVNFSPYFYL
 FLTVLLFDRAFRDDRRCATKYGQDWKKYCELVPYKIVPFLI

5.5) Alignment of DHCR7



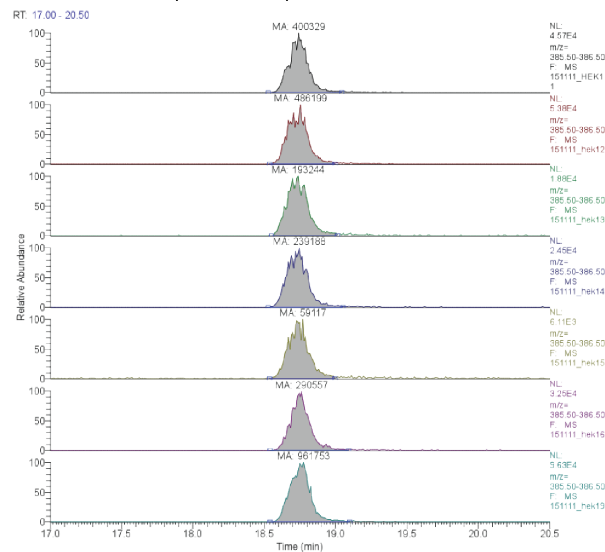
5.6) Phylogeny tree of DHCR7



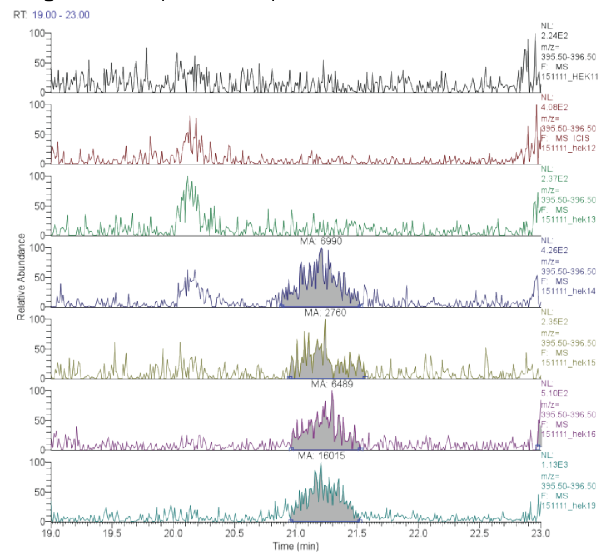
5.7) GC-MS measurement of cholesterol

An example of GC-MS measurements of different samples for four different ion mass (386 for cholesterol, 412 for stigmasterol, 398 for brassicasterol and 396 for ergosterol) is shown below. Integral of peak area was calculated automatically for each ion. Experiments were performed as triplicate and averaged for each point as shown in the results.

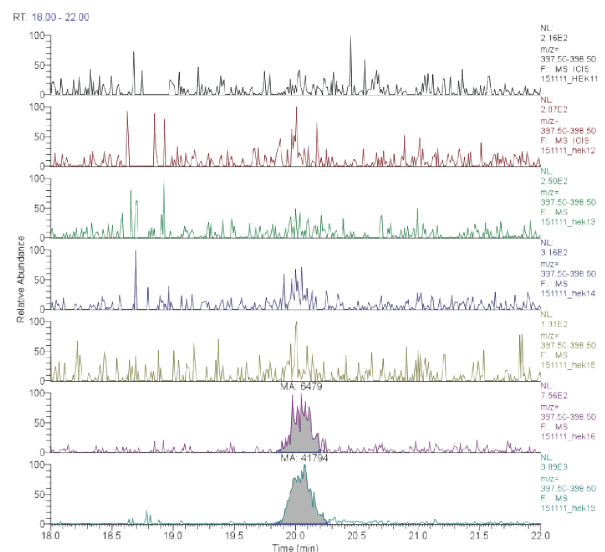
Cholesterol (m/z 386)



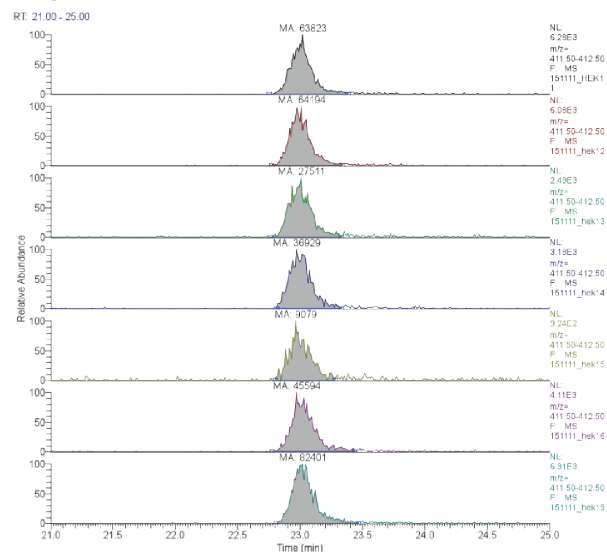
Ergosterol (m/z 396)



Brassicasterol (m/z 398)



Stigmasterol (m/z 412)



6) Glossary

α -tubulin	Is G-protein that together with β -tubulin forms a dimer to form the basic structure of microtubule
β -tubulin	Is a GTPase that binds to α -tubulin and later to the plus end of microtubules. Upon incorporation into microtubules, it hydrolyzes GTP
Actin	ATP-binding protein that polymerizes to form elongated filaments involved in contractility and cell motility
Actomyosin	Actin and major motor protein are arranged in microfibrils that consume ATP to produce contractile force
Anillin	A protein with actin and septin binding domains
APC	Anaphase promoting complex, which is active during late mitosis and early G1 committing cells to finish the cell cycle
BD domain	Is a borg specific domain responsible for binding and bundling of septin
Bem3	Is a GAP for Cdc42p
Borg superfamily	Is a family proteins with CRIB and BD3 domain responsible for septin regulation in mammalian cells
Bub2-Bfa1	Is a GAP for Tem1
Bud	Refers to daughter cell during cell division of <i>S. cerevisiae</i>
Budding neck	The area between the mother and the daughter cell
Cdc	Cell division cycle are proteins with diverse functions, which are active through the cell cycle
Cdc5	A polo kinase that activates MEN in yeast
Cdc14	Is phosphatase responsible to revert Cdc28/C1b2 mediated phosphorylation
Cdc24	Is a GEF for Cdc42p
Cdc28	A catalytic domain of the main yeast's Cdk, which associates with Cln or Clb cyclins
Cdc42p	Small GTPase involved in establishment of polarity in budding yeast
Cdk	Cyclin dependent kinase responsible for phosphorylation during mitosis
Cilium	Cellular projections involved in movement and sensation
Cla4	Is a kinase with a CRIB domain that interacts with Cdc42 and organizes septin by phosphorylating Cdc3 and Cdc10

Clb	B-type cyclin that activates Cdc28 to promote cell cycle in yeast
Cln	G1-type cyclin that activates Cdc28 to promote G1 phase in yeast
CRIB domain	Cdc42/Rac-interactive binding
Cyclin	A family of proteins that control the progression of cell cycle via Cdk
Cyclodextrin	Is a compound used to extract cholesterol from cell membrane
DHCR7	7-dehydrocholesterol reductase that removes C7-8 double bond from 7-dehydrocholesterol
Electron crystallography	A method to study the structure of membranes reconstituted in lipid bilayer using EM
Elm1	Is kinase that regulates septin structure
Fritz	An essential protein required to establish planar polarity
G3 domain	Is a domain with the consensus sequence of DXXG required for Mg ⁺² coordination and contact with γ -phosphate
G4 domain	Is a domain with the consensus sequence of KXD responsible for guanosine base recognition in G-proteins
G1 phase	The 1 st phase of the cell cycle
G2 Phase	The 3 rd phase of the cell cycle
GAP	GTPase activating protein that promotes hydrolysis of GTP in GTPases
GDP	Guanosine diphosphate
GEF	GTPase exchange factor that exchanges GDP to GTP in GTPases
Gic	GTPase interacting component that participates in early recruitment of septin to the budding neck
Gin4	A kinase that phosphorylates Shs1
G-interface	An interface among septin subunits in which nucleotide binding domains contact each other
GMP	Guanosine monophosphate
GppNHp	5'-Guanylyl imidodiphosphate is a nonhydrolyzable analog of GTP
GTP	Guanosine triphosphate
HMG-CoA reductase	Is the second and rate-limiting enzyme in the cholesterol biosynthesis pathway, which produces mevalonatic acid
Insig	Insulin induced gene, is a hydroxycholesterol sensing protein and regulates SREBP and

	cholesterol synthesis pathways
Kin4	Is a kinase that regulates septin
Lte1	Is a GEF for Tem1
Mitosis	The last phase of the cell cycle, which entails separation of duplicated chromosomes into mother and daughter cells
MEN	Mitosis exit network
NC-interface	An interface among septin subunits in which N and C termini contact each other
Paraseptin	A bacterial homologue of septin
PIP2	phosphatidylinositol-4,5-bisphosphate
P-loop	Is a domain with the consensus sequence of GXXXXGK(S/T) required to coordinate Mg ⁺² and contact phosphate
Restriction point	Is a point in lower eukaryotes that cell becomes committed to go through cell division
Rga1	Is a GAP for Cdc42p
Rga2	Is a GAP for Cdc42p
Rsr1	GTP binding protein required for bud site selection
SCAP	SREBP cleavage activating protein, is a cholesterol sensing protein, which escorts SREBP from ER to Golgi apparatus for cleavage
Septin hourglass	A septin structure at the budding neck resembling an hourglass that exists when bud grows
Septin ring	A single septin ring forming early in G1 between mother and daughter cells
Septin split ring	Two separate septin rings forming late in telophase each in mother and daughter cells
Single particle analysis	An EM-based method used to build up a 2D reconstruction of macromolecules
SLOS	Smith Leemli Optiz syndrom in which DHCR7 is deficient
Sonic hedgehog (Shh)	Is a pathway regulated by cholesterol required for pattern formation during development
S phase	The 2 nd phase of the cell cycle
Sporulative cycle	A cycle in budding yeast in which cells are diploid and divide mitotically or meiotically
SREBP	Sterol regulatory element binding protein, is an ER-residing transcription factor that upon cleavage and activation in Golgi regulates genes related to cholesterol
Start point	Is synonym for restriction point in higher eukaryotes

Statin	Is a family of HMG-CoA reductase inhibitors widely used to lower cholesterol levels in blood
Sterol sensing domain (SSD)	Is a domain in higher eukaryotic proteins responsible for binding and sensing different sterols
Switch I	Is a domain in G-proteins that together with Switch II participate in GTP hydrolysis
Switch II	Is another name for G3 domain, which together with Switch I domain participate in GTP hydrolysis
Tem1	A GTPase that activates MEN by releasing Cdc14
UTR	5' or 3' untranslated region are regions in mRNA that play translational regulatory role
Vegetative cycle	A cycle in budding yeast in which cells are haploid and divide mitotically
Yeast Septin Complex (YSC)	Filament forming octamer composed of Cdc3, Cdc10, Cdc11 and Cdc12

7) Index

- 2D crystallography, 50, 79, 134, 135, 141
3D crystallography, 49, 50, 62, 80, 141
7-dehydrocholesterol, 4, 37, 39, 42, 43, 144, 152, 153, 159, 160, 169
7DHC, 42, 43, 131, 132
Actin, 30, 168
Bfa1, 12, 31
Brassicasterol, 8
Bud, 168
Bud2, 30
Budding neck, 168
Cdc10, 6, 7, 18, 20, 21, 22, 23, 28, 32, 34, 61, 72, 86, 87, 88, 89, 90, 91, 92, 93, 94, 101, 102, 104, 106, 108, 109, 110, 111, 112, 114, 118, 119, 120, 163, 164, 165, 168, 171
Cdc10Δ, 6, 21, 72, 89, 90, 92, 93, 94, 102
Cdc11, 6, 7, 18, 20, 21, 22, 23, 24, 32, 34, 61, 72, 74, 81, 82, 84, 86, 87, 88, 89, 90, 91, 92, 93, 94, 109, 110, 111, 112, 118, 120, 163, 164, 165, 171
Cdc11Δ, 21, 72, 74, 89, 90, 92, 93
Cdc12, 18, 20, 21, 22, 23, 28, 32, 61, 82, 84, 87, 90, 91, 93, 94, 109, 110, 120, 163, 164, 165, 171
Cdc14, 11, 159, 168, 171
Cdc24, 145, 168
Cdc3, 12, 18, 20, 21, 22, 23, 24, 32, 34, 61, 72, 81, 82, 83, 84, 87, 88, 91, 93, 94, 103, 104, 109, 110, 112, 120, 163, 164, 165, 168, 171
Cdc42p, 6, 7, 21, 26, 30, 31, 32, 33, 34, 54, 57, 60, 61, 67, 72, 74, 75, 76, 81, 83, 92, 95, 96, 97, 98, 99, 100, 101, 102, 103, 104, 105, 106, 107, 108, 109, 111, 112, 113, 115, 116, 117, 118, 119, 120, 144, 145, 148, 151, 152, 155, 168, 170
Cdc5, 12, 26, 158, 168
Cholesterol, 36, 37, 38, 43, 51, 78, 128, 132, 145, 159
Cla4, 30, 31, 34, 160, 161, 168
CMC, 44, 49, 127, 134, 142
Cryo-electron tomography, 4, 47, 72
Cryo-EM, 150
C-terminal extension, 14, 20, 21, 22, 82, 84, 119
DHCR7, 4, 6, 7, 8, 36, 37, 39, 40, 41, 42, 43, 57, 60, 67, 68, 80, 121, 128, 130, 132, 133, 135, 136, 137, 138, 139, 140, 141, 142, 148, 151, 161, 165, 166, 167, 169, 170
DLPC, 51, 79, 134, 135
DOPC, 4, 51, 73, 79, 85, 86, 134, 135
Electron crystallography, 48, 156, 169
Electron microscopy, 4, 45, 73
Ergosterol, 8, 132
Fluorescence, 77
Fos-choline®-13, 49, 67, 68, 122, 123, 124, 125, 126, 127, 128, 129, 130, 131, 134, 135, 141
G3, 23, 24, 112, 169, 171
G4, 23, 24, 112, 163, 169
GAP, 4, 12, 30, 31, 103, 119, 168, 169, 170
GC-MS, 4, 6, 8, 58, 63, 79, 132, 133, 142, 143, 167
GEF, 4, 12, 30, 31, 168, 169, 170
Gic1, 6, 7, 31, 32, 33, 56, 60, 61, 66, 72, 74, 81, 83, 84, 85, 86, 87, 88, 89, 90, 91, 92, 93, 94, 95, 99, 100, 102, 104, 105, 106, 107, 108, 109, 111, 112, 113, 114, 115, 116, 117, 118, 119, 120, 145, 150
Gic2, 7, 31, 32, 33, 83, 104, 118, 145, 150, 155
Gin4, 12, 28, 34, 169
G-interface, 17, 19, 20, 23, 169
GTPase, 4, 12, 23, 25, 30, 31, 75, 96, 103, 104, 109, 110, 118, 147, 152, 168, 169, 171
HMG-CoA reductase, 26, 36, 37, 39, 40, 41, 43, 121, 133, 141, 143, 145, 148, 155, 169, 171
HPLC, 4, 53, 76, 96, 103
Insig, 38, 41, 128, 130, 156, 169
Insig, 156, 169
IPTG, 4, 44, 52, 64, 65, 66, 67, 68, 83, 95, 121, 122, 124, 125
LPR, 49, 79, 134, 135
Lte1, 12, 31, 170
MEN, 4, 12, 31, 150, 168, 170, 171
NBD, 80, 130, 131, 142
NC-interface, 6, 17, 18, 19, 20, 81, 83, 93, 94, 102, 103, 110, 112, 170
Ni-NTA, 62, 67, 68, 70, 80, 81, 83, 84, 122, 123, 126, 127, 129, 130, 131
P450 oxidoreductase, 42, 155
P-loop, 16, 23, 24, 112, 153, 170
POR, 42, 132
SCAP, 38, 41, 49, 121, 128, 130, 133, 135, 155, 156, 170

-
- SEPT2, 14, 15, 17, 18, 19, 20, 23, 27, 28, 29, 93, 94, 110, 151
SEPT2/6/7, 19
SEPT6, 14, 17, 18, 19, 20, 24, 28, 29
SEPT7, 14, 15, 17, 18, 19, 20, 27, 28, 29, 32
SEPT9, 14, 15, 16, 19, 20, 29, 143, 146, 152, 157, 159
Septin, 12, 13, 14, 18, 21, 26, 27, 28, 29, 30, 56, 65, 74, 76, 81, 86, 90, 104, 116, 145, 146, 147, 148, 151, 153, 154, 155, 160, 161, 170, 171
Septin ring, 148, 151, 170
Shs1, 14, 22, 34, 148, 151, 164, 169
Single particle analysis, 20, 46, 102, 170
SLOS, 5, 6, 7, 39, 41, 43, 133, 142, 170
SREBP, 38, 40, 132, 135, 155, 169, 170
SSD, 41, 42, 80, 121, 171
Sterol, 5, 37, 41, 42, 61, 146, 150, 170, 171
Sterol sensing domain, 61, 171
Stigmasterol, 79
Switch I, 24, 163, 171
Switch II, 24, 163, 171
Tem1, 12, 31, 168, 170, 171
Yeast two-hybrid assay, 5, 61, 75, 90, 91
 β -methyl-cyclodextrin, 138, 139, 140

Acknowledgments

I would like to acknowledge and appreciate the following people who provided me with tremendous help and advice through this work.

I would like to appreciate,

Dr. Stefan Raunser who supervised and assisted me in designing the experiments and the manuscript.

Prof. Dr. Roger S. Goody for discussing our results and accepting to be the first referee.

Prof. Dr. Roland Winter who accepted to be the second referee.

Dr. Marian Farkasovsky who initiated the project, purified proteins, performed the yeast two-hybrid assay and discussed the data through the work on septin.

Dr. Christos Gastogiannis who helped me with cryo-electron tomography and reconstruction.

Dr. Oliver Hofnagel who helped with cryo-data acquisition.

Prof. Dr. Alfred Wittinghofer who initiated the septin project and discussed the data.

Dr. Jürgen Nolte and Rita Fobbe at ISAS, Dortmund who performed the GC-MS measurements.

IMPRS-CB office (Prof. Dr. Martin Engelhard, Dr. Waltraud Hofmann-Goody and Christa Hornemann) for financial support and organizing office work.

Sandra Bergberde for technical assistance in the lab.

In the end, I would like thank my parents, my family and my friends including Stefan, Matthias, Shyamal, Amir Abbas, Armisha, Bamdad, Peiman and Mohsen who made my life fabulous in Dortmund.